Implications des modifications post-transcriptionnelles dans la régulation de l'activité de MITF in vivo : un facteur de transcription essentiel pour la lignée mélanocytaire

Julien Debbache

UNIVERSITÉ DE RENNES 1

ueb

THÈSE / UNIVERSITÉ DE RENNES 1
sous le sceau de l'Université Européenne de Bretagne

pour le grade de

DOCTEUR DE L'UNIVERSITÉ DE RENNES 1

Mention: Biologie

École Doctorale: Vie – Agro – Santé

presentée par

Julien DEBBACHE

préparée dans les 2 unités de Recherche
"Mammalian Development Section" au NINDS/NIH, Bethesda, MD USA
& IGDR UMR6061 CNRS, Rennes, France
Composante Universitaire: Sciences de la Vie et de l'Environnement

_____

**Implications des modifications post-transcriptionnelles dans la régulation de l'activité de MITF *in vivo* :
Un facteur de transcription essentiel pour la lignée mélanocytaire**

Thèse soutenue à : **Rennes, France**
Le 9 Décembre 2011

Devant le jury composé de:

Pr. Colin R. Goding
Professeur au Ludwig Institute for Cancer Research,
Oxford, UK   /*Rapporteur*

Dr. Lionel Larue
Directeur de Recherche INSERM U1021, CNRS UMR3347,
Institut Curie, Orsay, FR   /*Rapporteur*

Dr. Catherine André
Chargée de recherché CNRS IGDR, UMR60611
Rennes, FR   /*Examinatrice*

Pr. Gilles Salbert
Directeur de Recherche CNRS UMR6026
Rennes, FR   /*Examinateur*

Pr. Marie-Dominique Galibert
PU-PH CNRS, IGDR, UMR60611
Rennes, FR   /*Co-directrice de thèse*

Dr. Heinz Arnheiter
Directeur de Mammalian Development Section au NINDS/NIH
Bethesda, MD USA   /*Directeur de thèse*

APPRECIATIONS & ACKNOWLEDGMENTS

Table of Contents

Figures

Figure 1: The various functions of pigmentation

Figure 2: Differentiation of melanocyte precursor cells

Figure 3: Schematic distribution of the major mouse alleles and the position of their respective mutations on the gene

Figure 4: Sequence conservation of MiT family members and their homologs across animal species

Figure 5: Representation of *Mitf* alternative promoter use and subsequent alternative splicing of exon 2B and 6A

Figure 6: Regulation of transcriptional activation of the M-Mitf isoform

Figure 7: Illustration of diversity of mouse *Mitf* alleles and their corresponding phenotypes

Figure 8: Representation of the major types and positions of MITF post-translational modifications and their respective signaling pathways.

List of Abbreviations

α-MSH : α-Melanocyte Stimulating Hormone
BAC: Bacterial Artificial Chromosome
Bcl2: B-cell Lymphoma 2 Gene
bHLH-LZ: Basic Helix-Loop-Helix Leucine-Zipper
BrdU: Bromo Deoxy-Uridin
cAMP: Cyclic Adenine Mono Phosphate
cDNA: Complementary Deoxyribo Nucleic Acid
CREB: Cyclic-AMP Response Element Binding Protein
DCT: Dopachrome Tautomerase
E9.5: Embryonic Stage 9.5 Days
E-box: Ephrussi-box
EGFP: Enhanced/Eukaryotic Green Fluorescent Protein
ENU: N-ethyl N-nitrosourea
ESE: Exonic Splice Enhancer
GSK3: Glycogen Synthase Kinase 3
Kit: Kit-ligand Receptor, Stem cell factor Receptor.
MAPK: Mitotic Activated Protein Kinase
MC1R: Melano-cortin Receptor 1
MelSC: Melanocyte Stem Cells
MiT family: Mitf-Tcfe Transcription Factor Family
Mitf: Microphthalmia-Associated Transcription Factor Gene (Mouse)
MITF: Mitf Gene (Human)
Mitf: Mitf Transcript
MITF: Mitf Protein
mRNA: Message Ribo Nucleic Acid
NC: Neural Crest
NCC: Neural Crest Culture
NMD: Non-sense Mediated Decay
NRAS: Neuroblastoma-Ras protein homologue
PIAS3: Protein Inhibitor of activated STAT3
Pax3: Paired-Box Transcription Factor 3
RNAi: Ribo Nucleic Acid Interference
RPE: Retinal Pigmented Epithelium
RSK1: Ribosomal Protein S6 Kinase 1
RT-PCR: Real-Time Polymerization Chain Reaction
S73: Serine 73
S73A, D, S: Mutated Serine into Alanine, Aspartate, Serine
Sox10: SRY-like HMG Box Containing Gene 10
SRp: Serine-arginine Rich Protein
SRY: Sex-Determining Region Y
STAT3: Signal Transducer and Activator of Transcription 3
SUMO: Small Ubiquitin-related Modifiers
TYR: Tyrosinase
TYRP1: Tyrosinase-Related Protein 1
UV: Ultra Violet
Wnt: Wingless Integration 1 homolog

Introduction

Introduction

Pigmentation is one of the features in biology that presents a tremendous variety in terms of colors, shades, patterns and locations. It is seen by animals with eyes and depends on light. In fact, in places were light is absent, multi-cellular organisms generally lose their vision along with their pigmentation even though the loss of these two traits is not necessarily molecularly connected. Pigmentation functions are extremely diverse, protecting against ultra violet-radiation (UV), providing camouflage, male/female distinction, intra and inter-species communication and signaling (Figure 1). Easy visibility is likely a prime reason why pigmentation has been one of the first animal traits studied in modern biology. In addition, in vertebrates, pigment-bearing cells called melanocytes have been implicated in the normal development of several sensory organs, including the inner ear, where melanocytes play a critical role in the formation and the maintenance of the homeostasis of the endolymph and are necessary for hearing (Tachibana, 1999), and the eye, where retinal pigmented epithelium (RPE) cells play a supportive role for the retina and serve as a light screen (Bharti et al., 2006).

In humans, besides protection against UV induced DNA damage of the outer layers of the skin, pigmentation carries a cultural weight that seems to fluctuate with time and customs. For Middle-Age occidental and Asian societies, pale skin was very often associated with beauty or high societal rank. Nowadays, however, the pursuit of skin tanning has become a trend, which unfortunately has dramatic health consequences.

Fig.1A : Protection against UV damage

Fig.1B : Protection against predators, camouflage

Fig.1B : Male/Female distinction

Fig.1C : Intra-species communication

Fig.1D : Inter-species communication/signaling

Figure 1 : The various functions of pigmentation

Melanocyte-derived tumors, known as melanomas, have become one of the major public health issues in countries where the environment as well as individual genetic susceptibilities play key roles in the development of such pathologies. A good example for the interaction between genetic susceptibilities and the environment is the comparison of lifetime risk of cutaneous melanoma between the UK and Australian populations. With essentially the same genetic background, Australians have on average a 4 times higher risk to get melanoma than their relatives from the UK (Giblin and Thomas, 2007). Among the few high penetrance factors greatly correlated with the appearance of melanomas, we find inactivation of several key proteins involved in cell cycle regulation such as CDKN2A (encoding p16^{INK4a} and p14^{ARF}), cell and DNA integrity maintenance such as P53 or survival signaling pathways inhibition such as the Phosphatase and Tensin homolog (PTEN) (Meyle and Guldberg, 2009).

Although the vast majority of melanoma susceptibility gene mutations have a much lower penetrance, they can have a great importance in tumor formation, though not alone, but in combinations with other susceptibility genes. In fact, the purpose of this thesis is not to investigate what are the bold and dramatic effects of the lack of a protein on pigment cells, but rather to understand how minute genetic changes, either in the germ line or induced somatically, can have significant effects on a cell type or an entire living organism. Hence, the study of such a sensitive process like pigmentation offers the opportunity to understand molecular changes at the macroscopic, phenotypic level.

The study of coat pigmentation presents three critical advantages to biological experimentation: Pigmentation phenotypes are easily noticeable without any alteration to

the animal, the pigmentation process involves many of the major cellular parameters such as cell proliferation, differentiation, migration, maintenance, survival and death. Nevertheless pigmentation defects do not affect the development of a viable and fertile adult animal.

This thus motivated our group to study the development and functions of melanocytes. To do so, we chose the mouse model, which provides for powerful genetic manipulations. The mouse also has a relatively short generation time and shares with humans a similar number of conserved genes in a genome of similar size, enabling us to assess biological relevance within the time constrains of a thesis project.

1) The developmental origin of pigment cells:

In mammals, pigment cells, located throughout the dermis and the epidermis in the adult, originate from a very unique embryonic structure called the Neural Crest (NC) (Sommer, 2011). This transient structure forms at the margin of the developing neural tube from ectodermal tissue. The Neural Crest is capable of generating a great variety of cells. Among them, we find neurons, glia, chondrocytes, osteoblasts, smooth muscle cells, and melanocytes (Calloni et al., 2009; Le Douarin et al., 2008). After an epithelial to mesenchymal transition, NC derived cells can start migrating and differentiating into various cell types. The position of the progenitor cells along the axial level seems to pre-determine their fate during later differentiation steps. While some cell types such as sensory neurons, glial cells or pigment cells originate from the entire neuraxis, the source

of skeletal muscle precursor cells, for instance, is limited to the cranial neural crest (Le Douarin et al., 2008).

NC cells are originally pluripotent but lose this feature during their developmental specification. Melanocyte progenitor cells called melanoblasts are defined by the co-expression of early differentiation markers. Among them is KIT, the receptor for KIT Ligand, which plays a vital role in the survival and migration of progenitor cells. Alterations of the KIT signaling pathway lead to significant pigmentation defects in the mouse (Hou et al., 2000; Seldin et al., 1990). However, *in vitro*, KIT null NC cells can give rise to melanoblasts expressing a number of markers also found in melanocytes, with the exception of the pigmentation gene Tyrosinase (*Tyr*) (Hou et al., 2000). Another marker is MITF, a basic-helix-loop-helix leucine-zipper transcription factor, whose expression is turned on strongly during the specification of the pigment cell lineage, starting as early as E9.5 and staying high throughout life in mature melanocytes. A third one is EDNRB, the receptor for Endothelin 3, which promotes melanocyte proliferation. In fact, full differentiation of mature melanocytes can be obtained *in vitro* from E9.5 NC explants cultured in the presence of Endothelin 3 and KIT-ligand (Hou et al., 2000). A fourth one is Dopachrome Tautomerase (*Dct*), whose expression product is involved in pigment synthesis. The timing of *in vitro* differentiation follows the pattern observed *in vivo*, where *Dct* expression is seen at day 1 corresponding to E10.5 *in vivo*, followed by the expression of the pigmentation gene Tyrosinase related protein 1 (*Tyrp1*) seen at day 5 (E14.5 *in vivo*), and by the expression of *Tyr* at day 6 (E16.5 *in vivo*). Pigmentation then occurs around day 10 (Figure 2). In contrast to differentiated melanocytes, melanocyte stem cells (MelSC) are immature melanoblasts, which do not produce
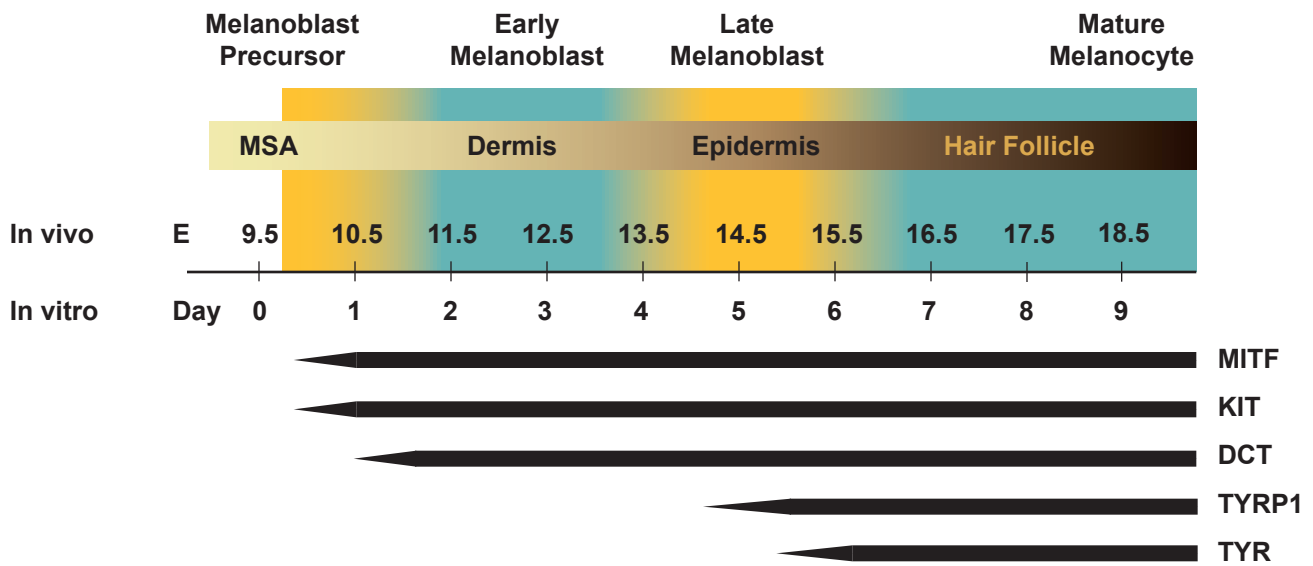
Figure 2: Differentiation of Melanocytes from precurssor cells. Schematic timeline representation of the transcriptional activation of several key differentiation markers in Neural crest cultures.

(From Hou *et al*. 2000)

melanin. They are maintained in a MITF/KIT-independent manner but retain high levels of DCT expression (Nishimura, 2011; Nishimura et al., 2002; Sommer, 2011). To this day, however, no marker or set of markers distinguishing MelSC from differentiated melanocytes have been identified. The branching out of MelSC from the melanocyte differentiation pathway occurs during the initial melanoblast migration to the hair follicle. Melanoblasts migrate to a specific stem cell niche in the upper part of the hair follicle, called the bulge, where they become MelSC, whereas cells migrating to the lower part of the hair follicle, called the bulb, terminally differentiate. During each hair cycle, MelSC located in the bulge area migrate to the hair bulb and mature to become pigmented melanocytes, while MelSC remaining in the bulge would settle in a quiescent/self renewal pathway. The switch between differentiation and "stemcellness" seems to be dictated by one or more extrinsic factors within the local environment surrounding the cell, but such factors are no longer required once the fate switch has been achieved. In fact, "stemcellness" of melanoblasts can be preserved in culture under simple conditions. One of the likely targets of these fate-switching factors might be the differential expression regulation of a specific set of genes.

2) Genes involved in melanocyte development:

So far, 378 loci have been identified to have an impact of melanocyte biology, of which only 171 genes have been cloned to this date in the mouse (http://www.espcr.org/micemut). Among them, we find genes implicated commonly in developmental signaling pathways, such as Wnt and Notch signaling, genes specifically

involved in the pigmentation pathway, such as the Melano-Cortin Receptor 1 (MC1R), or genes that are ubiquitously expressed and present, when mutated, a pigmentation phenotype, such as the B-cell lymphoma 2 gene (Bcl2) implicated in the inhibition of apoptosis. Out of this extensive list, the Microphthalmia-Associated Transcription Factor (MITF) has been demonstrated to be the melanocyte master regulator (Levy et al., 2006a; Vance and Goding, 2004), because it controls all the major cellular processes of the melanocyte cell lineage, such as differentiation, proliferation, and survival. Therefore, we focused our interest on how MITF is regulated and what consequences result from the modification of some of its activities.

Among the main regulatory mechanisms linking extracellular signaling pathways to MITF function, we find phosphorylation, which can adjust MITF target gene activation and its biological availability through the modulation of MITF stability. MITF Serine 73 phosphorylation is one of the critical sites that has been linked to modulations of MITF activity (Hemesath et al., 1998). It has so far been extensively studied, but for most of it, only *in vitro*.

In order to study the function of MITF phosphorylation *in vivo*, or the consequences resulting from its lack, we generated MITF S73 phosphorylation mutant animals. In this thesis we focused on the role of this particular MITF posttranslational modification, using both MITF transgenic animals and MITF knock-in mutant mice, on pigment cell biology *in vivo*.

3) History of *Mitf*:

The *microphthalmia* locus has first been described in 1942 by a German geneticist, Paula Hertwig (Hertwig, 1942). Intriguingly, the feature that led to the name of this particular locus was not the lack of pigmentation, but rather the resulting eye phenotype that mutant locus provoked. Only in 1993, the corresponding gene, *Mitf,* was cloned through the result of an insertional null allele, known now as *Mitf^{mi-vga9}* (Hodgkinson et al., 1993). When homozygous, this allele presented the same phenotypic characteristic as the original *Mitf^{mi}* allele and intercrosses between the original *Mitf^{mi}* allele and a *Mitf^{mi-vga9}* showed no complementation. MITF was found not only to be expressed in NC-derived pigment cells but also at high levels in the RPE where it has been shown to play a key role in the regulation of normal eye development (Hodgkinson et al., 1993; Nakayama et al., 1998). Mitf is also expressed in mast cells, which are cells of the adaptive immune system, and osteoclasts and at low levels in many other cell types. While Mitf expression in heart is low per cell, the fact that every cell expresses it leads to high signals in tissue extracts. Nonetheless, apart from the pigment cells, mast cells and osteoclasts, none of the other cell types seems to be severely affected by the impairment of MITF expression.

Since *Mitf* was cloned, more than 30 different spontaneous or chemically or radiation-induced *Mitf* alleles have been described in the mouse alone. The identification of this relatively high number of alleles can be explained by the ease with which coat color mutants can be seen in mouse colonies and highlights the sensitivity of pigmentation to

change in MITF activity. As described in more details later, the list of *Mitf* alleles represent many types of genetic mutations: single amino acid changes, single amino acid deletion, protein truncations, exon skipping mutations, promoter deletions, repeat element insertions and frame shift mutations (Hallsson et al., 2000; Steingrimsson et al., 1994) (Figure 3). Some of these alleles have been extensively analyzed and their associated phenotypes explained, but for others, such as *Mitf^{mi-bws}*, the amount of information is still insufficient to establish a direct genotype/phenotype correlation (Hallsson et al., 2000; Wen et al., 2010).

Mitf is at the "epicenter" of melanocyte biology:

In mammals, birds and fish, *Mitf* has been shown to promote differentiation functions, by direct activation of genes involved in pigmentation including, *Tyr*, *Dct*, *Tyrp1*, *Pmel17*, *Silver* among others (Hemesath et al., 1994). It has also been shown to control the cell cycle through the regulation of *p21* and *p27* via diaphanous-1 (Carreira et al., 2006). Furthermore it may control cell survival with the positive activation of *Bcl2* (McGill et al., 2002). However, there is little evidence that MITF is pro-proliferative. Bismuth *et al.* published a set of experiments with MITF transfected HEK293 cells, showing that MITF lacking exon 6A had a higher rate of BrdU incorporation than EGFP-transfected cells (Bismuth et al., 2005). In the total absence of MITF, however, melanoblasts are absent. Whether they die or whether their development is diverted to other lineages, such as Schwann cells, is not yet clear, however, Dupin *et al.* argue that cultured avian Schwann cells can transdifferentiate into melanoblasts, and melanoblasts into Schwann cells (Dupin et al., 2003). Therefore, it is conceivable that the number of Schwann cells
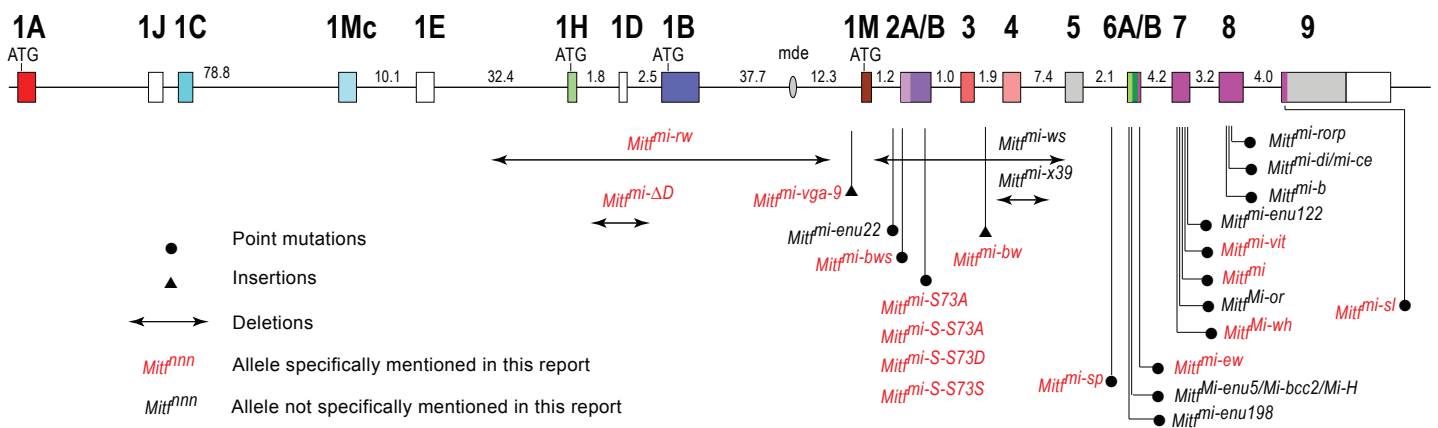
Figure 3: Schematic distribution of the major mouse *Mitf* alleles and the positions of their respective genetic mutations on the gene

increases in Mitf null mutants, but direct evidence for this is not available. In zebrafish, activation of Wnt signaling has been demonstrated to increase pigment cell numbers at the expense of sensory neuron and glial cell populations (Dorsky et al., 1998). The loss of Wnt signaling has the opposite effect of increasing sensory neurons and glial cell numbers at the expense of melanoblasts. In contrast, a gain of Wnt signaling results in an increase of the number of sensory neurons but not melanocytes, at the expense of other neural crest derivatives. The lack of Wnt signaling in NC-derived cells leads to the loss of the pigmentary cell population with a gain in the number of glial cells (Hari et al., 2002).

4) Genetic and biochemical characteristics of MITF:

MITF is a nuclear protein and contains a nuclear localization signal (IERRRR) located in its basic domain (Takebayashi et al., 1996). It is a member of the large family of basic Helix-Loop-Helix Leucine-Zipper transcription factors (bHLH-LZ), like *MAD* and *MAX*, and binds DNA on E-box derived sequence motifs, CACGTG or CATGTG, called M-boxes (Aksan and Goding, 1998; Hemesath et al., 1994; Strub et al., 2011). Specifically, it belongs to a subfamily called MiT transcription factors (*Mitf-Tcfe*) consisting of *Tcfe3*, *Tcfeb* and *Tcfec*, with which Mitf has been shown to directly interact to form heterodimers *in vitro*. However, it is not quite clear if these heterodimers have any functional relevance *in vivo*, as melanoblasts are not affected by Tcfe gene mutations (Steingrimsson et al., 2002). Nevertheless, genetic interaction has been shown between dominant negative *Mitf^{mi}* and a null allele of *Tcfe3* in osteoclasts (Hershey and Fisher, 2004). Such interactions are not seen with the Mitf null allele *Mitf^{mi-vga9}*. Mitf is highly

conserved throughout the animal kingdom. It is found in C. elegans, D. melanogaster, fish, reptiles, birds, and mammals with high similarity scores (Figure 4). 74% of its basic DNA binding domain are fully conserved amino acids or conservative substitutions. It reaches 100% of conservation if only amino acids making contacts to DNA are taken in to account (Hallsson et al., 2007). Mutations in the Mitf gene have also been found in many species, including zebra fish, quail and many mammals (rat, guinea pig, dog, human, pig) (Hodgkinson et al., 1998; Opdecamp et al., 1998; Tachibana, 2000).

5) Clinical significance:

In humans, *MITF*-mutations can lead to depigmentation of the skin, light hair color, and in some cases deafness and developmental defects of the eye (Tassabehji et al., 1994), a syndrome called Waardenburg syndrome type 2A and/or Tietz syndrome. In some cases, Mitf mutations previously characterized in mice are also found in patients. For instance, the deletion of an arginine in the basic domain of the $Mitf^{mi}$ allele is equivalent to the deletion reported in 2 families with Tietz syndrome (Izumi et al., 2008). In contrast to mice heterozygous for $Mitf^{mi}$, heterozygous humans display strong pigmentary deficiencies not only in the skin but also in the eye, and they are hearing-impaired. No homozygous patient has been recorded so far, perhaps because the loss of MITF function in human is lethal during the development of the fetus.
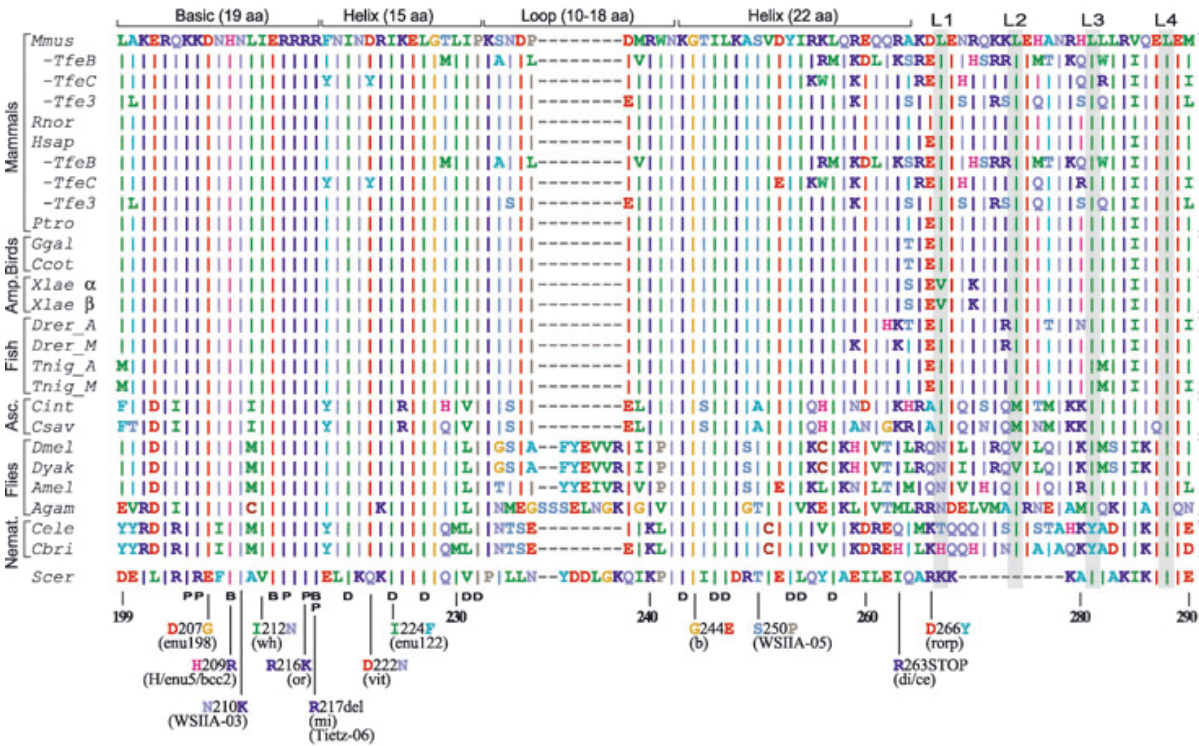
Fig. 4A: Protein sequence alignement of MITF against MiT family members and protein homologs from other animal species.
Critical mutants are annotated with their corresponding effect on the protein.
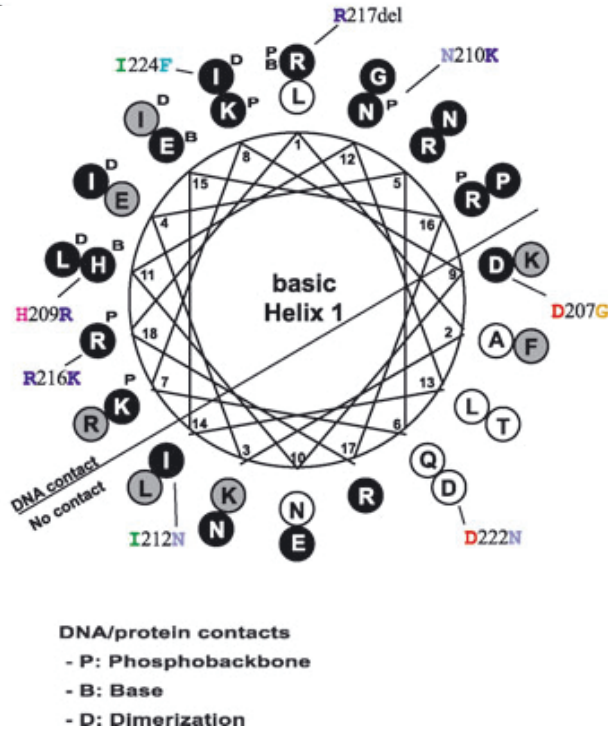
Fig. 4B: Structural representation of the basic and Helix 1 domain and localisation of the mutations of several Mitf alleles

Figure 4: Sequence conservation of MiT family members and their homologs across animal species.

(From Hallsson *et al.* 2007)

6) *Mitf* gene structure and expression profile:

The *Mitf* gene, spread over 214 kb in the mouse, is relatively complex with currently 9 known alternative promoters: A, J, C, Mc, E, H, D, B and M. A tenth promoter, CM, has been described in human *MITF* (Shiohara et al., 2009). For some, the first exon is non-coding, for others it is coding, leading to MITF protein isoforms differing at the amino-terminus (Figure 5). These alternative promoters bear very specific activation profiles among the different cell types of the organism. For instance, isoforms A, B, H and J are expressed ubiquitously in the mouse (Amae et al., 1998). H-Mitf is present at high levels in heart, D-Mitf is exclusively found in the RPE (Bharti et al., 2008), and M-Mitf is exclusively expressed in the melanocyte cell lineage (Amae et al., 1998; Fuse et al., 1999; Yasumoto et al., 1998). The body of the gene carries 8 exons, common to all isoforms (2-9). Of the later, one, exon 2, contains a 5' alternative splice site, and another, exon 6, contains a 3' alternative splice site. Indeed, alternative splicing leads to exclusion of exon 2B and exon 6A in 5 to 10% and 50% respectively of Mitf transcripts (Bismuth et al., 2008; Hallsson et al., 2000). The DNA binding and dimerization domains are covering a sequence from exon 6B to exon 8. *Mitf* contains both symmetric and asymmetric exons. Symmetric exons consist of multiples of 3 base pairs, resulting in the conservation of the reading frame if they are skipped in the mature mRNA. Asymmetric exons, in contrast, are not multiples of 3 base pairs. Therefore, asymmetric exon skipping results in a shift of the reading frame and likely protein truncation due to premature stop codons and/or non-sense mediated decay (NMD) of the mRNA when a premature translation termination codon appears in internal exons.
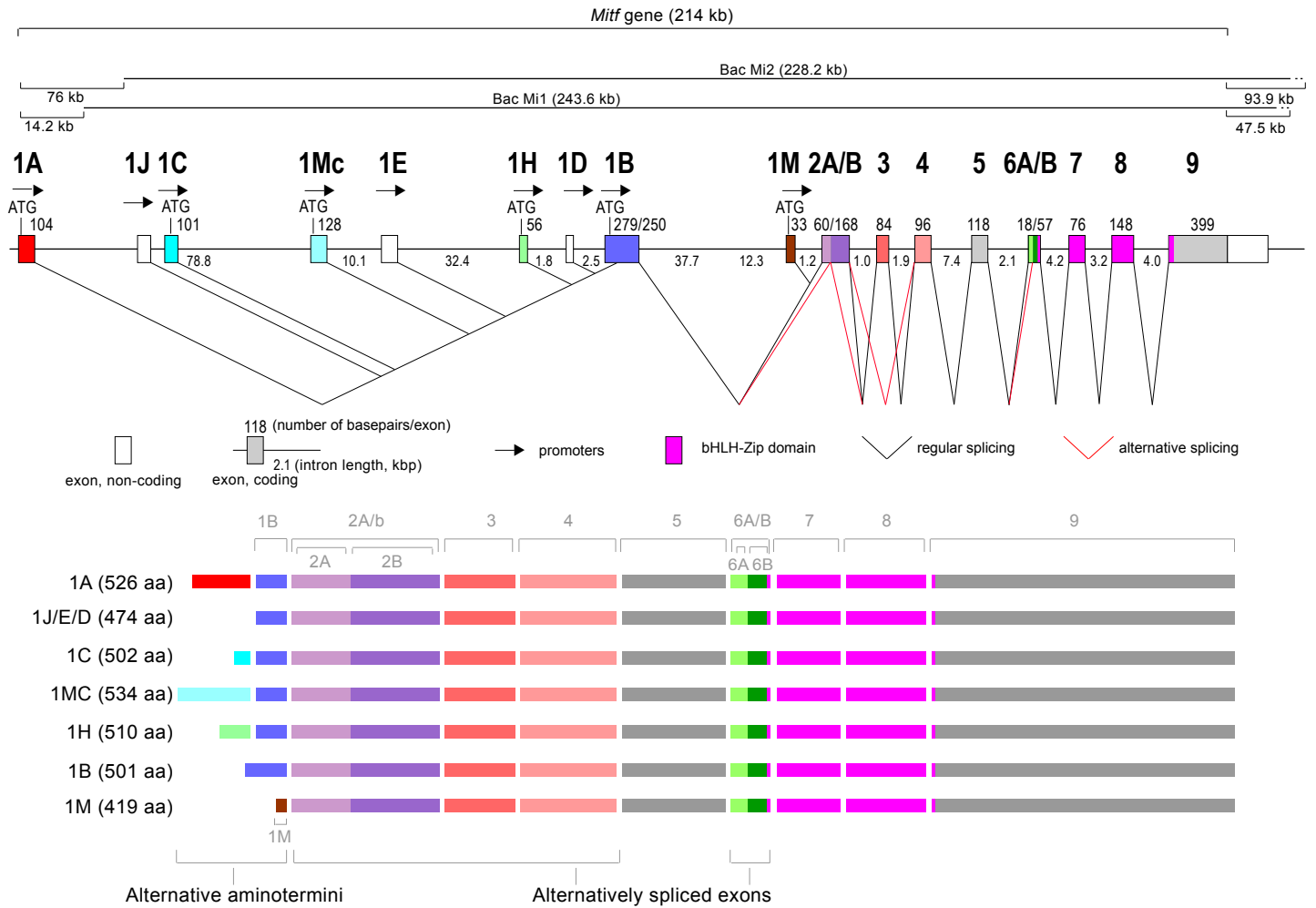
Figure 5: Representation of *Mitf* alternative promoter use and subsequent alternative splicing of exons 2B and 6A.

Intriguingly, while exons 2 to 5 can be excluded individually or all together with conservation of the open reading frame, the exons coding for the DNA binding and dimerization domains are all asymmetrical. cDNA cloning experiments performed by Steingrimsson's group, showed a glimpse of *Mitf* mRNA diversity, some of which lacking several exons. The possibility for these truncated transcripts to have any functional significance or to be just failed spliced materials, is yet to be determined (Hallsson et al., 2000).

All Mitf transcripts A, C, D, E, H, J, and Mc initiated from either one of the promoters lying upstream of B are spliced into exon 1B and subsequently into exon 2A, 3 etc. M-Mitf derived isoforms are the only transcripts that do not contain exon 1B. Although shown for only a few isoforms, it is conceivable that each of them may or may not contain the alternativly spliced exons 2B or 6A. Exon 6A alternative splicing and its consequences have been well documented with respect to the M-MITF isoform and biology of melanocytes. The presence of exon 6A in M-MITF leads to an increase in transcriptional activity on its target genes and an increased inhibition of cell cycle progression (Bismuth et al., 2005). Although evidence exists with respect to the alternative splicing of exon 6A in other isoforms, such as A-Mitf or H-Mitf, little is known about its biological relevance in cell types other than melanocytes. Exon 6A is included in 50 to 60% of the M-Mitf transcripts. Galibert's group has shown, however, that the splicing of exon 6A was highly variable in melanoma cells, with a much higher ratio for exon 6A exclusion compared to normal melanocytes (Primot et al., 2010). The same group has shown evidence linking the MAPK pathway with exon 6A splicing. The

inhibition of ERK leads to an increase of exon 6A exclusion in melanoma cells. Although MITF 6A+ protein has been shown to inhibit DNA synthesis more strongly than MITF 6A(-), it is not clear if the MAPK regulation of exon 6A splicing is part of a feedback loop in order to maintain the cell cycle progression, or if it is a way to further decrease Mitf-mediated cell survival.

In contrast, exon 2B alternative splicing has been more recently discovered and bears more complex mechanisms of activity regulation of MITF. Exon 2B inclusion seems to occur in the vast majority of Mitf transcripts, of which normally no more than 10% lack exon 2B . Bismuth *et al.* showed that MITF 2B+ has a higher ability to block cell cycle progression than MITF lacking the amino-terminus including exon 2B, suggesting that MITF 2B- proteins might have a reduced transcriptional activity, similar to the activity reduction seen in the MITF 6A- (Bismuth et al., 2005). In addition, this decreased inhibition was only observed with MITF containing exon 6A. Interestingly, somatic mutations resulting in exon 2B exclusion have recently been identified in melanoma samples, suggesting exon 2B is biologically relevant in melanoma proliferation (Cronin et al., 2009). However, so far, little is known about the regulation of exon 2B splicing and its consequences on melanocytes under normal conditions.

7) *Mitf* transcriptional regulation:

M-Mitf expression is regulated during melanoblast development by a set of transcription factors and signaling pathways.

Among them, four transcription factors, SOX10, PAX3, CREB and LEC/TCF, as well as two signaling pathways, Wnt/β-catenin and cAMP, play major roles in the transcription activation and maintenance of Mitf expression (Figure 6).

A) M-Mitf regulation through SOX10 transcription factor:

Sox10 (Sry-like HMG box containing gene) belongs to the SRY (sex determining region Y) transcription factor family, contains a High Mobility Group DNA binding domain, and binds (A/T)(A/T)CAA(A/T)G consensus motifs (Kuhlbrodt et al., 1998). Mutations of *SOX10* in humans are associated with Waardenburg-Shah syndrome type 4 (WS4), resulting in a combination of Waardenburg syndrome and Hirschprung disease (Pingault et al., 1998), that is various degrees of hearing loss, pigmentation defects, and distal motility defects in the large intestines due to the absence of myenteric plexus neurons. In the mouse, the dominant allele *Sox10^{DOM}* can lead to a depigmented belly spot – as seen in numerous *Mitf* mutants – and a megacolon (Mollaaghababa and Pavan, 2003). *Sox10^{DOM}/+*; *Mitf^{mi}/+* double mutant mice show aggravated coat depigmentation compared to single mutants. Several groups showed direct activation of the M-*Mitf* promoter by SOX10, consistent with the observed genetic interaction (Lee et al., 2000; Mollaaghababa and Pavan, 2003; Verastegui et al., 2000). In addition, it has been found that SOX10 and MITF can act in synergy on different promoters, such as the *Dct* and *Tyr*
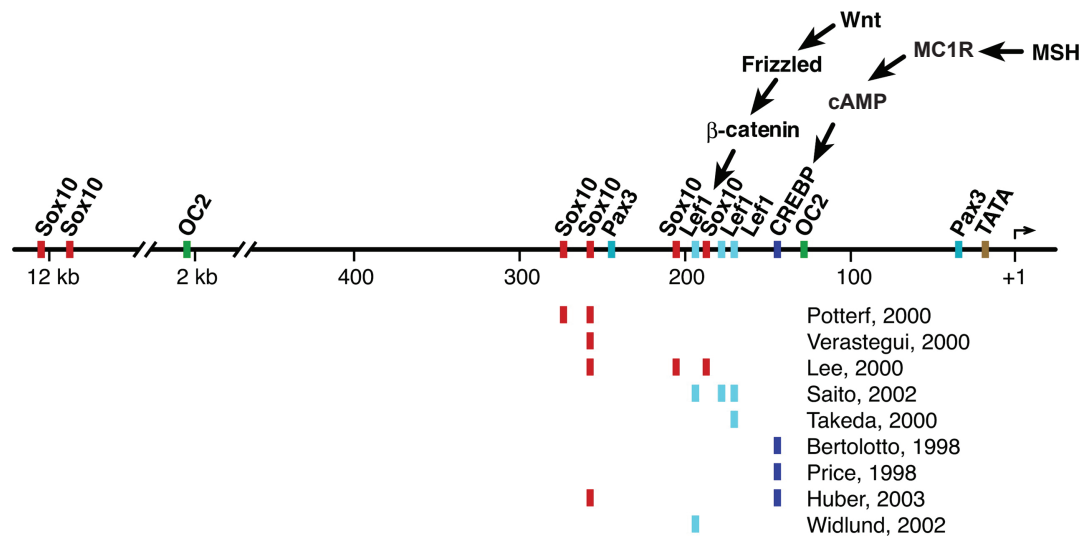
Figure 6: Regulation of transcriptional activation of the M-Mitf isoform
(From Steingrimsson *et al.* 2004)

promoters, without direct physical interaction. Complementary studies realized by Fisher's group have shown that SOX10 binding on the M-*Mitf* promoter allowed the binding and the activation of *Mitf* transcription by CREB and reciprocally, CREB binding on the M-*Mitf* promoter increased SOX10-mediated transcriptional activation of *Mitf* (Huber et al., 2003). This process is thought to increase M-*Mitf* expression specificity to melanocytes only.

B) M-Mitf regulation through Pax3 transcription factor:

Pax3 belongs to the Paired-Box (PAX) transcription factor family. Members of the PAX family typically contain a paired box domain and a paired-type homeodomain and play significant roles in the developing embryo. In humans, mutations in *PAX3* are associated with Waardenburg syndrome type 1 and 3 manifested by cranio-facial abnormalities, skin and hair pigmentation defects, and inner ear and eye development defects. Like SOX10, PAX3 promotes *Mitf* transcription activation (Watanabe et al., 1998), but can also collaborate with MITF to activate the *Tyrp1* promoter (Galibert et al., 1999).

C) M-Mitf regulation through cAMP signaling pathway:

Ballotti R.'s group showed in B16 melanoma cells that an increased concentration of cAMP by Forskolin treatment led to an increase of MITF protein expression (Bertolotto et al., 1998). In melanocytes, intracellular cAMP levels can be regulated by the α-MSH/MC1R pathway. Keratinocyte-secreted α-melanocyte stimulating hormone (α-MSH) binds to melanocortin receptor 1 (MC1R), a G-protein coupled receptor expressed by melanocytic cells, and leads to an increase of the cAMP concentration (Price et al.,

1998). Protein Kinase A is then subsequently activated which promotes the phosphorylation of cyclic-AMP response element binding protein (CREB). CREB then homodimerizes and can bind its DNA target sequences, one of which is located on the M-*Mitf* promoter.

D) M-Mitf regulation through the canonical Wnt/β-catenin signaling pathway:

Frizzled receptor bound WNT protein leads to a dissociation of the Axin/APC/GSK3/β-catenin complex (Hart et al., 1998). β-Catenin is no longer phosphorylated and stabilized and is then translocated to the nucleus and cooperates with LEF/TCF to bind on one or more of the 3 sites present on the M-Mitf promoter and activate its transcription (Takeda et al., 2000b). In several animal models, canonical WNT signaling has been shown to play an important role in the generation of pigment cells. Dorsky *et al.* showed that WNT is required for the development of melanophores in zebra fish and several groups showed that WNT1 and WNT3 were able to influence the number of melanoblasts in the developing mouse embryo (Dorsky et al., 1998; Dunn et al., 2005; Dunn et al., 2000). In addition, an increase of the β-catenin pathway in B16 melanoma cells leads to an increase in MITF protein expression (Saito et al., 2003; Takeda et al., 2000b).

8) *Mitf* and melanoma:

Melanoma, the melanocyte-derived cancer, ranks among the highest in cancer-related death in humans. Its high resistance to chemo and radiation-therapy leaves only little flexibility other than the surgical removal of the primary tumor before it

metastasizes and spreads to other organs. Given *Mitf*'s major role in melanocyte biology, it's not surprising that *Mitf* is also a major regulator of melanoma formation and metastasis (Vance and Goding, 2004). Interestingly, metastatic tissues have been demonstrated to be associated with very disparate Mitf levels. Although Comparative Genomic Hybridization assays from metastatic melanoma samples suggest that *microphthalmia* locus can be amplified multiple times in some cases (Garraway et al., 2005; Gast et al., 2010; Jonsson et al., 2007), Mitf mRNA and protein levels do not necessarily correlate with *microphthalmia* locus copy numbers. In addition, Samuels' group was able to identify the occurrence of various *MITF* mutations that arose specifically in tumor and metastasis samples from melanoma patients (Cronin et al., 2009). All of these mutations were tested *in vitro* and lead to a decrease of MITF transcriptional activation on two target gene promoters. This heterogeneity in MITF activity levels is also reflected by the heterogeneous nature of melanoma itself, where even within a tumor, great heterogeneity can arise and reveal an underlying genomic or epigenetic instability of these malignant cells.

Hence, the variations not only of MITF levels but more importantly its biological activity may reveal the underlying pathways that are differentially activated in one tumor versus another. It also seems that MITF levels fluctuate between different tumor growth stages, allowing cancer cells to oscillate between differentiated, proliferative and invasive phenotypes, a phenomenon called "phenotype-switching" (Hoek and Goding, 2010).

Among the principle signaling pathways involved in melanocyte proliferation control, the MAPK pathway is one most often genetically altered. B-RAF and N-RAS mutations are found, respectively, in 60% and 30% of melanoma cases and are mutually exclusive

(Meyle and Guldberg, 2009). In both genes, the large majority of the mutations corresponds to an increase of the kinase activity of the protein. The MAPK pathway is altered in a quantitative or qualitative manner in 100% of the melanoma cases. Under normal conditions, constitutive activation of MAPK results in the induction of senescence related cell cycle arrest (Dhomen et al., 2009). To overcome this barrier that normally prevents further progression, additional alterations affecting cell cycle regulators such as *Cdkn2a*, *Cdk4* or *p53* are required (Bennett, 2008; Dahl and Guldberg, 2007; de Snoo and Hayward, 2005). Very specific growth characteristics are associated with the accumulation of mutations in these genes, from radial to vertical growth and, ultimately, migration to other organs.

Although MITF doesn't directly regulate the MAPK activity, the MAPK pathway is directly linked to post-translational modifications of MITF and is able to regulate MITF activity and stability (Hemesath et al., 1998; Wu et al., 2000). In this particular case, the MAPK pathway plays a dual role by increasing MITF target gene activation and decreasing MITF levels by subsequent poly-ubiquitination and proteasome-mediated degradation.

Besides proliferation, another critical parameter for an increase in cell number is survival. In melanocytes, *Bcl2* and Melanoma-inhibitor of apoptosis protein (*ML-IAP* or *Livin* or *Birc7*) have been shown to be key factors to prevent cells from entering apoptosis prematurely. *Bcl2* is one of the many critical target genes regulated by *Mitf* and *Bcl2* deficient mice display premature graying, which is greatly amplified with a reduction in MITF activity (McGill et al., 2002). In melanoma cell lines, down regulation of Mitf by RNAi has been shown to decrease *Bcl2* expression leading to a decrease in cell numbers

(McGill et al., 2002). In contrast, *Mitf* overexpression in melanoma cell lines leads to cell cycle arrest (Carreira et al., 2006). The above evidence emphasizes the ambivalent role that Mitf play by affecting cell proliferation, differentiation and survival. Small changes in MITF activity can therefore have drastic consequences with respect to melanocyte biology. The use of the genetic mouse model allows us to molecularly dissect MITF functions and provides a very well buffered biological system that prevents the interference of experimental artifacts that one often encounters *in vitro*.

9) *Mitf* alleles in mice:

Among the 36 different mutant alleles that have been described in the mice, most affect the bHLH domain of MITF protein through various ways such as single amino acid deletion (*Mitf^{mi}*: deletion of one of the 4 arginines in the basic domain), single amino acid changes (*Mitf^{Mi-wh}*: I212N, *Mitf^{mi-or}*: R216K), and splice defects resulting in a missing exon (*Mitf^{mi-ew}*: ΔExon 6A/6B). A special case is presented by *Mitf$^{mi-S73A}$* where the primary mutation is a point mutation in Serine-73 that also leads to preferential elimination of the corresponding exon from mature mRNA (Bauer et al., 2009; Bismuth et al., 2008; Steingrimsson et al., 1994) (Figure 7). In addition to these 36 alleles, 6 novel alleles are described in this thesis: *Mitf$^{mi-S-S73ANeo}$*, *Mitf$^{mi-S-S73AΔNeo}$*, *Mitf$^{mi-S-S73DNeo}$*, *Mitf$^{mi-S-S73DΔNeo}$*, *Mitf$^{mi-S-S73SNeo}$* and *Mitf$^{mi-S-S73SΔNeo}$*.
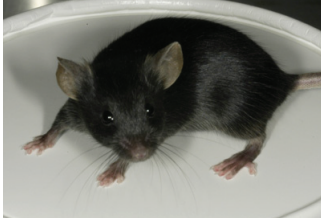
Fig.7A : C57BL6/J
Wild type allele
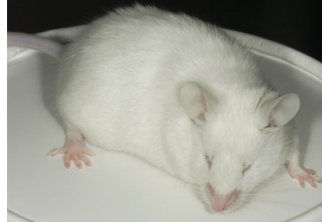
Fig.7B : $Mitf^{mi\text{-}vga9}/Mitf^{mi\text{-}vga9}$
Functionnally null
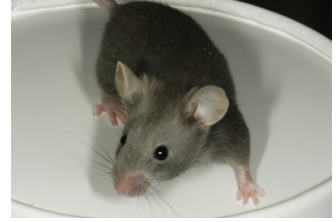
Fig.7C : $Mitf^{Mi\text{-}wh}/Mitf^{+}$
Dominant Negative
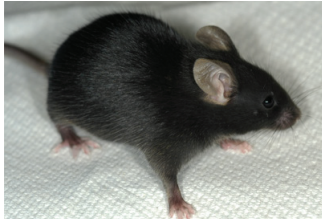
Fig.7D : $Mitf^{mi\text{-}sp}/Mitf^{mi\text{-}sp}$
Hypomorphic splice mutant
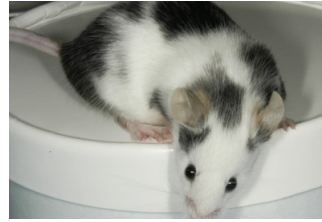
Fig.7E : $Mitf^{mi\text{-}sp}/Mitf^{mi\text{-}vga9}$

Fig.7F : $Mitf^{mi\text{-}bws}/Mitf^{mi\text{-}bws}$
Splice mutant
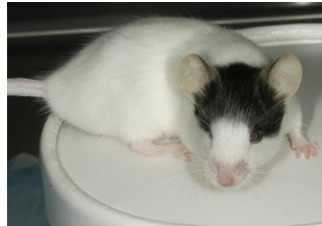
Fig.7G : $Mitf^{mi\text{-}rw}/Mitf^{mi\text{-}rw}$
Isoform specific mutant
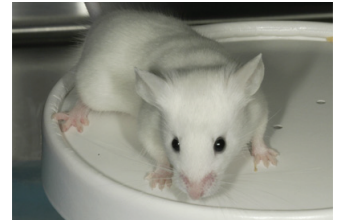
Fig.7H : $Mitf^{mi\text{-}bw}/Mitf^{mi\text{-}bw}$
Insertional mutant
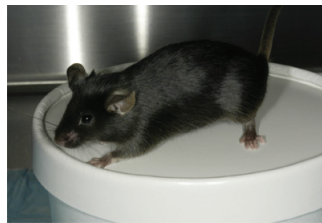
Fig.7I : $Mitf^{mi\text{-}\Delta D}/Mitf^{mi\text{-}\Delta D}$
Isoform specific mutant

Figure 7 : Illustration of the diversity of *Mitf*
alleles and their corresponding phenotypes

A) Historical and principal mutants:

 All bHLH-domain mutants present similar phenotypes as the null $Mitf^{mi-vga9}$ allele when homozygous, with absence of neural-crest derived melanocyte, small eyes (microphthalmia) and a loss of hearing. However, subtle biologically relevant differences exist and help reveal differences in the underlying molecular mechanisms. For instance, most *Mitf* mutations have, in the mouse, very small effects or none at all at the heterozygous state. For instance, a small white belly spot can be present in $Mitf^{mi-or}$ or $Mitf^{mi}$ mice and hearing may be normal. More severe pigmentation defects are only observed when the gene dose or MITF activity is reduced to 50% or less of wild type, depending on the allele. In humans, however, alteration of only one of the two *MITF* alleles is often sufficient to display phenotypic defects including hearing deficiencies (Nobukuni et al., 1996; Pingault et al., 2010).

The $Mitf^{mi-vga9}$ null allele, the historically important allele that led to the cloning of the *Mitf* gene (Hodgkinson et al., 1993), is the result of insertions of tandem repeats of a vasopressin-β galactosidase transgene construct, 800 bp upstream of the exon 1M. The consequence of this insertion consists in the disruption of any Mitf transcript produced by the 8 upstream promoters as well as the deregulation of the downstream M promoter.

In fact, the $Mitf^{mi-vga9}$ allele produces no Mitf RNA and protein in most tissues including heart and skin. In RPE, however, *in situ* hybridization using a full length cDNA probe have shown a reduced Mitf signal but this signal can potentially be attributed to aberrant transcripts initiated from the transgene or to a cross reactivity with the closely related Tcfec transcript, which has recently been shown to be upregulated in the developing RPE

in the absence of *Mitf* expression (Rowan et al., 2004). In any event, even the RPE shows no MITF protein accumulation (Nakayama et al., 1998).

The *Mitf$^{mi\text{-}or}$* and *Mitf^{mi}* alleles display similar phenotypic characteristics as both of these alleles affect one of four arginines clustered in exon 7. These mutations interfere with DNA binding of the resulting proteins (Steingrimsson et al., 1994). In addition, the *Mitf^{mi}* mutation affects MITF's nuclear localization signal, such that the mutated protein is no longer strictly nuclear. *Mitf^{mi}* is associated with the most severe phenotype in the homozygous conditions resulting in death after weaning as a result of severe osteoporosis and starvation linked to the lack of tooth eruption. These extra phenotypic features associated with the *Mitf^{mi}* allele can be attributed to the inability of MITF^{mi} heterodimers to bind DNA as well as the sequestration of other MIT family members, leading to a further decrease of their respective availability to bind DNA.

The *Mitf$^{Mi\text{-}wh}$* allele presents a unique feature among all *Mitf* alleles as it displays a strong coat color dilution along with a loss of hearing at the heterozygous state (Takebayashi et al., 1996). This apparent dominant-negative activity is paired with a homozygous phenotype similar to, but less severe than in *Mitf^{mi}* or *Mitf$^{mi\text{-}vga9}$* null mutant homozygous animals. In fact, although the lack of NC-derived melanocytes is complete, the severity of the microphthalmia of *Mitf$^{Mi\text{-}wh}$*/*Mitf$^{Mi\text{-}wh}$* mice is reduced compared to that of *Mitf$^{mi\text{-}vga9}$*/*Mitf$^{mi\text{-}vga9}$* mice. *Mitf$^{Mi\text{-}wh}$* is also one of the few alleles known to display allelic complementation, meaning that compound heterozygotes such as *Mitf$^{Mi\text{-}wh}$*/*Mitf^{mi}* or *Mitf$^{Mi\text{-}wh}$*/*Mitf$^{mi\text{-}vga9}$* show eyes of normal size unlike their microphthalmic homozygous parents. Recent unpublished biochemical work performed by Steingrimmsson's group on the crystal structure and binding capacity of the MITF$^{Mi\text{-}wh}$ protein shows that the protein

is capable of binding M-boxes, but is also capable of binding other E-box-like motifs with a higher affinity than wild-type MITF. These results suggest that MITF^{Mi-wh} could shift the transcription activation from melanocyte-specific genes to normally non-MITF-specific target genes and thereby interfere with, or alter the normal melanocyte differentiation and maturation pathway (Steingrimsson E unpublished).

B) Splice mutants:

Among the mutant *Mitf* alleles that carry splice defects, *Mitf*$^{mi-sp}$ (*mi-spotted*) and *Mitf*$^{mi-bws}$ (*mi-black and white spots*) present complex mechanisms that bring only partial answers to explain their phenotypes. The *Mitf*$^{mi-sp}$ allele is the result of an insertion of an extra Cytidine in the alternatively spliced exon 6A between the F190 codon and the P191 codon. This insertion results in a shift in the open reading frame and the generation of a stop codon shortly after the beginning of exon 6B in mRNAs that have exon 6A included. As mentioned above, exon 6A is generally included in about 50% of the M-Mitf transcripts; hence half of the mRNAs should carry a premature STOP codon in exon 6B, within 60 bases of the exon-exon junction and therefore triggering NMD of the Mitf 6A+ mRNA. Alternatively, it is possible that the extra Cytidine disrupts the polypyrimidine tract that regulates splicing. Despite this genetic alteration, *Mitf*$^{mi-sp}$/*Mitf*$^{mi-sp}$ mice are fully pigmented with normal-sized eyes (Boissy and Lamoreux, 1995). Nevertheless, they display Mitf RNA levels close to 80%, rather than the expected 50%, hence showing that there is a compensatory upregulation of transcription or a reduction in production of the 6A+ isoform, reducing the amount of Mitf message subject to NMD. *Mitf*$^{mi-sp}$ is a hypomorphic allele that displays its phenotype only in the presence of another null or dominant-negative *Mitf* allele. Regardless of its reduced transcript level, *in vitro* results

with Mitf cDNA over-expression have shown that MITF 6A- has a lower activity on differentiation genes, and a lower DNA binding affinity compared to the MITF 6A+ isoform (Murakami et al., 2007). In addition, MITF cell cycle arrest related activities are significantly decreased in the presence of MITF 6A- compared to MITF 6A+ (Bismuth et al., 2005).

The *Mitf^{mi-bws}* allele was historically the first *Mitf* mutant that was demonstrated to affect exon 2B with *Mitf* transcripts lacking exon 2B (Mitf 2B-) representing ~50% rather than the normally observed ~10% (Hallsson JH 2000). The molecular analysis revealed a G>A mutation 12 base pairs upstream of exon 2A. *Mitf^{mi-bws}* / *Mitf^{mi-bws}* homozygous mice display large white areas with black spots which tend to gray with aging. Therefore, loss of exon 2B was thought to be associated with a great loss of MITF activity. However, new evidence presented in this thesis suggest that this allele is associated with a substantial reduction of Mitf RNA levels, reflecting additional alterations yet to be identified.

C) Isoform specific mutants:

A few alleles are known to affect specifically a set of isoforms and have therefore been useful to study the particular role of some of these isoforms during development. For instance, the *Mitf^{mi-rw}* (*mi-red eye white*) allele is characterized by a deletion spanning the H, D and B promoters and corresponding exons (Bharti et al., 2008; Hallsson et al., 2000). This genomic deletion leads to the absence of H-Mitf, D-Mitf and B-Mitf transcripts. It also results in an upregulation of the upstream A, J and E isoforms. Both J and E isoforms normally use the start codon located in exon 1B as translation initiation

site (Bharti et al., 2008). But in the case of *Mitf^{mi-rw}*, exon 1B is missing, hence the next available start site is located in exon 2B, resulting in a M-MITF-like isoform truncated at its N-terminal end. The *Mitf^{mi-rw}*/*Mitf^{mi-rw}* is very particular and reflects the complexities resulting from the expression of aberrant isoforms at abnormal levels. The homozygous mice are mostly white with a variably-sized black spot on the head and occasionally on the belly. The eye size is much reduced but there is considerable variability.

The *Mitf^{mi-bw}* allele (*mi-black-eye white*) is characterized by the insertion of a 7 kb L1 SINE element in intron 3 resulting in the specific down regulation of the expression of the M-Mitf isoform (Yajima et al., 1999). *Mitf^{mi-bw}* / *Mitf^{mi-bw}* homozygous mice display a white coat with the complete lack of NC-derived melanocytes, due to the lack of the melanocyte specific Mitf isoform. Eye size and pigmentation remain, however, unaffected as the maintenance of significant Mitf expression in the RPE of the A-Mitf and H-Mitf isoform may be sufficient to support normal development of this tissue.

More recently, Mitf-isoform targeted knockouts have been generated in our group in order to understand the role of some of the major MITF isoforms, such as A-MITF and D-MITF. Although these specific mutants do not display strong phenotypes on their own, a striking phenotype can be revealed, for instance, in *Mitf$^{mi-\Delta D}$*/*Mitf$^{mi-\Delta D}$* mice in combinations with gene dose changes in the eye transcription factor *Pax6*.

While the lack of availability of isoform-specific antibodies has restricted the analysis of isoform distribution mainly to mRNA expression by real-time PCR, the sensitivity of this technique has allowed precise measurements of the level of specific isoform per cell, even when only small amounts of tissue are available. Nonetheless, it remains an open question whether all the full-length and some of the truncated mRNA isoforms are

translated into protein. Furthermore, even if they were all translated, it remains unclear whether all protein isoforms would be biologically relevant. In that regard, mechanisms such as RNA interference and micro RNA regulations are efficient ways to modify the ability of a specific RNA to lead to a specific protein. In the case of Mitf, several binding sites of miRNA, though mostly confined to the 3' untranslated region, have been identified using bioinformatic tools several years ago, but it is not until recently that breakthrough discoveries in the miRNA world were linked to *Mitf* regulation. In fact, *Mitf* regulates and is regulated by RNAi and the miRNA machinery. The mouse M-Mitf message is over 4.5 kb long with more than half of the sequence being non coding. Recent work done by Haflidadottir *et al.* has demonstrated the effect of two miRNA, miR-148 and miR-137 binding to the 3' untranslated region, on the expression of MITF protein in melanocytes and melanoma cells (Haflidadottir et al., 2010). More strikingly, Mitf has been associated with the regulation of a key enzyme in the miRNA-processing machinery: DICER (Levy et al., 2010). DICER plays a critical role in the maintenance and function of a large number of cell types. Hence, one of the ubiquitous roles of Mitf could be associated with the maintenance and survival of differentiated cells through the expression of a vital enzyme such as DICER. In melanocytes, both *in vitro* and *in vivo* DICER expressions are required for survival even in the presence of functional Mitf.

The above-mentioned elements on Mitf post-transcriptional regulations are further evidence supporting the inadequacy of the *in vitro* model to integrate the diversity of Mitf regulation, and further motivated us to pursue the study of Mitf activity regulation *in vivo*.

10) The roles of post-translational modifications for modulating activity:

As it has been described earlier, MITF is able to control proliferation, differentiation, migration, death, and other melanocyte specific processes. These processes, like cell death and proliferation, are sometimes biologically synergistic and make sense when one single transcription factor, by acting positively on target genes, can promote cell division and inhibit cell death at the same time. However, the positive regulation of two fundamentally opposed biological processes, such as differentiation and proliferation, by one single transcription factor may not be easy to understand. In the case of Mitf, proliferating, migrating or differentiating melanocytes must be able to modulate specific sets of target genes by molecular modifications of MITF to allow the cells to choose between these distinct biological behaviors. Hence MITF transcriptional activation is unlikely to be linear on each of its target genes and may be dependent on a particular set of post-transcriptional modifications. One possibility is that different isoforms have different specific activities and the outcome of the regulation of the combination of these isoforms ultimately results in the fine-tuning of target gene expression. Thus, it would only be correct to refer to MITF "activities" and not generalize MITF activity as a single term. In addition to this transcription regulation, post-translational modifications are usually important regulators of protein activity. They can act on various levels by changing protein stability and target-binding affinity, cellular localization, or interaction with partners or co-factors. Like with a large majority of eukaryotic proteins, MITF protein is subject to various post-translational modifications,

including serine/threonine phosphorylation, lysine mono and poly-ubiquitination, acetylation, and SUMOylation (Figure 8).

A) M-MITF SUMOylation in melanocytes:

SUMOylation stands for the enzymatic reaction catalyzing the conjugation of Small Ubiquitin-related Modifiers on an amino acid sequence, through three individual steps involving different proteins: activation, involving the E1 enzyme (SAE1/SAE2), conjugation, involving the E2 enzyme (UBC9) and transfer on the protein substrate involving the cooperation of E2 and E3 protein ligase (Miller et al., 2005; Murakami and Arnheiter, 2005). The fixation of SUMO occurs on Lysines belonging to the Ψ-K-x-D/E consensus site, where Ψ is stands for a hydrophobic amino acid. Three types of SUMO proteins are known so far: SUMO-1, SUMO-2 and SUMO-3. Although mixed chains of these proteins can be formed, SUMO-1 protein itself lacks a SUMOylation site and therefore prevents the further branching of additional SUMO proteins. MITF contains at least two SUMOylation sites on K182 and K316. SUMOylation on either or both sites has been shown to decrease the transcriptional activity of multiple M-box containing promoters but not on single M-box containing promoters *in vitro* (Miller et al., 2005; Murakami and Arnheiter, 2005). This alone shows that post-translational modifications can affect MITF activities in a target gene specific manner *in vitro*, even if signaling pathways resulting in MITF SUMOylation have yet to be identified. In addition, recent epidemiological data have identified a SUMOylation mutant in the European population. This variant is a p>E318K germline mutation and is associated with a higher risk of both sporadic and familial melanoma (Bertolotto et al., 2011a; Yokoyama et al., 2011).
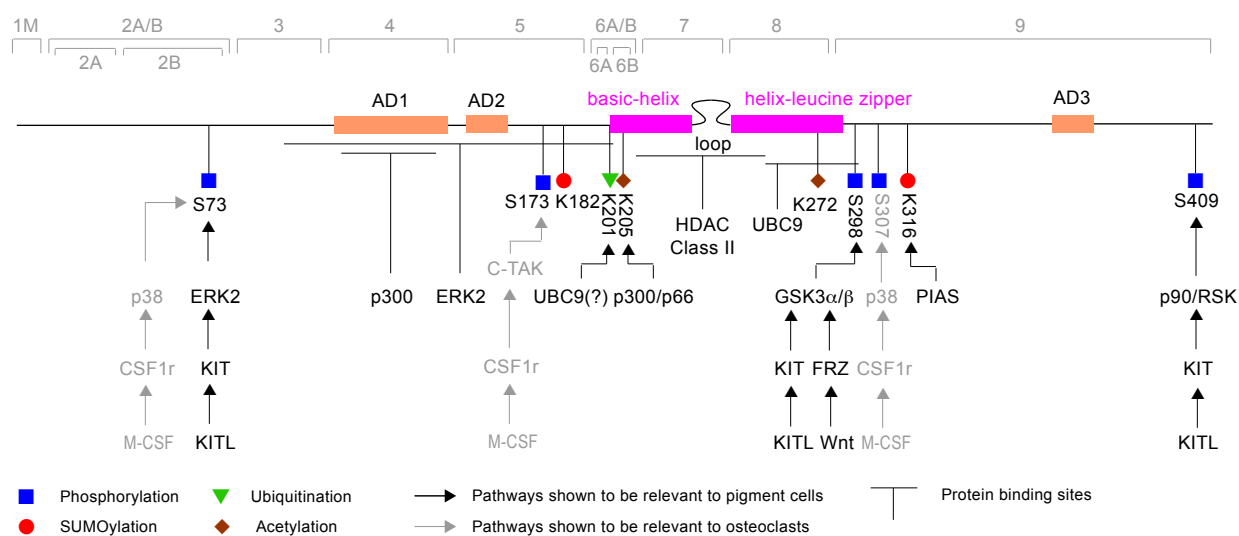
Figure 8: Representation of the major types and positions of MITF post-translational modifications and their respective signaling pathways.

B) M-MITF Acetylation in melanocytes:

MITF contains two known aceylation sites on K206 and K243. However, the effect of MITF acetylation seems to depend on the location of these modifications. Unpublished work performed by Schepsky *et al.* suggest that, on the one hand, K206 acetylation leads to an increased transcriptional activity of MITF. On the other hand, K243 seems to be constitutively acetylated *in vitro*, and the prevention of acetylation at this position leads to a significant increase in activity (Schepsky A, Steingrimsson E Unpublished). Like for SUMOylation however, no clear signaling pathway leading to a change in MITF acetylation has been identified so far.

C) M-MITF phosphorylation in melanocytes:

Phosphorylation of M-MITF protein has been demonstrated on several sites along its amino acid sequence as a result of the activation of two principle signaling pathways in melanocytes.

    <u>KIT-ligand signaling:</u> The serine at position 73 in the M-MITF 2B+ 6A+ isoform, is subject to phosphorylation by ERK subsequent to KIT-ligand signaling in melanocytes, which activates the Mitotic-Activated Protein Kinase (MAPK) pathway (Hemesath et al., 1998). Ser73-Phosphorylated MITF was shown to have an increased transcriptional activity on a tyrosinase reporter gene. In addition, activation of the MAPK pathway through KIT-ligand binding is thought to lead to the phosphorylation of another serine at position 409 in the M-MITF 2B+ 6A+ isoform through RSK1 (Wu et al., 2000). The role of this Ser409 phosphorylation remains, however, controversial. The original publication

stated that a protein non-phosphorylatable at both S73 and Ser409 was not able to bind DNA, and had a much smaller apparent molecular weight than the single mutated proteins (Wu et al., 2000). More recent publications demonstrated that S73/409A double mutant proteins do not show this apparent smaller molecular weight and were able to activate a reporter gene (Phung et al., 2011). Therefore this raises the possibility the protein presented in the original paper had additional alterations besides the serine substitutions.

Nevertheless, S73/409 doubly phosphorylated MITF was shown to be subject to ubiquitination on K201 and subsequent proteasome-mediated degradation. USP13, a de-ubiquitinase, has recently been involved in the regulation of the ubiquitination rate of MITF (Zhao et al., 2011). Modulations of USP13 expression drastically modify the level of MITF protein *in vitro*.

Hence phosphorylation of S73 shows a dual effect: on the one hand, it increases the binding activity of MITF protein, and on the other, it decreases the amount of available protein by targeting MITF protein for degradation.

WNT signaling: Mitf also bears additional phosphorylation sites, such as S298 activated by GSK-3β, and S307 activated by p38 MAPK (Takeda et al., 2000a). The biological relevance of these sites in melanocytes still needs to be explored in detail.

In a first attempt to assess the question of the role of phosphorylation, a mouse with a mutation at MITF serine-73 *Mitf*$^{mi-S73A}$ was generated by Bismuth *et al.* and analyzed for

both pigmentation phenotypes and proliferation rates of E9.5 derived Neural Crest Cultures (NCC). RT-PCR measurement of Mitf isoform distribution in three mutant mice revealed, however, that the mutation affected the proper inclusion of exon 2B in Mitf mRNA, resulting in the apparent exclusion of exon 2B in >90% of Mitf transcripts in both heart and skin (Bismuth et al., 2008). Nevertheless, the lack of Mitf 2B+ expression did not show any visible pigmentation phenotype in the homozygous adult mouse. $Mitf^{mi-S73A}$ melanocytes proliferate more readily compared to wild type melanocytes. Moreover, heterologous cells transfected with Mitf 2B- expression plasmids proliferate normally while those transfected with Mitf 2B+ expression plasmids were inhibited (Bismuth, unpublished observation). Hence, this sensitization of exon 2B exclusion seems to have drastic consequences on melanocyte behavior depending on whether the melanocytes are in their natural *in vivo* environment or *in vitro*. This differential behavior suggests that extracellular signals, as well as the direct microenvironment surrounding the melanocyte, play key roles in switching between proliferation and differentiation states.

The complexity of Mitf isoform distribution, the unexpected alteration in the alternative splicing profile of Mitf messages, and its consequences on melanocyte biology motivated us to develop quantitative methods, such as Real-Time PCR, to measure the amount of transcripts initiated from specific promoters as well as the amount of specific alternative splice variants in the total transcript pool.

Using these techniques, we carried out a first study aimed at identifying the molecular mechanisms that are involved in the genetic interaction of the Kit^{w-LacZ} allele with only

very specific *Mitf* alleles. Among them, the *Mitf^(mi-bws)* allele is associated with an unexpectedly severe pigmentation defect when crossed with *Kit^(w-LacZ)*. We, therefore, attempted to explain how this *Mitf* allele, originally characterized as an Mitf exon 2B splice mutant, was leading to such a dramatic phenotype in combination with a reduction of the MAPK signaling pathway.

Despite the failure of the *Mitf^(mi-S73A)* genetic model to dissociate two very distinct and perhaps independent mechanisms, MITF S73 Phosphorylation and Mitf exon 2B alternative splicing, this sensitized *Mitf* allele can be used to study the molecular mechanisms linking exon 2B alternative splicing regulation with the S73 codon. However, in order to understand the full extent of the influence of both mechanisms on melanocyte biology, it is crucial to be able to dissociate them from one another. Hence, we first collaborated with the Steingrimsson group who used a BAC-rescue transgenic approach in order to answer several critical questions assessing the link between phosphorylation, splicing and MITF activity.

We then addressed the need for a genetic model, which allows the dissociation of S73 codon mutation from exon 2B alternative splicing regulation, and used the presence of the floxed Neo cassette as a way to exacerbate the phenotypes of mice bearing single amino acid differences at residue-73. By extensive intercrosses with various Mitf alleles as well as molecular quantification of message and protein levels, we characterized the role of S73 phosphorylation *in vivo*.

Ultimately, we analyzed a particular allele found through the analysis of a ENU mutagenesis screen aiming to identify modifiers of the *Mitf* gene network. Such modifiers would enhance or suppress the pigmentation defects associated with the sensitized genetic background.

The results of these studies presented in the next section of this thesis attempt to answer several critical questions about *Mitf* regulations:

- What are the molecular bases of the genetic interactions observed in *Mitf*$^{mi-bws}$/+; *Kit*$^{w-LacZ}$ double mutant mice?

- Is an S73A/S409A double mutant MITF protein truly functionally dead *in vivo*?

- How is exon 2B alternative splicing regulated by a single amino acid change at the S73 position?

- What are the *in vivo* consequences of a forced incorporation of a non-phosphorylatable alanine on MITF activity?

Résultats

Résultats

1 – Méthodes de biologie moléculaire pour l'analyse de l'épissage alternatif et de l'initiation de la transcription du facteur de transcription bHLH-LZ Mitf.

L'activité de facteurs de transcription est souvent régulée par des modifications post traductionnelles. Une des conditions requise pour ce type de modifications correspond à la présence, dans l'ARNm correspondant, des exons qui sont directement sujets à ces modifications, ou codent pour des domaines protéiques qui influencent ces modifications de façon indirecte. L'incorporation ou l'exclusion de ces exons sont régulées principalement par épissage alternatif, mais peuvent également dépendre de la sélection du site d'initiation de la transcription et/ou de poly-adénylation. Ainsi, la collecte d'informations sur ces évènements d'inclusion et d'exclusion d'exons, à la fois quantitatives et qualitatives, présente un grand intérêt pour des projets expérimentaux visant à muter de façon endogène certains codons, car dans certains cas, ces mutations peuvent entrainer des défauts d'épissage. C'est pour cette raison qu'ici, nous avons choisi l'exemple du facteur de transcription Mitf pour décrire des méthodes de quantification d'épissage alternatif et de sélection de promoteur chez la souris.

Ces méthodes de quantification ainsi que les protocoles utilisés pour l'extraction des échantillons biologiques nécessaires aux expériences sont décrites dans l'**Article 1**.

The following results present a set of methods to determine, with quantitative and qualitative data, the expression profile of a complex gene, such as *Mitf* that uses differential promoter initiation as well as alternative splicing. The publication answers the critical need of quantifying specific RNA isoforms in cases where the absence of isoform-specific antibodies restricts the analysis to the RNA level.

The strategy and the protocol used to obtain the biological materials necessary for the measurement of gene product variants are described in the following **Article 1**

Article 1

The basic-helix-loop-helix-leucine zipper gene *Mitf*: analysis of alternative promoter choice and splicing.

The Basic-Helix-Loop-Helix-Leucine Zipper Gene *Mitf*: Analysis of Alternative Promoter Choice and Splicing

Kapil Bharti, Julien Debbache, Xin Wang, and Heinz Arnheiter

Abstract

The activity of transcription factors is often regulated by Post-translational modifications. A precondition for such modifications is the presence, in the corresponding mRNAs, of the exons that either directly encode the modifiable residues in question, or encode protein domains that influence their modification indirectly. The inclusion or exclusion of coding exons is regulated predominantly by alternative splicing but can also depend on promoter choice and polyadenylation site selection. Information about exon inclusion and exclusion, both qualitatively and quantitatively, is particularly important for experiments designed to mutate endogenous codons because such mutations can alter splicing patterns. Therefore, we here describe methods employed to quantitate exon inclusion and exclusion, using as example a mouse transcription factor gene, *Mitf*.

Key words: Reverse transcriptase polymerase chain reaction, Real-time PCR, Serine phosphorylation, Knock-in allele

1. Introduction

A prerequisite for Post-translational modifications is the incorporation of the specific exons coding for the modifiable residues. It is particularly important to determine the relative efficiency of exon inclusion or exclusion in cases where endogenous genes are mutated in codons that affect modifiable residues as such mutations can lead to the absence rather than the (intended) presence of the modifiable residue. It is for this reason that we here describe methods that can be employed to analyze and quantitate promoter and splice choices that determine the presence or absence of specific exons.

Our description focuses on a model gene, *Mitf*. This gene encodes a basic helix-loop-helix–leucine zipper transcription factor whose major role in vertebrates is the regulation of the

development and function of melanin-bearing pigment cells (that is, melanocytes and retinal pigment epithelium or RPE cells) (1). Mutations in *Mitf* can lead to severe deficiencies in neural crest-derived melanocytes which in mammals are not only associated with loss of coat pigmentation but also with deafness (2). In man, for instance, about 20% of congenital hearing deficiencies of the type "Waardenburg syndrome II" are associated with heterozygosity for mutations in *MITF* (3). In birds and rodents, homozygosity for *Mitf* mutations can also be associated with the "transdifferentiation" of retinal pigment epithelium cells into a retina-like tissue, a developmental aberration associated with small eyes (called microphthalmia, hence the name, Mitf = *mi*crophthalmia-associated *t*ranscription *f*actor) (4). Nevertheless, although *Mitf* is expressed in many more cell types besides pigment cells, most of them do not display overt phenotypes when *Mitf* is mutated. Among those that are affected are mast cells, B cells, and osteoclasts. The latter cells show severe impairments when *Mitf* is mutated in such a way that the mutant protein, which forms obligatory homo- and heterodimers, acts in a dominant-negative manner. Mice with such mutations can have an osteopetrosis leading to premature death at weaning (5).

Although encoded by a single gene, MITF is not a single protein but represents a family of isoforms generated by alternative promoter choice, alternative splicing, and a series of functionally relevant post-translational modifications (reviewed in ref. (2)). In fact, the 214,000 bp gene (mouse, human) has at least nine different promoters, at least six of which associated with
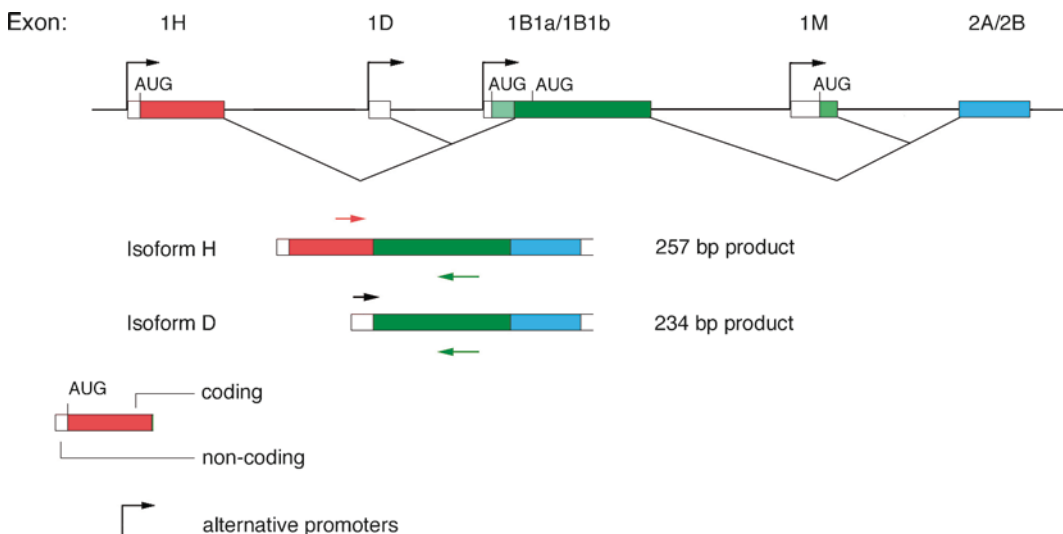
Fig. 1. Partial gene structure of *Mitf*, focusing on alternative promoters D and H and showing noncoding/coding parts of 5′ exons, splice patterns and primer selection for quantitative determination of promoter choices. Note that isoform H utilizes an translational start codon in exon H, and isoform D a start codon in the 3′ part of exon 1B, called exon 1B1b. For results obtained using these primers, see ref. (6).

unique amino-terminal protein sequences. Some of these promoters show a precise tissue-specific and developmental regulation (ref. (6), see also Fig. 1). Moreover, modifications of splicing patterns have been associated with specific pigmentary phenotypes in mice (7). Lastly, serine phosphorylation, sumoylation, and acetylation have all been shown to affect MITF activity in vitro. For instance, sumoylation at lysine-182 and lysine-316 decreases MITF activity in a promoter-specific way that depends on the number of cognate promoter motifs (E-boxes) capable of interacting with MITF (8, 9). Moreover, it has been reported that MAPK-mediated phosphorylation at serine-73 increases the protein's capacity to stimulate the promoter of *tyrosinase*, a melanocyte differentiation gene, and that double phosphorylation at serine-73 and serine-409 leads to increased MITF protein degradation (10, 11). Serine-73 is present in exon 2B (see Fig. 2), an
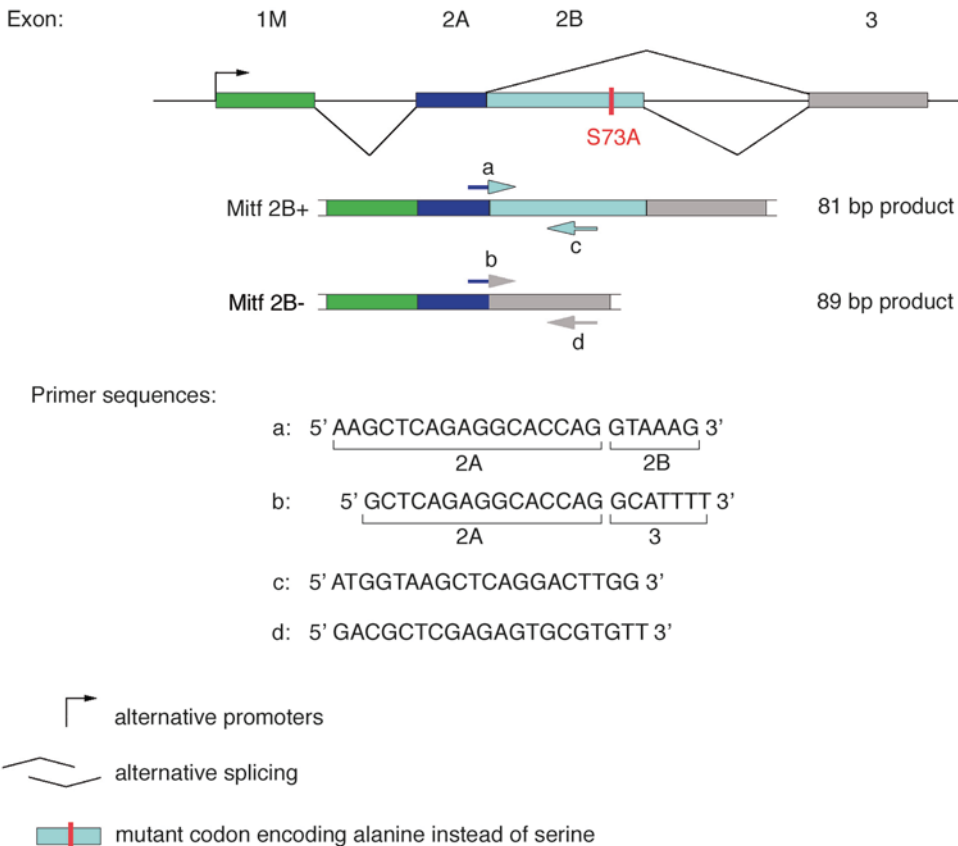
Fig. 2. Partial gene structure of mouse *Mitf*, focusing on exon 2A/2B and showing alternative splice products and primer choices for quantitative determination of exon inclusion. The *top* shows a partial gene structure for the region spanning exon 1B and 3. Note that two alternative promoters linked to either exon 1B or 1M and the common splice acceptor in exon 2A. Exon 2 is bipartite, with exon 2B either included (Mitf 2B+) or excluded (Mitf 2B−) from the mRNA. Primers overlapping the 2A/2B junction or the 2A/3 junction are shown, with reverse primers placed such that similar size products result for the two exon 2B splice versions. The schematic also shows the relative position of a serine-73-to-alanine codon mutation (S73A). This mutation favors exon 2B exclusion.

exon that is normally absent in only 5–10% of Mitf mRNAs, but is absent in over 95% of mRNAs transcribed from a mutant *Mitf* allele characterized by a serine-73-to-alanine codon change (12). These observations suggest that the serine-73 codon is part of an exonic splice enhancer sequence that binds specific arginine/serine-rich proteins which are known to regulate mRNA splicing (for a recent review, see ref. (13)). This example highlights the importance of exonic sequences in determining splice choices and hence, ultimately, whether the protein can be Post-translationally modified or not (see Fig. 3).
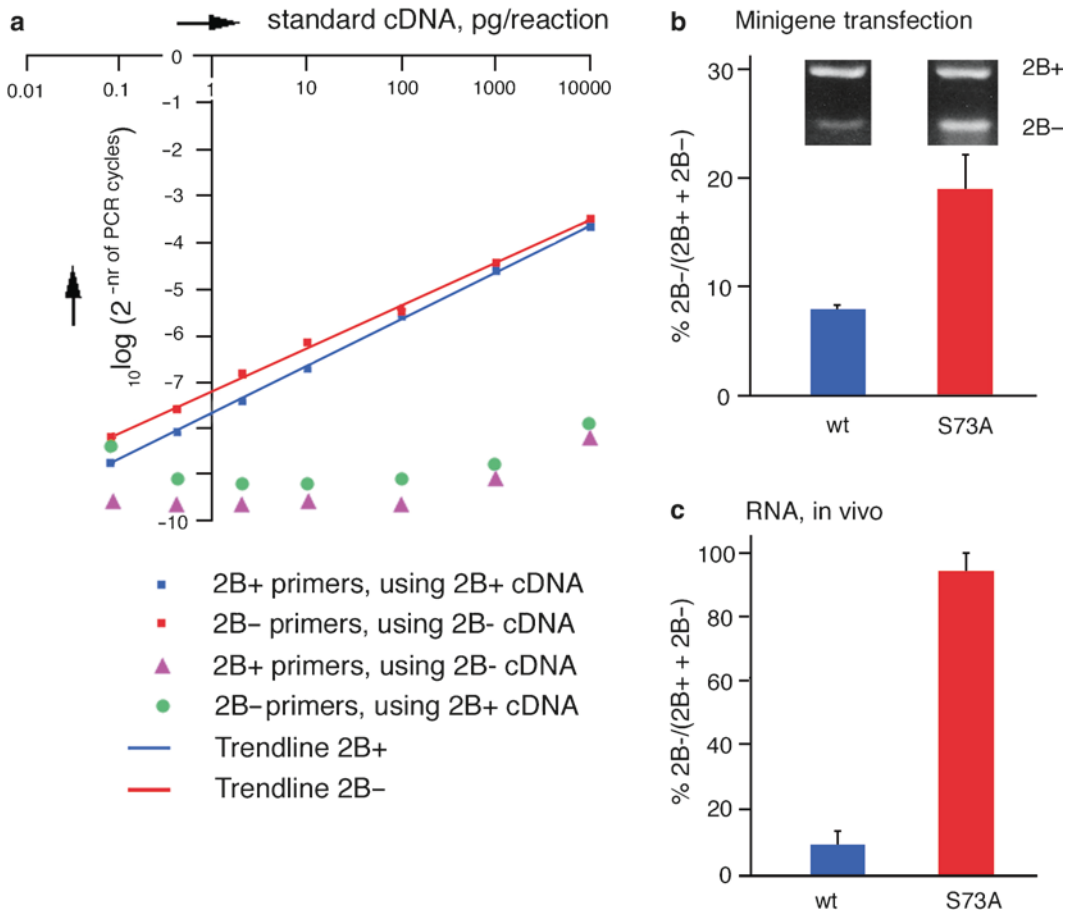
Fig. 3. Real-time PCR to quantify exon inclusion/exclusion. (**a**) Establishment of standard curves. Graded amounts of mouse Mitf standard cDNA were mixed with heterospecific cDNA, and real-time PCR was performed as indicated in the text. 2B+ primers correspond to primer pair a–c from Fig. 2, and 2B– primers correspond to primer pair b–d from Fig. 2. (**b**) Quantitation of exon 2B exclusion in RNA prepared from HEK293 cells transfected with the minigene as described in text and Fig. 2. Regular PCR followed by product identification by gel electrophoresis was done with a forward primer in exon 1M and a reverse primer in exon 3. This yields a product of 312 bp when exon 2B is included, and of 144 bp product when exon 2B is excluded. S73A corresponds to a minigene with a two base-pair change in codon 73 (AGC-to-GCC). Results are given as mean with bars indicating standard deviation from three measurements. (**c**) Similar quantitative assay performed with cDNA obtained from hearts of wild type mice or mice with the S73A codon change as indicated for (**b**). Note that the difference between wild type and mutant is more pronounced in vivo compared to minigene-transfected cells. *wt* wild type.

2. Materials

2.1. Embryo Harvesting and Tissue Grinding

1. Pregnant mouse females, for instance C57BL/6J (Jackson Labs, Bar Harbor, ME).

2. RNaseZap (Ambion, Austin, TX), RNase inhibitor solution for cleaning surgical instruments. Store at room temperature.

3. Straight surgical scissors (27 mm for mouse dissection and 15 mm for removing embryos from the uterus, ROBOZ Scientific, Gaithersburg, MD).

4. Two pairs of microdissection tweezers (tips 0.05×0.01 mm) (ROBOZ Scientific, Gaithersburg, MD).

5. 10 cm and 3.5 cm Petri dishes (Becton Dickinson and Company, Franklin Lakes, NJ).

6. DEPC-treated Molecular Biology grade water (Quality Biologicals, Inc., Gaithersburg, MD). Store at room temperature.

7. 10× PBS (Quality Biologicals, Inc., Gaithersburg, MD). Mix 100 ml of 10× PBS with 900 ml of DEPC-treated water to make 1× PBS. Store at 4°C.

8. 1.5 ml microcentrifuge tubes (Denville Scientific, Metuchen, NJ).

9. Plastic tissue grinders (Bel-art Products, Pequannock, NJ).

2.2. Cell Culture and Transfection

1. Dulbecco's Modified Eagle's Medium (DMEM) supplemented with 10% fetal bovine serum (FBS) and 1% Penicillin/ Streptomycin (Gibco/BRL, Carlsbad, CA). Store all reagents at 4°C.

2. Solution of 0.05% trypsin and ethylenediamine tetraacetic acid (EDTA) (Gibco/BRL, Carlsbad, CA). Store at 4°C.

3. 10 and 6 cm tissue culture grade dishes (Becton Dickinson and Company, Franklin Lakes, NJ).

4. Tris/EDTA (TE): 10 mM Tris-Hcl, 1 mM EDTA, pH 7.4 (Quality Biologicals, Inc., Gaithersburg, MD). Store at room temperature.

5. Effectene Transfection Kit (Qiagen, Valencia, CA). Store at 4°C.

6. 15 ml centrifuge tubes (Denville Scientific, Metuchen, NJ).

2.3. RNA Extraction and cDNA Preparation

1. RNeasy Mini RNA Extraction Kit (Qiagen, Valencia, CA). Store at room temperature.

2. Ethanol 200 proof (The Warner-Graham Company, Cockeysville, MD). Mix 70 ml of 200 proof ethanol with 30 ml of DEPC-treated water to make 70% ethanol.

3. RNase-free-DNase (3,000 Kunitz units/ml, Qiagen, Valencia, CA).

4. Nanodrop Spectrophotometer (Nanodrop Technologies, Wilmington, DE).

5. SuperScript First-Strand Synthesis System for RT-PCR (Invitrogen, Carlsbad, CA). Store at –20°C.

2.4. Polymerase Chain Reaction

1. Taq 2000 Polymerase (5 units/µl) (Stratagene, La Jolla, CA). Store at –20°C.

2. 2 mM dNTPs (MBI Fermentas, Glen Burnie, MD). Store at –20°C.

3. Primers, final concentration 10 pmole/µl (Genelink, Hawthorne, NY). Store at –20°C.

4. PCR tubes 0.2 ml (Denville Scientific, Metuchen, NJ).

5. Molecular biology grade water (Quality Biologicals, Inc., Gaithersburg, MD). Store at room temperature.

6. Dyad DNA Engine Themocycler (MJ mini, now Bio-Rad, Hercules, CA).

7. 5× DNA loading dye (Teknova, Hollister, CA).

2.5. Agarose Gel

1. Ultra pure agarose (Invitrogen, Carlsbad, CA). Store at room temperature.

2. 50× TAE (Quality Biologicals, Inc., Gaithersburg, MD). 50× TAE is diluted to 1× by mixing 20 ml of 50× TAE in 980 ml of deionized water.

3. Ethidium bromide 10 mg/ml (Sigma, St. Louis, MO).

4. Sub-Cell GT agarose gel electrophoresis unit (Bio-Rad, Hercules, CA).

5. Pharmacia EPS 250/200 power supply (GE Healthcare, Pharmacia, Uppsala, Sweden).

6. Molecular weight marker, DNA ladder mix (MBI Fermentas, Glen Burnie, MD). Store at –20°C.

2.6. Real-Time PCR Analysis

1. Power SYBR Green Mix (2×) (Applied Biosystems, Foster City, CA). Store at 4°C.

2. 96-well optical reaction plate (Applied Biosystems, Foster City, CA).

3. ABI Prism 7000 Sequence Detection System (Applied Biosystems, Foster City, CA).

3. Methods

3.1. Sample Preparation for Isoform Analysis

3.1.1. Harvesting Embryonic Tissue for Detection of Alternate Promoter Isoforms of Mitf at Different Developmental Stages. Example Eye Tissue

1. Pregnant C57BL/6J females: To calculate the developmental time point for harvesting embryos, the morning that the vaginal plug is first detected is considered embryonic day (E) 0.5. For instance, E11.5 embryos are collected 11 days following the day of plug detection (E0.5). For detailed information about embryo collection, see ref. (14).

2. Harvesting tissue for RNA extraction requires precautions to avoid RNase contamination. Before starting to dissect the pregnant female, treat all instruments with RNase inhibitor solutions (RNaseZap), and prepare the solutions needed for this procedure with DEPC-treated molecular biology grade water. A separate set of tweezers, which has not been used during mouse dissection, is used for the dissection of the eye tissue. Two sets of appropriately labeled 1.5 ml microcentrifuge tubes are stored in dry ice.

3. Euthanize the pregnant females according to methods approved by your Animal Care and Use Committee (for instance CO_2). Harvest embryos using 27 mm scissors and tweezers and place the embryos in cold 1× PBS in a 10-cm dish. Remove the placenta and the chorionic membranes from each embryo, one at a time, using a pair of 15 mm scissors, and transfer the embryos to cold 1× PBS in a second 10 cm dish.

4. Using the clean set of tweezers, carefully remove both eyes from an embryo under a dissection scope and transfer the eyes to cold 1× PBS in a 3.5 cm dish. While holding the eyeball with one tweezer, use the other tweezer to enlarge the optic pit hole at the back of the eye. Push the retina/lens through the optic pit hole by squeezing/pushing at the anterior part of the eye. Collect the separated RPE/mesenchyme and retina/lens tissue into separate 1.5 ml microcentrifuge tubes stored on dry ice (see Note 1). Freeze these tubes at –80°C until further processing.

5. For other tissues, proceed accordingly.

3.1.2. Harvesting Transfected Cells for Assaying Alternative Splicing of Different Mitf Exons

1. Human embryonic kidney cells (HEK293) are cultured in DMEM medium with 10% FBS and 1% Penicillin/Streptomycin at 37°C in an incubator with 6% CO_2/air. Passage the cells as they approach 70% confluency, using 0.05% trypsin/EDTA, and replate at a dilution of 1:5 (see Note 2).

2. The methods described here are applicable to analyzing the relative and absolute levels of different splice isoforms of

endogenous Mitf mRNAs. Because one of the goals is to analyze the sequence requirements for regular and alternative splicing, we use wild type and various mutated minigene constructs that are transfected into cultured cells. Generally, these minigene constructs contain a part of the gene where the exon to be tested for alternative splicing is flanked, at least, by the two neighboring introns and adjacent exons. For instance, to analyze alternative splicing of exon 2B of *Mitf*, the reporter construct contains part of the gene from exon 1M to exon 3, including introns 1 and 2 (see Fig. 2). For expression, these minigenes are placed under the control of a CMV promoter and contain a 3′ untranslated region and polyadenylation signal. The strength of alternate splicing is analyzed by comparison with constructs where splice junctions or splice enhancer and silencer sequences are mutated.

3. For transfection, plate one million of freshly trypsinized cells in a 6 cm dish and transfect them the following morning using the Effectene Transfection Kit (Qiagen). Dilute 1 μg of the minigene construct dissolved in TE into 150 μl of DNA condensation buffer (Buffer EC) in a 1.5 ml microcentrifuge tube. Add 8 μl of enhancer solution and vortex the tubes for 1 s (see Note 3).

4. Incubate at room temperature for 2–5 min, then briefly spin the tubes to collect drops from the tube top.

5. Add 25 μl of effectene reagent to the tubes and vortex for 10 s. Incubate tubes at room temperature for 10 min.

6. While the DNA-transfection complexes are forming, aspirate the medium from the cells and gently wash cells with 4 ml 1× PBS. Add 4 ml fresh DMEM medium to the cells and return the dishes to the incubator.

7. Add 1 ml DMEM medium to the tube containing the DNA-transfection complex and mix gently by pipetting up and down. Add the transfection mix to the cells and gently swirl the dish to ensure uniform distribution of the DNA-transfection mix. Return the dishes to the incubator.

8. After 16 h of incubation, collect cells for RNA extraction. Aspirate the medium from the dish and wash cells with 4 ml 1× PBS. Trypsinize cells with 1 ml 0.05% trypsin/EDTA. Add 5 ml of fresh medium to the cells and transfer detached cells to a 15 ml centrifuge tube and pellet by centrifugation at $300 \times g$ for 5 min. Aspirate the medium from the cell pellet without disturbing the pellet. Wash the cells with 1× PBS and spin the tubes again at $300 \times g$ for 5 min. Aspirate the supernatant fluid and flash freeze the tubes in dry ice. Store tubes at –80°C until further processing.

3.2. Preparation of RNA and cDNA From Embryonic Tissue or Transfected Cells

3.2.1. RNA Extraction Using RNeasy Mini RNA Extraction Kit From Qiagen

1. To grind embryonic tissue, use plastic tissue grinders fitting the conical bottom of a 1.5 ml microcentrifuge tube. Before grinding, clean the grinders with RNase inhibitor solution (RNaseZap) and store at –20°C to keep them cold. Add 50 μl of RLT buffer from the Kit (add 10 μl of β-mercaptoethanol to 1 ml RLT buffer before use) to the frozen tissue and grind it on dry ice using the prechilled plastic grinders. After grinding, add an additional 300 μl of RLT buffer to the tissue and freeze on dry ice until other tubes are processed. Once all the tubes are processed, thaw them on ice and process for RNA extraction starting at step 3.

2. To lyse frozen tissue culture cells, add 350 μl RLT buffer to the cell pellet immediately after taking it from the freezer. Vortex the tube to ensure a homogenous suspension of the cells and proceed to step 3.

3. Pipette the tissue lysate from step 1 or the cell suspension from step 2 onto a QIAshredder column placed in a 2 ml collection tube. Centrifuge tubes for 2 min at maximum speed to lyse the cells.

4. Add 350 μl of 70% ethanol to the homogenized cell lysate and mix thoroughly by pipetting up and down. Do not vortex or centrifuge the samples at this step.

5. Pipette all 700 μl of the sample mixture, including any precipitates that may have formed in the previous step, to an RNeasy mini spin column placed in a 2 ml collection tube. Centrifuge the samples for 30 s at $9,300 \times g$.

6. Discard the flow-through. Add 500 μl of buffer RW1 from the kit to the RNeasy column and spin the columns for 30 s at $9,300 \times g$.

7. Discard the flow-through along with the collection tube and transfer the column to a new collection tube.

8. Add RNase-free-DNase, in a mixture of 75 μl of buffer RDD from the kit and 5 μl of DNase (15 Kunitz units totally), onto each column. Make sure that the DNase solution covers the entire surface of the membrane and incubate columns at room temperature for 30 min.

9. Add another 500 μl of buffer RW1 to the column and spin the columns for 30 s at $9,300 \times g$.

10. Transfer RNeasy column to a new collection tube, add 500 μl of buffer RPE from the kit to the column, and spin for 30 s at $9,300 \times g$.

11. Add another 500 μl of buffer RPE onto each column and spin for 2 min at $9,300 \times g$ to dry the column.

12. Transfer the column to a 1.5 ml microcentrifuge tube and add 50 µl of 65°C RNase-free water onto the membrane. Incubate at room temperature for 5 min and spin the columns for 30 s at $9,300 \times g$.

13. The eluate contains pure RNA. Measure concentration using a nanodrop spectrophotometer using 1.3 µl of the undiluted RNA solution.

3.2.2. cDNA Preparation Using Superscript First-Strand Synthesis System for RT-PCR

1. Mix 1 µg of RNA with 1 µl of 10 mM dNTP mix, and 2 µl of random hexamers (50 ng/µl) in a 0.2 ml PCR tube. Adjust the final volume of the mixture to 10 µl with DEPC-treated water (see Note 4).

2. Incubate tubes at 65°C for 5 min and then transfer them to ice for 2–3 min.

3. While the samples are cooling on ice, prepare a second reaction mix containing 2 µl of 10× RT buffer, 4 µl of 25 mM $MgCl_2$, 2 µl of 0.1 M DTT, 1 µl of RNaseOUT recombinant (Ribonuclease inhibitor) and 1 µl of Superscript II Reverse Transcriptase (50 units). Add 10 µl of the reaction mixture to each RNA/primer mixture. Mix the solutions gently and spin the tubes briefly to collect all of the solution at the bottom.

4. Incubate the tubes for 2 min at 25°C. Transfer the tubes to 42°C for 1 h.

5. Terminate the reaction by incubating tubes at 70°C for 15 min and then place tubes on ice.

6. Add 1 µl of RNase H to each tube and incubate at 37°C for 20 min.

7. Dilute the cDNA 1:5 in water. The cDNA is now ready for PCR.

8. Before using this cDNA for real-time analysis, check the quality of each sample by PCR amplification of an unrelated cDNA.

3.2.3. Setting Up a PCR

1. For a 20 µl PCR reaction, mix 2 µl of 10× reaction buffer, 2 µl of 2 mM dNTPs, 2 µl of 10 pmole/µl of each forward and reverse primers, 1 µl of the cDNA template, 11.75 µl of molecular biology grade water, and 1 unit (0.25 µl) of Taq Polymerase in a 0.2 ml PCR tube. For primer choice, see Figs. 1 and 2 and ref. (6).

2. Place the tubes in the thermocycler block and set up a cycling program as follows: 92°C, 2 min (step 1), 92°C, 20 s; 55°C, 30 s; 72°C, 1 min (step 2, repeat for 29 cycles), 72°C, 7 min (last step). Start the cycling program. The program is designed for DNA Engine DYAD thermocycler from MJ mini (see Note 5).

3. Once the PCR is finished, add 5 μl of 5× DNA gel loading buffer to each tube. The samples are now ready to load on an agarose gel.

3.2.4. Agarose Gel Electrophoresis

1. The agarose gel set up is described for Sub-Cell GT agarose gel electrophoresis unit from Bio-Rad.

2. To prepare a 1.5% agarose gel for a chamber that holds 150 ml of gel solution, weigh 2.25 g of agarose in a 250 ml Erlyenmeyer flask and add 150 ml of 1× TAE. Heat the solution with intermittent shaking until agarose dissolves completely. Let the gel solution cool to about 50°C. Add ethidium bromide at a final concentration of 1 μg/ml. Pour the gel solution into the gel tray with stoppers on each side. Add the combs to the tray and let the gel solidify.

3. Remove the combs and the stopper from the solidified gel and submerge the gel into 1× TAE running buffer in the gel electrophoresis unit.

4. Load 10 μl total of sample and 1×loading buffer per well.

5. In a corner well, load 3 μl of DNA ladder mix as a molecular weight marker.

6. Run the gel at constant 75 V. Stop the gel when the dye front has reached 2/3rd of the total running distance. Take a picture of the gel, using a UV-gel documentation unit.

3.3. Quantitative Real-Time PCR

3.3.1. Primer Design for Alternative Promoter Isoforms

To detect alternative promoter choice for the *Mitf* gene in different tissues at various developmental stages, forward primers specific for the alternative exons are used in combination with a reverse primer that is common to all isoforms. Forward primers are designed in a way that the PCR products amplified for the different isoforms are of similar size. For details, see ref. (6).

3.3.2. Primer Design for Alternatively Spliced Exons

To detect alternatively spliced exons, forward primers are unique to the exon–exon junctions of the differently spliced products. For the situation where the alternative exon is spliced-in, the forward primer is positioned at the exon junction in a way that part of the primer hybridizes with the 3′ end of the upstream exon, and part with the 5′ end of the downstream exon. For the situation where the alternative exon is spliced-out, forward primers are placed accordingly in a way that they span the expected junction formed by the absence of the alternative exon. Hence, the 5′ parts of both types of forward primers are identical, but because their 3′ parts are different, cross-priming is not usually a problem. For reverse primers, sequences in the downstream common exon are chosen at locations that assure a similar length of the two expected products (Fig. 2).

3.3.3. Generation of Standard Curve and Real-Time Analysis of Alternative Promoter Isoforms

1. Amplify standard cDNA products corresponding to each isoform, using primer pairs as described in Subheading 3.3.1, step 1. Using amplified DNA allows for the generation of linear standard DNAs of a size similar to the cDNAs present in the test samples and is to be preferred over the use of plasmids for standard curve purposes.

2. Quantify the amounts of standard DNA products both spectrophotometrically and by agarose gel electrophoresis (see below).

3. Dilute appropriate concentrations of the standard DNA, for instance in steps of tenfold dilutions, into a cDNA source that does not contain the isoforms to be tested. For instance, in the case of Mitf-promoter isoforms, cDNA from hearts of $Mitf^{mi-rw/mi-rw}$ animals was used (6). These mutant mice lack the exon corresponding to the common reverse primer (exon 1B) but provide a complexity of cDNAs similar to that expected in the test sample. This is critical as primer efficiency differs depending on the amplification environment. In the absence of appropriate mutants, use heterospecific cDNA and species-specific primers.

4. Perform real-time PCR on these samples using a set of primers that represent a nested set to the original pair used to amplify the standard DNAs (for details, see ref. (6). An ABI Prism 7000 real-time PCR machine is used for the real-time analysis.

5. A log of the amount of standard DNA (weight/reaction) is plotted against the threshold cycle (cT) values obtained for each concentration. A best-fit regression plot is drawn for each standard curve. Using the average molecular weight of a basepair as 660 Daltons, the weight can be converted into the number of DNA molecules.

6. Generate standard curves for each isoform, and separately for each repeat assay performed with the test samples.

7. Perform the real-time PCR of the test samples (for instance, cDNA obtained from E11.5 RPE and retina), by using the same set of nested primers as used in step 4. Normalize each sample by quantifying an unrelated cDNA, again using real-time PCR (see Note 6). The absolute amount of cDNA molecules in test samples is determined by using the appropriate previously determined isoform-specific standard curves and linear regression plots.

3.3.4. Generation of Standard Curve and Real-Time Analysis of Alternatively Spliced Exons

1. The principles of standard curve determination are according to the methods described above for promoter choice determination (see Note 7).

2. Standard templates of mouse cDNA are diluted in a cDNA mixture from a human cell line (see Notes 2 and 7).

The primers used for this analysis are made specific to mouse sequences so that human Mitf cDNA is not amplified in this mixture of mouse standard cDNAs and human cell line cDNA. An example of a standard curve determination is shown in Fig. 3A. Note that inappropriate cross-priming (for instance, 2B+ primers on 2B– cDNA) for cDNA concentrations above 1 pg/reaction gives results that are 1–4 logs below those obtained for appropriate priming (for instance 2B+ primers on 2B+ cDNA).

3. Using the above methods of standard curve determination, test samples are subjected to real-time PCR as mentioned. Use quantification of an unrelated cDNA for normalization of the test samples (see Note 6). Results can be expressed in absolute numbers of cDNA molecules, or, as shown in Fig. 3B and 3C, as relative amounts of exon 2B-lacking cDNAs compared to the sum of exon 2B-lacking and exon 2B-containing cDNAs.

4. Notes

1. If embryos need to be genotyped, separate each embryo into an individual tube and remove a portion from each embryo for PCR or other appropriate genotyping reaction.

2. Instead of using heterospecific cells to prepare cDNA to be used during standard curve determination, one may also use cell types in which the gene of interest is not expressed (or expressed below threshold levels for the chosen PCR conditions).

3. The method of transfection has to be adapted to the type of cell line used.

4. The amount of RNA used for the RT reaction can be lower but each test sample should contain the same amount of total RNA.

5. The annealing temperature may vary with the efficiency of the primer sets, and the number of cycles for step 2 may vary depending on the abundance of the cDNA of interest in the sample. An optimum number of cycles is considered to be that which gives amplification in the linear range.

6. For normalization, use an unrelated cDNA whose threshold cycle time is similar to that of the test cDNA. For the analysis of exon 2B splice variants, for instance, we used USF, a cDNA whose relative abundance is similar to that of Mitf exon 2B– cDNA in wild type, and does not change significantly between samples obtained from different genotypes.

7. If one wants to avoid the use of nested primer set-PCR to generate standard DNAs from appropriate plasmids, one can use the respective plasmids directly as standard cDNAs. In this case, only one primer set is used both for the generation of the standard curve and for the analysis of the test samples.

Acknowledgments

References

1. Hodgkinson CA, Moore KJ, Nakayama A, Steingrimsson E, Copeland NG, Jenkins NA, Arnheiter H (1993) Mutations at the mouse microphthalmia locus are associated with defects in a gene encoding a novel basic-helix-loop-helix-zipper protein. Cell 74:395–404

2. Arnheiter H, Hou L, Nguyen MTT, Bismuth K, Csermely T, Murakami H, Skuntz S, Liu W, Bharti K (2006) Mitf – A matter of life and death for the developing melanocyte. In: Hearing V, Leong SPL (eds) From melanocytes to malignant melanoma. Humana, Totowa, NJ

3. Tassabehji M, Newton VE, Read AP (1994) Waardenburg syndrome type 2 caused by mutations in the human microphthalmia (MITF) gene. Nat Genet 8:251–255

4. Bharti K, Nguyen MT, Skuntz S, Bertuzzi S, Arnheiter H (2006) The other pigment cell: specification and development of the pigmented epithelium of the vertebrate eye. Pigment Cell Res 19:380–394

5. Steingrimsson E, Copeland NG, Jenkins NA (2004) Melanocytes and the microphthalmia transcription factor network. Annu Rev Genet 38:365–411

6. Bharti K, Liu W, Csermely T, Bertuzzi S, Arnheiter H (2008) Alternative promoter use in eye development: the complex role and regulation of the transcription factor MITF. Development 135:1169–1178

7. Hallsson JH, Favor J, Hodgkinson C, Glaser T, Lamoreux ML, Magnusdottir R, Gunnarsson GJ, Sweet HO, Copeland NG, Jenkins NA, Steingrimsson E (2000) Genomic, transcriptional and mutational analysis of the mouse microphthalmia locus. Genetics 155:291–300

8. Murakami H, Arnheiter H (2005) Sumoylation modulates transcriptional activity of MITF in a promoter-specific manner. Pigment Cell Res 18:265–277

9. Miller AJ, Levy C, Davis IJ, Razin E, Fisher DE (2005) Sumoylation of MITF and its related family members TFE3 and TFEB. J Biol Chem 280:146–155

10. Hemesath TJ, Price ER, Takemoto C, Badalian T, Fisher DE (1998) MAP kinase links the transcription factor Microphthalmia to c-Kit signalling in melanocytes. Nature 391:298–301

11. Wu M, Hemesath TJ, Takemoto CM, Horstmann MA, Wells AG, Price ER, Fisher DZ, Fisher DE (2000) c-Kit triggers dual phosphorylations, which couple activation and degradation of the essential melanocyte factor Mi. Genes Dev 14:301–312

12. Bismuth K, Skuntz S, Hallsson JH, Pak E, Dutra AS, Steingrimsson E, Arnheiter H (2008) An unstable targeted allele of the mouse Mitf gene with a high somatic and germline reversion rate. Genetics 178:259–272

13. Lin S, Fu XD (2007) SR proteins and related factors in alternative splicing. Adv Exp Med Biol 623:107–122

14. Nagy A, Gertenstein M, Vintersten K, Behringer R (2003) Manipulating the mouse embryo. A laboratory manual, 3rd edn. Cold Spring Harbor Laboratory Press, Cold Spring Harbor, NY

2 – Les interactions génétiques entre *Mitf* et *Kit* sont allèle-spécifiques et mettent en évidence de nouveaux éléments sur la nature moléculaire de l'allèle murin *Mitf^{mi-bws}*.

Le récepteur tyrosine kinase KIT et le facteur de transcription MITF, tous deux requis dans le développement des mélanocytes, ont été démontrés comme interagissant de façon fonctionnelle *in vitro* et *in vivo*. *In vitro*, l'activation de la voix de signalisation KIT entraine la phosphorylation de MITF, ce qui affecte son activité ainsi que sa stabilité. *In vivo*, la présence de l'allèle « mi-*white* » *Mitf^{Mi-wh}* accentue le phénotype de dépigmentation associé aux mutations hétérozygotes du gène *Kit*. Ici nous démontrons que parmi une série d'autres allèles de Mitf, seul l'allèle récessif « mi-*black-and-white spots* » ou *Mitf^{mi-bws}* parvient à reproduire l'interaction génétique observée entre l'allèle *Mitf^{Mi-wh}* et *Kit*. De façon intéressante, *Mitf^{mi-bws}* a été caractérisé au niveau transcriptionnel par une réduction du niveau d'inclusion de l'exon 2B, qui code, entre autres, pour la Serine 73, qui se trouve être un des sites de phosphorylation de la voix de signalisation KIT. Cependant, d'autres allèles de Mitf qui génèrent des altérations similaires de l'inclusion de l'exon 2B ou qui altèrent le niveau d'expression du gène, ne présentent pas d'interactions similaires avec *Kit in vivo*. De ce fait, nous supposons que l'allèle récessif *Mitf^{mi-bws}* est un allèle complexe et non complètement caractérisé qui peut présenter un effet dominant-négatif lorsqu'il est présent sur un fond génétique sensibilisé par *Kit*. Nous suggérons ainsi que la variabilité de certaines pathologies génétiques humaines peuvent, elles aussi, être liées à l'interaction allèle-spécifique de variants alléliques complexes de différents gènes.

Les résultats expérimentaux liés à cette étude sont présentés dans l'**Article 2**.

In the following study, we characterized a new genetic interaction between the *Mitf*$^{mi\text{-}bws}$ and the *Kit*$^{W\text{-}LacZ}$ alleles, showing a similar effect as the interaction of *Mitf*$^{Mi\text{-}wh}$ with *Kit*$^{W\text{-}LacZ}$. The *Mitf*$^{mi\text{-}bws}$ allele is characterized by an exon 2B splice defect which promotes the exclusion of exon 2B in about 50% of Mitf transcripts compared to the normally ~5% in wild type *Mitf*. In contrast, mice carrying the *Mitf*$^{mi\text{-}S73A}$ allele, which also presents a significant exclusion of *Mitf* exon 2B at the mRNA level, do not show similar interactions with *Kit*. In this study, we show that in addition to the exon 2B exclusion, *Mitf*$^{mi\text{-}bws}$ mice display abnormally reduced levels of Mitf messages. Nonetheless the attempt to mimic the molecular phenotype observed in *Mitf*$^{mi\text{-}bws}$; *Kit*$^{W\text{-}lacZ}$/+ mice by further reducing the *Mitf* levels in *Mitf*$^{mi\text{-}S73A}$ by genetic means still did not lead to mice with phenotypes similar to *Mitf*$^{mi\text{-}bws}$/*Mitf*$^{mi\text{-}bws}$; *Kit*$^{w\text{-}LacZ}$/+. The results suggest that the *Mitf* exon 2B exclusion cannot be the only reason for the observed interaction seen with *Kit* and *Mitf*$^{mi\text{-}bws}$. Hence, the *Mitf*$^{mi\text{-}bws}$ allele may have additional genetic and functional alterations besides what is currently known about this allele.

The experimental work related to this study is presented in the following **Article 2**.

Article 2

Allele-specific genetic interactions between *Mitf* and *Kit* affect melanocyte development.

Allele-specific genetic interactions between *Mitf* and *Kit* affect melanocyte development

Bin Wen[1,2], Yu Chen[1,2], Huirong Li[1], Jing Wang[1], Jie Shen[1], Aobo Ma[1], Jia Qu[2], Keren Bismuth[3], Julien Debbache[3], Heinz Arnheiter[3] and Ling Hou[1,2]

1 Developmental Cell Biology and Disease Program, School of Ophthalmology and Optometry and Zhejiang Eye Hospital, Wenzhou, Zhejiang, China **2** State Key Laboratory Cultivation Base and Key Laboratory of Vision Science of Ministry of Health of China, Wenzhou Medical College, Wenzhou, Zhejiang, China **3** Mammalian Development Section, National Institute of Neurological Disorders and Stroke, National Institutes of Health, Bethesda, MD, USA

CORRESPONDENCE Ling Hou, PhD, e-mail: lhou88@gmail.com

Summary

The tyrosine kinase receptor KIT and the transcription factor MITF, each required for melanocyte development, have been shown to interact functionally both in vitro and in vivo. In vitro, KIT signaling leads to MITF phosphorylation, affecting MITF activity and stability. In vivo, the presence of the *Mitf^{Mi-wh}* allele exacerbates the spotting phenotype associated with heterozygosity for *Kit* mutations. Here, we show that among a series of other *Mitf* alleles, only the recessive *Mitf^{mi-bws}* mimics the effect of *Mitf^{Mi-wh}* on *Kit*. Intriguingly, *Mitf^{mi-bws}* is characterized by a splice defect that leads to a reduction of RNAs containing MITF exon 2B which encodes serine-73, a serine phosphorylated upon KIT signaling. Nevertheless, other *Mitf* alleles that generally affect Mitf RNA levels, or carry a serine-73-to-alanine mutation that specifically reduces exon 2B-containing RNAs, do not show similar interactions with *Kit* in vivo. We conclude that the recessive *Mitf^{mi-bws}* is a complex allele that can display a semi-dominant effect when present in a *Kit*-sensitized background. We suggest that human disease variability may equally be due to complex, allele-specific interactions between different genes.

Introduction

Interactions between different genes are often difficult to assess because they may be subtle and the corresponding phenotypes not easily visible to the naked eye. Such interactions can be probed readily, however, for genes affecting pigmentation because pigmentary alterations can serve as a highly sensitive read-out of the modification of the action of one gene by another (Barsh, 1996; Baxter et al., 2009; Quevedo and Holstein, 1992; Spritz, 1997). In fact, given that over 200 loci are known to affect pigmentation in mice alone, pigmentation may be among the first phenotypes for which an extensive if not complete genetic network can be established (Baxter et al., 2004; Bennett and Lamoreux, 2003; Hearing and Jimenez, 1989; Hou and Pavan, 2008).

Genetic interactions often reflect functional interactions where the gene products in question feed into common molecular pathways (Drees et al., 2005). This is perhaps best illustrated by interactions between transcription factor genes on the one hand and genes controlling signaling pathways that modify the activities of these transcription factor genes or their products on the other. For instance, mice that are heterozygous for a mutation in the gene encoding the signaling receptor *Kit* and also heterozygous for a mutation in the gene encoding the *microphthalmia*-associated transcription factor *Mitf* (a basic-helix-loop-helix-leucine zipper protein which binds DNA as homo- or heterodimers) can show much more extensive white spotting than would be expected from heterozygosity for mutations in either gene alone (Beechey and Harrison, 1994; Diwakar et al., 2008; Hou et al., 2000). This phenomenon may indeed reflect functional interactions as it is well documented in vitro that *Mitf* is needed for the maintenance of KIT expression in melanoblasts and that *Kit* signaling affects *Mitf* both at the transcriptional and post-translational levels (Hemesath et al., 1998; Opdecamp et al., 1997; Price et al., 1998). Interactions have also been observed between the transcription factor PAX3 and KIT (Guo et al., 2010), between genes encoding signaling components, such

as endothelin receptor B (*Ednrb*) and Kit ligand (*Kitl*), or between transcription factors, such as *Sox10* and *Mitf* (Hou et al., 2006; Potterf et al., 2000; Rhim et al., 2000). Moreover, an interaction has been observed between *Mitf* and *Bcl2*, a gene that is involved in the cell death pathway and is regulated by *Mitf* (McGill et al., 2002).

The fact that pigmentation defects caused by mutations in one gene can be affected by mutations in a second gene have also made it possible to search for mutant pigmentation genes that by themselves would hardly produce a visible phenotype in heterozygotes. For example, a number of novel mutations affecting the pigment cell lineage have recently been identified in mice by combining a null mutation for *Sox10* with germline mutations obtained after treatment with N-ethyl-N-nitrosourea (Matera et al., 2008). When designing such sensitized genetic screens, however, one has to take into account that gene interactions may be allele-specific. The above mentioned interaction between *Kit* and *Mitf*, for instance, although seen with several *Kit* alleles (Beechey and Harrison, 1994; Diwakar et al., 2008; Hou et al., 2000), has so far been tested only for the semi-dominant *Mitf*$^{Mi-wh}$ (*Microphthalmia-white*) allele. *Mitf*$^{Mi-wh}$ is characterized by a codon change in exon 7 and produces at least one protein isoform that is unable to bind DNA but still able to form dimers with wild-type dimerization partners (Hemesath et al., 1994). The enhanced spotting phenotype of *Mitf*$^{Mi-wh}$/*Kit* mutant mice could be explained, therefore, by reduced phosphorylation, and hence increased stability and dominant-negative action, of this isoform (Arnheiter et al., 2006). If so, *Mitf* alleles lacking dominant-negative characteristics might not show similar interactions with *Kit*. In fact, as demonstrated here, many other *Mitf* alleles showed no interactions with the *Kit* null allele *Kit*^{tm1Alf} (Bernex et al., 1996; Hou et al., 2000), with the intriguing exception of a recessive allele, *Mitf*$^{mi-bws}$ (*microphthalmia-black and white spots*), prompting us to analyze this allele and its interactions with *Kit*^{tm1Alf} in more detail.

Mitf^{mi-bws}, when homozygous, produces extensive white spotting but when heterozygous, there is no visible phenotype. The allele is characterized by a point mutation in the *Mitf* intron preceding exon 2 but otherwise the coding region remains wild-type (Hallsson et al., 2000). *Mitf*$^{mi-bws}$ is associated with a severe

reduction of Mitf RNA levels when measured in an organ that shows no obvious phenotype, the heart (Bauer et al., 2009). It is also associated with a skewed splicing pattern that enriches RNAs excluding a part of exon 2, called exon 2B, at the expense of RNAs including this particular subexon (Hallsson et al., 2000). Intriguingly, exon 2B contains the codon for a serine, serine-73, that is phosphorylated in response to *Kit* signaling and whose phosphorylation affects the transcriptional activity and stability of MITF protein (Hemesath et al., 1998). Therefore, we used additional *Mitf* alleles that separately probe changes in Mitf RNA levels and changes in splicing patterns and mutations in serine-73, and analyzed the effects of these alleles in mice heterozygous for *Kit*. The results imply that *Mitf*$^{mi-bws}$ is a complex allele that may act in a semi-dominant fashion similar to *Mitf*$^{Mi-wh}$, but that is dissimilar from *Mitf*$^{Mi-wh}$ in that its semi-dominant activity may only be revealed when placed on a *Kit*-sensitized background.

Results and discussion

The *Kit* allele used in this study, *Kit*^{tm1Alf}, is characterized by an in-frame insertion of the bacterial *LacZ* gene, encoding nuclear LACZ, in the first exon of *Kit* in a way that the *Kit* gene becomes a functional null allele (Bernex et al., 1996; Hou et al., 2000). Homozygotes usually die in utero but heterozygotes display a belly spot, white feet and a white tail tip. Such mice were crossed with mice carrying either one of the following *Mitf* alleles: *microphthalmia-brownish* (*Mitf*$^{Mi-b}$), *microphthalmia-vga9* (*Mitf*$^{mi-vga9}$), *microphthalmia-eyeless-white* *Mitf*$^{mi-ew}$, *microphthalmia red-eyed white* (*Mitf*$^{mi-rw}$), *Mitf*$^{tm1.1Arnh}$ (here called *Mitf*^{S73A}), and *microphthalmia-black and white spots* (*Mitf*$^{mi-bws}$). Their molecular characteristics are schematically shown in Figure 1 and their phenotypes described in Table 1. *Mitf*$^{Mi-b}$ is inherited semi-dominantly and contains a point mutation in exon 8 that affects DNA binding. Homozygotes have a white coat and red eyes while heterozygotes have a brownish coat color, and pale ears and tails (Steingrimsson et al., 1996). The recessive allele *Mitf*$^{mi-vga9}$ is a transgenic insertional null allele and its homozygotes are white with small eyes (Hodgkinson et al., 1993). The recessive allele *Mitf*$^{mi-ew}$ has a point mutation close to the exon 6B/intron 6 splice junction, and its mRNA is
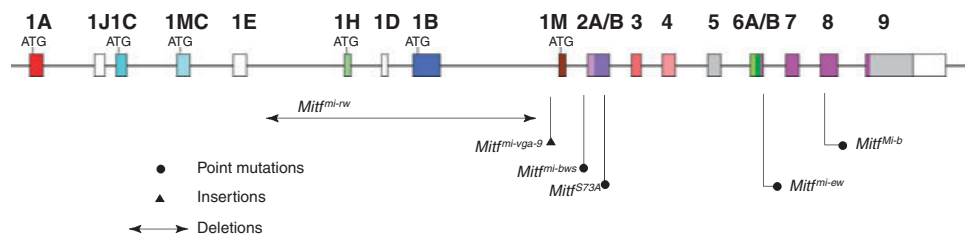

Figure 1. Schematic diagram of the mouse *Mitf* gene and the mutations used in this study. Filled boxes represent coding exons, and open boxes non-coding exons or non-coding parts of exons.

Table 1. Allele-specific interactions between *Mitf* alleles and the *Kit^{tm1Alf}* allele visualized by white spotting of the coat

Genotype 1	Inheritance	Genotype 2	Inheritance	Spotting phenotype	Interaction	Reference
Mitf+/+	–	*Kit+/+*	–	None	–	
Mitf+/+	–	*Kit^{tm1Alf}/+*	Sd	Belly spot, white feet and tail	–	Bernex et al., 1996
Mitf^{Mi-b}/+	Sd	*Kit+/+*	–	None	–	Steingrimsson et al., 1996
Mitf^{mi-ew}/+	Re	*Kit+/+*	–	None	–	Nakayama et al., 1998
Mitf^{mi-rw}/+	Re	*Kit+/+*	–	None	–	Bharti et al., 2008
Mitf^{mi-vga-9}/+	Re	*Kit+/+*	–	None	–	Hodgkinson et al., 1993
Mitf^{S73A}/+	Re	*Kit+/+*	–	None	–	Bismuth et al., 2008
Mitf^{mi-bws}/+	Re	*Kit+/+*	–	None		Hallsson et al., 2000
Mitf^{Mi-b}/+	Sd	*Kit^{tm1Alf}/+*	Sd	Belly spot, white feet and tail	NI	This study
Mitf^{mi-ew}/+	Re	*Kit^{tm1Alf}/+*	Sd	Belly spot, white feet and tail	NI	This study
Mitf^{mi-rw}/+	Re	*Kit^{tm1Alf}/+*	Sd	Belly spot, white feet and tail	NI	This study
Mitf^{mi-vga-9}/+	Re	*Kit^{tm1Alf}/+*	Sd	Belly spot, white feet and tail	NI	This study
Mitf^{S73A}/+	Re	*Kit^{tm1Alf}/+*	Sd	Belly spot, white feet and tail	NI	This study
Mitf^{mi-bws}/+	Re	*Kit^{tm1Alf}/+*	Sd	Extensive spotting around trunk, white feet, white tail	IN	This study
Ednrb^{tm1Myks}/+	Re	*Kit+/+*	–	Occasional belly spot	NI	This study
Ednrb^{tm1Myks}/+	Re	*Kit^{tm1Alf}/+*	Sd	Occasional belly spot	NI	This study

–, not applicable; NI, no gene interaction; IN, gene interaction; Sd, semi-dominant; Re, recessive.
Mice containing the indicated alleles were obtained by appropriate crosses to yield 14–18 doubly heterozygous mice. Note that while many mutant *Mitf* alleles, when homozygous, cause small eyes (microphthalmia), there were no obvious eye phenotypes in *Mitf* heterozygotes alone or in combination with *Kit^{tm1Alf}/+*.
Backgrounds of parental strains: *Mitf +/+;Kit +/+* (C57BL/6), *Mitf+/+; Kit^{tm1Alf}* (mixed C57BL/6;C3H/He), *Mitf^{Mi-b}* (C57BL/6J;C3H/RI), *Mitf^{mi-ew}* (C57BL/6Bn), *Mitf^{mi-rw}* (C57BL/6J), *Mitf^{mi-vga9}* (mixed C57BL/6J;C3H/He), *Mitf^{S73A}* (129S1/Sv;C57BL/6), *Mitf^{mi-bws}* (C57BL/10).

characterized by the absence of exon 6A/B and retention of the open reading frame between exons 5 and 7. The resulting protein affects DNA binding, with homozygotes showing a similar phenotype as *Mitf^{mi-vga9}* homozygotes (Nakayama et al., 1998; Opdecamp et al., 1997). The recessive allele *Mitf^{mi-rw}* contains a genomic deletion that encompasses the exons 1H, 1D, and 1B1a/1B1b and their flanking sequences (Bharti et al., 2008). *Mitf^{mi-rw}* homozygotes have eyes of variable sizes and a coat that is white except for a black spot on the head and/or belly or the base of the tail. The allele *Mitf^{S73A}* has been generated by gene targeting and encodes a non-phosphorylatable alanine instead of the phosphorylatable serine at position 73 (Bismuth et al., 2008). Because the codon change affects an exonic splice enhancer sequence (Wang et al., 2009), it leads to efficient skipping of exon 2B. Nevertheless, the corresponding mice, heterozygous or homozygous, have no visible phenotype. *Mitf^{mi-bws}* is characterized by a point mutation in intron 1 that results in partial skipping of exon 2B (Hallsson et al., 2000). Homozygotes have widespread white spotting but normal eyes.

It was possible that in contrast to the previously observed strong *Mitf^{Mi-wh}/Kit* interactions, the recessive *Mitf* alleles may show no or only mild (additive) interactions with *Kit*. Indeed, the recessive *Mitf^{mi-ew}* or *Mitf^{mi-rw}*, for instance, were unable to enhance the extent of the white spotting of *Kit^{tm1Alf}/+*, and even the mildy semi-dominant *Mitf^{Mi-b}* showed no interactions with *Kit^{tm1Alf}* (Figure 2A). In contrast, *Mitf^{mi-bws}/+*; *Kit^{tm1Alf}/+* mice were extensively spotted (Figure 2B),

and *Mitf^{mi-bws/mi-bws}*;*Kit^{tm1Alf}/+* mice were either completely white or occasionally retained just small pigmented spots on the head or the rump (Figure 2C, compare with *Mitf^{mi-bws/mi-bws}*;*Kit+/+* mouse in Figure 2B). To assay whether this interaction is *Kit*-specific or can also be seen with alterations in a different signaling pathway critical for melanocyte development, we generated double heterozygous combinations of *Mitf^{mi-bws}* and *Ednrb^{tm1Myks}* in which the receptor for endothelin-3, a G protein-coupled receptor, is non-functional (Lee et al., 2003; Hou et al., 2004; Saldana-Caboverde and Kos, 2010). These mice, however, did not show the exacerbation of white spotting seen in *Mitf^{mi-bws}/+*; *Kit^{tm1Alf}/+* mice (Figure S1A).

Because *Mitf^{mi-bws}* reduces both the overall Mitf RNA levels (as measured in the heart) and the relative amounts of Mitf RNA that contains exon 2B (for short, 2B+) versus Mitf RNA that lacks exon 2B (for short, 2B–), it was not a priori clear whether the above mentioned interaction with *Kit* was brought about by the general or the exon-specific reduction of Mitf RNA levels. Hence, we used additional alleles allowing us to test overall RNA levels separately from changes in exon 2B splicing. The allele *Mitf^{mi-vga9}* eliminates the production of Mitf RNA entirely so that in *Mitf^{mi-vga-9}/+* heterozygotes, Mitf RNA, all of which contributed from the remaining wild-type allele, accumulates to approximately 50% of what is seen in a normal animal, measured either in heart or skin (Bauer et al., 2009). However, *Mitf^{mi-vga-9}/+*;*Kit^{tm1Alf}/+* mice showed a spotting phenotype just as *Mitf+/+*; *Kit^{tm1Alf}/+* mice, suggesting that the

A

B

C
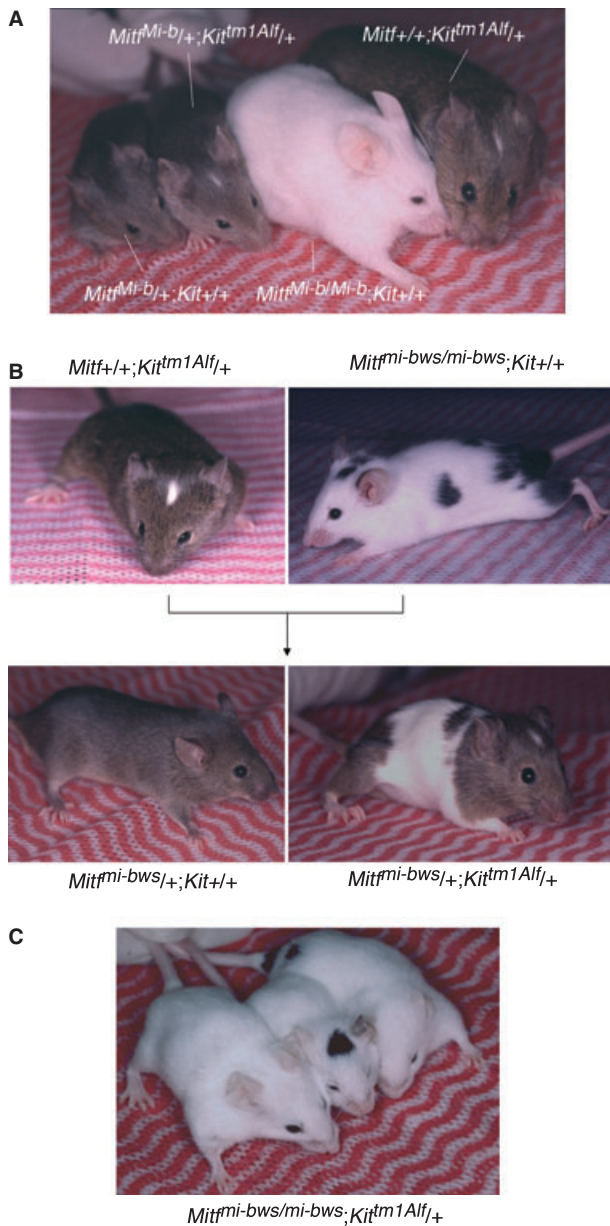
Figure 2. Genetic interactions between *Mitf* and *Kit*. (A) Lack of genetic interactions between *Mitf^Mi-b^* and *Kit^tm1Alf^*. The corresponding genotypes are indicated in the figure. Note that *Mitf^Mi-b^/+;Kit^tm1Alf^/+* mice show a phenotype indistinguishable from that of *Mitf+/+;Kit^tm1Alf^/+* mice. (B) Interaction between *Mitf^mi-bws^* and *Kit^tm1Alf^*. Mice of the indicated genotypes were crossed and their offspring genotyped. Note that *Mitf^mi-bws^/+; Kit+/+* mice are fully pigmented whereas *Mitf^mi-bws^/+;Kit^tm1Alf^/+* offspring show extensive white spotting in the trunk area, different from *Mitf+/+;Kit^tm1Alf^/+* mice. (C) *Mitf^mi-bws/mi-bws^;Kit^tm1Alf^/+* mice are either totally white or retain just small pigmented spots.

exacerbated phenotype in *Mitf^mi-bws^/+; Kit^tmAlf^/+* mice is not simply due to a reduction in total Mitf RNA.

Because the above mentioned exon 2B splicing alteration in *Mitf^mi-bws^* mice has not so far been demonstrated specifically for melanocytes, we analyzed by

standard RT-PCR reactions the exon distribution in the melanocyte-specific M-Mitf RNA. For these tests, we used dorsal skin from C57BL/6 control mice, and dorsal black skin from *Mitf^mi-bws/mi-bws^* and *Kit^tm1Alf^/+* mice (Figure S2). The results showed exon 2B splicing patterns as expected from the analysis of heart RNA from the respective mice. There was, however, no obvious reduction in M-Mitf RNA levels in black *Mitf^mi-bws/mi-bws^* skin. Conceivably, the corresponding melanocytes represent a pool of cells with higher *Mitf* levels which have allowed them to escape the developmental demise of *Mitf^mi-bws^* melanoblasts which on average may express lower levels of *Mitf*. In *Kit^tm1Alf^/+* skin, however, M-Mitf and total Mitf RNA were indeed reduced, consistent with the pigment dilution characteristics of these mice.

To test whether a skewed exon 2B splicing might contribute to the *Mitf/Kit* interaction independently of overall M-Mitf RNA level changes, we used the *Mitf^S73A^* allele. This allele produces normal levels of total Mitf RNA in heart or skin, normal levels of M-Mitf in skin (not shown), but a 2B+/2B− ratio of approximately 0.1, as compared to wild type, where this ratio is approximately 0.9 (Bismuth et al., 2008). The phenotype of *Mitf^S73A^/+; Kit^tm1Alf^/+* and *Mitf^S73A/S73A^; Kit^tm1Alf^/+* mice (Figure S1B), suggests, however, that the exon 2B splice change can also not account separately for the *Mitf^mi-bws^/Kit* interaction, with the only caveat that the remaining 10% of 2B+ RNA derived from the *Mitf^S73A^* allele contains the serine-to-alanine mutation while in *Mitf^mi-bws^*, the serine residue is unchanged. Given the above results, we also tested whether a combination of splice changes *and* a reduction in overall RNA levels would mimic the *Mitf^mi-bws^/Kit* gene interactions. To this end, we generated compound heterozygotes between *Mitf^mi-vga9^* and *Mitf^S73A^* and combined them with *Kit^tmAlf^/+*, but even this allelic combination (*Mitf^mi-vga9/S73A^;Kit^tm1Alf^/+*) yielded mice with just the *Kit* phenotype (not shown). Quantitations of Mitf RNA (total, 2B+ and 2B−) for heart and skin of mice carrying the various alleles alone and in some combinations are shown in Figure S3.

Finally, to determine whether the extensive white spotting in post-natal *Kit^tm1Alf^/+;Mitf^mi-bws^/+* mice already originates during development, at the melanoblast stage, or, conversely, whether the absence of enhanced white spotting in the other crosses might be the result of a post-natal compensation of an early developmental alteration, we made use of the fact that the *Kit^tm1Alf^* allele produces melanoblasts that can be labeled by the X-GAL reaction. Figure 3 shows examples of labeled embryos at day 12.5 of gestation from groups that contained 9–15 embryos and that showed little embryo-to-embryo variation within one genotypic cohort. As shown in Figure 3A, in *Kit^tm1Alf^/+* embryos, individual *β*-Gal-positive cells in the area of the trunk are normally distributed in the dorsolateral migration pathway underneath the surface ectoderm where earlier studies have
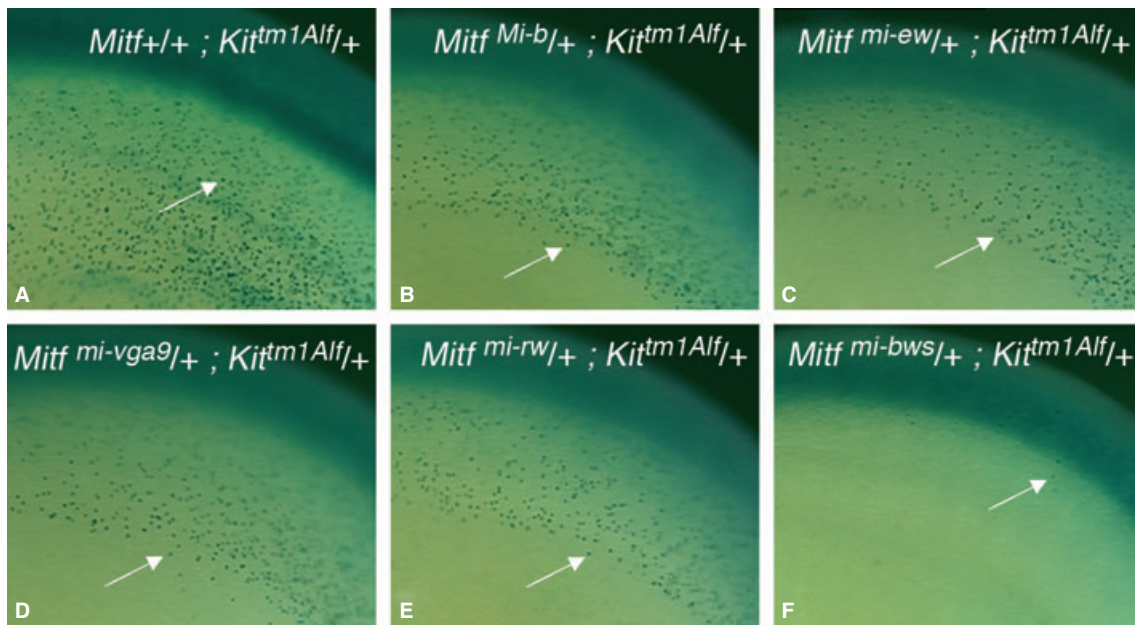
Figure 3. Tracking of β-Gal-positive melanoblasts in embryogenesis. Embryos of the indicated genotypes were harvested at 12.5 days of gestation and processed for β-Gal labeling. Arrows point to individual β-Gal-positive melanoblasts in the dorsolateral migration pathway underneath the surface ectoderm in the trunk area. (A–E) Note similar distribution but slightly reduced numbers and densities of β-Gal-positive melanoblasts in embryos carrying a mutant *Mitf* allele together with the *Kit*[tm1Alf] allele as opposed to a wild-type *Mitf* allele along with the *Kit*[tm1Alf] allele, consistent with earlier findings that *Mitf* gene dosage affects melanoblast numbers early in development (Hornyak et al., 2001). (F) Melanoblasts in embryos double heterozygous for *Mitf*[mi-bws] and *Kit*[tm1Alf] are very sparse and largely restricted to the area over the neural tube.

identified MITF-positive cells (Nakayama et al., 1998) that depend on functional MITF (Hou et al., 2000). Double heterozygous embryos for *Kit*[tm1Alf] and either *Mitf*[Mi-b], *Mitf*[mi-vga9], *Mitf*[mi-ew], *Mitf*[mi-rw] or *Mitf*[S73A] displayed a distribution pattern of β-Gal-positive melanoblasts that was similar to that observed in *Mitf* wild-type embryos heterozygous for *Kit*[tm1Alf] (Figure 3B–E, and data not shown). In contrast, the numbers of labeled cells were severely reduced in the middle trunk region of *Kit*[tm1Alf]/+;*Mitf*[mi-bws]/+ embryos (Figure 3F). Hence, these latter embryos, but not the former ones, have a severe defect in melanoblasts, suggesting that the adult white spotting of *Kit*[tm1Alf]/+;*Mitf*[mi-bws]/+ mice is set at an early developmental stage.

Earlier results have clearly indicated that *Kit*-mediated phosphorylation of serine-73 regulates MITF protein activity and stability in vitro (Hemesath et al., 1998). Nevertheless, neither direct targeting of the corresponding codon in the endogenous gene or in transgenic, bacterial artificial chromosome rescue constructs have been able to demonstrate a clear role for this serine in vivo (Bauer et al., 2009; Bismuth et al., 2008). An isolated serine-to-alanine change, with no effect on exon 2B splicing, however, has not so far been obtained, and so the exact role of serine-73 in an otherwise entirely normal gene has not been formally addressed. Nevertheless, as here demonstrated genetically, neither RNA level changes, nor exon 2B splice changes associated with the ser-

ine73-to-alanine mutation, alone or in combinations, can account for the *Mitf*[mi-bws]/*Kit* interaction phenotype. Hence, *Mitf*[mi-bws] is an allele that is likely altered in one or several more ways than would be suggested solely from its point mutation in intron 1. In fact, an explanation for the *Mitf*[mi-bws] phenotype may be found only when additional promoter- and splice-isoforms have been analyzed, an undertaking that may require the sequencing of the entire 200 kb *Mitf*[mi-bws] gene.

Acknowledgements

References

Arnheiter, H., Hou, L., Nguyen, M.T.T., Bismuth, K., Csermely, T., Murakami, H., Skuntz, S., Liu, W., and Bharti, K. (2006). MITF-A matter of life and death for developing melanocytes. In From Melanocytes to Melanoma: The Progression to Malignancy, V.J.,

Hearing, and S.P.L., Leong, eds. (Totowa, NJ: Human Press, Inc.), pp. 27–49.

Barsh, G.S. (1996). The genetics of pigmentation: from fancy genes to complex traits. Trends Genet. 12, 299–305.

Bauer, G.L., Praetorius, C., Bergsteinsdottir, K. et al. (2009). The role of MITF phosphorylation sites during coat color and eye development in mice analyzed by bacterial artificial chromosome transgene rescue. Genetics 183, 581–594.

Baxter, L.L., Hou, L., Loftus, S.K., and Pavan, W.J. (2004). Spotlight on spotted mice: a review of white spotting mouse mutants and associated human pigmentation disorders. Pigment Cell Res. 17, 215–224.

Baxter, L.L., Loftus, S.K., and Pavan, W.J. (2009). Networks and pathways in pigmentation, health, and disease. Wiley Interdiscip. Rev. Syst. Biol. Med. 1, 359–371.

Beechey, C.V., and Harrison, M.A. (1994). A new spontaneous W allele, W36H. Mouse Genome 92, 502.

Bennett, D.C., and Lamoreux, M.L. (2003). The color loci of mice – a genetic century. Pigment Cell Res. 16, 333–344.

Bernex, F., De Sepulveda, P., Kress, C., Elbaz, C., Delouis, C., and Panthier, J.J. (1996). Spatial and temporal patterns of c-kit-expressing cells in WlacZ/+ and WlacZ/WlacZ mouse embryos. Development 122, 3023–3033.

Bharti, K., Liu, W., Csermely, T., Bertuzzi, S., and Arnheiter, H. (2008). Alternative promoter use in eye development: the complex role and regulation of the transcription factor MITF. Development 135, 1169–1178.

Bismuth, K., Skuntz, S., Hallsson, J.H., Pak, E., Dutra, A.S., Steingrimsson, E., and Arnheiter, H. (2008). An unstable targeted allele of the mouse Mitf gene with a high somatic and germline reversion rate. Genetics 178, 259–272.

Diwakar, G., Zhang, D., Jiang, S., and Hornyak, T.J. (2008). Neurofibromin as a regulator of melanocyte development and differentiation. J. Cell Sci. 121, 167–177.

Drees, B.L., Thorsson, V., Carter, G.W., Rives, A.W., Raymond, M.Z., Avila-Campillo, I., Shannon, P., and Galitski, T. (2005). Derivation of genetic interaction networks from quantitative phenotype data. Genome Biol. 6, R38.

Guo, X.L., Ruan, H.B., Li, Y., Gao, X., and Li, W. (2010). Identification of a novel nonsense mutation on the Pax3 gene in ENU-derived white belly spotting mice and its genetic interaction with c-Kit. Pigment Cell Melanoma Res. 23, 252–262.

Hallsson, J.H., Favor, J., Hodgkinson, C. et al. (2000). Genomic, transcriptional and mutational analysis of the mouse microphthalmia locus. Genetics 155, 291–300.

Hearing, V.J., and Jimenez, M. (1989). Analysis of mammalian pigmentation at the molecular level. Pigment Cell Res. 2, 75–85.

Hemesath, T.J., Steingrimsson, E., McGill, G., Hansen, M.J., Vaught, J., Hodgkinson, C.A., Arnheiter, H., Copeland, N.G., Jenkins, N.A., and Fisher, D.E. (1994). Microphthalmia, a critical factor in melanocyte development, defines a discrete transcription factor family. Genes Dev. 8, 2770–2780.

Hemesath, T.J., Price, E.R., Takemoto, C., Badalian, T., and Fisher, D.E. (1998). MAP kinase links the transcription factor Microphthalmia to c-Kit signalling in melanocytes. Nature 391, 298–301.

Hodgkinson, C.A., Moore, K.J., Nakayama, A., Steingrimsson, E., Copeland, N.G., Jenkins, N.A., and Arnheiter, H. (1993). Mutations at the mouse microphthalmia locus are associated with defects in a gene encoding a novel basic-helix-loop-helix-zipper protein. Cell 74, 395–404.

Hornyak, T.J., Hayes, D.J., Chiu, L.Y., and Ziff, E.B. (2001). Transcription factors in melanocyte development: distinct roles for Pax-3 and Mitf. Mech. Dev. 101, 47–59.

Hou, L., and Pavan, W.J. (2008). Transcriptional and signaling regulation in neural crest stem cell-derived melanocyte development: do all roads lead to Mitf? Cell Res. 18, 1163–1176.

Hou, L., Panthier, J.J., and Arnheiter, H. (2000). Signaling and transcriptional regulation in the neural crest-derived melanocyte lineage: interactions between KIT and MITF. Development 127, 5379–5389.

Hou, L., Pavan, W.J., Shin, M.K., and Arnheiter, H. (2004). Cell-autonomous and cell non-autonomous signaling through endothelin receptor B during melanocyte development. Development 131, 3239–3247.

Hou, L., Arnheiter, H., and Pavan, W.J. (2006). Interspecies difference in the regulation of melanocyte development by SOX10 and MITF. Proc. Natl. Acad. Sci. USA 103, 9081–9085.

Lee, H.O., Levorse, J.M., and Shin, M.K. (2003). The endothelin receptor-B is required for the migration of neural crest-derived melanocyte and enteric neuron precursors. Dev. Biol. 259, 162–175.

Matera, I., Watkins-Chow, D.E., Loftus, S.K., Hou, L., Incao, A., Silver, D.L., Rivas, C., Elliott, E.C., Baxter, L.L., and Pavan, W.J. (2008). A sensitized mutagenesis screen identifies Gli3 as a modifier of Sox10 neurocristopathy. Hum. Mol. Genet. 17, 2118–2131.

McGill, G.G., Horstmann, M., Widlund, H.R. et al. (2002). Bcl2 regulation by the melanocyte master regulator Mitf modulates lineage survival and melanoma cell viability. Cell 109, 707–718.

Nakayama, A., Nguyen, M.T., Chen, C.C., Opdecamp, K., Hodgkinson, C.A., and Arnheiter, H. (1998). Mutations in microphthalmia, the mouse homolog of the human deafness gene MITF, affect neuroepithelial and neural crest-derived melanocytes differently. Mech. Dev. 70, 155–166.

Opdecamp, K., Nakayama, A., Nguyen, M.T., Hodgkinson, C.A., Pavan, W.J., and Arnheiter, H. (1997). Melanocyte development in vivo and in neural crest cell cultures: crucial dependence on the Mitf basic-helix-loop-helix-zipper transcription factor. Development 124, 2377–2386.

Potterf, S.B., Furumura, M., Dunn, K.J., Arnheiter, H., and Pavan, W.J. (2000). Transcription factor hierarchy in Waardenburg syndrome: regulation of MITF expression by SOX10 and PAX3. Hum. Genet. 107, 1–6.

Price, E.R., Ding, H.F., Badalian, T., Bhattacharya, S., Takemoto, C., Yao, T.P., Hemesath, T.J., and Fisher, D.E. (1998). Lineage-specific signaling in melanocytes. C-kit stimulation recruits p300/CBP to microphthalmia. J. Biol. Chem. 273, 17983–17986.

Quevedo Jr, W.C., and Holstein, T.J. (1992). Molecular genetics and the ontogeny of pigment patterns in mammals. Pigment Cell Res. 5, 328–334.

Rhim, H., Dunn, K.J., Aronzon, A., Mac, S., Cheng, M., Lamoreux, M.L., Tilghman, S.M., and Pavan, W.J. (2000). Spatially restricted hypopigmentation associated with an Ednrbs-modifying locus on mouse chromosome 10. Genome Res. 10, 17–29.

Saldana-Caboverde, A., and Kos, L. (2010). Roles of endothelin signaling in melanocyte development and melanoma. Pigment Cell Melanoma Res. 23, 160–170.

Spritz, R.A. (1997). Piebaldism, Waardenburg syndrome, and related disorders of melanocyte development. Semin. Cutan. Med. Surg. 16, 15–23.

Steingrimsson, E., Nii, A., Fisher, D.E., Ferre-D'Amare, A.R., McCormick, R.J., Russell, L.B., Burley, S.K., Ward, J.M., Jenkins, N.A., and Copeland, N.G. (1996). The semidominant Mi(b) mutation identifies a role for the HLH domain in DNA binding in addition to its role in protein dimerization. EMBO J. 15, 6280–6289.

Wang, X., Debbache, J., and Arnheiter, H. (2009). Alternative splicing and cell regulation in vertebrate pigment cells. Dev. Biol. 331, A108.

Supporting information

Additional Supporting Information may be found in the online version of this article:

Figure S1. (A) The *Mitf*$^{mi\text{-}bws}$/*Kit* interaction is *Kit*-specific as no interaction is seen between *Mitf*$^{mi\text{-}bws}$ and *Ednrb*^{tm1Myks}, an *Ednrb* null allele. (B) No interaction between *Kit*^{tm1Alf} and *Mitf*^{S73A}. Note white feet characteristic of the *Kit*^{tm1Alf}/+ genotype but no extensive spotting, unlike what is seen in *Mitf*$^{mi\text{-}bws}$/+; *Kit*^{tm1Alf}/+ mice.

Figure S2. RT-PCR using RNA from black dorsal skin of C57BL/6 wild type (wt), *Mitf*$^{mi\text{-}bws/mi\text{-}bws}$ (*mi-bws/mi-bws*), and *Kit*^{tm1Alf}/+ mice. Primers mapped to Mitf or Usf1 (upstream stimulatory factor-1) exons as indicated. Note that wt contains more M-Mitf exon 2B+ compared to M-Mitf exon 2B− cDNA while the M-Mitf exon 2B+/2B− cDNA ratio is reversed in *mi-bws/mi-bws* (primers 1M-3). The total levels of M-Mitf cDNA is, however, similar for wt and *mi-bws/mi-bws* skin and only lower for *Kit*^{tm1Alf}/+ skin for which, because of the lower levels, it becomes difficult to assess the relative 2B+/2B− ratio. Total Mitf cDNA levels (measured using primers 6B-8, amplifying Mitf from melanocytes and the remainder of skin tissue), are only slightly lower in *mi-bws/mi-bws* or *Kit*^{tm1Alf}/+ skin compared to wt. Note similar levels of control Usf1 cDNA for all samples.

Figure S3. Real time RT-PCR for the tissue samples and genotypes indicated. Separate quantitation was performed for exon 2B+ and exon 2B− cDNA, using primers giving equal length products as described in Bharti et al., in press. (A) Wild type, and heterozygous and homozygous single-gene mutant genotypes. (B) Wild type and *Mitf*$^{mi\text{-}vga9/S73A}$ compound mutants either lacking or carrying *Kit*^{tm1Alf}.

Please note: Wiley-Blackwell are not responsible for the content or functionality of any supporting materials supplied by the authors. Any queries (other than missing material) should be directed to the corresponding author for the article.

3 – Les transgènes de type BAC qui expriment les mutants MITF S73A, MITF S409A, MITF 2B- et le double mutant MITF S73/409A sont tous capables de restaurer la fonctionnalité de MITF.

Le facteur de Transcription Mitf apparaît comme un modèle important pour la régulation génique chez les organismes eucaryotes. Chez les vertébrés, Mitf régule le développement de plusieurs types cellulaires parmi lesquels se trouvent les melanocytes, et a été démontré comme ayant un rôle important dans le mélanome. *In vitro*, parmi les voix de signalisations qui régulent l'activité de MITF, se trouve la voix des MAP Kinases qui a pour conséquence la phosphorylation de MITF aux postions S73 et S409. Cependant, le rôle précis de cette voix de signalisation reste mal caractérisé *in vivo*. Ici nous utilisons une approche « BAC rescue » afin d'introduire des mutations spécifiques du gène *Mitf* dans le but d'étudier l'importance de ces sites de phosphorylation et des domaines protéiques qui les environnent. Nous démontrons que des transgènes mutés sur un seul acide aminé peuvent restaurer le phénotype de souris qui portent un allèle nul de *Mitf* de façon homozygote. Ainsi, ces résultats jouent un rôle dans l'intégration des interactions entre les voix de signalisations extra-cellulaires et de l'activité de facteurs de transcription. De plus, MITF ainsi que la voix des MAP Kinases jouent des rôles cruciaux dans le mélanome ; ces résultats peuvent donc apporter de nouveaux éléments dans la compréhension de cette pathologie.

Ce travail est présenté dans l'**Article 3**.

Here we use a bacterial artificial chromosome (BAC) transgenic rescue strategy to probe the role of S73 and S409 phosphorylation as well as exon splicing of *Mitf*. BACs were

modified by a "hit and fix" strategy using homologous recombination in bacteria. We demonstrate for instance, that a S73A/S409A double mutant still rescues *Mitf^{mi-vga9}/Mitf^{mi-vga9}* homozygous mutants. Because of the variability of expression levels seen with different BAC transgenics, however, we cannot conclude from these experiments that S73A/S409A double mutated MITF has an activity equivalent to wild-type. Nevertheless it is clear that it retains considerable DNA binding capacity and transcriptional activity *in vivo*. S409 phosphorylation has been suggested to play a role in the interaction with the Protein Inhibitor of activated STAT3 (PIAS3). Experiments performed by Levy *et al.* showed that the presence of a charged amino acid like aspartate at position 409, which mimics constitutive phosphorylation, prevents the PIAS3/MITF interaction (Levy et al., 2006b). This interaction has been shown to play an important role in the inhibition of Mitf activation of the mMCP-6 promoter in mast cells.

Corroborating the previous results observed in *Mitf^{mi-S73A}* knock-in mouse, the BAC transgenic lines expressing MITF S73A also display an abnormally high rate of exon 2B exclusion in both heart and skin tissue.

Additional transgene constructs carrying various internal intron and exon deletions all show partial to almost complete rescue of the *Mitf^{mi-vga9}/Mitf^{mi-vga9}* phenotype.

The details of this research study are described in the following **Article 3**.

Article 3

The role of MITF phosphorylation sites during coat color and eye development in mice analyzed by bacterial artificial chromosome transgene rescue.

The Role of MITF Phosphorylation Sites During Coat Color and Eye Development in Mice Analyzed by Bacterial Artificial Chromosome Transgene Rescue

Georg L. Bauer,* Christian Praetorius,* Kristín Bergsteinsdóttir,* Jón H. Hallsson,*,[1] Bryndís K. Gísladóttir,* Alexander Schepsky,* Deborah A. Swing,† T. Norene O'Sullivan,† Heinz Arnheiter,‡ Keren Bismuth,‡,[2] Julien Debbache,‡ Colin Fletcher,§ Søren Warming,†,[3] Neal G. Copeland,** Nancy A. Jenkins** and Eiríkur Steingrímsson*,[4]

*Department of Biochemistry and Molecular Biology and Biomedical Center, Faculty of Medicine, University of Iceland, 101 Reykjavik, Iceland, †Mouse Cancer Genetics Program, Center for Cancer Research, National Cancer Institute, Frederick, Maryland 21702, ‡Laboratory of Developmental Neurogenetics, National Institute of Neurological Disorders and Stroke, Porter Neuroscience Research Center, Bethesda, Maryland 20892-3706, §Knock Out Mouse Program, National Human Genome Research Institute, National Institutes of Health, Bethesda, Maryland, 20892-9305 and **Institute of Molecular and Cell Biology, Proteos, Singapore 138673

ABSTRACT

The microphthalmia-associated transcription factor (Mitf) has emerged as an important model for gene regulation in eukaryotic organisms. In vertebrates, it regulates the development of several cell types including melanocytes and has also been shown to play an important role in melanoma. *In vitro*, the activity of MITF is regulated by multiple signaling pathways, including the KITL/KIT/B-Raf pathway, which results in phosphorylation of MITF on serine residues 73 and 409. However, the precise role of signaling to MITF *in vivo* remains largely unknown. Here, we use a BAC transgene rescue approach to introduce specific mutations in MITF to study the importance of specific phospho-acceptor sites and protein domains. We show that mice that carry a BAC transgene where single-amino-acid substitutions have been made in the *Mitf* gene rescue the phenotype of the loss-of-function mutations in *Mitf*. This may indicate that signaling from KIT to MITF affects other phospho-acceptor sites in MITF or that alternative sites can be phosphorylated when Ser73 and Ser409 have been mutated. Our results have implications for understanding signaling to transcription factors. Furthermore, as MITF and signaling mechanisms have been shown to play an important role in melanomas, our findings may lead to novel insights into this resilient disease.

THE bHLH-Zip transcription factor MITF (microphthalmia-associated transcription factor) was initially found as the gene mutated at the mouse microphthalmia locus (HODGKINSON *et al.* 1993). Subsequent work has led to the proposal that MITF acts as a master regulator of melanocyte development by regulating proliferation, survival, and differentiation of this cell type (reviewed by HOU and PAVAN 2008). MITF has also been implicated as a regulator of melanocyte stem cell maintenance (NISHIMURA *et al.* 2005) as well as a melanoma oncogene (LEVY *et al.* 2006). In addition, the human MITF gene is mutated in individuals with

Waardenburg syndrome type 2 and Tietz syndrome (reviewed in STEINGRÍMSSON *et al.* 2004). Clearly, MITF is an important decision maker in melanocytes and may be an important player in melanomas as well.

The many mutations at the mouse *Mitf* locus have provided key insights into the structure–function relationship of this transcription factor. All of the mouse *Mitf* mutations affect melanocytes to a varying degree, resulting in animals with coat color phenotypes ranging from white spotting and coat color dilution to a completely white coat due to lack of melanocytes (reviewed in STEINGRÍMSSON *et al.* 2004). Some of the mutations also affect retinal pigment epithelial (RPE) cells, resulting in unpigmented or hypopigmented microphthalmic eyes. Other cell types affected by *Mitf* mutations include osteoclasts and mast cells as well as natural killer cells, basophils, macrophages, and B cells (reviewed in STEINGRÍMSSON *et al.* 2004). Interestingly, the phenotypes of *Mitf* mutations overlap partly with the phenotypes of mutations in the *Kit* and *Kitl* genes in the mouse. Mutations in these three genes affect melanocyte development, resulting in pigmentation defects

(often leading to white coat color), and all have effects on mast cells. However, only mutations in *Mitf,* and not *Kit* or *Kitl,* affect eye development. On the other hand, *Kit* and *Kitl* mutations affect hematopoiesis and germ-cell development whereas mutations in *Mitf* do not, at least not to the same degree.

As *Kit* and *Kitl* encode a receptor tyrosine kinase and its ligand, respectively, it was proposed that they form a signaling cascade that culminates in effects on the MITF protein (DUBREUIL *et al.* 1991). Indeed, a number of signaling pathways, including KITL and KIT, have been shown to regulate the activity of the MITF protein. In a landmark series of experiments, David Fisher's group showed that MITF is an important downstream target of the KIT tyrosine kinase receptor. They showed that treating human 501-mel melanoma cells with KIT ligand (KITL) resulted in the phosphorylation of the Ser73 and Ser409 amino acids of MITF (HEMESATH *et al.* 1998; WU *et al.* 2000). Signaling to MITF involved the receptor ty-rosine kinase KIT, the mitogen-activated protein kinase ERK2, and the serine–threonine kinase p90RSK and resulted in the phosphorylation of Ser73 by ERK2 and of Ser409 by p90RSK (HEMESATH *et al.* 1998; WU *et al.* 2000). Phosphorylation of Ser73 increased the trans-activation potential of MITF by specifically recruiting the co-activator p300/CBP to the phosphorylated pro-tein (PRICE *et al.* 1998). KITL stimulation was also shown to result in the ubiquitination of MITF and its sub-sequent proteasome-mediated degradation (WU *et al.* 2000; XU *et al.* 2000). Interestingly, when either Ser73 or Ser409 alone are mutated to alanine *in vitro,* transcrip-tion activation potential is only mildly affected, whereas mutating both sites simultaneously obliterates the tran-scription activation ability of the MITF protein in *in vitro* assays (WU *et al.* 2000). These findings, together with the fact that mice that carry mutations in *Kit* and *Kitl* are white with normal eye development, have suggested that this signaling pathway is essential for MITF function in melanocytes.

Here, we use a BAC transgene rescue strategy to in-vestigate the *in vivo* role of signaling to MITF in the mouse. Recombineering was used to generate specific mutations in a BAC clone containing the *Mitf* gene. BAC transgenic animals were made and then crossed to *Mitf* loss-of-function mutants to determine if the BAC could rescue the *Mitf* phenotype. Using this method, we show that mutating either Ser73 or Ser409 to alanine leads to rescue of the melanocyte and RPE defects associated with *Mitf* mutations. Similarly, deletion studies show that the domains encoded by exons 1A, 2A, and 2B do not seem to be essential for MITF function. Our results present a novel and rapid method for analyzing the role of individual amino acids and functional domains in the mouse. The results have implications for our under-standing of transcription factor function in general and for melanocyte development in particular. And as MITF and signaling mechanisms have been shown to play an important role in melanoma, our findings may lead to novel insights into this disease.

MATERIALS AND METHODS

Recombineering and generation of transgenic mice: The BAC-Mi1 (RP23-9A13) and BAC-Mi2 (RP23-21E20) clones were selected from the RPCI-23 BAC library (female C57BL/ 6J mouse). The BAC-Mi1 clone was introduced into the DY380 strain of *Escherichia coli,* and the Ser73Ala and Ser409Ala mu-tations were introduced using the two-step hit-and-fix method as described in YANG and SHARAN (2003) and outlined in Figure 1. The deletion mutations were made using the method of WARMING *et al.* (2005). The oligos used for recombineering and BAC screening are listed in Tables 1 and 2. The BACs were screened for the presence of the hit-and-fix sequences using PCR, and the mutated regions were sequenced to verify that the correct changes had been introduced. BAC DNA was pre-pared for pronuclear injections according to SHARAN *et al.* (2004), and pronuclear injections of supercoiled BAC DNA were performed as described by HOGAN *et al.* (1994).

Analysis of mutations: Genomic DNA was extracted from mouse tail tips according to JENKINS *et al.* (1982). For detecting the *MITF^{mi-vga9}* transgene, we used the primers vga9-for and mitf-rev, and for detecting the CMr sequence of the BAC transgene, we used the primers CMr-F and CMr-R (see primers in Table 1). To verify that the mutations had been correctly introduced into the transgenic mice, RT–PCR was performed on heart tissue using the appropriate *Mitf* primers, and the resulting product was sequenced.

Analysis of alternative splicing: Tissues were collected and deposited directly into liquid nitrogen and total RNA ex-tracted using TRIZOL reagent (Invitrogen). RNA quantity was measured on a Nanodrop spectrophotometer, and integrity was determined on an Agilent 2100 Bioanalyzer RNA Nano chips. RNA with an RNA integrity number >7.0 was treated with DNase (Qiagen) to remove genomic contamination and purified on an RNeasy MinElute column (Qiagen). RNA quantity was measured again, and integrity was determined. RNA samples were then reverse transcribed using the Revertaid H first-strand synthesis kit (Fermentas) with both oligo(dT) and random hexamer primers, and the two reactions were com-bined for subsequent analysis. PCR was performed using the primers indicated in each case and listed in Tables 1–3.

Relative quantification by quantitative PCR: RNA was isolated as described above. The presence of inhibitory factors in the RNA samples was tested using the SPUD assay (NOLAN *et al.* 2006). Two micrograms of total RNA were reverse tran-scribed into cDNA using Superscript III reverse transcriptase and anchored oligo(dT)$_{20}$ primers (Invitrogen). To find ap-propriate reference genes, the expression of 12 housekeeping genes (TATAA Biocenter, Göteborg, Sweden) was evaluated in cDNA samples prepared from heart tissues of six wild-type mice, and GeNorm software (VANDESOMPELE *et al.* 2002) used to identify the most stable reference gene. Quantitative real-time PCR was performed using the SybrGreen I Master^{PLUS} mix and the LightCycler (Roche Diagnostics) and normalized to the expression of the most stable reference gene (*Hprt1*). Three mice from each group of BAC transgenic lines were analyzed for *Mitf* expression. Primers were designed using the Primer3 program (ROZEN and SHALETSKY 2000). Each sample assay included a cDNA template equivalent to 50 ng of total RNA; each PCR assay was performed in duplicate. Negative controls consisting of non-reverse transcribed samples were included in each set of reactions. Amplification efficiency was determined for the primers using a dilution-curve fivefold series of 6 points) and was 1.03 and 0.978, respectively, for the

TABLE 1

Primers used in the study for BAC recombineering

Primer	Sequence
	Ser73
Ser73HitF	5′-ACATGCCAGCCAAGTCCTGAGCTCACCATGTCCAAACCAGCCTGGCGACCATGCCATGCCACCAGTGCCGGGGAGCAGCGAAGCTTACTGTCAGCTCGAG-3′
Ser73HitB	5′-AGTTAATGGAATGTAAGAAACAGAGGAGAAGAGGAGACGTGAATTACCTCTTTTTCACAGTTGGAGTTAAGAGTGAGCATCTCGAGCTGACAGTAAGCTT-3′
Ser73FixF	5′-ACATGCCAGCCAAGTCCTGAGCTCACCATGTCCAAACCAGCCTGGCGACCATGCCATGCCACCAGTGCCGGGGAGCAGCGCACCCAAC*GCC*CCTATGGCT-3′
Ser73FixB	5′-AGTTAATGGAATGTAAGAAACAGAGGAGAAGAGGAGACGTGAATTACCTCTTTTTCACAGTTGGAGTTAAGAGTGAGCATAGCCATAGG*GGC*GTTGGGTG-3′
	Ser409
Ser409HitF	5′-GGACGATGCCCTCTCACCTGTTGGAGTCACCGACCCACTGCTGTCATCAGTGTCGCCAGGAGCTTCAAAAACAAGCAGCCAAGCTTACTGTCAGCTCGAG-3′
Ser409HitB	5′-AGTCTCCTGAAGAAGAGAGGGAGCGGTCCGTGCAGAGGCAGAGCAAGGCAGGCTCGCTAACACGCATGCTCCGTTTCTTCCTCGAGCTGACAGTAAGCTT-3′
Ser409FixF	5′-GGACGATGCCCTCTCACCTGTTGGAGTCACCGACCCACTGCTGTCATCAGTGTCGCCAGGAGCTTCAAAAACAAGCAGCC*GGAGGAGC*GCTATGAGCGCA-3′
Ser409FixB	5′-AGTCTCCTGAAGAAGAGAGGGAGCGGTCCGTGCAGAGGCAGAGCAAGGCAGGCTCGCTAACACGCATGCTCCGTTTCTTCTGCGCTCAT*AGC*GCTCCTCC-3′
	Del(int1/2A)
Mitf galK F	CTGCCTGAAACCTTGCTATGCTGGAAATGCTAGAATACAGTCACTACCAGCCTGTTGACAATTAATCATCGGCA
Mitf galK R	ACTTGGCTGGCATGTTTATTTGCTAAAGTGGTAGAAAGGTACTGCTTTACTCAGCACTGTCCTGCTCCTT
galK del(int1/2a)up	CTGCCTGAAACCTTGCTATGCTGGAAATGCTAGAATACAGTCACTACCAGGTAAAGCAGTACCTTTCTACCACTTTAGCAAATAAACATGCCAGCCAAGT
galK del(int1/2a)low	ACTTGGCTGGCATGTTTATTTGCTAAAGTGGTAGAAAGGTACTGCTTTACCTGGTAGTGACTGTATTCTAGCATTTCCAGCATAGCAAGGTTTCAGGCAG
	Del(2B/int2)
Mitf2B galK F	ACCTGGAAAACCCCACCAAGTACCACATACAGCAAGCTCAGAGGCACCAGCCTGTTGACAATTAATCATCGGCA
Mitf2B galK R	CCTGGGCACTCACTCTCTGCCCTGCTCTGCTCCTCAAACTTATAAAATGCTCAGCACTGTCCTGCTCCTT
Mitf2B S	ACCTGGAAAACCCCACCAAGTACCACATACAGCAAGCTCAGAGGCACCAGGCATTTTATAAGTTTGAGGAGCAGAGCAGGGCAGAGAGTGAGTGCCCAGG
Mitf2B AS	CCTGGGCACTCACTCTCTGCCCTGCTCTGCTCCTCAAACTTATAAAATGCCTGGTGCCTCTGAGCTTGCTGTATGTGGTACTTGGTGGGGTTTTCCAGGT
	Del(int2)
Mitf intr2 galK F	CCAACAGCCCTATGGCTATGCTCACTCTTAACTCCAACTGTGAAAAAGAGCCTGTTGACAATTAATCATCGGCA
Mitf2B galK R	CCTGGGCACTCACTCTCTGCCCTGCTCTGCTCCTCAAACTTATAAAATGCTCAGCACTGTCCTGCTCCTT
Mitf intr2 S	CCAACAGCCCTATGGCTATGCTCACTCTTAACTCCAACTGTGAAAAAGAGGCATTTTATAAGTTTGAGGAGCAGAGCAGG
Mitf intr2 AS	ATGCACGACGCTCGAGAGTGCGTGTTCATACCTGGGCACTCACTCTCTGCCCTGCTCTGCTCCTCAAACTTATAAAATGC

Mitf (mMitf-e6-8qF and mMitf-e6-8qR) and *Hprt1* (*Hprt1*-F2 and *Hprt1*-R2) primers. Cycling conditions were the following: denaturation at 95° for 10 min, followed by 45 cycles at 95° for 10 sec, 59° for 10 sec, and 72° for 25 sec. Melting curve analysis and agarose gel electrophoresis were performed to confirm the specificity of the product. Data were analyzed using the Genex program (VANDESOMPELE *et al.* 2002). Quantitation of *Mitf* isoforms containing or lacking exon 2B was performed as described in BHARTI *et al.* (2009).

RESULTS AND DISCUSSION

BAC transgene strategy: To determine the *in vivo* role of signaling to MITF, we used a BAC rescue strategy. Two BACs that contain the *Mitf* gene were obtained and characterized with respect to end sequences and the presence of the *Mitf* gene. The BACs, termed BAC-Mi1 (rpci-23-9a13t7) and BAC-Mi2 (rpci-23-21e20sp6), are

TABLE 2

Primers used in this study for BAC and genomic screening

Primer	Sequence	Function
Hit ScreenF	5′-AAGCTTACTGTCAGCTCGAG-3′	For screening Hit clones
S73FixScr	5′-GGGAGCAGCGCACCCAACGCCCCTATGGCT-3′	For screening 73 fixed clones
S409FixScr	5′-ACAAGCAGCCGGAGGAGCGCTATGAGCGCA-3′	For screening 409 fixed clones
Ex2/F	5′-TGTTGGTCAACTGGTCAGTCT-3′	For sequencing exon 2
Ex2/R	5′-AGGACAGAGGTTGGTGACAAT-3′	For sequencing exon 2 and for screening hit-and-fix clones
RecEx9Scr5A	5′-CCTGATCTGGTGAATCGGATCATCAAGC-3′	For sequencing part of exon 9
RecEx9Scr3A	5′-CAGATACTGCACGCTGAAGGTACAATAC-3′	For sequencing part of exon 9 and for screening hit-and-fix clones
vga9-for	5′-CTGCAGCACGGACAATAAACCTCC-3	Mitf: specific for vga9 mutation
mitf-rev	5′-AAACAAGGCATCCCGAGGCACC-3′	Mitf: for screening vga9 mutation
Mitf-2BtestF	5′-CAGGGACGTTAAACAGGATAGT-3′	For screening deletions
Mitf-2BtestR	5′ -AGGTCCTGAAGTCATCAGGA-3′	For screening deletions
CMr-F	5′-AGCATTCTGCCGACATGGAAGC-3′	BAC clone forward
CMr-R	5′-CACGACGATTTCCGGCAGTTTC-3′	BAC clone reverse

shown in Figure 1A. Although they differ at the 5′- and 3′-ends, they contain the entire *Mitf* gene except exon 1A. We used a two-step recombineering protocol called "hit and fix" (outlined in Figure 1B) for introducing specific mutations into the BAC (YANG and SHARAN 2003) and the *GalK* recombineering strategy (WARMING *et al.* 2005) for introducing deletion mutations.

Phenotypic rescue of wild-type BACs: To test if the wild-type BAC clones can rescue the *Mitf* mutant phenotype, transgenic mice that carry the BAC-Mi1 clone were made. The transgenic mice were made using *Mitf^{mi-ew}* heterozygous embryos, and the resulting carriers were then crossed to *Mitf^{mi-ew}* homozygous animals to generate *Mitf^{mi-ew}*/*Mitf^{mi-ew}* animals, which also carry the BAC clone. Homozygous *Mitf^{mi-ew}*/*Mitf^{mi-ew}* animals are completely white, due to a lack of melanocytes, and have severe microphthalmia due to developmental defects in the retinal pigment epithelium (Figure 1C) (STEINGRÍMSSON *et al.* 2004). However, homozygous *Mitf^{mi-ew}* mice that are also homozygous for the BAC-Mi1 clone are normally

pigmented and have normal eyes (Figure 1C), suggesting that the BAC-Mi1 clone can rescue the phenotype completely, despite lacking exon 1A; they are normally pigmented in every respect, including the belly region (Figure 2A). Transgenic mice were also made using the BAC-Mi2 clone and, again, the BAC can rescue the *Mitf^{mi-ew}* mutant phenotype with respect to both coat color and eye developmental defects (Figure 2B). The *Mitf^{mi-ew}* mutation results in a MITF protein that lacks the DNA-binding domain (STEINGRÍMSSON *et al.* 1994; HALLSSON *et al.* 2000), and *in vitro* studies suggest that the protein acts in a dominant-negative fashion (HEMESATH *et al.* 1994); detailed phenotypic characterization has suggested a mild dominant-negative action of the mutant protein in osteoclasts (STEINGRÍMSSON *et al.* 2002). To avoid possible problems with dominant-negative behavior of the *Mitf^{mi-ew}* mutation, we also performed rescue studies using the recessive *Mitf^{mi-vga9}* mutation, a transgene insertion mutation that obliterates *Mitf* expression in most tissues (HODGKINSON *et al.* 1993) and is

TABLE 3

Primers used in this study for RT–PCR and qPCR

Primer	Sequence	Position
Exon 1bF	5′-GACACCAGCCATAAACGTCA-3′	Exon 1b forward
Exon 9R	5′-TGCTTGATGATCCGATTCAC-3′	Exon 9 reverse
Exon 3R	5′-TGTTCATACCTGGGCACTCA-3′	Exon 3 reverse
Mitf-q3-rev	5′-CATCAATTACATCATCCATCTGC-3′	Exon 4 reverse
Mitf-1M-e4F	5′-ACTAAGTGGTCTGCGGTGTCTC-3′	Exon M forward
Mitf 1M-e4R	5′-TAACTTGATTCCAGGCTGATGA-3′	Exon 4 reverse
Mitf-1H-e9F	5′-TGAGTCAGACACCAGCCATAA-3′	Exon 1H forward
Mitf-1H-e9-Rev	5′-TGCTTGATGATCCGATTCAC-3′	Exon 9 reverse
Mitf-e6-8qF	5′-AGCAAGAGCATTGGCTAAAGA-3′	Exon 6 forward
mMitf-e6-8qR	5′-GCATGTCTGGATCATTTGACTT-3′	Exon 8 reverse
mHPRT1-for2	5′-GTTGGATACAGGCCAGACTTTGTTG-3′	Hprt control
mHPRT1-rev2	5′-GATTCAACTTGCGTCATCTTAGGC-3′	Hprt control
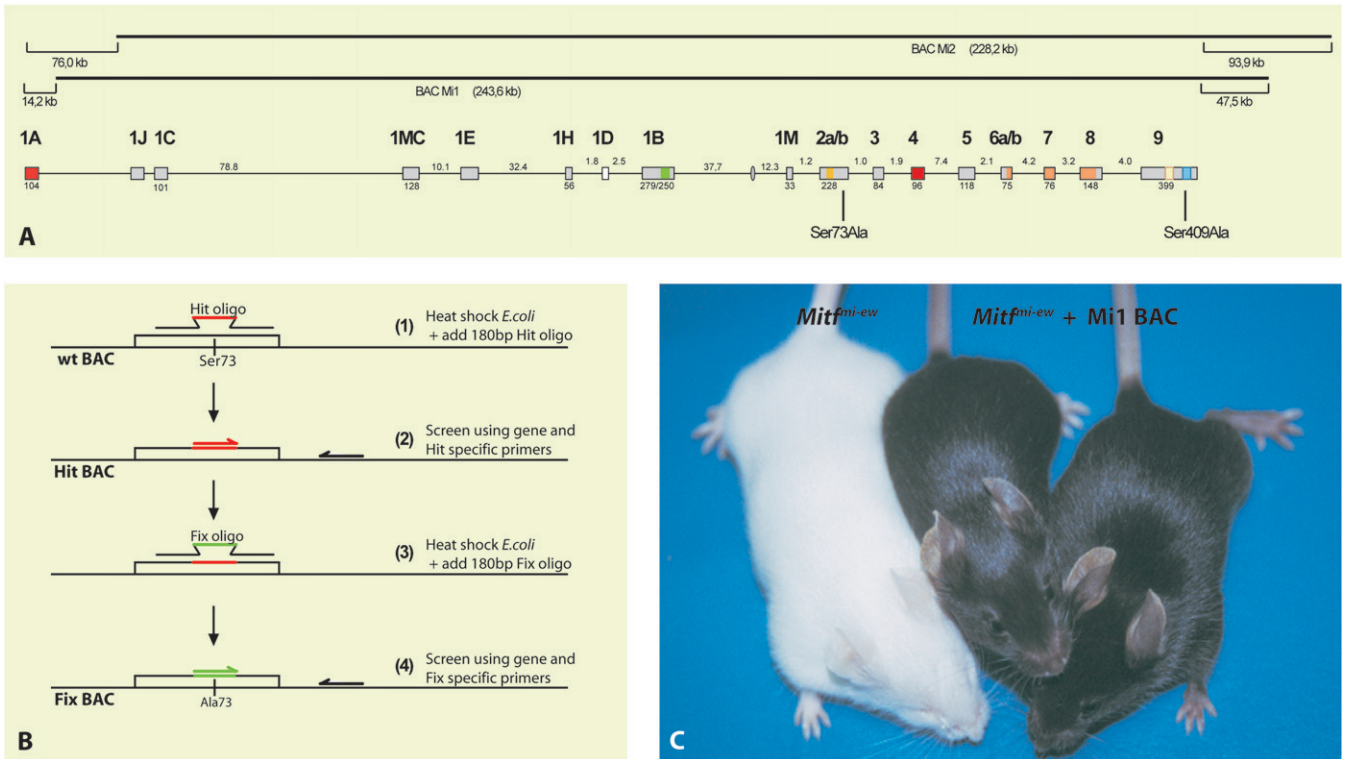
FIGURE 1.—The BAC clones and recombineering strategy. (A) The two BAC clones isolated in the study are shown with respect to the structure of the *Mitf* gene. The size of the two clones are indicated in parentheses. Also indicated is the distance from the ends of the first and last known exons of *Mitf* to the ends of each clone. BAC Mi1 lacks 14.2 kb of DNA with respect to the first nucleotide of exon 1A whereas it contains an additional 47.5 kb of DNA from the last known nucleotide of exon 9. Similarly, BAC Mi2 lacks 76 kb with respect to the first nucleotide of exon 1A and contains additional 93.9 kb at the 3′-end. The relative sizes of the exons and introns are indicated but are not shown in the correct proportional sizes. The locations of amino acid residues Ser73 and Ser409 are indicated. (B) The two-step recombineering strategy used for generating the Ser73 and Ser409 mutations. The hit oligo was recombineered into the *Mitf* locus, and successful recombinants were screened using Hit-specific primers. After verifying the recombineered Hit clone, the Fix oligo was recombineered into the positive Hit-BAC and screened by PCR using fix-specific oligos. The resulting mutated BAC clones were further screened for the presence of the mutation and the absence of the Hit sequences before they were used for generating transgenic mice. (C) BAC transgene rescue of the *Mitf^mi-ew* mutation. All three mice are homozygous for the *Mitf^mi-ew* mutation, and therefore all should have the phenotype of the mouse on the left showing a white coat and microphthalmia. However, the two mice on the right also carry the BAC Mi1 clone, which fully rescues both phenotypes.

therefore considered a null mutation. Homozygotes are white and have severe microphthalmia although there is no evidence of a dominant or semidominant phenotype in any tissue, including bone (HODGKINSON *et al.* 1993; STEINGRÍMSSON *et al.* 2004). Two different transgenic lines were made on the *Mitf^mi-vga9* mutant background and, as can be seen in Figure 2, C and D, the BAC-Mi1 clone fully rescues the *Mitf^mi-vga9* mutant phenotype, with respect to both coat color and eye development. Both lines are maintained as homozygotes for both the *Mitf^mi-vga9* mutation and the BAC transgenes. Thus, we conclude that the BAC clones Mi1 and Mi2 rescue the *Mitf* mutant phenotype fully and therefore contain all the sequences necessary for normal *Mitf* expression and function in melanocytes and RPE cells. These results suggest that exon 1A is not necessary for Mitf function in these cell types. This is interesting in light of the relatively high level of conservation of amino acid sequence in this exon between different mammalian

species (>95% amino acid conservation between mice and humans) (HALLSSON *et al.* 2007).

Phenotypic rescue of serine-mutant BACs: To determine the *in vivo* significance of the Ser73 and Ser409 phosphorylation sites of MITF, we mutated these sites in the BAC-Mi2 clone to alanine using the recombineering strategy described in Figure 1B. We generated three different mutant BAC clones: a Ser73Ala mutation (changing AGC to GCC), a Ser409Ala mutation (changing AGT to GCC), and a clone containing the Ser73Ala and Ser409Ala mutations. After confirming the presence of each mutation, the BACs were used to generate transgenic mice using *Mitf^mi-vga9*/+ heterozygous zygotes, and the resulting transgenic animals were mated to generate animals that were homozygous for the *Mitf^mi-vga9* mutation and for the BAC transgene.

Three independent lines that carry the BAC containing the Ser73Ala mutation were generated (Figure 3, A–C). These lines all rescue the *Mitf^mi-vga9* phenotype

FIGURE 2.—Wild-type BAC clones rescue *Mitf* mutant phenotypes. The two wild-type BAC clones rescue *Mitf* mutant phenotypes completely. (A and B) The BAC Mi1 and Mi2 wild-type BAC clones rescue the phenotype of the *Mitf*^{mi-ew} mutation fully; no belly spot is visible in the mice (right panels). (C and D) The BAC Mi1 clone also rescues the *Mitf*^{mi-vga9} loss-of-function phenotype fully as seen in two independent transgenic lines. Again, not even a belly spot is visible, suggesting full rescue. The inserts show the eyes of the BAC transgenic mice.

significantly, but to a different extent. The TG21055-Ser73Ala line fully rescues the eye developmental phenotype whereas coat color is partially rescued, resulting in mice with normal eyes, a white belly, and white spots over the rest of the coat (Figure 3A). The TG8260-Ser73Ala line fully rescues the eye defect of the *Mitf*^{mi-vga9} mutation, and the coat color is rescued apart from a belly spot (Figure 3B). The TG8250-Ser73Ala line does not rescue the eye developmental defect but rescues the

coat color defect nearly fully, leaving a small white belly spot (Figure 3C). Together, the rescue observed with these lines suggests that the Ser73Ala mutant BAC can rescue the eye developmental phenotype and the coat color defects of *Mitf* mutations, apart from leaving an unpigmented belly spot. Small belly spots are commonly seen in the C57BL/6J strain (ARNHEITER 2007), on which the *Mitf*^{mi-ew} and *Mitf*^{mi-vga9} mutations are maintained, suggesting that in fact we observe almost full rescue with the TG8260-Ser73Ala line and full rescue with respect to coat color in the TG8250-Ser73Ala line. The difference in the ability of these three lines to rescue the phenotype probably reflects the integration sites involved.

We obtained one line each of transgenic mice that carry the Ser409Ala single mutant and the Ser73Ala; Ser409Ala double-mutant BAC clones (Figure 3, D and E). Both the TG11223-Ser409 transgenic line and the double-mutant TG32643-Ser73/409Ala transgenic line rescue the eye and coat color phenotype of the *Mitf*^{mi-vga9} mutation fully, resulting in normally pigmented mice (Figure 3, D and E). In the TG11223-Ser409 line, some animals show a belly spot (Figure 3D) whereas a belly spot is rarely seen in the double-mutant TG32643-Ser73/409Ala line. Together, these data suggest that the Ser73Ala and Ser409Ala mutations can fully rescue the *Mitf*^{mi-vga9} mutation, even in a double-mutant combination. This indicates that these two serines are not essential for MITF function during mouse melanocyte development.

Splicing of Mitf is affected in the Ser73Ala BACs: A knock-in mutation has been made in the *Mitf* gene where Ser73 was replaced with alanine (BISMUTH *et al.* 2008). This knock-in mutation is the very same mutation that we made in the BAC mice, except it also introduced a silent *Apa*LI restriction site a few base pairs upstream of the Ser73Ala mutation and a LoxP site in the downstream intron (BISMUTH *et al.* 2008). Mice homozygous for this knock-in mutation are normally pigmented and have normal eyes, supporting our conclusions from the BAC rescue experiments. However, the knock-in mutation affected splicing of the *Mitf* gene such that a normally minor alternative product lacking exon 2B became the major product (BISMUTH *et al.* 2008). We used RT–PCR on heart tissue to determine if the splicing of *Mitf* was affected in the BAC transgenic mice. Heart tissue expresses the *Mitf* mRNA at a significant level in wild-type mice as well as in most of the available *Mitf* mutants but is absent in hearts from animals carrying the *Mitf*^{mi-vga9} mutation (HODGKINSON *et al.* 1993; STEINGRÍMSSON *et al.* 1994). As all the BAC clones are maintained on the *Mitf*^{mi-vga9} mutant background, the only *Mitf* mRNA expressed in the BAC transgenic mice is derived from the BAC clone. The primers used span from exon 1B to exon 3 and resulted in two bands in wild-type mice: a 359-bp full-length band and a 191-bp band that represents a product lacking exon 2B (Figure 4).
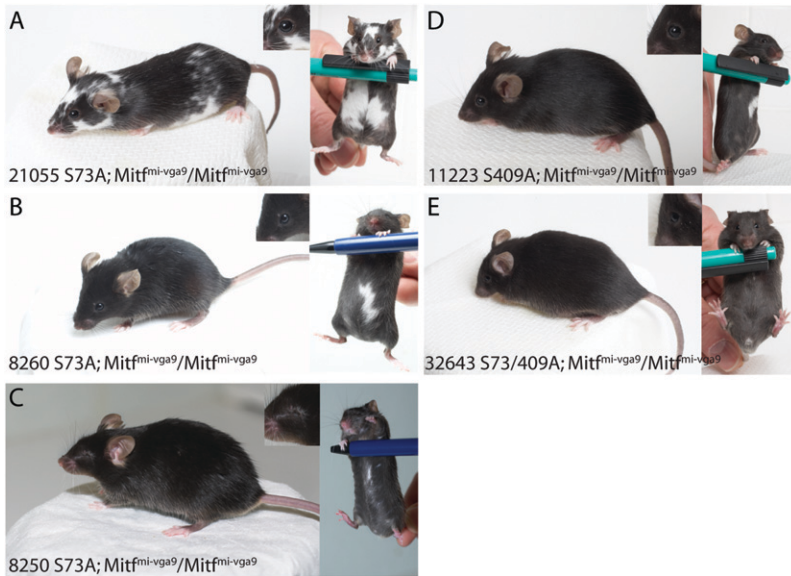
FIGURE 3.—The mutant BAC clones Ser73Ala and Ser409Ala rescue the *Mitf* mutant phenotype. The BAC clones containing the Ser73Ala and Ser409Ala mutations rescue the phenotype of the *Mitf*[mi-vga9] loss-of-function mutation fully in either single or double-mutant combination. (A–C) Three different transgene lines that contain the Ser73Ala mutation were obtained. The line 21055 fully rescues the microphthalmia associated with the *Mitf*[mi-vga9] mutation whereas the coat color phenotype is rescued only partially (A). These animals lack pigmentation on the belly and have small unpigmented spots over the rest of the body. However, a significant proportion of the coat is pigmented, suggesting significant rescue in this line; the spots on the back are rather small, suggesting failure to rescue during late melanocyte development or differentiation. (B) The line 8260 rescues the phenotype fully, apart from a small belly spot (right). (C) The line 8250 rescues the coat color phenotype fully except for a minor belly streak seen in most of the animals. However, eye development is not rescued. The phenotypic differences in these three lines are most likely due to differences in the integration event of the transgenes. (D) The Ser409Ala mutant BAC clone can rescue the phenotype of the *Mitf*[mi-vga9] mutation completely, although many animals show a significant belly spot. (E) The BAC clone containing the double mutation Ser73Ala; Ser409Ala can also rescue the phenotype of the *Mitf*[mi-vga9] mutation completely, and in this case belly spots are rarely seen. The inserts show the eyes of the BAC transgenic mice.

The same bands are present in all the transgenic lines, and all show the same ratio of the two bands, except in the BAC lines that contain the Ser73Ala mutation, either alone or in the double-mutant combination with Ser409. Quantitative PCR (qPCR) analysis shows that in the two lines containing the Ser73Ala mutation there is approximately three times more of the smaller 198-bp band lacking exon 2B than in either the other BAC lines or wild-type mice (Figure 4). This suggests that the presence of the Ser73Ala mutation alone is sufficient to affect splicing of exon 2B such that the shorter product becomes more abundant than in the other lines. This is consistent with the splicing defect observed in the Ser73Ala knock-in mice and with the idea that the sequence around the Ser73 codon represents an exon splice enhancer sequence (BISMUTH *et al.* 2008). The only difference between the Ser73Ala knock-in and BAC transgene mutations is the ratio of the two bands. In the knock-in mice, the shorter band represents a majority (~90%) of the resulting *Mitf* products whereas in the BAC mice it is ~40–45%. This difference may be due to the more extensive changes introduced in the knock-in mutation than in the BAC as the knock-in mutation generated an *Apa*LI restriction site (changing a C to a T 10 bp upstream of the Ser73Ala codon) and placed a floxed neo-cassette in a nearby intron, in addition to the Ser73Ala modification.

Exon 2 deletion mutations: Ser73 is located in exon 2B of the *Mitf* gene. The phenotype of the Ser73Ala knock-in (BISMUTH *et al.* 2008) and BAC transgenic mice suggests that the absence of exon 2B in a majority of the *Mitf* transcripts produced is not detrimental for the function of the MITF protein. To detail the functional role of exon 2 of *Mitf*, we created three different deletion mutations in the BAC and generated transgenic mice on the *Mitf*[mi-vga9] background. The mutations represent a deletion of intron 1 and exon 2A, resulting in a fusion of exon 1M with exon 2B [del(int1/2A)]; deletion of exon 2B and intron 2, creating a fusion of exon 2a and exon 3 [del(2B/int2)]; and deletion of only intron 2, creating a fusion of exon 2B and exon 3 [del(int2)] (Figure 5A). For the del(int1/2A) and del(2B/int2) deletions, we obtained one transgenic line each, whereas for del(int2) we obtained two independent lines (Figure 5, B–E). The transgenic line carrying the del(int1/2A) deletion fully rescues the eye developmental defect of the *Mitf*[mi-vga9] mutation as well as the coat color, except for a belly spot (Figure 5B). Similarly, the del(2B/int2) transgene rescues the eye and coat color phenotype, apart from a small belly spot seen in most of the mice (Figure 5C). The two different del(int2) lines fully rescue the eye developmental phenotype of the *Mitf*[mi-vga9] mutation and the coat color phenotype, leaving a large belly spot and occasional white spots on other body regions (Figure 5, D and E). Interestingly, the two independent del(int2) lines have near-identical phenotypes.

We used RT–PCR to characterize expression and splicing of the *Mitf* gene in mice carrying the BAC-deletion mutations. First, we characterized expression of *Mitf* in heart tissue using primers extending from exon 1B to exon 3 or exon 4 (Figure 6A). In wild-type hearts, both primer sets produced two bands, representing a full-length transcript and a transcript lacking exon 2B, at a ratio of ~20:1 (Figure 6A). This is consistent with previous results (HALLSSON *et al.* 2000). In the
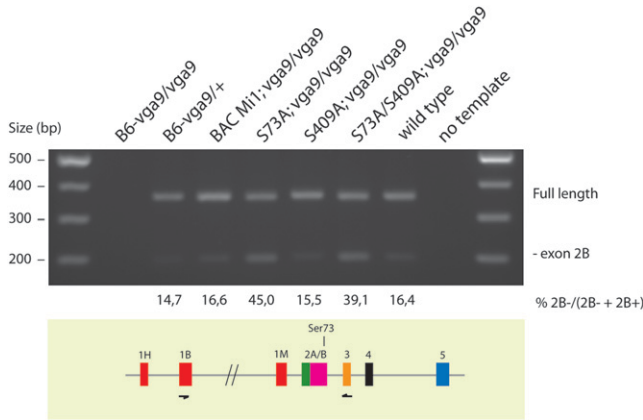
FIGURE 4.—Splicing of exon 2 of *Mitf* is affected in the BAC transgenic mice containing the Ser73Ala mutation. RT–PCR was used to determine if splicing of exon 2 was affected in the BAC transgenic mice. Primers spanning from exons 1B to exon 3 (bottom) were used to amplify cDNAs isolated from the indicated BAC transgenic mice (top). No products were amplified in the homozygous *Mitf* $^{mi\text{-}vga9}$ mice whereas two bands were amplified in *Mitf* $^{mi\text{-}vga9}$ heterozygotes and in wild-type mice as well as in all the other BAC transgenic lines. The 359-bp top band represents the full-length product whereas the 191-bp bottom band represents an alternative product lacking exon 2B. Quantitative PCR using exon-specific primers was used to determine the relative amount of these two products in the different BAC transgenic lines. The results are indicated as the percentage of the product lacking exon 2B over the total amount of products lacking and containing exon 2B. The shorter product is relatively more abundant in the lines that contain the Ser73Ala mutation.

del(int1/2A) transgenic mice, each primer set resulted in the production of only one product. The size of these products suggests that they are missing exons 2A and 2B, and this was further confirmed by sequencing. These results were expected in this line as exons 2A and 2B are not split by an intron; in wild-type mice, the mRNA product lacking exon 2B is produced by the use of an alternative splice donor. As the deletion removes intron 1 and exon 2A, this alternative splice donor is not present and the only possible product in this case fuses exon 1B to exon 3. RT–PCR performed on hearts from the del(2B/int2) deletion mutation also results in only one product for each primer set (Figure 6A). Sequencing shows that, as expected, these products lack exon 2B whereas exon 2A is present.

The two del(int2) transgenic lines (13627 and 13628) affect mRNA splicing similarly, with some minor differences. Using primers from exon 1B to exon 3, only one product is produced, representing a full-length *Mitf* transcript (Figure 6A, top). This transcript is produced from the transgene by the splicing of exon 1B to exon 2A/B, which is then fused directly to exon 3 due to the deletion of intron 2. No alternative product is detected lacking exon 2B using this primer combination because

such a product is not possible when intron 2 has been removed. RT–PCR performed using primers from exon 1B to exon 4 results in two products in the transgenic line TG13628, representing a full-length product and a truncated product lacking exons 2B and 3 (Figure 6A, bottom). This smaller PCR product is produced by alternative splicing from exon 2A to exon 4 using the alternative splice donor at the juncture of exons 2A and B, which is then spliced to the acceptor in exon 4 rather than the acceptor in exon 3 as it is lacking due to the deletion. In transgenic line TG13627, only the smaller product lacking exons 2B and 3 is detected using the primer set from exon 1B to exon 4, whereas in line TG13628, the full-length product is also detected. Clearly, the full-length product is expressed in both transgenic lines at some level since a product is observed using the primers extending from exon 1B to exon 3. However, the absence of such a product in the TG13627 line using the exon 1B to exon 4 primer set suggests that this is a minor product and that the majority of transcripts are lacking exons 2B and 3. Nevertheless, the phenotypes of both transgenic lines are nearly identical (Figure 5, D and E), suggesting that, although a MITF protein lacking exons 2B and 3 is able to rescue eye development fully, it is not quite able to fully rescue the coat color phenotype of the *Mitf* $^{mi\text{-}vga9}$ mutation. Because the transgene deleting only exon 2B can rescue the phenotype, this would indicate that the simultaneous absence of both domains encoded by exons 2B and 3 is detrimental to function. Alternatively, it is possible that exon 3 plays a more important functional role than exon 2B. Sequence comparison of representative species of the mammalian, avian, amphibian, fish, and echinoderm lineages reveals that exon 3 is found only in mammals and birds. Although this means that exon 3 is not evolutionarily conserved in all species, it is possible that the recruitment and retention of this sequence in mammalian and avian species indicates a functional role. At this point, however, this function is not known.

The deletion del(int1/2A) fuses exons 1M and 2B of *Mitf*, and as exon 1M is melanocyte specific and thus not expressed in the heart, we also performed RT–PCR on skin tissue from all deletion strains using primers extending from exon 1M to exon 4. As seen in Figure 6B, the RT–PCR results indicate the presence of the expected *Mitf* transcripts in skin. Using primers extending from exon 1M to exon 4 results in a 440-bp normal band whereas in the transgenic strain carrying the del(int1/2A) deletion this results in two bands: one major 380-bp band missing exon 2A and one minor 212-bp band missing both exons 2A and 2B. This suggests that the splice donor in exon 1M is functional when fused to exon 2B. This is consistent with the fact that the splice donor sequence remains the same (ACCAG/GT). In the del(2B/int2) strain, the primer pair resulted in a major 272-bp band missing exon 2B and a minor band lacking also exons 2A and 3. This smaller product

A

Genomic structure:

wild type

del(int1/2A)

del(2B/int2)

del(int2)

B

7082 del(int1/2A); Mitf^mi-vga9^/Mitf^mi-vga9^

C

22816 del(2B/int2); Mitf^mi-vga9^/Mitf^mi-vga9^

D

13627 del(int2) ; Mitf^mi-vga9^/Mitf^mi-vga9^

E

13628 del(int2); Mitf^mi-vga9^/Mitf^mi-vga9^
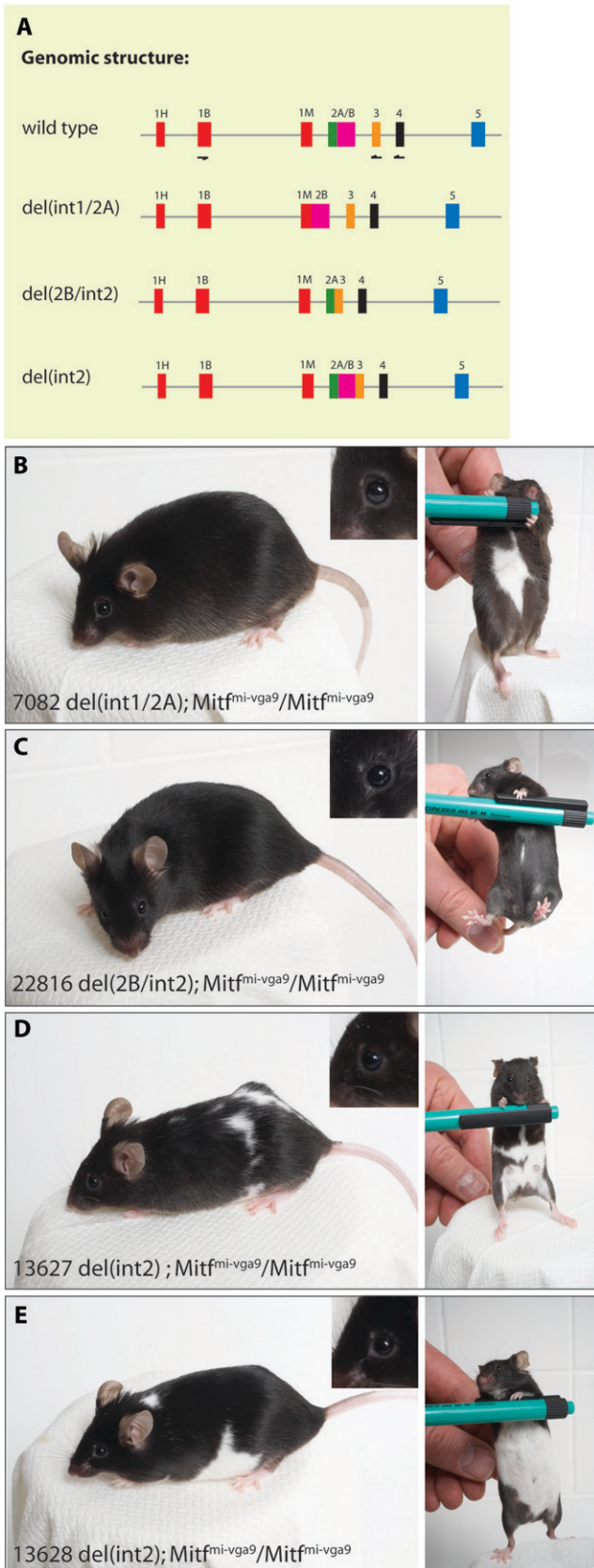
represents a rare alternative *Mitf* transcript, where exon 1M has been spliced directly to exon 4. A similar *Mitf* transcript, extending from exon 1A to exon 4, has been shown to exist in heart (HALLSSON *et al.* 2000). In the two del(int2) transgenic strains, the only product present is a 188-bp band lacking exons 2B and 3. This is the major band seen in skin from the mutants, suggesting that the full-length transcript observed in heart is rarely, if at all, expressed in skin.

Our analysis of *Mitf* expression and splicing in skin is consistent with the results obtained using heart tissue. Because the del(int1/2A) and del(2B/int2) BAC transgenes rescue the *Mitf*^mi-vga9^ phenotype (Figure 5, B and C), we conclude that neither exon 2A nor exon 2B is essential for MITF function in eye or melanocyte development in the mouse. Exon 2B contains the codon for amino acid Ser73, so these results are consistent with results obtained by the Ser73Ala knock-in mutation (BISMUTH *et al.* 2008) and the Ser73Ala BAC transgenes described above. These results are rather surprising because a section of exon 2A (amino acids 11–39) is highly conserved among different species (HALLSSON *et al.* 2007).

The *Mitf*^mi-enu22(398)^ mutation: Analysis of a novel *Mitf* mutation called *Mitf*^mi-enu22(398)^ provides independent support for the molecular and phenotypic characteristics of the deletion mutations. This mutation was induced by treatment with ethylnitrosourea as part of a genetic screen performed at the Novartis Institute for Functional Genomics. Animals homozygous for this mutation have normally developed eyes, a white belly, and large unpigmented spots over the rest of the coat (Figure 7A). The phenotype is remarkably similar to the phenotype of the del(int2) transgenic lines on the *Mitf*^mi-vga9^ background (compare Figure 7A to Figure 5, D and E), except *Mitf*^mi-enu22(398)^ has a bit more extensive white spotting. Sequence analysis shows that the mutation is a C-to-T change at nucleotide position 205 of the cDNA, which introduces a stop codon in exon 2A,

FIGURE 5.—Generation and analysis of exon 2 deletion mutations. Several different deletion mutations were generated to analyze the role of exons 2A and B in Mitf function. (A) The genomic structure of the deletion mutations that were generated. The exons are indicated as colored boxes. (B–E) The transgenic mice carrying the different deletion mutations. The left panels show a side view of the mice and the right panels show the belly region. The inserts in the upper right corner of the left panels show the eyes of the BAC transgenic mice. (B) The BAC carrying the del(int1/2A) mutation rescues the phenotype of the *Mitf*^mi-vga9^ mutation to a large extent, leaving a sizable belly spot. (C) The BAC carrying the del(2B/int2) mutation also rescues the phenotype of the *Mitf*^mi-vga9^ mutation; a small belly spot is visible in most of the animals. (D and E) Two different transgenic lines were generated which carry the BAC with the del(int2) mutation. These lines fully rescue the microphthalmia associated with the *Mitf*^mi-vga9^ mutation whereas coat color is rescued only partially. These animals have an extensive belly spot in addition to white spots over the rest of the coat.
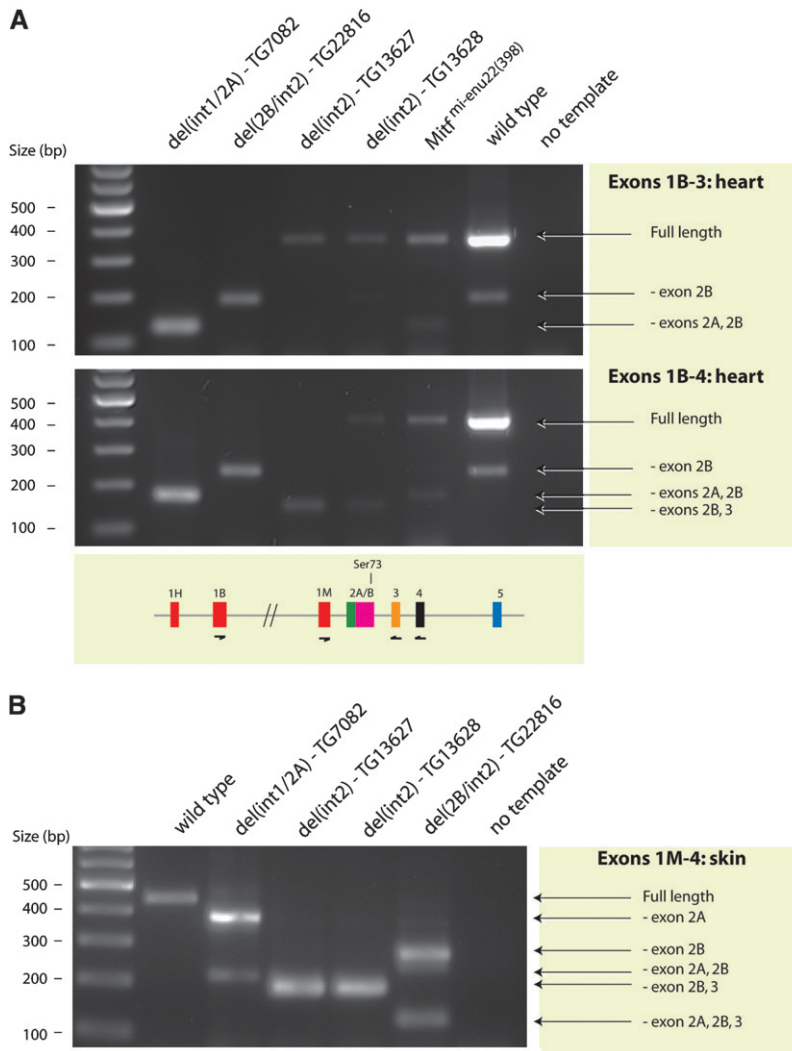
FIGURE 6.—Analysis of splicing in BAC transgenic mice carrying *Mitf* deletion mutations. RT–PCR analysis was performed on both heart and skin to characterize *Mitf* transcripts in mice carrying the BAC deletion mutations. (A) Splicing of *Mitf* in heart tissue was characterized using two primer sets. The first primer set (top) extended from exon 1B to exon 3. In wild-type mice, these primers result in two bands: a full-length 359-bp band and a shorter 191-bp band lacking exon 2B. The full-length band is more prominent, representing 90–95% of the product. In the del(int1/2A) mutation, a single 131-bp PCR product was made, representing a transcript lacking both exons 2A and 2B. Because exon 2A is missing, the only product possible is made by splicing exon 1B directly to exon 3. In the del(2B/int2) mutation, only the 191-bp product lacking exon 2B is generated, as expected. The two del(int2) lines generate only the full-length product. The *Mitf*[mi-enu22(398)] mice express both the full-length product and the 131-bp product missing both exons 2A and 2B. The second primer pair (bottom) extended from exon 1B to exon 4. The results are largely the same as above. The only exception is that the two del(int2) lines produce a smaller band in addition to the full-length product observed in line TG13628. The smaller product represents transcripts that lack exons 2B and 3, suggesting that exon 2B is spliced directly to exon 4 in these mice. (B) Splicing of Mitf in skin was analyzed using primers extending from exon 1M to exon 4. In control (B6) animals, this primer set results in the production of a single 440-bp full-length product. These primers result in two products in skin from mice carrying the del(int1/2A) deletion mutation, a 380-bp band representing a transcript lacking exon 2A, and a smaller 212-bp band lacking exons 2A and 2B. This deletion fuses exon 1M directly to exon 2B so none of the products will contain exon 2A. However, the smaller product suggests that the splice donor in exon 1M is still active and that this exon can be fused directly to exon 3. The del(2B/int2) deletion also results in the production of two fragments using this primer set: a 272-bp fragment lacking exon 2B and a fragment lacking exons 2A, 2B, and 3. In these mice, exon 2A is fused directly to exon 3 so all products will lack exon 2B. The small alternative product indicates that exon 1M can also be spliced directly to exon 4. Both del(int2) lines result in only one product, representing a transcript lacking exons 2B and 3. Clearly, the absence of intron 2 leads to the skipping of the two flanking exons, and the only product produced fuses exon 2A directly to exon 4.

changing glutamine at position 26 of the MITF protein to STOP (Figure 7B). This would terminate the MITF protein prematurely, producing only a short peptide. RT–PCR analysis using primers that extend from exon 1B to exon 9 results in multiple bands in wild-type hearts, indicating the multiple alternative splice products made; sequencing confirms that the full-length product is the most prominent product and that another prominent product lacks exon 2B (Figure 7C). However, in hearts from *Mitf*[mi-enu22(398)] homozygous animals, the major *Mitf* product lacks exons 2A, 2B, and 3, resulting in a product in which exon 1B is fused to exon 4 (Figure 7C). A functional protein can be made although it lacks the domains encoded by these three exons. The molecular characteristics of this mutation are similar to the del(int2) transgenic lines on the *Mitf*[mi-vga9] background in that all

are lacking exons 2B and 3. They are different, however, in that the del(int2) lines retain exon 2A and express the full-length wild-type transcript at a low level, at least in heart, whereas in *Mitf*[mi-enu22(398)] hearts, exon 2A is largely missing. The full-length RNA product is also made in *Mitf*[mi-enu22(398)] animals, as well as a product lacking exons 2A and 2B (Figure 6A). However, the full-length transcript can be translated only into a truncated peptide. The phenotypic similarity of animals carrying the del(int2) BACs and the *Mitf*[mi-enu22(398)] mutations suggests that the transgenic approach accurately reflects the functional aspect of *Mitf* during melanocyte and eye development.

The *Mitf*[mi-black-and-white spot] (*Mitf*[mi-bws]) mutation also results in black and white animals (HALLSSON *et al.* 2000). The molecular defect described in this mutation is an alteration in a splice acceptor site 12 bp upstream of
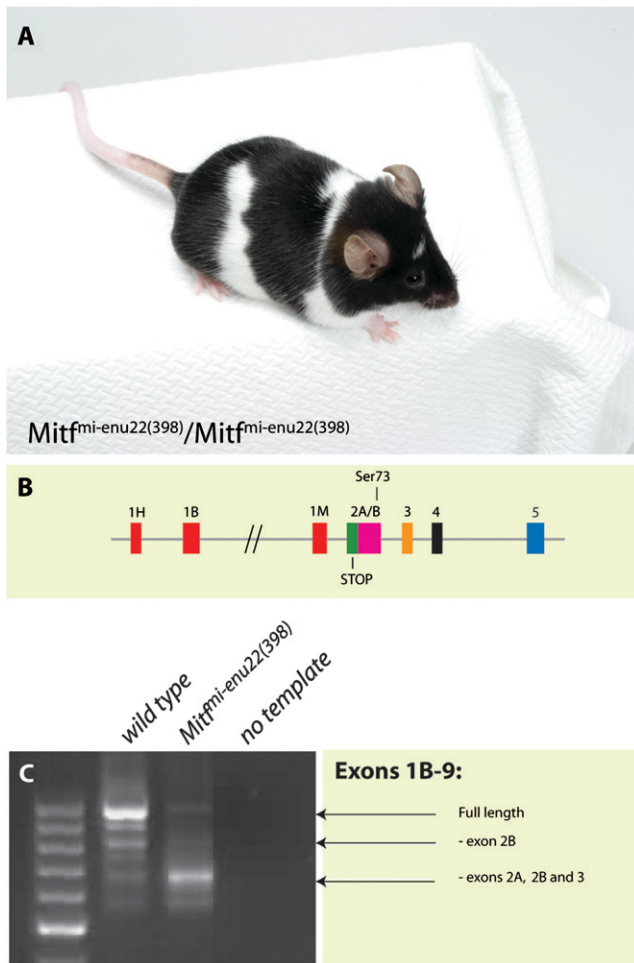
FIGURE 7.—Molecular and phenotypic characterization of the *Mitf^mi-enu22(398)* mutation. (A) The phenotype of the *Mitf^mi-enu22(398)* mutation. The mice have normal eye size. However, although they have extensive white belly spots and white spots over the rest of the body, a significant portion of their coat is normally pigmented. (B) The mutation associated with this phenotype is a stop codon in exon 2A of the *Mitf* gene. The position of the Ser73 amino acid is also indicated. (C) Characterization of splicing of the *Mitf* gene in normal and *Mitf^mi-enu22(398)* mutant mice using primers extending from exon 1B to exon 9. In normal mice, this results in the production of a major 997-bp full-length band and several alternative splice products, including the 829-bp product lacking exon 2B. In the *Mitf^mi-enu22(398)* mutation, the major 685-bp product is lacking exons 2A, 2B, and 3.

exon 2A, which results in partial exon skipping such that exon 2B is missing in a significant portion of the transcripts (HALLSSON *et al.* 2000). This is therefore not consistent with our BAC results or with our analysis of the *Mitf^mi-enu22(398)* mutation. Thus, we used quantitative PCR to characterize the expression of the *Mitf* gene in the *Mitf^mi-bws* mutation. This shows that ~40% of *Mitf* transcripts in the hearts of *Mitf^mi-bws* animals lack exon 2B. However, the total expression of the *Mitf* transcript is only 9.5% in *Mitf^mi-bws* animals as compared to wild type when analyzed using primers from exon 6 to exon 7 or from exon 7 to exon 8. Thus, the level of Mitf expression

is significantly affected in *Mitf^mi-bws* animals. At present, it is not well understood how the intron mutation found in *Mitf^mi-bws* results in the alternative splicing of a downstream exon or how it affects expression of the gene.

Relative quantification of MITF expression in BAC transgenic mice: To determine the expression level of the *Mitf* gene in BAC transgenic mice, we performed qPCR analysis on tissues from the transgenic animals as well as from controls. We followed the protocols and recommendations of NOLAN *et al.* (2006) and tested for inhibitory factors using the SPUD assay, tested 12 different housekeeping genes to identify the most stable reference gene (we used *Hprt1*), and determined amplification efficiency for each primer pair used. The primers used for quantifying *Mitf* extend from exon 6 to exon 8 and should quantify all currently know splice forms of the gene. We measured expression in hearts from three animals and skin from two animals of each genotype, and each reaction was performed in duplicate using identical amounts of total RNA in each case. Expression of *Mitf* was first determined in heart, a tissue that expresses significant levels of *Mitf* in wild-type mice, as well as in mutants that lack melanocytes and show severe microphthalmia (STEINGRÍMSSON *et al.* 1994). In the *Mitf^mi-vga9* mutants, however, we detected no *Mitf* expression because no significant difference was found in *Mitf* expression between cDNA samples prepared from *Mitf^mi-vga9* homozygotes and from no-template controls (average cycle threshold values were 32.5 ± 0.95 and 33.2 ± 1.34, respectively). Thus, the *Mitf^mi-vga9* mutants do not express the *Mitf* gene in heart, and the only transcripts detected in the BAC transgenic lines must therefore be expressed from the transgenes and not from the *Mitf^mi-vga9* locus.

The results of the qPCR analysis in heart are presented in Table 4 as the fold change of *Mitf* expression as compared to the control after normalization. The data show that expression of the *Mitf* transcript in heart from the BAC transgenic lines ranges from −1.15-fold to 0.55-fold as compared to controls. Interestingly, expression of *Mitf* in *Mitf^mi-vga9* heterozygotes is −0.9-fold less than in controls, indicating that they have half the amount of the *Mitf* transcript as compared to controls. This is exactly as expected, given that these animals express *Mitf* from only one copy of the gene. Expression of *Mitf* in the BAC-Mi1 transgene, which contains the wild-type BAC, is very similar to controls or −0.17-fold. This suggests that the BAC construct truly replicates expression of the wild-type *Mitf* gene in heart. These data confirm both the robustness of our qPCR analysis and the BAC transgene rescue method. Analysis of *Mitf* expression in the remaining BAC transgenic lines shows that expression in heart is in most cases similar to wild type, or lower [the Ser73Ala, Ser73Ala;Ser409Ala double mutant, del(2B/int2), Ser409Ala, del(int2)13628, and del(int1/2A) transgenic lines]. In only one case is *Mitf* expressed at a level higher than seen in the controls [the

TABLE 4

Relative expression of Mitf in heart and skin

	Fold change[a]			
	Heart		Skin	
B6	0	±0,62	0	±1.51
B6-vga9/+	−0.90	±0,26	−1.05	±0.33
BAC-Mi1	−0.17	±0,62	−0.22	±1.70
Ser73Ala	−0.50	±0,32	−1.31	±1.53
Ser409Ala	−0.82	±0,19	−2.04	±2.55
Ser73/409Ala	−0.13	±0,60	−4.80	±0.25
del(int2)13627	0.55	±0,25	−0.19	±1.73
del(int2)13628	−0.88	±1,40	−1.27	±1.68
del(int1/2A)	−1.15	±0,53	−1.70	±3.45
del(2B/int2)	−0.52	±0,60	−2.18	±2.00

[a] Relative to the reference gene Hprt1.

BAC transgene line del(int2)13627]. This line, however, shows a phenotype identical to the phenotype of the del(int2)13628 line, suggesting that expression levels are less important for phenotypic expression than the molecular defect involved. The results suggest that the BAC transgenes more or less replicate the wild-type expression of the *Mitf* gene in heart.

Melanocytes are the cells responsible for pigmentation. To determine *Mitf* expression levels in melanocytes of the BAC transgenic mice, skin of transgenic 5-day-old mice was prepared for RNA isolation, cDNAs were prepared, and qPCR analysis was performed as described above. The results are shown in Table 4 and show that in all the lines but one, *Mitf* is expressed at lower levels than seen in controls, ranging from 0.19- to 4.80-fold lower expression. Again, the expression of *Mitf* in *Mitf*[mi-vga9] heterozygotes is at half the level seen in the controls, suggesting that our method accurately measures expression of the gene in skin. In conclusion, the gene expression data in both heart and skin show that most of the transgenes express *Mitf* at a level similar to or lower than what is seen in wild-type mice. Thus, we conclude that the rescue observed is not due to overexpression of the *Mitf* gene. The level of transcripts is of course only one parameter in determining the levels of functional protein, and it is possible that the cells can compensate for the lack of transcripts through regulating translation, activity, or other aspects of producing a transcriptionally active MITF protein.

Conclusions: We have used a BAC transgene rescue method to determine the *in vivo* functional role of two phospho-acceptor sites in the MITF protein, serine 73 and serine 409, as well as of two domains encoded by exons 2A and 2B. These two phospho-acceptor sites had previously been suggested to be important for MITF function, although the effects observed differed depending on the cell type used. HEMESATH *et al.* (1998) showed that in baby hamster kidney (BHK) cells the wild-type and Ser73Ala mutant MITF proteins can ac-

tivate expression of the tyrosinase promoter at equal levels. However, in BHK cells harboring constitutively active Raf, the wild-type protein was a 2.5 times more potent activator of tyrosinase than the Ser73Ala mutant protein, suggesting that the Raf signaling pathway affects transactivation specifically through this phospho-acceptor site. PRICE *et al.* (1998) showed that the increased transcription activity was due to the recruitment of the co-activator p300 to the phosphorylated protein; a protein containing the Ser73Ala mutation failed to activate expression. WU *et al.* (2000) then showed that in NIH3T3 cells the Ser73Ala mutant protein is significantly less able to activate transcription than the wild-type protein whereas the Ser409Ala mutation is similar to wild type. In these cells, the Ser73Ala; Ser409Ala double-mutant protein is not able to activate transcription at all. In 501mel melanoma cells, the wild type, Ser73Ala, and Ser409Ala proteins are similar in their transcription activation potential whereas the double mutant is transcriptionally inactive (WU *et al.* 2000). From these data and the fact that the phenotypes of *Mitf*, *Kitl*, and *Kit* mutations all affect coat color, we would have expected that mutations in these phospho-acceptor sites in mice would result in mice with a white coat color. Our results, however, indicate that, *in vivo*, neither of the two phospho-acceptor sites is essential for MITF function.

We believe that our results accurately depict the *in vivo* roles of these amino acids and domains. First, the BAC transgene rescue strategy clearly works because wild-type BACs rescue the *Mitf*[mi-vga9] phenotype fully and replicate the endogenous expression of the *Mitf* gene. It should be emphasized that this strategy calls for the rescue of a severe phenotype, where melanocytes are missing and where RPE cells have lost their normal identity. The strategy therefore represents a "positive" test of *Mitf* function *in vivo*. Second, expression of the *Mitf* gene in heart and skin from the BAC transgenic mice is in the range (or less) observed in wild-type and *Mitf*[mi-vga9] heterozygous mice, which have normal coat color and eye development. This suggests that the transgenes have not resulted in overexpression of the *Mitf* gene, which might have confounded the results. Third, our results are consistent with a previous characterization of the role of Ser73 using a knock-in strategy (BISMUTH *et al.* 2008). Fourth, the phenotype and molecular defect of the *Mitf*[mi-enu22(398)] mutation is consistent with the phenotype of the del(int2) mutations, suggesting that the BAC constructs can replicate the phenotype of *Mitf* mutations.

So how can we then explain the discrepancy between the *in vitro* and the *in vivo* observations? One possible explanation is that *in vivo*, alternative phospho-acceptor sites take over when Ser73 and Ser409 have been mutated to alanine, thus leading to total rescue of the phenotype. Due to differences in the environment (culture conditions *vs.* *in vivo* development) this compensation may not take place in the *in vitro* assays, leading to the

observed effects on transcription activation and protein stability. This would imply that there is a redundancy in the signaling mechanisms to ensure that the protein receives the signal. Detailed analysis of MITF phosphorylation would need to be performed to test this. Another possibility is that KITL and KIT signal to other phospho-acceptor sites in the MITF protein. Several other phospho-acceptor sites are known in the MITF protein, including Ser307, which has been shown to be phosphorylated by p38 upon RANKL/RANK signaling in osteoclasts (Mansky *et al.* 2002), and Ser298, which was shown to be phosphorylated by GSK3β (Takeda *et al.* 2000). In contrast to KIT signaling to MITF in melanocytes, the RANKL/RANK signaling to Ser307 of MITF in osteoclasts appears to be persistent and not transient (Mansky *et al.* 2002). Little is known about the biochemical consequences or *in vivo* significance of this signaling event, and currently it is not known if it is also active in melanocytes. Studies seem to indicate that Ser298 is crucial for normal DNA binding and transcription activation of the MITF protein and that this phosphorylation is an important regulatory event. At present it is not clear whether Ser298 is constitutively phosphorylated or regulated in a cell-specific or developmental manner or whether it is a *bona fide* GSK3β phospho-acceptor site (Frame and Cohen 2001). In addition to Ser307 and Ser298, additional, yet uncharacterized phosphorylation sites of functional importance may exist in the MITF protein. A third explanation for the differences observed between the *in vivo* and *in vitro* results might be that the *in vitro* assays used to determine protein stability and transcription activation (Wu *et al.* 2000; Xu *et al.* 2000) are more sensitive to subtle differences between the different mutations than the *in vivo* assay. This higher sensitivity would lead to significant differences in cell assays, whereas no such differences would be detected in the organism. The mice do not appear to be sensitive to *Mitf* dose as the phenotype of some of the mutant BAC-transgenic mice is normal although the *Mitf* gene is expressed at lower levels as compared to wild-type controls. In some cases, only ~30% of the *Mitf* transcript is sufficient for a normal phenotype, and in *Mitf^{mi-bws}* mutant mice the *Mitf* gene is expressed at only 9.5% level in heart as compared to wild-type controls. Reduced expression would presumably enhance the sensitivity of *Mitf* to mutations that affect the function of the gene. Finally, it is possible that the stability of the MITF protein is affected in the Ser73Ala and Ser409Ala BAC mutant mice such that the protein is more stable and therefore present for a longer time in the BAC mice than in wild-type mice. This would be consistent with the observation that the Ser73Ala; Ser409Ala double-mutant protein is more stable in cell culture than the wild-type protein (Wu *et al.* 2000; Xu *et al.* 2000). Despite being a poor transcription activator *in vivo* (due to the Ser73 and Ser409 mutations), a more stable protein might be able to rescue

the phenotype as it persists for longer in the cells. If this were the case, one would not necessarily expect *Kitl* and *Kit* mutant mice to share a phenotype with *Mitf* mutations as the lack of signaling would presumably lead to a more stable MITF protein. This requires further studies on protein stability in the transgenic mice.

Our studies have also addressed the roles of several different exons in the *Mitf* gene. The lack of exon 1A from both BAC constructs used in these studies indicates that this exon is dispensable for *Mitf* function in melanocytes as well as during eye development. Like exon 1A, exons 2A and 2B seem to be dispensable for Mitf function. This is consistent with the normal phenotype of Ser73Ala mutant mice. The del(int2) BACs, together with the del(int1/2A) and del(2B/int2) mutations, suggest that exon 3 may play a more important role than exon 2. However, the role of exon 3 is currently not known.

In summary, our studies imply that signaling to *Mitf* may be more complex *in vivo* than the *in vitro* experiments would suggest. It may involve alternative phospho-acceptor sites or even alternative signaling mechanisms downstream of the *Kit* and *Kitl* signaling pathway. Further studies on this fascinating transcription factor are needed to characterize the role of signaling in melanocyte development.

LITERATURE CITED

Arnheiter, H., 2007 Mammalian paramutation: A tail's tale? Pigment Cell Res. **20:** 36–40.

Bharti, K., J. Debbache, J. Wang and H. Arnheiter, 2009 The basic helix-loop-helix leucine-zipper gene Mitf: analysis of alternative promoter choice and splicing in *Methods in Molecular Biology: Transcription Factors,* edited by Paul Higgins. Humana Press, Totowa, NJ (in press).

Bismuth, K., S. Skuntz, J. H. Hallsson, E. Pak, A. S. Dutra *et al.*, 2008 An unstable targeted allele of the mouse *Mitf* gene with a high somatic and germline reversion rate. Genetics **178:** 259–272.

Dubreuil, P., L. Forrester, R. Rottapel, M. Reedijk, J. Fujita *et al.*, 1991 The c-fms gene complements the mitogenic defect in mast cells derived from mutant W mice but not mi (microphthalmia) mice. Proc. Natl. Acad. Sci. USA **88:** 2341–2345.

Frame, S., and P. Cohen, 2001 GSK3 takes centre stage more than 20 years after its discovery. Biochem. J. **359:** 1–16.

Hallsson, J. H., J. Favor, C. Hodgkinson, T. Glaser, M. L. Lamoreux *et al.*, 2000 Genomic, transcriptional and mutational analysis of the mouse microphthalmia locus. Genetics **155:** 291–300.

Hallsson, J. H., B. S. Haflidadottir, A. Schepsky, H. Arnheiter and E. Steingrímsson, 2007 Evolutionary sequence comparison of the Mitf gene reveals novel conserved domains. Pigment Cell Res. **20:** 185–200.

Hemesath, T. J., E. Steingrímsson, G. McGill, M. J. Hansen, J. Vaught *et al.*, 1994 Microphthalmia, a critical factor in

melanocyte development, defines a discrete transcription factor family. Genes Dev. **8:** 2770–2780.

HEMESATH, T. J., E. R. PRICE, C. TAKEMOTO, T. BADALIAN and D. E. FISHER, 1998 MAP kinase links the transcription factor microphthalmia to c-Kit signalling in melanocytes. Nature **391:** 298–301.

HODGKINSON, C. A., K. J. MOORE, A. NAKAYAMA, E. STEINGRÍMSSON, N. G. COPELAND *et al.*, 1993 Mutations at the mouse microphthalmia locus are associated with defects in a gene encoding a novel basic-helix-loop-helix-zipper protein. Cell **74:** 395–404.

HOGAN, B., R. BEDDINGTON, F. COSTANTINI and E. LACY, 1994 *Manipulating the Mouse Embryo: A Laboratory Manual.* Cold Spring Harbor Laboratory Press, Cold Spring Harbor, NY.

HOU, L., and W. J. PAVAN, 2008 Transcriptional and signaling regulation in neural crest stem cell-derived melanocyte development: Do all roads lead to Mitf? Cell Res. **18:** 1163–1176.

JENKINS, N. A., N. G. COPELAND, B. A. TAYLOR and B. K. LEE, 1982 Organization, distribution and stability of endogenous ecotropic murine leukemia virus DNA sequences in chromosomes of *Mus musculus.* J. Virol. **43:** 26–36.

LEVY, C., M. KHALED and D. E. FISHER, 2006 MITF: master regulator of melanocyte development and melanoma oncogene. Trends Mol. Med. **12:** 406–414.

MANSKY, K. C., U. SANKAR, J. HAN and M. C. OSTROWSKI, 2002 Microphthalmia transcription factor is a target of the p38 MAPK pathway in response to receptor activator of NF-kappa B ligand signaling. J. Biol. Chem. **277:** 11077–11083.

NISHIMURA, E. K., S. R. GRANTER and D. E. FISHER, 2005 Mechanisms of hair graying: incomplete melanocyte stem cell maintenance in the niche. Science **307:** 720–724.

NOLAN, T., R. E. HANDS, W. OGUNKOLADE and S. A. BUSTIN, 2006 SPUD: a quantitative PCR assay for the detection of inhibitors in nucleic acid preparations. Anal. Biochem. **351:** 308–310.

PRICE, E. R., H. F. DING, T. BADALIAN, S. BHATTACHARYA, C. TAKEMOTO *et al.*, 1998 Lineage-specific signaling in melanocytes. C-kit stimulation recruits p300/CBP to microphthalmia. J. Biol. Chem. **273:** 17983–17986.

ROZEN, S., and H. SHALETSKY, 2000 Primer3 on the WWW for general users and for biologist programmers., pp. 365–386 in *Bioinformatics Methods and Protocols: Methods in Molecular Biology*, edited by S. KRAWETZ and S. MISENER. Humana Press, Totowa, NJ.

SHARAN, S. K., A. PYLE, V. COPPOLA, J. BABUS, S. SWAMINATHAN *et al.*, 2004 BRCA2 deficiency in mice leads to meiotic impairment and infertility. Development **131:** 131–142.

STEINGRÍMSSON, E., K. J. MOORE, M. L. LAMOREUX, A. R. FERRE-D'AMARE, S. K. BURLEY *et al.*, 1994 Molecular basis of mouse microphthalmia (mi) mutations helps explain their developmental and phenotypic consequences. Nat. Genet. **8:** 256–263.

STEINGRÍMSSON, E., L. TESSAROLLO, B. PATHAK, L. HOU, H. ARNHEITER *et al.*, 2002 Mitf and Tfe3, two members of the Mitf-Tfe family of bHLH-Zip transcription factors, have important but functionally redundant roles in osteoclast development. Proc. Natl. Acad. Sci. USA **99:** 4477–4482.

STEINGRÍMSSON, E., N. G. COPELAND and N. A. JENKINS, 2004 Melanocytes and the microphthalmia transcription factor network. Annu. Rev. Genet. **38:** 365–411.

TAKEDA, K., C. TAKEMOTO, I. KOBAYASHI, A. WATANABE, Y. NOBUKUNI *et al.*, 2000 Ser298 of MITF, a mutation site in Waardenburg syndrome type 2, is a phosphorylation site with functional significance. Hum. Mol. Genet. **9:** 125–132.

VANDESOMPELE, J., K. DE PRETER, F. PATTYN, B. POPPE, N. VAN ROY *et al.*, 2002 Accurate normalization of real-time quantitative RT-PCR data by geometric averaging of multiple internal control genes. Genome Biol **3:** RESEARCH0034.

WARMING, S., N. COSTANTINO, D. L. COURT, N. A. JENKINS and N. G. COPELAND, 2005 Simple and highly efficient BAC recombineering using galK selection. Nucleic Acids Res. **33:** e36.

WU, M., T. J. HEMESATH, C. M. TAKEMOTO, M. A. HORSTMANN, A. G. WELLS *et al.*, 2000 c-Kit triggers dual phosphorylations, which couple activation and degradation of the essential melanocyte factor Mi. Genes Dev. **14:** 301–312.

XU, W., L. GONG, M. M. HADDAD, O. BISCHOF, J. CAMPISI *et al.*, 2000 Regulation of microphthalmia-associated transcription factor MITF protein levels by association with the ubiquitin-conjugating enzyme hUBC9. Exp. Cell Res. **255:** 135–143.

YANG, Y., and S. K. SHARAN, 2003 A simple two-step, 'hit and fix' method to generate subtle mutations in BACs using short denatured PCR fragments. Nucleic Acids Res. **31:** e80.

4 – Le codon S73 du gène *Mitf* fait partie d'une séquence d'enhancer exonique d'épissage impliquée dans la régulation de l'incorporation de l'exon 2B.

Le facteur de transcription MITF, connu principalement pour ses implications dans la biologie des melanocytes et du mélanome, représente une famille d'isoformes générées par l'utilisation alternative de différents promoteurs, par épissage alternatif et par modification post-traductionnelles. Ici nous démontrons que le codon 73 de Mitf ne code pas seulement pour une serine, dont la phosphorylation contrôle l'activité et la stabilité de la protéine, mais fait également partie d'une séquence d'enhencer exonique d'épissage, qui régule l'incorporation de l'exon 2B sur lequel il se situe. D'ailleurs, de nombreuses permutations de ce codon dans des mini gènes, y compris un codon alternatif codant pour une serine, provoquent tous une augmentation de l'exclusion de l'exon 2B. L'exclusion de cet exon est favorisée par un membre de la famille des SR protéines SRp30c et son inclusion par SF2/ASF, SRp55, SC35 et SRp40. Ce dernier facteur présente une affinité de fixation à l'enhancer exonique différente entre le codon témoin et le codon muté pour une alanine non-phosphorylable à cette position. Les résultats présentés ici confirment les observations précédentes chez la souris avec l'allèle *Mitf*$^{mi-S73A}$ et suggèrent que la phosphorylation de MITF est non seulement régulée par les kinases correspondantes mais aussi de façon indirecte par les activités relatives de SR protéines spécifiques.

Les travaux liés à cette étude sont décrits dans l'**Article 4**.

The following results present the identification of the molecular mechanism involved in the linkage between the *Mitf^mi-S73A* allele and the large exclusion of exon 2B, which contains the mutated codon.

We first determined that the alteration of the exon 2B inclusion, originally observed *in vivo* in the *Mitf^mi-S73A* knock-in mice, can be reproduced in an heterologous context *in vitro* using an artificial pCMV driven *Mitf* minigene, which contains only the genomic sequence from exon 1M to exon 3. We then demonstrated that the splice alteration is solely caused by the S73A mutation and many of the 14 possible additional permutations leading to amino acid changes at this position. Hence, a S73S mutation displays a similar reduction of exon 2B inclusion *in vitro*. Hence, the splice alterations observed in *Mitf^mi-S73A* mice is unlikely due to the mutated protein itself as it can be reproduced with expression of wild-type protein.

 In silico prediction tools reveal that the S73 codon sequence is part of an Exonic Splice Enhancer sequence (ESE) for several splice regulatory serine/arginine rich proteins. In fact in silico, the tools predict that one of them, SRp40, has a reduced binding score for all of the 15 distinctly mutated codons.

We then characterized a number of SR proteins for their effects on the splicing pattern of the Mitf minigene by co-transfection of SR protein expression vector and the minigene in HEK293 cells. The results show that SRp40 in addition to SRp55 and SC35, is able to correct exon 2B exclusion in presence of the S73A mutation; SRp30c increases exon 2B exclusion.

Additional biochemical tests indicate that SRP40 indeed shows reduced affinity for short mutated RNA compared to wild type RNA on RNA affinity columns.

We, therefore, propose a straightforward mechanism involving SR proteins to explain the fine-tuning of Mitf exon 2B alternative splicing regulation. A relative excess of SRp40

(and some others) over SRp30c leads to exon 2B inclusion, and a relative excess of SRp30c over SRP40 (and others) to its exclusion. In experiments not shown, we find that different cell lines, or cells in different proliferative stages, change the ratios of these proteins and that their relative ratios correlate with the relative inclusion or exclusion of exon 2B from Mitf. Because the absence of exon 2B is associated with a reduced anti-proliferative activity, relative SR protein abundance would be predicted to regulate cell proliferation. The equilibrium between exon 2B inclusion and exclusion can therefore be easily switched by tweaking the relative activity of SR protein, ultimately affecting the proliferative state of melanocytes.

The experimental work related to this study is presented in the following **Article 4**.

Article 4

The codon for a phosphoacceptor site in the microphthalmia-associated transcription factor MITF has a role as regulator of splicing.

(DRAFT)

THE CODON FOR A PHOSPHOACCEPTOR SITE IN THE MICROPHTHALMIA-ASSOCIATED TRANSCRIPTION FACTOR MITF HAS A ROLE AS REGULATOR OF ALTERNATIVE SPLICING

Xin Wang[1], Julien Debbache[1], Ruiling Mu[2], Susan Skuntz[1], Keren Bismuth[1], and Heinz Arnheiter[1]

From the Mammalian Development Section[1], National Institute of Neurological Disorders and Stroke, and the GNRL Immunology Section, National Institute of Allergy and Infectious Diseases[2], National Institutes of Health, Bethesda, Maryland 20892

Running head: Regulation of MITF splicing

Address correspondence to: Heinz Arnheiter, MD, 35 CONVENT DRIVE, Building 35/2A-201, Bethesda, MD 20892-3706. Fax 301-480-2737; E-mail: ha3p@nih.gov

The transcription factor MITF, known primarily for its roles in pigment cell biology and melanoma, represents a family of isoforms generated by alternative promoter use, alternative splicing, and post-tanslational modifications. Here we show that MITF codon-73 not only encodes a serine whose phosphorylation regulates the protein's activity and stability, but is also part of an exonic splice enhancer sequence that regulates the splicing of its own exon, exon 2B. In fact, multiple permutations of the codon in corresponding minigenes, including an alternative serine codon, all lead to enhanced exclusion of this exon. Exon 2B exclusion is favored by the serine/arginine-rich protein SRp30c and its inclusion by SF2/ASF, SRp55, SC35 and SRp40, the latter showing differential binding to the splice enhancer sequence containing the wild-type codon versus one encoding a non-phosphorylatable alanine at this position. The results are consistent with previous observations in knock-in mice with serine-73-to-alanine mutations and suggest that MITF phosphorylation is not only regulated directly by the corresponding kinases and phosphatases but also indirectly via the relative activities of specific serine/arginine-rich splicing factors.

The vertebrate microphthalmia-associated transcription factor MITF is a basic-helix-loop-helix-leucine zipper protein that controls many cellular processes, most notably specification, proliferation and differentiation of melanin-bearing pigment cells. Mutations in *Mitf*, which have been found from fish to man, commonly affect pigmentation of the integument and, depending on the species, also the development of the eye and inner ear. In humans, heterozygosity for *MITF* mutations are associated with Waardenburg type IIa and Tietz syndrome which are characterized by pigment abnormalities in skin and iris, premature hair greying, and varying degrees of congenital hearing loss (1,2). Recently, *MITF* has also been found to function as a "lineage addiction" oncogene during melanoma formation (3).

Over the years it has become clear that MITF is not a single protein but a family of isoforms which are generated by alternative promoter use, alternative splicing, and post-translational modifications. For instance, based on in vitro data, MITF serine-73 is phosphorylated by the MAP kinase pathway through the action of ERK1/2 (4). Serine-73 phosphorylation increases the protein's activity but also promotes, along with phosphorylation at serine 409, its degradation (5). To assess whether serine-73 phosphorylation would play a role in vivo, we have previously generated knock-in mice in which two basepairs of the highly conserved codon for serine-73 were changed in such a way that a non-phosphorylatable alanine-73 is encoded instead (hereafter called S73A mutation) (6). To our surprise, this codon change led to a change in the extent of alternative splicing of subexon 2B, the very subexon that harbors codon-73. In mice and other mammals, exon 2 of Mitf is comprised of two subexons, subexon 2A (hereafter called exon 2A) containing 20 codons and subexon 2B (hereafter called exon 2B) containing 56 codons. Quantitative real-time RT-PCR assays and direct cDNA cloning have shown that normally, approximately 90% of Mitf mRNAs from heart, skin, or melanocytes of mice contain both exons and about 10% lack exon 2B, meaning that in this case, exon 2A is spliced directly into exon 3

(6-9). In contrast, in the knock-in mice, only 10% of Mitf mRNAs contain both exons 2A and 2B and 90% lack exon 2B. This splice alteration was confirmed in BAC rescue transgenics carrying the S73A mutation (7). Although the splice change does not lead to an overt phenotype, it does affect, at least in vitro, cell proliferation: MITF containing exon 2B is anti-proliferative whilst MITF lacking exon 2B leaves cell proliferation untouched (unpublished observation). Intriguingly, a line of metastatic human melanoma has also recently been found to generate MITF mRNAs lacking exon 2B as a result of a mutation at the 5' splice site of this exon (10). Presumably, this mutation is one of many that has arisen to allow for increased rates of melanoma cell proliferation.

The above findings, together with the recognition that alternative splicing is an important parameter of eukaryotic gene function in general, prompted us to analyze the MITF codon-73-associated splice change in greater detail. The formation of mature mRNAs from intron-containing pre-mRNAs has been shown to depend on both cis-acting RNA elements and trans-acting factors. The main cis-acting elements are short, degenerate sequences around the 5' splice site, the 3' splice site, the polypyrimidine tract, and the branch point, and they are recognized by a set of trans-acting factors which together form the catalytically active spliceosome (11,12). Splice site selection is influenced by a family of conserved serine/arginine-rich (SR) proteins, which interact with specific RNA sequences via their RNA recognition domains and with spliceosomal proteins via their RS domains. Specific RNA sequence elements are called exonic or intronic splice enhancer elements (ESEs or ISEs) when they lead to inclusion of a particular exon, and exonic or intronic splice silencer elements (ESSs or ISSs) when they lead to exon skipping. In fact, the splicing of most alternative exons is controlled by multiple enhancer and silencer elements. It has to be kept in mind, however, that many of these elements are not strict silencers or enhancers but can act in one way or the other depending on the context, including their position relative to an alternatively spliced exon (13).

Given the above information, it was conceivable that codon-73 of Mitf is part of a splice regulating cis-acting sequence and as such might interact with specific SR proteins. Indeed, we found that the mutated two bases are part of an ESE and that they regulate the interaction with SRp40. Moreover, we found that while overexpression of SRp40 and other SR proteins leads to enhanced inclusion of exon 2B, overexpression of SRp30c leads to its enhanced exclusion. The results suggest that distinct SR proteins and their relative activities in a given cell are part of the regulatory splicing machinery that determines MITF alternative splicing and hence, potentially, the rate of cell proliferation both during development and in malignancies.

Experimental Procedures

Mice and preparation of melanocyte lines- Mice carrying the Ser-73-Ala mutation along with a silent *Apa*LI site have been described (designation: *Mitf*$^{tm1.1Arnh}$, kept on a background that involves 129S1/Sv*C3H/He*C57BL/6). They were crossed with mice carrying a targeted mutation in the *Ink4a/Arf* locus (designated *Cdkn2a*^{tm1Rdp}, background C57BL/6) to generate mice homozygous for both mutations. Dorsal skin of one-day old pups from these latter mice and homozygous *Cdkn2a*^{tm1Rdp} mice were used to produce melanocyte cultures according to established protocols. The cells were kept in RPMI 10% fetal calf serum, 1% non-essential amino acids, 1% penicillin/streptomycin, 1% L-Glutamine, 200 nM 12-O-tetradecanoylphorbol-13-acetate (TPA) (Sigma), 40 pM hFGF2 (Peprotech), 20 ng/ml mSCF (Peprotech) and 10 nM EDN3 (Sigma). After 2-5 days, cultures were trypsinized and approximately 100 pigmented cells were picked microscopically, using a 40x objective. These were designated passage 1 of pure melanocytes. Cells were usually used between passage 10 and 20 to assess splicing of endogenous Mitf RNAs.

Cell culture and transfections- For most transfection experiments, HEK293 cells which do not express MITF were used. Some experiments were done in ARPE19 cells which are *MITF* expressing spontaneously immortalized human retinal pigment epithelium cells. The cells were grown in DMEM

supplemented with 10% fetal bovine serum and penicillin-streptomycin (Invitrogen, Carlsbad, CA, USA). Cotransfections in HEK293 cells were done at 60-70% confluence in 60 mm dishes, using Effectene reagent (Qiagen) and one μg each of minigene DNA and SR protein expression vector. ARPE19 cell transfections were done with two μg of the respective minigene constructs in 30 mm wells. Melanocytes were transfected with one μg each of minigene DNA, SR protein expression vector, and a green fluorescent protein (GFP) expression vector. Twenty-four to 48h after transfection, the cells were harvested and processed for RNA isolation. RNAs were analyzed by regular and real time reverse transcriptase (RT)-PCR.

RT-PCR- Total RNA was isolated from transfected cells, using RNA easy mini kit (QIAGEN), and converted into cDNA using superscript III reverse transcriptase (Invitrogen). The location of Mitf primers used for regular and qRT-PCR are shown in Fig. 1A, and their sequences along with those of primers specific for control genes and used for normalizations are shown in Suppl. Table S1. qRT-PCR reactions were performed as recently described in detail (14).

Immunoblotting- Extracts from transfected HEK293 cells and purified SR fusion proteins were separated by 4-12% Bis-Tris SDS-PAGE and transferred to nitrocellulose membranes (Bio-Rad Laboratories). Splicing factor-specific primary antibodies were: Rabbit-anti-SC35 (1:2,000 dilution, Abcam), Goat anti-SRp40 (1:200 dilution, Santa Cruz Biotechnology), and mouse monoclonal anti-SRp30c (1:500 dilution, Abcam). A mouse anti-His Tag (1:1,000 dilution, Millipore) was used to detect the tag-only *E. coli*-derived protein. Horseradish peroxidase-conjugated goat anti-rabbit, goat anti-mouse, or mouse anti-goat IgG (Thermo scientific) were employed as secondary antibodies. In addition, the mouse monoclonal antibody MAb104, which recognizes a phosphoepitope on SR proteins, was produced from a corresponding hybridoma line (ATCC CRL-2067) and used in conjunction with a horseradish peroxidase-conjugated goat anti-mouse IgM antibody (1:20,000, Thermo

scientific). A mouse monoclonal anti-β-actin antibody (1:25,000 dilution, Sigma) was used for control purposes. Positive bands were detected using the chemiluminescent blotting kit (SuperSignal West Pico, Thermo scientific).

Constructs and plasmids- Minigene constructs: A 2.55 kb fragment containing exon 1M to exon 3 of the *Mitf* gene was generated by PCR amplification from mouse *Mitf* Bac 369-C11 (6,7). This fragment was cloned into the pcDNA3.1/V5-His TOPO TA mammalian expression vector (Invitrogen) following the manufacturer's instructions. Mutated minigenes were engineered using appropriate mutated primers and the quickchange site-directed mutagenesis kit (Stratagene). Plasmids were verified by sequencing. SRp20, SRp30c, SRp40, SRp55, SC35, SF2, and 9G8 pCG expression vectors were a gift from Dr. Thomas Misteli.

Synthesis of DIG-labelled riboprobes- Synthesis of the Mitf wild-type or mutated exon 2B DIG-labelled riboprobe was carried out by in vitro transcription of an Mitf wild-type or mutated exon 2B cDNA inserted into pBluscript II. To generate sense probes, the plasmid was linearized with XhoI and transcribed with T3 RNA polymerase in the presence of DIG-UTP (Roche). The 3xCE9 plasmid (kindly provided by Benoit Chabot) was linearized with *Cla*I and transcribed with T3 RNA polymerase (EPICENTRE Biotechnologies) to serve as a positive control for binding of SRp30c protein. The h 3'int and ESE2-DSX plasmids (kindly provided by Francisco E. Baralle and James G. Patton) were linearized with *Nde*I and *Mlu*I separately and transcribed with T7 RNA polymerase (EPICENTRE Biotechnologies) to serve as positive controls for binding of SRp40 or SC35 protein, respectively.

Cloning, expression and purification of SR fusion proteins- The sequences for the respective SR proteins were amplified by PCR from corresponding plasmids, digested with *Sal*I and *Not*I, and cloned into a modified pET30a (Novagen) vector allowing for expression of fusion proteins with GB1 and NusA protein and an 8x His tag. Coding frames were verified by DNA sequencing. The respective plasmids were expressed in *E. coli* BL21 (DE3). The cultures were grown at 37^0C and induced by using auto-induction LB media (Novagen) for 12 h. The

cells were harvested by centrifugation at 4000 rpm, 30 min, at 4^0C, resuspended in 25 mM Tris pH 8.0, 125 mM NaCl, 10 mM imidazole, lysed by sonication, and centrifuged at 30,000 rpm for 25 min at 4^0C. The lysate, supernatant, and pellet were subjected to SDS–PAGE followed by Coomassie staining. The supernatant was then loaded onto HisPrep™ FF 16/10 affinity columns (GE Healthcare). The columns were washed, and using an imidazole gradient on an AKTA-FPLC system, the proteins were eluted at 60-100 mM imidazole at 4^0C. Desalting was done with Zeba™ Micro Desalt spin columns.

Nitrocellulose filter binding assays- RNA-protein filter-binding assays (15) were adapted to accommodate the use of DIG-labelled RNA probes instead of radioactive probes in the following ways. Mixes between protein and DIG-labeled RNAs were incubated in a total volume of 50 μl binding buffer for 30 min at 30^0C and spotted onto the pretreated MF membranes. The filters were then washed with 4 ml binding buffer, and 1 μl of this solution were spotted at 2-fold dilutions (in triplicates) onto nitrocellulose membranes. The membranes were then subjected to chemiluminescent detection of the DIG labeled probe following the manufacturer's instructions (Roche). We found that unlike purified *E.coli*-derived SRp40 and SC35, purified *E.coli*-derived SRp30c had no measurable binding activity to positive control 3xCE9 probes. However, after incubation with a HeLa cytosolic S100 extract lacking SR proteins but containing all other required splicing components (Protein One), SRp30c showed binding activity.

RNA affinity chromatography- Chromatography columns were prepared and coupled with modified RNAs as described (16,17) (wild-type sequence: 5'-N6-GCA CCC AAC AGC CCU AUG GCU A-3'; mutant sequence: 5'-N6-GCA CCC AAC GCC CCU AUG GCU A-3', 100 nmol each, Thermo scientific Dharmacon). Control columns were prepared in the same way except that RNA was omitted in the coupling step. Purified SR proteins (10 μg each) were applied to the columns and incubated at room temperature for 20 min in binding buffer (20 mM Tris-HCl [pH 8.0], 100 mM KCl, 0.5 mM dithiothreitol [DTT], 0.2 mM EDTA, 5% glycerol), and the flow-through reapplied for 10

min. After two washes with the binding buffer, bound proteins were eluted by step-wise application of binding buffer containing 0.2, 0.5, 0.75 and 1.0 M KCl concentrations, followed by a final elution in 8 M urea-20 mM Tris-HCl (pH 8.0). Fractions were separated on 4-12% Bis-Tris SDS-polyacrylamide gels, and the proteins analyzed by silver staining.

RESULTS

The S73A codon change is sufficient to affect exon 2B splicing. The original observation of the splice alteration associated with the S73A mutation in *Mitf* was made in vivo in knock-in mice. In these mice, the mutated allele also contains a silent *Apa*LI restriction site close to the S73A mutation and a loxP site in intron 2 (6). Therefore, we first tested which of these alterations were responsible for the splice change, using appropriate mini-genes transfected into cultured cells. To this end, we engineered constructs that placed genomic mouse *Mitf* sequences spanning exon 1M to exon 3 between a CMV promoter and a bovine growth hormone polyadenylation site. As shown in Fig. 1, these sequences contained either the wild-type serine codon at position 73 or the S73A change alone or in conjunction with the *Apa*LI site. We did not include the loxP site as we reasoned that this site was unlikely to influence exon 2B splicing because mice harboring just the loxP site or the full loxP-neomycine resistance cassette showed similar 2B+/2B- ratios. The minigene constructs were expressed in HEK293 cells and the RNAs subjected to an RT-PCR assay that allowed distinction between Mitf RNAs containing or lacking exon 2B. Fig. 1C shows the results using primers a and g from Fig. 1A. In wild type, a predominant band of 345 bp was seen, corresponding to the sequence containing exon 2B, and a barely visible band of 177 bp, corresponding to the sequence lacking exon 2B. The three mutant constructs all showed a clearly visible band of 177 bp in addition to one of 345 bp, with the lowest apparent ratio of 2B+/2B- seen with the S73A mutation alone. These results indicated that the in vivo splice alteration could be reproduced in heterologous cells in vitro and that the S73A codon change was

sufficient to affect the respective splice choices in the context of a minigene.

Additional S73 codon changes, including an S73S codon change, affect exon 2B splicing. The original S73A change involved the first two bases of the respective codon (**AG**C to **GC**C). Hence, we tested, again in minigenes, whether any of the additional 14 possible permutations of these two bases would affect splicing. The corresponding plasmids were generated by in vitro PCR site-directed mutagenesis, sequence-confirmed, and transfected into HEK293 and ARPE19 cells. The latter cells were chosen because they are derived from an *MITF* expressing, pigmented cell type, the human retinal pigment epithelium, express low amounts of endogenous MITF, and can be transfected with high efficiency. For HEK293 cells, RT-PCR was performed using the primer pair a/g (Fig. 1A,C), and for ARPE19 cells, the minigene-specific primer pair b/f (Fig. 1A) was used. The results showed that in both cell types, all mutations affected the exon 2B+/2B- ratio of Mitf RNAs to some extent (Fig. 2A, shown for ARPE19 cells). For quantification, we performed real time PCR assays as previously described in detail (14). For these assays, we used primers specific for either mouse *Mitf* exon 2A-3 (primer d, spanning the exon 2A-3 junction, and primer f in Fig. 1A) or exon 2B-3 (primer c, spanning the exon 2A-2B junction, and primer e in Fig. 1A) that yielded single bands when assayed by gel electrophoresis and did not show significant cross-priming on the inappropriate splice form (i.e. exon 2A-3 primers on 2B+ cDNA and vice versa) (three independent transfections, each assayed in triplicates). As shown at the bottom of Fig. 2A, the quantifications of splicing isoforms showed relatively large standard deviations, suggesting that splicing may be sensitive to slight variations in culture conditions between experiments. Nevertheless, the quantifications largely confirmed the observation made by gel electrophoresis. For instance, the average $2B^-/(2B^+ + 2B^-)$ ratio was nearly 0 in wt but 0.15 in S73A. Intriguingly, the most prominent change was seen with TCC, one of the alternative serine codons, which showed an average $2B^-/(2B^+ + 2B^-)$ ratio of 0.35. Hence, even a "silent" serine-

to-serine mutation may not easily be tolerated at this position.

The S73 codon is predicted to be part of an ESE that interacts with SR proteins. Given that all tested codon mutations altered exon 2B splicing, we concluded that the S73 codon is part of an ESE affected by mutation rather than that the different mutations would each have created a novel ESS. Using a bioinformatics approach, we next assessed whether the respective wild type sequence might indeed serve as an ESE, and, if so, which SR protein would be predicted to consistently show reduced binding when the sequence was mutated in any of the 15 ways tested above. To this end, we used the web-based ESE finder tool (18,19) and identified several putative sequence motifs in exon 2B predicted to bind SR proteins, among them also the sequence that included codon 73. As shown in Fig. 2B, above-threshold scores were noted for this sequence with respect to binding SRp40 and SF2/ASF, though not for SC35 and SRp55, the other two SR proteins represented by this informatics tool. Interestingly, all mutations reduced the binding scores for SRp40 while the scores for SF2/ASF were changed by some but not other mutated sequences. Furthermore, some of the mutations gave an above-threshold score for SC35 and SRp55 (Fig. 2B). Given these predictions, we proceeded to test the role of these SR proteins for alternative Mitf splicing and the potential interaction of these proteins with the corresponding Mitf RNA sequences.

SR proteins affect exon 2B splicing in transfected cells. To test the effects of overexpression of SR proteins on exon 2B splicing, we co-transfected the wild-type and S73A minigene constructs along with various SR protein expression vectors, alone and in combinations, into HEK293 cells and assessed the effciency of exon 2B splicing by regular and real time RT-PCR. As shown in Fig. 3A, western blot assays using antibodies specific for SRp30c, SC35 or SRp40 indicated that the individual SR proteins were expressed above the levels of the respective endogenous proteins. In fact, the endogenous proteins were below detection limit using these antibodies and exposure times although their corresponding RNAs could be revealed by RT-PCR (not shown). Using the monoclonal antibody

mAB104, which detects the phosphorylated, active forms of SR proteins, suggested that the overexpressed proteins were indeed active. As shown in Fig. 3B, overexpression of SC35, SRp40, SF2/ASF and SRp55 led to an increase in exon 2B inclusion compared to control, as did SRp20 (not shown), and this regardless of whether the minigene contained the wild-type or the S73A codon. Overexpression of 9G8, however, had little if any effect (not shown). Interestingly, overexpression of SRp30c led to a relative decrease in exon 2B inclusion, again regardless of whether the wild-type or S73A codon was present in the minigene. To assess whether these proteins were co-dominant or not, we then co-transfected equal amounts of expression vector for the negatively acting SRp30c with those for the positively acting SRp40 or SC35. As shown in Fig. 3C, in these assays, SC35 and SRp40 dominated over SRp30c. Furthermore, the effect of transfected SRp30c, SRp40 and SC35 on exon 2B splicing was dose-dependent (Suppl. Fig. S1A). Because splicing efficiency may depend in part on the amount of pre-mRNA a cell expresses, we also tested whether splicing of minigene-derived RNA depended on the amount of minigene DNA used for transfection. We did not, however, observe significant changes in the exon 2B splice ratio over a 19-fold concentration range of S73A minigene DNA, resulting in a 10-fold range of Mitf RNA levels (not shown) (Suppl. Fig. S1B). Taken together, the results suggested that Mitf minigene splicing was influenced by the relative levels of specific SR proteins.

SR proteins affect exon 2B splicing of endogenous Mitf RNA. To test whether the above experiments showing the effect of SR protein overexpression on splicing of minigene-derived RNA can be extended to endogenous Mitf RNA, we used lines of skin-derived melanocytes that were prepared from either *Mitf* wild-type or S73A mutant mice. Using a growth factor-enriched medium supplemented with TPA, such melanocytes can be propagated as pure cultures of pigmented cells. Because of their high expression of *Mitf*, however, non-transfected cells would contribute a high background of unaltered Mitf RNA, and so we used co-transfection of a green fluorescent protein expression vector along with the respective SR protein expression vector and standard fluorescence activated cell sorting to obtain a highly enriched population of transfectants before RT-PCR analysis. As shown in Fig. 3D, when SR protein expression vectors were omitted, sorted wild-type cells showed a ratio of exon $2B^-/(2B^+ +2B^-)$ RNA of approximately 0.3 while this ratio was about 0.7 in cells carrying the S73A mutation. Ectopic expression of SRp30c increased this ratio in both types of cells, to 0.45 and 0.95 respectively, and ectopic expression of SRp40 or SC35 decreased the ratio to less than 0.05 in wild-type and 0.35-0.4 in S73A cells. We conclude, therefore, that as observed for minigene constructs, the respective SR proteins affect exon 2B splicing also of endogenous Mitf RNA.

Differential binding of SRp40 to wild type and S73A mutated Mitf RNA. The above experiments indicate that ectopically expressed SR proteins influence the efficiency of exon 2B inclusion in mature Mitf mRNA. They do not, however, address the question of whether this effect is mediated by direct binding of these proteins to Mitf RNA, and in particular to the sequence around codon-73, or whether it is due to indirect effects on other factors involved in the splicing reaction. To test for direct protein/RNA interactions, we first used a filter binding assay modified to allow for non-radioactive measurements. Digoxigenin-labeled target RNA corresponding to the wild-type or S73A exon 2B sequence (168 bases) was first prepared in vitro using appropriate plasmids. SRp40, SC35 and SRp30c fusion proteins were prepared in *E.coli* and purified by affinity chromatography, using the 8x His tag and appropriate His columns (Fig. 4A). After interaction of purified protein with labeled RNA, the mixtures were spotted onto MF filters. The filters were then washed, the flow-through collected, and an aliquot in serial dilutions assayed for the amount of free labeled RNA, using a filter spotting assay and antibody-mediated detection of digoxigenin. Each assay was done in triplicate and included published SR protein-specific positive controls and a bacterial neomycin resistance gene-derived RNA as negative control. The results are shown in Fig. 4B-E. SRp40 (Fig. 4B) showed high affinity binding to positive control and wild-type exon

2B RNA, lower affinity to S73A mutated RNA, and base line binding to the negative control RNA. This was consistent with the functional assays performed with SRp40 and suggested that indeed, SRp40 interacted with exon 2B RNA and that even though it might interact with multiple sites on this piece of RNA, codon-73 was likely part of a major binding site. SC35 (Fig. 4C) showed lower affinity binding compared to SRp40, but no significant difference was seen between binding to the wild-type or the S73A sequence. This was also consistent with the above functional assays. Nevertheless, as mentioned earlier, the ESE finder program predicted a high score for SC35 binding to the S73A sequence, though not the wild-type sequence. It was conceivable, therefore, that SC35 binding to other sites on exon 2B masked potential differences at the site of codon-73. Alternatively, the site at this codon, or its mutation, were irrelevant with respect to SC35 binding despite the binding score difference assigned to this site by the ESE finder tool. Unlike SRp40 and SC35, SRp30c (Fig. 4D) had to be activated by an SR protein-free Hela S100 extract in order to render it capable of interacting with the positive control RNA. Nevertheless, even when activated in this way, it showed no binding to exon 2B RNA, suggesting that exon 2B does not contain a binding site for SRp30c. Likewise, no binding was seen to a probe representing exon 2A (not shown). The results also indicated that the presence of the fusion tag on the recombinant proteins did not provide for unspecific interaction with exon 2B RNA. This latter point was confirmed in assays in which the tag alone, with no SR protein sequence, was used (Fig. 4E).

Differential binding of SRp40 to short RNAs containing codon-73. The above filter binding assays suggested that SRp40 binds to exon 2B target RNA and that this binding is influenced by the S73A mutation but do not positively identify the S73 codon as being part of the direct SRp40/RNA interaction. To define the binding site more precisely, we finally prepared RNA affinity columns containing equal amounts of covalently attached wild-type or S73A mutated, 22-base RNA sequences and used the columns to assess the binding and step-wise salt elution profile of the respective recombinant SR proteins. The results are shown in Fig. 5. After washing with 100 mM KCl, SRp40 could be eluted from the wild-type RNA column with 200-1000 mM KCl, giving positive signals on silver-stained polyacrylamide gels. In contrast, most of the SRp40 bound to the mutant RNA was eluted already with 500 mM KCl (Fig. 5A). The results suggested that the recombinant protein apparently consists of different subpopulations that bind RNA with different affinities, but that high affinity binding (resisting 500 mM KCl) was seen only on wild type but not mutant RNA. In contrast, SC35 gave similar elution profiles from wild-type and mutant RNA, suggesting similar affinities of this SR protein to the two types of RNAs (Fig. 5B). Only minimal amounts of SRp30c could be eluted from either of the two RNA columns (Fig. 5C). We did not, however, test Hela cell extract-activated SRp30c as we reasoned that the presence of the extract might interfere with binding on the columns. Figures 5A-C also show the elution profiles of the respective proteins from a column to which no RNA was coupled. While little if any SR proteins could be eluted from this column using KCl, stripping with 8 M urea eluted a small amount of residual protein (particularly SRp40 and SC35), suggesting that at least part of the proteins eluted with 8M urea from the RNA-containing columns was bound non-specifically. As expected, little if any SRp30c protein could be eluted from the RNA-free column (Fig. 5C), and the purified tag alone did also not show any binding (not shown). In sum, the results are in line with those obtained from filter binding assays and suggest that the effect of SRp30c on exon 2B skipping is mediated either by binding to another sequence, or sequences, of Mitf pre-mRNA, or indirectly by affecting other genes influencing the exon 2A/B splice choice.

DISCUSSION

Here we show that an AGC codon of the pigment cell transcription factor gene *Mitf* plays a crucial role not only as the codon for a functionally relevant phosphoacceptor serine but also as a part of an exonic splice enhancer (ESE) sequence regulating the alternative splicing of its own exon 2B. As shown in Fig. 6, this codon

and its surrounding sequence are largely conserved throughout vertebrate evolution, and so are the respective exon 2A/2B and exon 2B/intron 2 splice junctions. Nevertheless, neither of these splice junctions fully corresponds to consensus splice sequences (C/AAG▼GUA/GAGU) and hence, they may be suboptimal, rendering them particularly susceptible to regulation by transacting factors. Indeed, we find that splicing of this exon is antagonistically regulated by SRp30c on the one hand and SF2/ASF, SRp55, SC35 and SRp40 on the other. Among the latter, SRp40 binds the wild-type ESE sequence more efficiently than one containing a codon for a non-phosphorylatable alanine.

Interestingly, the opposing effects by SRp30c and the other SR proteins on exon 2B splicing appear to be independent of the cell type or the type of gene (minigene or endogenous gene) that we tested. This is in a way surprising given that overexpression (or knock-downs, for that matter) of these proteins would be expected to simultaneously affect the splicing patterns of RNAs of many genes, even genes encoding other splicing factors. It is reasonable to assume, therefore, that the SR proteins analyzed in this study all regulate exon 2B splicing by directly binding Mitf pre-mRNA, notwithstanding the fact that we have not so far been able to identify an SRp30c binding site near the alternative 5' splice site. In fact, it is likely that when ESE/SRp40 interactions are weak, SRp30c would guide the splicing machinery to the alternative 5' site and thereby favor exon 2A incorporation at the expense of still other potential splice events that would skip the entire exon 2 (2A and 2B). In this context, it is important to note that all Mitf isoforms, regardless of whether expressed from the M-promoter in melanocytes or additional upstream promoters in other cell types, usually contain exon 2A. Nevertheless, BAC rescue transgenics lacking intron 1/exon 2A have normal eyes and are normally pigmented, except for a white belly spot, indicating that exon 2A is largely dispensable (7).

ESE mutations can result in both reduced or enhanced interactions with specific RNA-binding SR proteins. As mentioned, the AGC-to-GCC (Ser-to-Ala) mutation led to a reduced

binding of SRp40, both predicted by the ESE finder informatics tool and confirmed in direct biochemical assays. In contrast, the ESE finder-predicted increase in affinity of the mutated site for SC35 could not be substantiated biochemically. Nevertheless, SC35 did show moderate binding to both the wild-type and the mutated ESE sequence, and when overexpressed, it increased incorporation of exon 2B expressed from minigenes or the endogenous gene. Because the predicted binding sites for SRp40 and SC35 overlap, it is unlikely that both proteins bind simultaneously to this site. One might assume, therefore, that because of the high avidity of SRp40 to the wild-type sequence and the similar avidities of SRp40 and SC35 to the mutated sequence, the wild-type sequence would preferentially be bound by SRp40 and the mutated sequence by either one of the two. Hence, if SC35 were expressed at higher levels than SRp40, it should be able to compensate for the loss of binding of SRp40 on the mutated sequence. In fact, in the cells tested, some codons showing relatively high SC35 binding scores (for instance GAC, encoding Asp, or AGC, encoding Thr, Fig. 2B) led to relatively modest increases in exon 2B exclusion, but others (for instance GCC, encoding alanine, or UCC, encoding serine, Fig. 2B) did not show this effect. These findings underscore the importance of functionally testing predicted ESE sequences and suggest that the regulation of splice site choices may involve additional factors and mechanisms besides the ones shown in the current study.

Our observations nevertheless suggest a straightforward model for the regulation of exon 2B splicing and hence the portion of MITF protein that contains exon 2B and can potentially be phosphorylated at serine-73. A high activity of SF2/ASF, SRp55, SC35 or SRp40 relative to that of SRp30c would favor exon 2B incorporation, and conversely, a low activity of these proteins relative to that of SRp30c would favor its exclusion. In turn, this regulation may then affect the balance between cell proliferation and differentiation as previous observations show that MITF without exon 2B lacks the anti-proliferative activity that is associated with MITF containing exon 2B (20, and unpublished observations), and that serine-73 phosphory-

lation is involved in the regulation of MITF protein activity and stability (4,5). This scenario suggests the further, intriguing possibility that MITF might regulate its own splicing if it were somehow capable of influencing the levels or activities of splicing factors. Currently, however, we have no experimental evidence for this possibility.

Given that the above model of exon 2B splicing regulation is entirely based on in vitro studies, it is finally important to discuss the relevance of our observations for the intact organism. In fact, mouse embryos and their pigment cells express both exon 2B-containing and exon 2B-lacking RNAs, and forced exon 2B incorporation throughout development and after birth, achieved by targeted mutation of the exon 2A/B splice junction, results in a pigmentary change (Debbache et al., unpublished). Nevertheless, targeted mice with partial exon 2B exclusion due to sequence changes in the ESE identified in our study show little if any phenotype in vivo although their isolated pigment cells have abnormally high proliferation rates in vitro (unpublished observation). Such in vitro/in vivo discrepancies, however, are not without precedent and suggest the existence of compensatory mechanisms that operate efficiently only in vivo and that may have been selected evolutionarily to safeguard organisms against natural fluctuations in gene expression. Such compensatory mechanisms might eventually be identified using splice-mutants as sensitized backgrounds for further mutagenesis screens. In sum, the results from our study not only suggest additional tests for the in vivo role of specific SR proteins but may also lead to wider studies exploring the role of alternative splicing of Mitf for development and for malignancies.

REFERENCES

1. Steingrimsson, E., Copeland, N. G., and Jenkins, N. A. (2004) *Annu Rev Genet* **38**, 365-411
2. Arnheiter, H., Hou, L., Nguyen, M. T. T., Bismuth, K., Csermely, T., Murakami, H., Skuntz, S., Liu, W., and Bharti, K. (2006) Mitf—A matter of life and death for the developing melanocyte. in *From Melanocytes to Melanoma: The progression to malignancy* (Hearing, V., and Leong, S. P. L. eds.), Humana Press, Totowa, NJ
3. Garraway, L. A., Widlund, H. R., Rubin, M. A., Getz, G., Berger, A. J., Ramaswamy, S., Beroukhim, R., Milner, D. A., Granter, S. R., Du, J., Lee, C., Wagner, S. N., Li, C., Golub, T. R., Rimm, D. L., Meyerson, M. L., Fisher, D. E., and Sellers, W. R. (2005) *Nature* **436**, 117-122
4. Hemesath, T. J., Price, E. R., Takemoto, C., Badalian, T., and Fisher, D. E. (1998) *Nature* **391**, 298-301
5. Wu, M., Hemesath, T. J., Takemoto, C. M., Horstmann, M. A., Wells, A. G., Price, E. R., Fisher, D. Z., and Fisher, D. E. (2000) *Genes Dev* **14**, 301-312
6. Bismuth, K., Skuntz, S., Hallsson, J. H., Pak, E., Dutra, A. S., Steingrimsson, E., and Arnheiter, H. (2008) *Genetics* **178**, 259-272
7. Bauer, G. L., Praetorius, C., Bergsteinsdottir, K., Hallsson, J. H., Gisladottir, B. K., Schepsky, A., Swing, D. A., O'Sullivan, T. N., Arnheiter, H., Bismuth, K., Debbache, J., Fletcher, C., Warming, S., Copeland, N. G., Jenkins, N. A., and Steingrimsson, E. (2009) *Genetics* **183**, 581-594
8. Hallsson, J. H., Favor, J., Hodgkinson, C., Glaser, T., Lamoreux, M. L., Magnusdottir, R., Gunnarsson, G. J., Sweet, H. O., Copeland, N. G., Jenkins, N. A., and Steingrimsson, E. (2000) *Genetics* **155**, 291-300.
9. Wen, B., Chen, Y., Li, H., Wang, J., Shen, J., Ma, A., Qu, J., Bismuth, K., Debbache, J., Arnheiter, H., and Hou, L. (2010) *Pigment Cell Melanoma Res* **23**, 441-447
10. Cronin, J. C., Wunderlich, J., Loftus, S. K., Prickett, T. D., Wei, X., Ridd, K., Vemula, S., Burrell, A. S., Agrawal, N. S., Lin, J. C., Banister, C. E., Buckhaults, P., Rosenberg, S. A., Bastian, B. C., Pavan, W. J., and Samuels, Y. (2009) *Pigment Cell Melanoma Res* **22**, 435-444

11.   Nilsen, T. W., and Graveley, B. R. (2010) *Nature* **463**, 457-463
12.   Licatalosi, D. D., and Darnell, R. B. (2010) *Nat Rev Genet* **11**, 75-87
13.   Hui, J., and Bindereif, A. (2005) *Biol Chem* **386**, 1265-1271
14.   Bharti, K., Debbache, J., Wang, X., and Arnheiter, H. (2010) *Methods Mol Biol* **647**, 237-250
15.   Darnell, J. C., Jensen, K. B., Jin, P., Brown, V., Warren, S. T., and Darnell, R. B. (2001) *Cell* **107**, 489-499
16.   Allerson, C. R., Martinez, A., Yikilmaz, E., and Rouault, T. A. (2003) *RNA* **9**, 364-374
17.   Crawford, J. B., and Patton, J. G. (2006) *Mol Cell Biol* **26**, 8791-8802
18.   Cartegni, L., Wang, J., Zhu, Z., Zhang, M. Q., and Krainer, A. R. (2003) *Nucleic Acids Res* **31**, 3568-3571
19.   Smith, P. J., Zhang, C., Wang, J., Chew, S. L., Zhang, M. Q., and Krainer, A. R. (2006) *Hum Mol Genet* **15**, 2490-2508
20.   Bismuth, K., Maric, D., and Arnheiter, H. (2005) *Pigment Cell Res* **18**, 349-359

ACKNOWLEDGMENTS

FIGURE LEGENDS

Fig. 1. The codon for Mitf S73 regulates exon 2B alternative splicing. *A*. Schematic representation of minigene constructs. Minigenes contain *Mitf* genomic DNA sequences from exon 1M to exon 3 fused to a bovine growth hormone polyadenylation site (BGH-PA) and are placed under the control of a CMV promoter. They are either wild type or contain a silent *Apa*LI site and/or the S73A mutation. The position of primers (see text and Supplementary Table S1) used for regular and real time RT-PCR assays are indicated. *B*. Minigene sequences around codon-73 in wild type and the three different mutations. The blue box marks the position of where the *Apa*LI site (GTGCAC) was introduced, and the red box the position of the serine-73 or alanine-73 codon. *C*. Alternative exon 2B splicing in HEK293 cells transfected with minigene constructs. RNA was assayed by RT-PCR, using primers a and g. The 345 bp band represents the sequence containing exon 2B, and the 177 bp band the sequence lacking exon 2B. Beta-actin was used as control.

Fig. 2. *A*. Effect of the 16 possible permutations of the first two bases of the S73 codon on exon 2B splicing after transfection of minigenes into ARPE19 cells. RNA was isolated 24 h after transfection and analyzed by RT-PCR, using minigene-specific primers b and g (see Fig. 1A). The bars underneath the gel picture indicate the quantitated percentage of exon 2B+/(2B- + 2B+) determined from real time PCR results, using primer pairs c/e for exon 2B+ and d/f for exon 2B- (see Fig. 1A). Note that only the wild type sequence (AGC) allows for high efficiency inclusion of exon 2B. *B*. ESE finder scores (version 3.0) for each of the 16 permutated sequences for predicted binding of SRp40, SF2/ASF, SC35 and SRp55. Values are indicated if they lie above the default threshold scores given by ESE finder for each of the four SR proteins.

Fig. 3. *A-C*. Ectopic expression of SR proteins influences exon 2B splicing in wild-type and S73A minigene transfected HEK293 cells. *A*. Western blot of HEK 293 cells, either untransfected or transfected with expression vectors for SRp30c, SC35 or SRp40 and probed with the corresponding specific antibodies or the monoclonal antibody MAb104, which recognizes phosphorylated SR proteins. Note that both total and phosphorylated (active) SR proteins are expressed at similar levels and above those of the endogenous proteins (the endogenous proteins are below the level of detection at the given exposure

times). Western blots for β-actin are shown as loading control. *B*. Top: Representative experiment showing effect of expression of indicated SR proteins on exon 2B inclusion. RT-PCR based on using primer pair a/g (Fig. 1A). Bottom: Quantitation based on RT-PCR as described for Fig. 2A. Results are given as mean and standard deviation based on three independent experiments. Note that SRp30c leads to increased exon 2B skipping on both wild-type and S73A mutant minigene-derived RNA, and SC35, SRp40, SF2/ASF and SRp55 to an increase in exon 2B incorporation. *C*. Top/Bottom: Cotransfections indicate dominance of SRp40 and SC35 over SRp30c. The respective expression vectors were cotransfected along with the indicated minigenes and RNAs were analyzed as for *B*, Top and Bottom. Quantification based on three independent experiments. *D*. Top: SR proteins influence exon 2B splicing of the endogenous *Mitf* RNA. Wild-type and S73A melanocytes were cotransfected with a GFP expression vector and expression vectors for either SRp30c, SRp40 or SC35, sorted for GFP expression using a fluorescence activated cell sorter, and RNAs assayed as for *B-C*. For quantification, the means of two independent experiments are shown. Note that similar to the effects on minigene-derived RNA, SRp30c favors exon 2B skipping in endogenous Mitf RNAs, and SRp40 and SC35 favor exon 2B inclusion.

Fig. 4. Demonstration of RNA/SR protein interactions using filter binding assays. *A*. SDS/Polyacrylamide gel electrophoresis of crude and His-affinity-purified extracts of *E.coli* expressing SR proteins fused with guanylate binding protein and an 8x His tag. Coomassie blue stained gel. *B-D*. Relative amount of RNA bound to the indicated recombinant SR proteins. Digoxigenin-labeled RNA corresponded to wild-type or S73A mutated exon 2B (168 bases), corresponding positive control RNAs, or a negative control RNA. Filter binding assays performed as described in Experimental Procedures. *E*. Control binding assay performed with purified fusion tag lacking SR protein sequences.

Fig. 5. Affinity chromatography of recombinant SR proteins on RNA columns. Equal amounts of 22-base RNAs corresponding to the portion of exon 2B surrounding codon-73 (either wild type or S73A, sequences, see Experimental Procedures) were covalently attached to thiol-modified NHS-activated Sepharose columns. Control columns were treated similarly but contained no RNA. Purified recombinant protein (see Fig. 4A, 10 μg each) was applied and the columns were then washed with binding buffer. Proteins were eluted with step-wise increasing KCl concentrations and finally stripped with 8 M urea as indicated. An aliquot of the eluates was subjected to SDS/polyacrylamide gel electrophoresis followed by silver staining. *A*. SRp40. Note that even 1M KCl and 8 M urea can elute substantial amounts of residual protein bound to the wild type column but not the S73A column, suggesting lower affinity of SRp40 protein to the mutated sequence. *B*. SC35 protein. Note similar elution profiles on both columns. *C*. SRp30c protein. Note similarly low level binding to either column. Also note that 8M urea was able to elute some residual SR proteins from the non-RNA control column, suggesting that a portion of the respective proteins binds non-specifically to the column material.

Fig. 6. Conservation of Mitf exon 2A/2B and 2B/intron 1 splice junctions (marked with inverted triangles on top of the mouse sequence) as well as the serine-73 codon (bold) and surrounding sequence in various vertebrates. Colored nucleotides mark changes from the mouse sequence. (---) no sequence available.

A

exons: 1M   2A   2B   3   BGH-PA

123 b   42 b

CMV

a
b

c   e

d

ApaLI   Ser or Ala

d

g
f
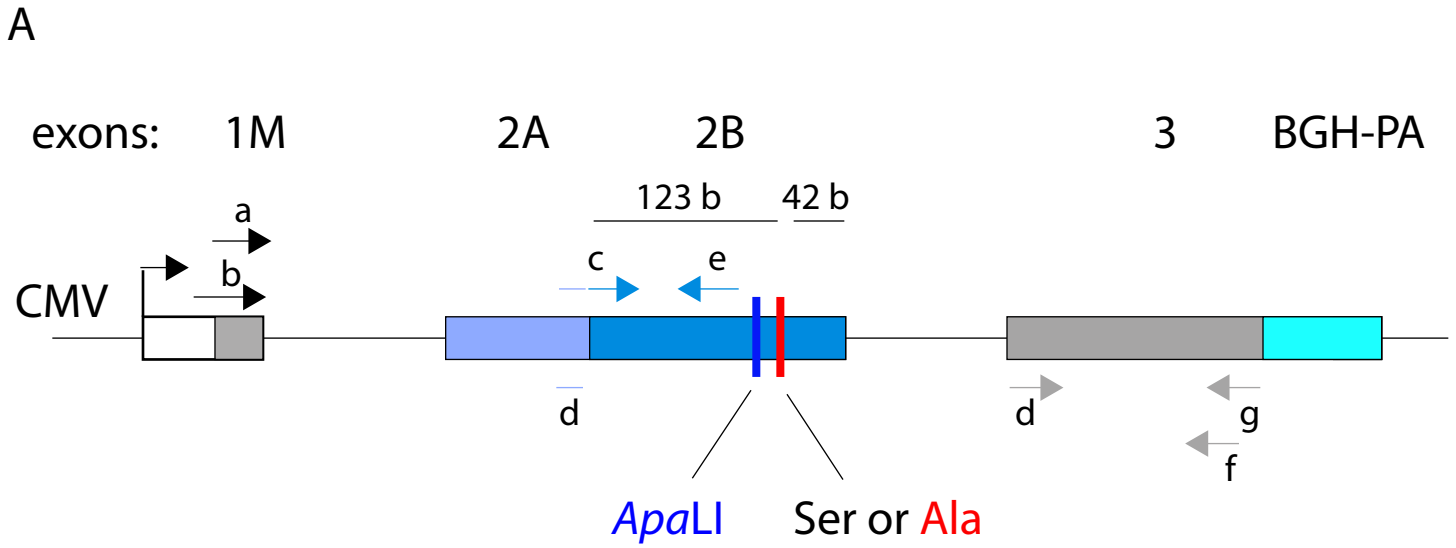
B

wt or ApaLI   Ser or Ala

wt S73   CAGCGCACCCAACAGCCCTA

ApaLI   CAGTGCACCCAACAGCCCTA

ApaLI/S73A   CAGTGCACCCAACGCCCCTA

S73A   CAGCGCACCCAACGCCCCTA

C

wt S73   ApaLI/S73A   ApaLI   S73A

345 bp

177 bp

β-actin
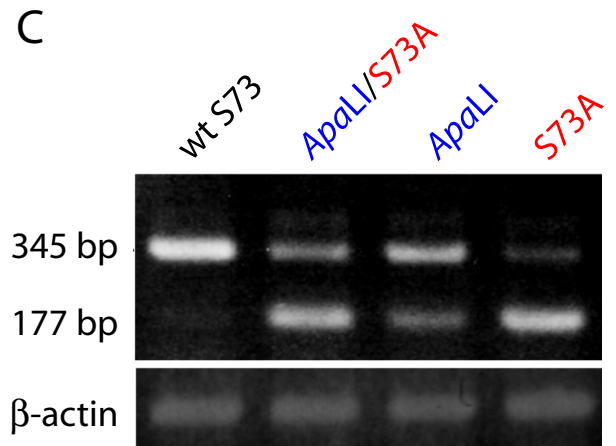
Wang et al., Fig. 1

A
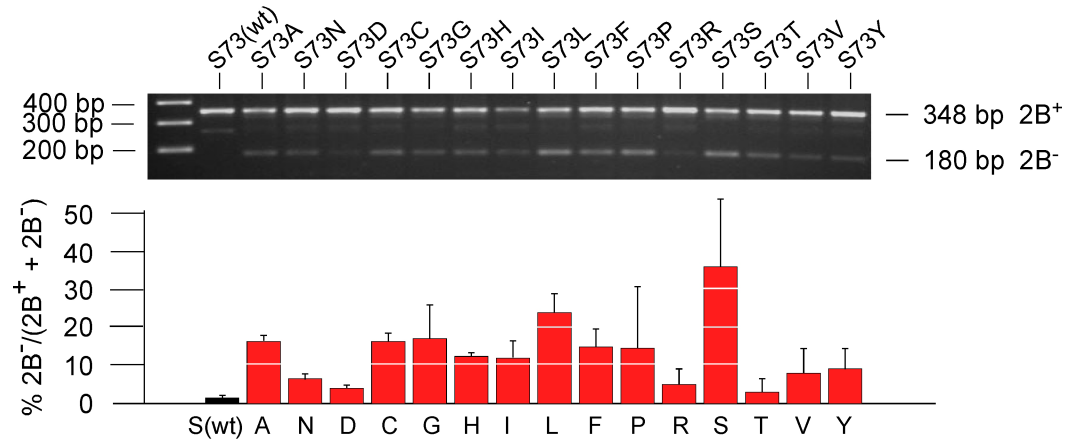
B

Encoded amino acid	SRp40		SF2/ASF		SC35		SRp55	
	Sequences	Score	Sequences	Score	Sequences	Score	Sequences	Score
S73(wt)	C*CAAC*AG*C*C	2.9	CCCAA *CAG**CCCU* AU	2.4	A*CAG**CCCUA* U	–	C*AAC*AG*C*C	–
S73A	.*CAAC*GC*C*.	–	..... *CGC**CCCU* ..	2.2	.*CGC**CCCUA* .	4.0	.*AAC*GC*C*.	–
S73N	.*CAAC*AA*C*.	–	..... *CAA**CCCU* ..	–	.*CAA**CCCUA* .	2.6	.*AAC*AA*C*.	–
S73D	.*CAAC*GA*C*.	–	..... *CGA**CCCU* .. .*CCAAC* GA	– 2.6	.*CGA**CCCUA* .	3.0	.*AAC*GA*C*.	–
S73C	.*CAAC*UG*C*.	–	..... *CUG**CCCU* ..	–	.*CUG**CCCUA* .	–	.*AAC*UG*C*.	–
S73G	.*CAAC*GG*C*.	–	..... *CGG**CCCU* ..	2.0	.*CGG**CCCUA* .	–	.*AAC*GG*C*.	2.8
S73H	.*CAAC*CA*C*.	–	..... *CCA**CCCU* .. .. *CA* *CCCUA*.	– 3.5	.*CCA**CCCUA* .	–	.*AAC*CA*C*.	–
S73I	.*CAAC*AU*C*.	–	..... *CAU**CCCU* ..	–	.*CAU**CCCUA* .	3.0	.*AAC*AU*C*.	3.0
S73L	.*CAAC*CU*C*.	–	..... *CCU**CCCU*.. ...... *CU* *CCCUA* .	– 2.4	.*CCU**CCCUA*.	–	.*AAC*CU*C*.	–
S73F	.*CAAC*UU*C*.	–	..... *CUU**CCCU* ..	–	.*CUU**CCCUA* .	2.8	.*AAC*UU*C*.	–
S73P	.*CAAC*CC*C*.	–	..... *CCC**CCCU* ..	–	.*CCC**CCCUA* .	–	.*AAC*CC*C*.	–
S73R	.*CAAC*CG*C*.	–	..... *CCG**CCCU* .. .. *CG* *CCCUA* .	– 3.0	.*CCG**CCCUA*.	–	.*AAC*CG*C*.	–
S73S	.*CAAC*UC*C*.	–	..... *CUC**CCCU* ..	–	.*CUC**CCCUA* .	3.3	.*AAC*UC*C*.	–
S73T	.*CAAC*AC*C*.	–	..... *CAC**CCCU*..	2.7	.*CAC**CCCUA* .	3.6	.*AAC*AC*C*.	–
S73V	.*CAAC*GU*C*.	–	..... *CGU**CCCU* .. .*CCAAC* GU	– 2.2	.*CGU**CCCUA* .	3.4	.*AAC*GU*C*.	3.6
S73Y	.*CAAC*UA*C*.	–	..... *CUA**CCCU* ..	–	.*CUA**CCCUA* .	–	.*AAC*UA*C*.	–

Wang et al., Fig. 2

Wang et al., Fig. 3

Wang et al., Fig. 4

	wt RNA column	S73A RNA column	No RNA column

A
SRp40

112 k —
60 k —

B
SC35

112 k —
60 k —

C
SRp30c

112 k —
60 k —

Mr

input, 100 mM KCl, 200 mM KCl, 500 mM KCl, 750 mM KCl, 1 M KCl, 8 M urea
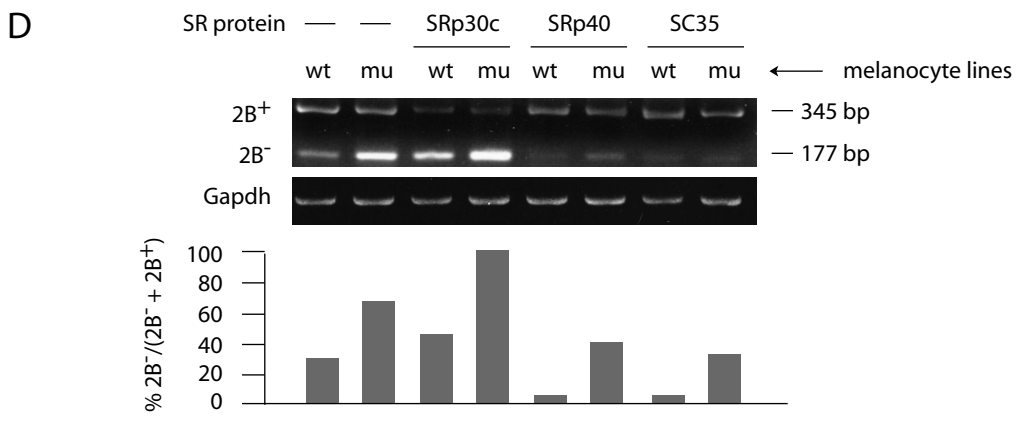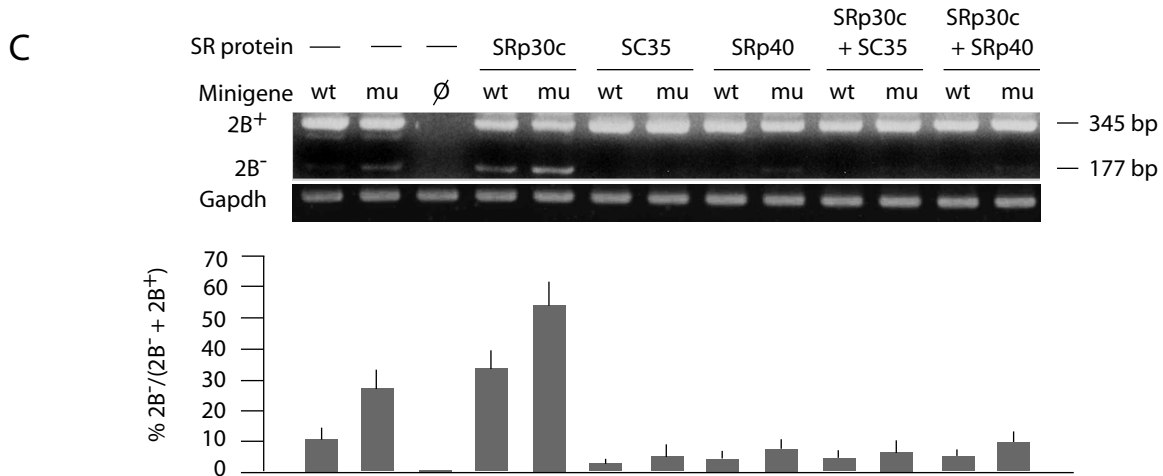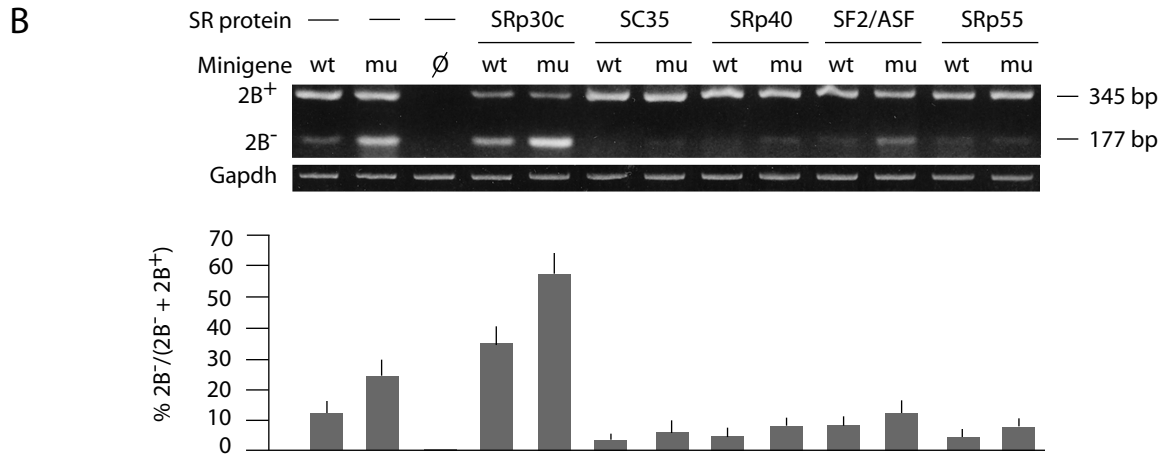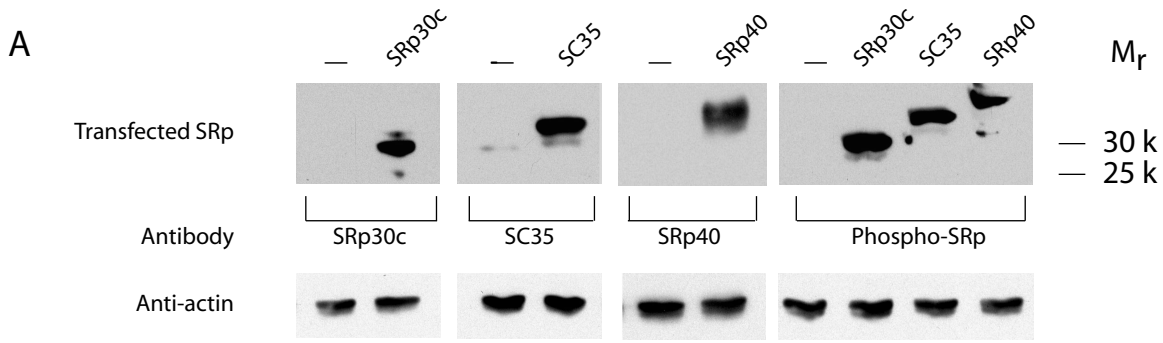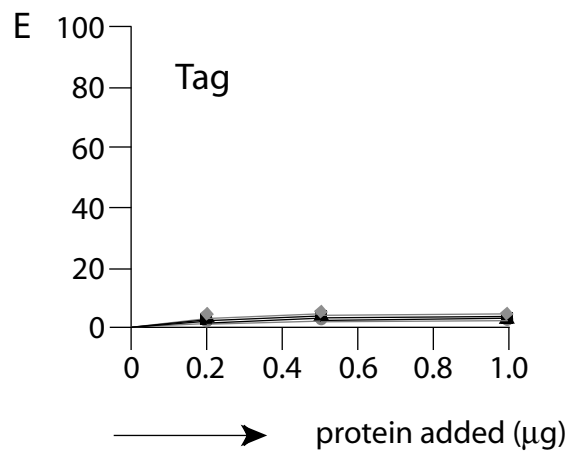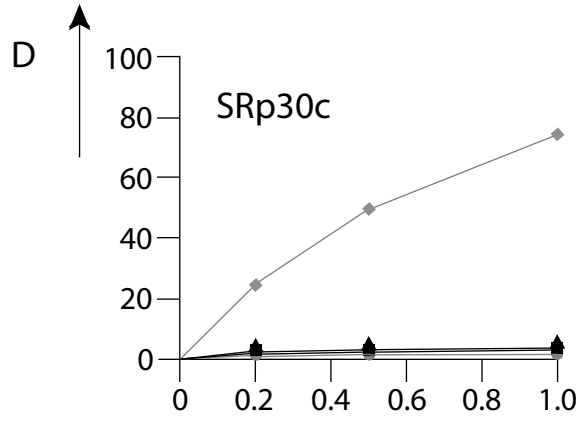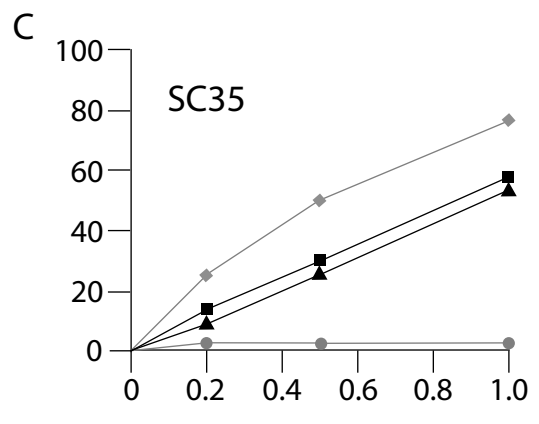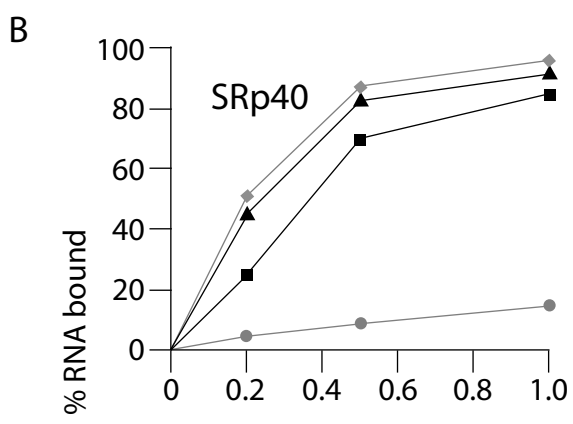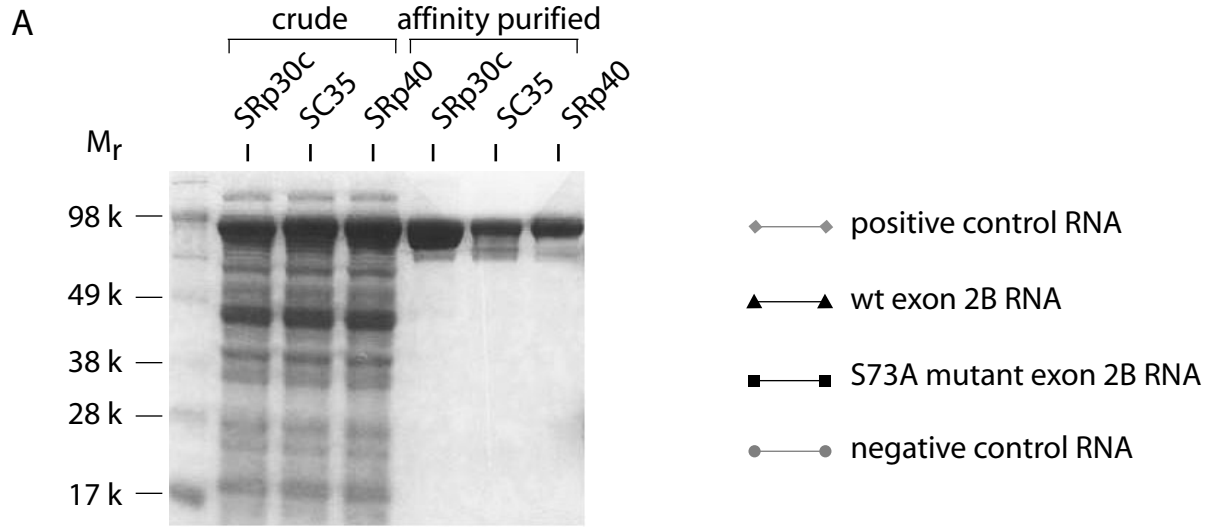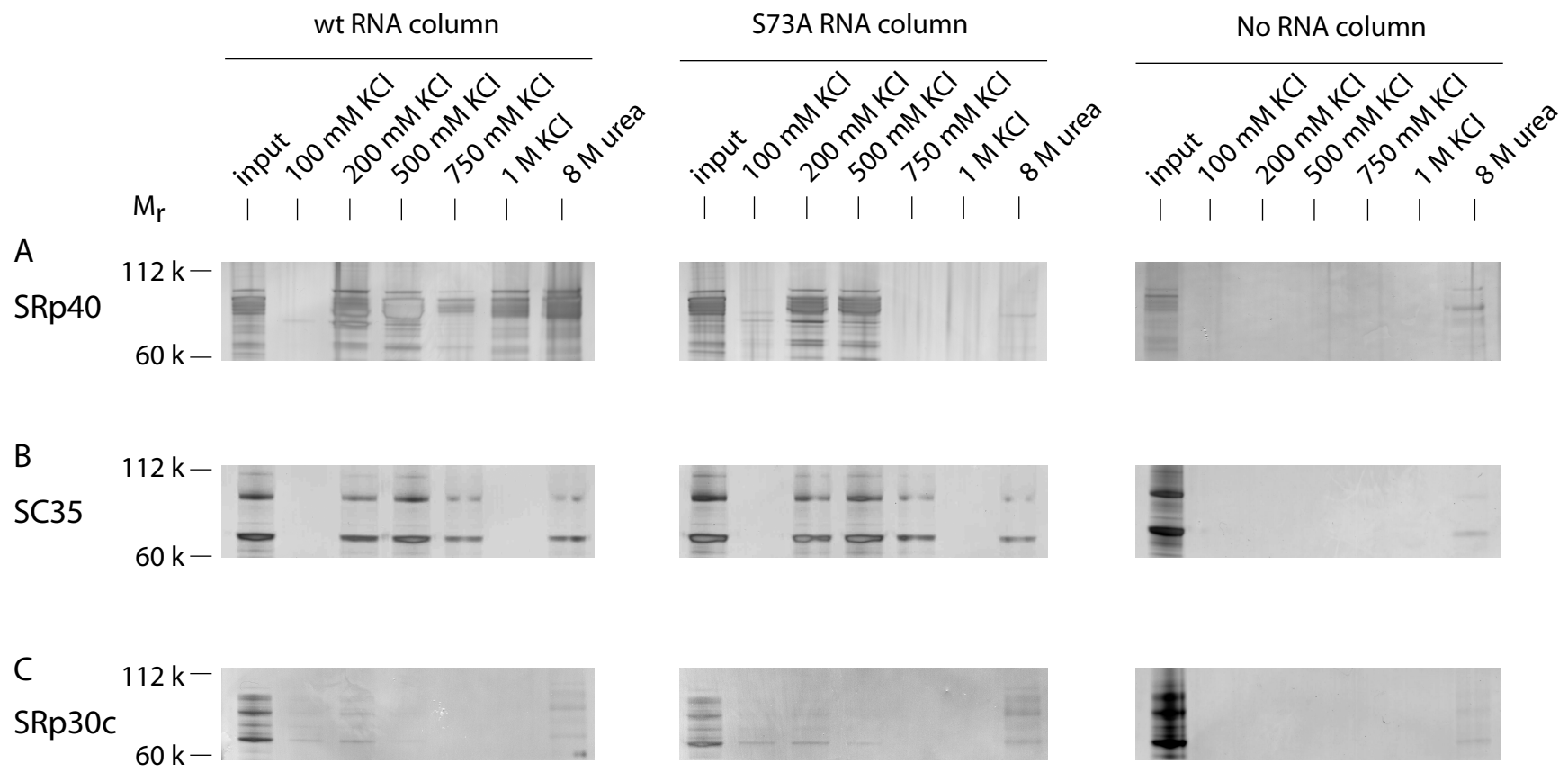
Wang et al., Fig. 5

Species	2A-2B Junction	Ser73 codon and surrounding sequence	2B-Intron 2 Junction
	▼	Ser	▼
Mus musculus	CACCAGGUAAAG	CCCAAC**AGC**CCUAUGG	AAAGAGGUAAUU
Rattus norvegicus	CACCAGGUAAAG	CCCAAC**AGC**CCCAUGG	AAAGAGGUAAUU
Cavia porcellus	CAGCAGGUAAAG	CCCAAC**AGC**CCCAUGG	AAAGAGGUAAUU
Homo sapiens	CAGCAGGUAAAG	CCCAAC**AGC**CCCAUGG	AAAGAGGUAAUU
Pan troglodytes	CAGCAGGUAAAG	CCCAAC**AGC**CCCAUGG	AAAGAGGUAAUU
Pongo pygmaeus	CAGCAGGUAAAG	CCCAAC**AGC**CCCAUGG	AAAGAGGUAAUU
Macaca mulatta	CAGCAGGUAAAG	CCCAAC**AGC**CCCAUGG	AAAGAGGUAAUU
Callithrix jacchus	CAGCAGGUAAAG	CCCAAC**AGC**CCCAUGG	AAAGAGGUAAUU
Canis familiaris	CAGCAGGUAAAG	CCCAAC**AGC**CCCAUGG	AAAGAGGUAAUU
Felis catus	CAGCAGGUAAAG	CCCAAC**AGC**CCCAUGG	AAAGAGGUAAUU
Equus caballus	CAGCAGGUAAAG	CCCAAC**AGC**CCCAUGG	AAAGAGGUAAUU
Bos taurus	CAGCAGGUAAAG	CCCAAC**AGC**CCCAUGG	AAAGAGGUAAUU
Loxodonta africana	CAGCAGGUAAAG	CCCAAC**AGC**CCCAUGG	AAAGAGGUAAUU
E. europaeus	CAGCAGGUAAAG	CCCAAC**AGC**CCCAUGG	AAAGAGGUAAUU
D. novemcinctus	CAGCAGGUAAAG	CCCAAC**AGC**CCCAUGA	------------
M. domestica	CAACAGGUAAAG	CCAAAU**AGC**CCCAUGG	AAAGAGGUAAUU
O. anatinus	CAGCAGGUAAAG	CCCAAC**AGC**CCAAUGG	AAAGAGGUAAUA
Gallus gallus	CAGCAGGUAAAG	CCCAAC**AGU**CCGAUGG	AAAGAGGUAAUA
Anolis carolinensis	CAGCAGGUCAAG	CCCAAC**AGC**CCCAUGG	AAAGAGGUAAGA
Xenopus tropicalis	CAGCAGGUAAAG	CCAAAC**AGU**CCAAUGG	AAAGAGGUAACU
Takifugu rubripes	CAGCACGUCCGG	CCCAGC**AGU**CCCAAAG	AAAGAGGU----
Danio rerio	CAGCAGGUGAAG	CCCAAC**AGC**CCUAUGG	AAAGAGGUACAU

Wang et al., Fig 6

A

5 1 0.3 µg of SR proteins

| SRp30c   SRp30c   SC35   SC35 | SRp40   SRp40

2B⁺ — 345 bp
2B⁻ — 177 bp
Gapdh — 386 bp

Minigene wt mu Ø ‾‾wt‾‾ ‾‾mu‾‾ ‾‾wt‾‾ ‾‾mu‾‾   ‾‾wt‾‾ ‾‾mu‾‾ wt mu

B

% 2B⁻/(2B⁻ + 2B⁺)

100
80
60
40
20
0
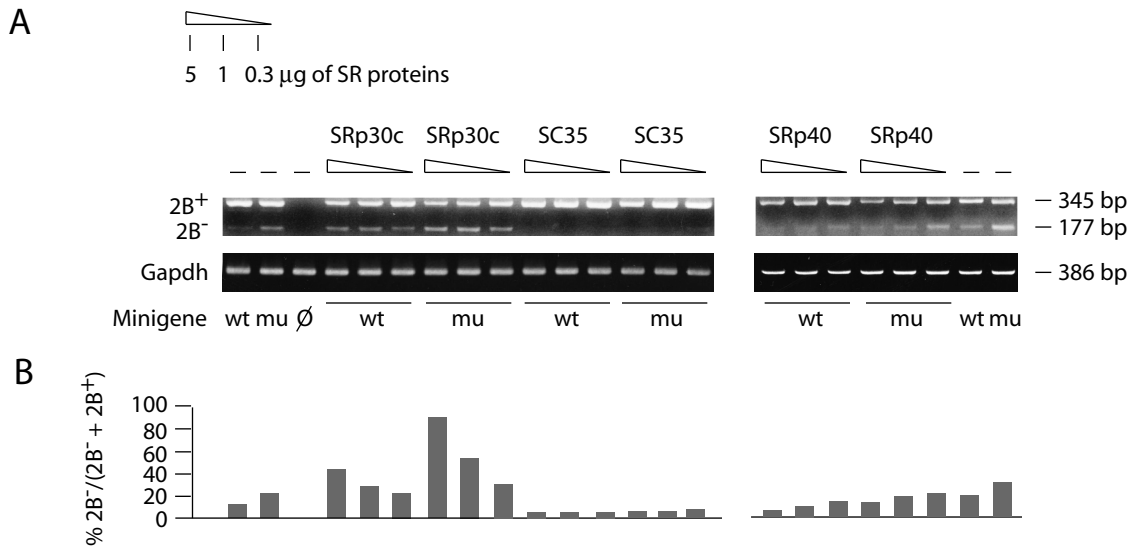
Supplemental Fig. 1. Effect of ectopic SR protein expression on exon 2B splicing of minigene-derived RNA is dose-dependent. Graded doses of expression vectors for the indicated SR proteins were transfected along with a constant amount of the wild-type or S73A minigene into HEK 293 cells. Twenty-four hours later, RNA was subjected to regular and real time RT-PCR as indicated in Fig. 3. *A.* Regular RT-PCR. *B.* Quantitative RT-PCR, showing means from two independent experiments.

% 2B⁻/(2B⁻ + 2B⁺)

25
20
15
10
5
0

| pcDNA (µg) | 1.9 | 1.5 | 1.0 | 0.5 | 0.1 |
| minigene S73A (µg) | 0.1 | 0.5 | 1.0 | 1.5 | 1.9 |
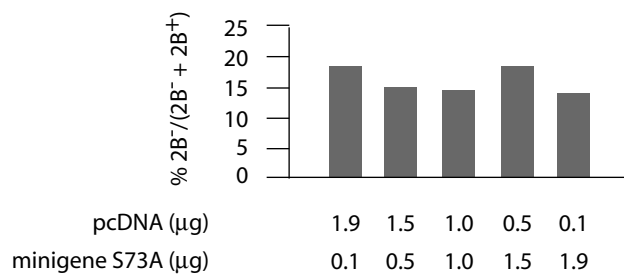
Supplemental Fig. 2. Exon 2B splicing of minigene-derived RNA does not depend on concentration of transfected DNA. Graded doses of the S73A mutated minigene were transfected into HEK293 cells and RNA assayed for exon 2B splicing as indicated for Fig. 3. No significant differences in the relative amounts of exon 2B inclusion were seen over a 19-fold concentration range of transfected DNA, resulting in a 10-fold difference in levels of Mitf RNA (not shown). Results are given as means from two independent experiments.

Supplemental Table S1: Primer Sequences

RT-PCR

Gene	Comb. Code Fig 1	Location	Sequence	Product length (bp)
Mitf	a	Exon 1M-F	5'-CACCATGCTGGAAATGC-3'	2B+ : 345
	g	Exon 3-R	5'-CTGCATGCACGACGCTCGAGAGTGC-3'	2B- : 177
Mitf	b	Exon 1M-F	5'-AATTGCCCTCACCATGCTG-3'	2B+ : 348
	f	Exon 3-R	5'-GACGCTCGAGAGTGCGTGTT-3'	2B - :180
β-actin	N/A	β -actin-F	5'-GATGACGATATCGCTGCG-3'	682
	N/A	β -actin-R	5'-GTGGCCATCTCCTGCTCG-3'	
Gapdh	N/A	Gapdh-F	5'-GCATTGTGGAAGGGCTCATGACC-3'	386
	N/A	Gapdh-R	5'-CGGCATCGAAGGTGGAAGAGTGG-3'	

qRT-PCR

Gene	Comb. Code Fig 1	Location	Sequence	Product length (bp)
Mitf	c	Exon 2A/B-F	5'-AAGCTCAGAGGCACCAGGTAAAG-3'	2B+ : 81
	e	Exon 2B-R	5'-AGGCTGGTTTGGACATGGTGAG-3'	2B - : N/A
Mitf	d	Exon 2A/3-F	5'-GCTCAGAGGCACCAGGCATTTT-3'	2B+ : N/A
	f	Exon 3-R	5'-GACGCTCGAGAGTGCGTGTT-3'	2B - : 89
Usf1	N/A	Exon5-F	5'-CAGGGCTCAGAGGCACTACT-3'	96
	N/A	Exon6 -R	5'-GCTCCCTCCCTGCAATACTT-3'	

5 – Une alanine non phosphorylable située au codon 73 de l'isoforme M-MITF induit un gain de fonction de la protéine MITF *in vivo.*

Nous avons préalablement montré que le codon de la Serine 73 du gène *Mitf* est implique directement dans la régulation de l'épissage alternatif de l'exon 2B qui contient ce site de phosphorylation. Les tentatives de mutation de cette serine de façon endogène ou par insertion de transgènes mutants ont pour même effet d'augmenter l'exclusion de cet exon. Ceci rend donc difficile la dissociation des rôles potentiellement distincts de la phosphorylation de S73 et de l'absence de l'exon 2B dans MITF. Ici, nous avons choisit d'étudier l'effet de l'absence de phosphorylation de MITF de façon endogène grâce à l'élaboration d'un contexte génétique qui empêche la reconnaissance de la jonction entre les exons 2A et 2B comme site potentiel d'épissage et force ainsi l'incorporation de l'exon 2B quelque soit la séquence du codon 73. Nous avons ainsi généré 3 nouveaux allèles ou l'exon 2B ne peut pas être exclus et comportant à la position 73 soit une Serine, soit un Aspartate mimant une phosphorylation constitutive, ou une Alanine. Nous avons ensuite comparé les phénotypes de ces 3 lignées de souris à la lignée originelle *Mitf*$^{mi-S73A}$. Nous avons également croisé ces souris avec d'autres allèles de Mitf en présence ou non de la cassette Neo, ce qui permet, lorsqu'elle est présente, d'obtenir une réduction du niveau d'expression de Mitf et d'exacerber les différences entre les phénotypes. Nous avons ainsi démontré que l'allèle S-S73A non-phosphorylable, lorsque l'exon 2B est retenu, présente un gain d'activité par rapport à l'allèle témoin S-S73S. Nous suggérons que ce gain d'activité est réalisé grâce à un gain de stabilité de MITF, une augmentation

du nombre de melanocytes au cours du développement *in vivo* et grâce à une réduction de

l'activité d'inhibition de la progression du cycle cellulaire, mesurée *in vitro*.

Les travaux associés à cette étude sont décrits dans l'**Article 5**.

As earlier described, exon 2B splicing is intrinsically linked to the sequence of the codon

for residue-73. Therefore, in order to study the role of S73 phosphorylation

independently of exon 2B exclusion, we chose a strategy to force the incorporation of

exon 2B regardless of the codon at position 73. This was achieved by additional nucleic

acid sequence modifications at the 5' alternative splice site. Like other alternative sub-

exons, exon 2B can either be recognized as part of the following intron (Mitf intron 2 in

that case), or as part of the preceding exon (exon 2A). One of the critical elements,

which allows to switch between the two splice sites, lies in the sequence of the junction

between exon 2A/2B. This sequence must match the 3' exon/intron consensus

sequence in order to allow the recognition of this site as a 3' exon definition site. The

introduction of mutations that would disrupt the recognition of this site by the splicing

machinery would then prevent exon 2B exclusion. Hence, to test if, a re-engineered

splice site, where exon 2B would be included in all Mitf transcripts, would have any

phenotypic effects on melanocytes, we generated three *Mitf* knock-in alleles. All three

alleles contain the 2A-2B exon junction mutations, and differ for residue 73, which either

encodes, a non-phosphorylatable alanine (S73A), a constitutively phospho-mimetic

aspartate (S73D) or a wild-type serine (S73S).

We first demonstrate that the exclusion of exon 2B normally seen in the presence of a

S73 codon mutation can be converted to a level of 100% of exon 2B incorporation by the

introduction of the corresponding modifications in a minigene comprising exon 1M-3.

Having demonstrated that this is indeed the case, we generated the above mentioned mouse lines in order to study the role of M-MITF phosphorylation.

We then tested the molecular and phenotypic consequences of each allele by themselves or in combination with several extant Mitf alleles and find that, perhaps surprisingly, the S73S (wild-type) allele acts as a hyp<u>o</u>morph, while the S73A and to a lesser extent, S73D, act as a hyp<u>er</u>morph. The simplest explanation for these findings is the fact that S73A protein accumulates to higher levels than S73S, likely because the lack of phosphorylation leads to an increased protein stability.

Interestingly, the S73D protein also shows an increase in protein levels, though less than the S73A protein, likely reflecting the fact that a permanent negative charge at this position neither reflects the effect on degradation seen with S73S MITF nor the absence of phosphorylation of S73A MITF.

The experimental work related to this study is described in **Article 5**.

Article 5

In vivo role of alternative splicing and serine phosphorylation of the microphthalmia-associated transcription factor MITF.

Soumis à Genetics

In vivo role of alternative splicing and serine phosphorylation of the microphthalmia-associated transcription factor MITF

Julien Debbache*, Raza Zaidi[§], Sean Davis**, Theresa Guo[§], Keren Bismuth*, Xin Wang*, Susan Skuntz*, Dragan Maric[§§], James Pickel[***], Paul Meltzer**, Glenn Merlino[§], and Heinz Arnheiter*

*Mammalian Development Section, NINDS, NIH, Bethesda, MD 20892-3706, USA

[§]Laboratory of Cancer Biology and Genetics, National Cancer Institute, NIH, Bethesda, MD 20892, USA

**Genetics Branch, National Cancer Institute, NIH, Bethesda, MD 20892, USA

[§§]NINDS Flow Cytometry Core Facility, NIH, Bethesda, MD 20892, USA

[***]Transgenic Core Facility, National Institute of Mental Health, National Institutes of Health, Bethesda, Maryland 20892

Corresponding author: Heinz Arnheiter
                               Building 35, Rm 2A-201
                               35 Convent Drive MSC 3706
                               Bethesda, Maryland 20892-3706
                               Phone: 301-496-1645
                               FAX: 301-402-7686
                               E-mail: ha3p@nih.gov

Abstract

The basic-helix-loop-helix-leucine zipper transcription factor MITF plays major roles in the development and physiology of vertebrate melanocytes and melanoma cells. It is regulated by post-translational modifications, including phosphorylation at serine-73, which based on in vitro experiments imparts on MITF an increased transcriptional activity paired with a decreased stability. Serine-73 is encoded by an alternatively spliced exon, exon 2B, which, intriguingly, is preferentially skipped in mice carrying a targeted serine-73-to-alanine mutation. Here, we measured the relative abundance of exon 2B+ and exon 2B- RNAs in freshly isolated and FACS-sorted wild-type melanoblasts and melanocytes and generated a series of knock-in mice allowing forced incorporation of either alanine, aspartate, or wild-type serine at position 73. None of these knock-in alleles, however, creates a striking pigmentation phenotype on its own, but differences between them can be revealed either by a general reduction of Mitf transcript levels or in heteroallelic combinations with extant *Mitf* mutations. In fact, compared with straight serine-73 knock-in mice with their relative reduction of 2B+ Mitf, forced incorporation of alanine-73 leads to greater increases in MITF protein levels, melanoblast and melanocyte numbers, and extent of pigmentation in particular allelic combinations. These results underscore, in vivo, the importance of the link between alternative splicing and post-translational modifications and may bear on the recent observation that exon 2B skipping can be found in metastatic melanoma.

Alternative splicing and post-translational modifications are among the major mechanisms by which individual genes generate multiple protein products. In fact, modern sequencing technologies and proteomic analyses have shown that most if not all multi-exon pre-mRNAs give rise to alternatively spliced mature mRNAs (NILSEN and GRAVELEY 2010) and that posttranslational modifications modulate the activities of most eukaryotic proteins (MANN and JENSEN 2003). In a simple sense, then, the two mechanisms are linked as posttranslational modifications depend on the presence of the particular exons encoding the modifiable residues or proteolytic cleavage sites. Here, we present a mouse model that allows us to probe this link in vivo by separately targeting a splice site and a codon for a biologically relevant phosphoacceptor site in the gene encoding the pigment cell transcription factor MITF. In fact, pigmentation is particularly suitable for such studies as it provides for an easily visible and highly sensitive read-out of gene function.

MITF, which stands for microphthalmia-associated transcription factor, plays a crucial role in the development and function of melanin-bearing pigment cells in skin, eye and inner organs (ARNHEITER 2010; ARNHEITER *et al.* 2006; HODGKINSON *et al.* 1993). Its protein product is a basic helix-loop-helix-leucine zipper transcription factor that regulates target gene promoters by binding specific E box sequences as homodimers or heterodimers with the related proteins TCFEB, TCFE3 and TCFEC (STRUB *et al.* 2011). *Mitf* mutations have been found from zebrafish to man and their analyses have established that *Mitf* controls specification, proliferation, death, differentiation and stress responses of normal pigment cells and regulates migration, metastasis, and death of melanoma cells (ARNHEITER *et al.* 2006; HOEK and GODING 2010).

In vitro experiments have shown that phosphorylation of MITF serine-73 increases the protein's transcriptional activity about three-fold (HEMESATH *et al.* 1998) and that serine-73 phosphorylation alone or double serine-73/serine-409

phosphorylation lead to polyubiquitination and degradation of MITF (WU *et al.* 2000; XU *et al.* 2000). To address the question of whether serine-73 phosphorylation plays a role in vivo, we have previously generated targeted mice in which codon-73 was changed to one encoding alanine-73 which cannot be phosphorylated (BISMUTH *et al.* 2008). These mice had a normally pigmented coat and normal eyes, a finding that was later confirmed by using a transgenic bacterial artificial chromosome (BAC) rescue strategy with BACs engineered to encode alanine-73 alone or alanine-73 and alanine-409 together (BAUER *et al.* 2009). A complication of these experiments was the fact that the Mitf exon which encodes serine-73, exon 2, contains a 5' alternative splice site that divides it into an exon 2A of 20 codons and an exon 2B of 56 codons, the latter including codon-73. This arrangement normally leads to a major transcript (at least 90% of total Mitf RNA in skin or heart) that contains the entire exon 2, and a minor one in which exon 2B, and hence codon-73, is missing although the open reading frame is maintained (BAUER *et al.* 2009; BISMUTH *et al.* 2008). Interestingly, the codon-73 mutation in both targeted mice and BAC transgenics is associated with a substantial decrease of the transcript containing exon 2B (only ~10% of total Mitf mRNA in the targeted mice and ~45% in the BAC rescue mice), and a concomitant increase of the transcript lacking exon 2B (BAUER *et al.* 2009; BISMUTH *et al.* 2008). This splice change, which is likely due to the fact that codon-73 is embedded in a splice enhancer sequence whose affinity for the serine/arginine rich splice regulator SRSF5 is reduced upon mutation (WANG *et al.* 2009), precluded meaningful conclusions on the specific role of serine-73. In order to separate the potential effects of mutations at residue 73 from the splice-dependent absence of this residue, we re-targeted *Mitf* in a way that renders the alternative 5' splice site non-functional and incorporates either a wild-type serine, a phosphomimetic aspartate, or an alanine at position 73. We find that although the new mutations cause no visible coat phenotypes on their own, they sensitize melanocytes to the phenotypic effects of

reductions in total *Mitf* levels and to the effects of extant *Mitf* alleles in compound heterozygotes. Intriguingly, when tested under such conditions, the targeted allele containing the wild-type serine behaves as a hypomorph while that containing the alanine behaves as a hypermorph. The results show that alternative splicing of exon 2B is indeed relevant in vivo, although in an unexpected manner and in a way that would be difficult to detect based solely on in vitro experiments.

Material and Methods

Melanoblast/melanocyte purification and RNA-Seq data

FVB/N melanocytes were purified by FACS sorting from doxycycline-treated bi-transgenic mice (iDct-GFP mice) that express H2B-GFP fusion proteins specifically in *Dct*-positive melanocytes, using previously published protocols (ZAIDI *et al.* 2011a; ZAIDI *et al.* 2011b; ZAIDI *et al.* 2011c). To purify melanoblasts from E15.5 and E17.5 C57BL/6 iDct-GFP embryos and P1 pups, the dams were fed doxycycline-fortified chow for the entire duration of gestation until harvest. For P3 and P7 pups, doxycycline was injected intraperitoneally at 80μg/g body weight 24 hours before harvest. Total RNA was prepared from FACS-sorted melanoblasts/melanocytes according to standard Illumina RNA-Seq paired-end protocol and then sequenced on the Illumina GAIIx to 80 base pairs per read. For analysis of alternative exon 2B splicing, a set of possible splice sites was determined and assigned to the aligner, indicating that a given splice variant might exist. The sequences were aligned using Genomic Short-Read Nucleotide Alignment Program (WU and NACU 2010) to mouse genome assembly mm9. A custom Python script was then used to count introns that had one boundary at position 97944374 on chromosome 6 (5' end of exon 3). The analysis revealed that only three splice sites were used, one at position 97943348, yielding 2B+ Mitf, one at position 97943180, yielding

2B- Mitf, and a single read for one at position 97879927, yielding Mitf with a junction between exon H and exon 3.

Targeting constructs, minigenes and expression plasmids

The 17.9 kb targeting construct described by Bismuth et al. (BISMUTH *et al.* 2008) was used as template to PCR-amplify a 1.2 kb *Eco*R1/*Hind*III-flanked fragment encompassing part of intron 1, exon2A/2B and part of intron2/Neo-loxP cassette. The PCR-amplified fragment was cloned into pcDNA 3.1 and used for PCR mutagenesis. In a first round, the exon 2A/2B junction was altered by changing 4 bases without changing the coding sequence. In a second round, the previously introduced *Apa*LI site was changed back to the wild-type sequence and codon A73 was either left intact or was changed into one encoding either aspartate or wild-type serine. Sequence-confirmed clones for each of the three different codons at residue 73 were digested with *Afl*II and *Age*I and used to replace the corresponding *Afl*II/*Age*I fragment in a 7.5 kb *Bam*H1 fragment representing the 3' arm of the original construct. The resulting constructs were digested with *Bam*H1 and ligated to a *Bam*HI-linearized construct containing the thymidine kinase gene and the 5' arm of the original construct, yielding three final re-engineered targeting constructs. The correct orientation of the 7.5 kb *Bam*HI fragment was verified by PCR with 2 primer pairs described in Supplemental Table 1. To test for the effect of the 5' splice junction mutation, an *Mitf* minigene comprising exon 1M, intron 1, exon 2A/B, intron 2 and exon 3 was subjected to PCR mutagenesis to alter the 5' splice junctions and codon-73 as in the targeting contructs, using Quickchange site-directed mutagenesis kit (Stratagene). For expression analysis, N-terminal estrogen-receptor (ER)-coupled Mitf 6a+ pBABE vectors were obtained from Colin Goding (CARREIRA *et al.* 2005) and subjected to PCR mutagenesis to obtain Mitf[S73A] (ER S73A)

and Mitf$^{\Delta 2B}$ (ER 2B-) expression plasmids, using a primer set described in Supplemental Table 1. All constructs were sequence-verified.

Mice

Mice carrying the allele *Mitf$^{tm1.2Arnh}$*, containing a S73A mutation with or without a floxed neo-cassette in intron 2, have been described (BISMUTH *et al.* 2008). For the purpose of this study, *Mitf$^{mi-S73A}$* mice from a separate targeting experiment were used and are designated *Mitf^{tm7Arnh}* (containing the neomycin resistance cassette) and *Mitf$^{tm7.1Arnh}$* (lacking the neomycin resistance cassette)(MGI:5050706). For targeting the exon 2A/2B 5' splice site in conjunction with mutations at serine-73, LC3 ES cells [genotype (C57BL/6Nx129S6)F1] were electroporated with 20 µg of the respective *Not*I linearized targeting constructs and grown under standard G418/FIAU selection protocols. After screening, targeted ES cells were injected into C57BL/6N blastocysts and chimeric mice were bred with C57BL/6J to test for germ line transmission and to establish Neo-cassette-containing targeted lines. To remove the floxed Neo-cassette, mice were bred with C57BL/6•129S4-Prm1-Cre deleter mice. After removal of the neo-casette, mice were either intercrossed to obtain homozygous targeted mice or were crossed with mice carrying other mutant *Mitf* alleles. The official designation of these targeted mice are: *Mitf^{tm4Arnh}* (MGI:5050700) and *Mitf$^{tm4.1Arnh}$* (MGI:5050701) for the splice junction/S73 allele; *Mitf^{tm5Arnh}* (MGI:5050702) and *Mitf$^{tm5.1Arnh}$* (MGI:5050703) for the splice junction/S73A allele; and *Mitf^{tm6Arnh}* (MGI:5050704) and *Mitf$^{tm6.1Arnh}$* (MGI:5050705) for the splice junction/S73D allele, each with or without the Neo-cassette, respectively. C57BL/6•129S2 *Kit^{tm1Alf}* (BERNEX *et al.* 1996) heterozygous males were bred with *Mitf$^{mi-S73A\Delta neo}$* and *Mitf$^{mi-S-S73A\Delta neo}$* homozygous females. Double heterozygous offspring were then crossed with the corresponding *Mitf* homozygotes to establish E12.5, E15.5 embryos and P1 pups homozygous for *Mitf* and heterozygous for *Kit^{tm1Alf}*. Xgal-labeling

was done as described (WEN *et al.* 2010). For generation of melanocyte lines, mice were crossed with B6•*Cdkn2a^{tm1Rdp}* mice to obtain double homozygous *Mitf/Cdkn2a* mutants. The bi-transgenic iDct-GFP mice (ZAIDI *et al.* 2011a) used for RNA-Seq were kept on a FVB/N background.

Reverse transcription, RT-PCR and Real-time (q)RT-PCR, western blots

Random primed cDNAs were made from 500 ng of total RNA extracted from heart or ng extracted from melanocyte lines using High Capacity cDNA Reverse Transcription Kit (Applied Biosystems) and RNAse inhibitor cocktail (Invitrogen). PCR and qPCR were performed as described (BHARTI *et al.* 2010), using primers described in Supplemental Table 1. For western blots, 600 µg of heart tissue or 120,000 cultured cells were separated by SDS-PAGE and blotted onto nitrocellulose membranes. The blots were exposed to appropriate antibodies and bands were revealed using SuperSignal West Pico Chemiluminiscent Substrate. Quantitation was done using a Biorad ChemiDoc XRS+ system.

Genotyping and Southern analysis

DNA extracted by standard procedures from tissue samples was analyzed by PCR, using primers indicated in Supplemental Table 1. For Southern blots, liver DNA was prepared, digested as indicated and probed using PCR-amplified probes as previously published (BISMUTH *et al.* 2008).

Photography

Photographs of knock-in mice and their intercrosses with other *Mitf* alleles were taken between 3 weeks and 2 months of age.

Cell lines stably expressing Mitf proteins

pBABE-ER vectors allowing expression of HA-tagged exon 6A+ MITF fused with the estrogen responsive portion of the estrogen receptor were obtained from Colin Goding (CARREIRA *et al.* 2005). Virus was produced by co-transfection of pBABE vectors and pCL Ampho vectors in 293T cells, and ARPE-19 cells (spontaneously immortalized human retinal pigment epithelium cells) were infected and selected with puromycin (1μg/ml) without subsequent cloning. Stable cell lines were prepared allowing expression of only ER (ER- Ø) or MITF-ER with wild-type S73 (ER-WT), S73A (ER-S73A), or 2B-MITF (ER-2B-). For induction, cells were treated with 300 nM 4-hydroxy-tamoxifen (TM) for 48 hours. Total extracts were probed with 6A5 anti-MITF antibodies (BHARTI *et al.* 2008).

Flow cytometry

For assaying MITF expression, ARPE19 cells were washed and fixed with 4% paraformaldehyde, permeabilized and incubated with mouse monoclonal antibody 6A5 and R-phycoerythrin-goat anti-mouse IgG1 as second antibody. Flow cytometry was performed using a FACSVantage SE flow cytometer (Becton Dickinson) and the data processed using CellQuest software. The gating was determined empirically and applied in the same way to all experiments.

Results

Alternative splicing of exon 2B of Mitf in melanocytes

Previous results have shown that heart and skin of wild-type mice express Mitf splice variants that specifically lack exon 2B (BAUER *et al.* 2009; BISMUTH *et al.* 2008; HALLSSON *et al.* 2000). To confirm these findings in freshly isolated embryonic and postnatal melanocytes, we purified the respective cells by FACS, using the recently

described bi-transgenic iDct-GFP mice that allow for tetracyclin-regulated expression of a histone H2B-GFP fusion protein in melanoblasts and melanocytes (ZAIDI *et al.* 2011a; ZAIDI *et al.* 2011b; ZAIDI *et al.* 2011c). For these experiments, we used wild-type embryos at E15.5, E17.5, and postnatal mice at P1, P3 and P7. RNA-Seq of sorted cells clearly showed the presence of Mitf RNA. As shown in Fig. 1A, detailed analyses revealed that although in all samples the majority of reads across the 5' alternative splice junctions of exon 2 corresponded to the exon 2B-exon 3 sequence, a small subset corresponded to the exon 2A-exon 3 sequence. To further confirm these results, we subjected RNA from P1 and P3 FACS-sorted cells to real-time RT-PCR as described (BHARTI *et al.* 2008). The results showed a 2B-/(2B- + 2B+) ratio of between 1.85 and 4.36%. These values were similar to those in passage 10 melanocytes obtained from P2 mice that were wild-type at *Mitf* and homozygous for a *Cdkn2a* targeted null allele used to prevent cell senescence (SVIDERSKAYA *et al.* 2002) (Fig. 1B). In contrast, in corresponding melanocytes from P2 skin of *Mitf*-S73A mutated, *Cdkn2a*^{-/-} mice (labeled S73A in Fig. 1B), the ratio was 90.75%. These results indicate that freshly isolated embryonic or postnatal melanocytes or cultured melanocytes express a small amount of Mitf mRNAs lacking exon 2B and that a serine-73 mutation substantially increases this alternatively spliced transcript.

A targeted mutation in the exon 2A/2B junction of Mitf prevents exclusion of exon 2B in vitro and in vivo

As shown in Fig. 2A and Suppl. Fig. 1, the RNA sequence of the alternative 5' splice site, CACCAG'GUAAAG, is close to the consensus splice sequence, C/AAG'GUA/GAGU. To ensure efficient inclusion of exon 2B despite codon-73 mutations, we deliberately mutated this splice site in genomic DNA to yield RNAs with the sequence CAUCAA'GUUAAA. The mutation was expected to render the 5' splice

junction non-functional without, however, changing the encoded aminoacid sequence. We first tested whether the mutation would function in the intended way in a minigene construct that comprised exon 1M-exon 3 of *Mitf*. Upon transfection into heterologous cells, this construct normally recapitulates the alternative exon 2B splicing and its dependence on the sequence of codon-73. When both the 5' splice junction and codon-73 were mutated, however, only exon 2B+ RNA and no aberrant splice products were produced in vitro (not shown). We then prepared 3 separate targeting constructs that carried the same splice mutation along with a codon for either wild-type serine, aspartate, or alanine (Fig. 2A; for details, see Materials and Methods). After electroporation into embryonic stem cells, three lines of targeted mice designated *Mitf*$^{mi-S-S73S}$, *Mitf*$^{mi-S-S73A}$ and *Mitf*$^{mi-S-S73D}$ (S-S for splice site and serine-73) were obtained and characterized by Southern blot analysis (Fig. 2B,C) and by sequencing (not shown). Together with *Mitf*$^{mi-S73A}$ mice, which do not carry the 5' splice site mutation, we established eight separate lines, four of them containing a floxed neomycin resistance cassette in intron 2 (see Fig. 2A), and four corresponding ones in which this cassette was removed by breeding with *Prm1-Cre* deleter mice.

For RNA analyses, we first used heart tissue because heart expresses relatively high levels of Mitf RNA and, unlike melanocytes, is not altered in a major way by *Mitf* mutations. RT-PCR analyses showed the presence of both exon 2B+ and exon 2B- RNA in wild-type mice; the predominant lack of exon 2B in mice homozygous for the *Mitf*$^{mi-S73A\Delta neo}$ allele; and the exclusive presence of exon 2B in hearts of mice homozygous for either of the three 5' splice-mutant alleles [regular RT-PCR in Suppl. Fig. 2A, qRT-PCR (BHARTI *et al.* 2010) in Suppl. Fig. 2B]. Total levels of Mitf RNAs, averaged from quantitative RT-PCR analyses using primers for exon 6-7 and 8-9 (Suppl. Table 1), were similar to wild type in the mutants in which the neo cassette has been removed (Suppl.

Fig. 2C). In order to determine RNA levels in mice in which the neo cassette was left intact, we used primers specifically covering the mutated exon 2 region to avoid measuring aberrant RNAs potentially starting from the neo cassette. The results showed that when the neo cassette was present, Mitf RNAs containing part or all of exon 2 were reduced by ~50-75% (Suppl. Fig. 2D). Immunoprecipitation/immunoblotting assays of hearts of the different mutants indicated that *Mitf*$^{mi-S73A^{\Delta}neo}$ mice produced MITF protein with a faster electrophoretic mobility, consistent with the predominant expression of MITF lacking exon 2B in such mice (Suppl. Fig. 2E). In contrast, the different S-S73 mutants all produced predominantly full-length MITF protein, but their relative expression levels differed. Compared to *Mitf*$^{mi-S-S73S^{\Delta}neo}$ mice, the levels were approximately 1.3 fold higher in *Mitf*$^{mi-S-S73D^{\Delta}neo}$ and 1.6 fold higher in *Mitf*$^{mi-S-S73A^{\Delta}neo}$ mice, suggesting that the particular residue at position 73 influences protein stability (Suppl. Fig. 2E).

To determine RNA and protein expression specifically in melanocytes, we then tested above described *Mitf*$^{+}$/*Mitf*$^{+}$;*Cdkn2a*$^{-/-}$ and *Mitf*$^{mi-S73A^{\Delta}neo}$/*Mitf*$^{mi-S73A^{\Delta}neo}$;*Cdkn2a*$^{-/-}$ melanocyte lines as well as a corresponding line derived from P2 skin of *Mitf*$^{mi-S-S73A^{\Delta}neo}$/*Mitf*$^{mi-S-S73A^{\Delta}neo}$;*Cdkn2a*$^{-/-}$ mice. RT-PCR assays showed a predominent band representing the Mitf 2B+ transcript in wild type, a double band representing the Mitf 2B+ and Mitf 2B- transcripts in *Mitf*$^{mi-S73A^{\Delta}neo}$ lines, and a single band representing the Mitf 2B+ transcript in *Mitf*$^{mi-S-S73A^{\Delta}neo}$ lines (Fig. 3A). As schematically depicted in Fig. 3B, MITF protein can undergo numerous post-translational modifications in melanocytes and other cell types, including phosphorylations, sumoylations and caspase cleavage. These modifications may lead to proteins with distinct electrophoretic mobilities on western blots. In fact, as shown in Fig. 3C, wild-type melanocytes showed the characteristic

13

double band of MITF protein representing S73-phosphorylated and S73-non-phosphorylated, exon 2B+ protein. *Mitf*$^{mi\text{-}S73A^{\Delta neo}}$ lines showed a more complex picture as

based on electrophoretic mobilities, there was a band corresponding to non-phosphorylated MITF 2B+ and one corresponding to MITF 2B-. In contrast to the relative

amounts of the respective transcripts, however, the MITF 2B+ protein band was more

prominent than the MITF 2B- protein band. This observation suggests that compared to

the wild-type full-length protein, either non-phosphorylated full-length MITF is more

stable or internally truncated MITF less stable, provided exon 2B+ and exon 2B- mRNA

share equal translational efficiency. In addition, *Mitf*$^{mi\text{-}S73A^{\Delta neo}}$ lines showed one band of

lower and one of higher electrophoretic mobility (marked with arrows in Fig. 3C) that may

represent differently modified or cleaved products. *Mitf*$^{mi\text{-}S\text{-}S73A^{\Delta neo}}$ lines showed a single

RT-PCR product corresponding to the Mitf 2B+ transcript and a simpler western blot

signal with a prominent band corresponding to non-phosphorylated MITF 2B+ protein

and one band each of higher and lower electrophoretic mobility (arrows), again

potentially representing differently modified or cleaved products. Quantitation of the

western blot bands revealed that *Mitf*$^{mi\text{-}S73A^{\Delta neo}}$ and *Mitf*$^{mi\text{-}S\text{-}S73A^{\Delta neo}}$ cells had higher MITF

levels than the corresponding wild-type cells (Fig. 3C), consistent with the notion that

lack of phosphorylation at residue 73 may increase accumulation of full-length MITF

because of increased protein stability.

Genetic dissection of pigmentation phenotypes associated with the targeted mutations

To determine the phenotypic consequences of the above mutations, we performed

extensive breeding tests. First, we generated mice containing the neomycin resistance

14

cassette that were either homozygous for the four targeted *Mitf* alleles or were compound heterozygotes with any of three extant Mitf alleles: *Mitf*$^{mi-vga9}$, which is a null allele due to insertion of a transgene array in the M-Mitf promoter (HODGKINSON *et al.* 1993); *Mitf*$^{Mi-wh}$, a semidominant allele characterized by a Ileu212-to-Asn mutation in the DNA-binding basic domain (STEINGRÍMSSON *et al.* 1994); and *Mitf*^{mi}, a semi-dominant allele characterized by the lack of an Arg in a row of four Arg in the basic domain (STEINGRÍMSSON *et al.* 1994). The targeted homozygotes showed normal eyes and normal pigmentation in coat, ears, and feet except for a white belly spot, which on average was largest in *Mitf*$^{mi-S-S73SNeo}$ but almost always absent in *Mitf*$^{mi-S-S73ANeo}$ mice (Fig. 4A-D). Similar phenotypic differences between the targeted alleles were seen in compound heterozygotes with *Mitf*$^{mi-vga9}$. While *Mitf*$^{mi-vga9}$/*Mitf*$^{+}$ mice are normally pigmented (Fig. 4E) and *Mitf*$^{mi-vga9}$/*Mitf*$^{mi-vga9}$ mice totally white and microphthalmic, the compound heterozygotes showed various extents of white spotting whereby *Mitf*$^{mi-S-S73ANeo}$/*Mitf*$^{mi-vga9}$ mice had the smallest areas of white coats; *Mitf*$^{mi-S-S73SNeo}$/*Mitf*$^{mi-vga9}$ mice were almost completely white; and *Mitf*$^{mi-S73ANeo}$/*Mitf*$^{mi-vga9}$ and *Mitf*$^{mi-S-S73DNeo}$/*Mitf*$^{mi-vga9}$ mice were intermediate (Fig. 4F,G,I,J). In contrast, no such differences between the targeted alleles were seen in combination with *Mitf*$^{Mi-wh}$ as all mice had a fawn coat with white spots of similar sizes (Supplemental Figure 2A). Only rarely did we observe small black spots in these mice that may reflect somatic loss-of-function mutations in the dominant-negative *Mitf*$^{Mi-wh}$ allele (an example shown in Supplemental Fig. 2A for *Mitf*$^{mi-S-S73ANeo}$/*Mitf*$^{Mi-wh}$). We also saw no major codon-73-dependent differences in combinations with *Mitf*^{mi} as all mice were totally white except for small black spots that appeared in highest frequency and sizes in *Mitf*$^{mi-S-S73ANeo}$/*Mitf*^{mi} mice but were always absent in *Mitf*$^{mi-S-S73SNeo}$/*Mitf*^{mi} mice (Supplemental Fig. 2B). These results indicate that in alleles containing the neomycin resistance cassette, the presence or absence of exon 2B and

the phosphorylatability or permanent negative charge of residue-73 are associated with phenotypic differences that are, however, only seen in particular allelic combinations.

In a second round of breedings, we used mice lacking the neomycin cassette to generate targeted homozygotes or compound heterozygotes as above. As shown in Fig. 4K-N, homozygotes were all normally pigmented regardless of the splice and serine-73 mutations. In contrast, phenotypic differences between the different targeted *Mitf* alleles were seen in combination with *Mitf*$^{Mi-wh}$ (Fig. 4O-R). Compared with *Mitf*$^{Mi-wh}$/*Mitf*$^{+}$ littermates, both *Mitf*$^{mi-S73A^{\Delta}neo}$/*Mitf*$^{Mi-wh}$ and *Mitf*$^{mi-S-S73A^{\Delta}neo}$/*Mitf*$^{Mi-wh}$ mice had a considerably darker coat, yet they still carried white belly spots typical of the presence of the *Mitf*$^{Mi-wh}$ allele. However, the coat was only slightly darker in *Mitf*$^{mi-S73D^{\Delta}neo}$/*Mitf*$^{Mi-wh}$ mice, and *Mitf*$^{mi-S73S^{\Delta}neo}$/*Mitf*$^{Mi-wh}$ mice were phenotypically indistinguishable from *Mitf*$^{Mi-wh}$/*Mitf*$^{+}$ mice (Fig. 4O-R). Because it was theoretically possible that the presence of MITF protein that cannot be phosphorylated at residue 73 might influence the phosphorylation status of the MITF^{Mi-wh} protein and so influence the stability and dominant-negative activity of the latter, we also performed immunoprecipitation/immunoblot assays of heart tissues of the different allelic combinations. As shown in Suppl. Fig. 2F, however, there was no clear indication for a change in phospho-MITF^{Mi-wh} as the bands in *Mitf*$^{mi-S73A^{\Delta}neo}$/*Mitf*$^{Mi-wh}$ hearts (lane 5) appeared as the sum of those seen in *Mitf*$^{mi-S73A^{\Delta}neo}$/*Mitf*$^{mi-S73A^{\Delta}neo}$ (lane 3) and *Mitf*$^{Mi-wh}$/*Mitf*$^{Mi-wh}$ (lane 8) hearts. Furthermore, none of the targeted alleles showed any differences in combinations with *Mitf*$^{mi-vga9}$ or *Mitf*^{mi} (Supplemental Fig. 2C,D). These results again indicate that phenotypic differences between the different targeted alleles can be revealed only in particular allelic combinations.

Melanoblast and melanocyte accumulation is differently affected by *Mitf*^mi-S73A^ and *Mitf*^mi-S-S73A^

The darker coat associated with the presence of the serine-73-to-alanine mutated MITF protein in *Mitf*^Mi-wh^ compound heterozygotes could be explained by the accumulation of a greater number of melanoblasts and melanocytes in the corresponding mice. The availability of *Kit*^tm1Alf^, a *Kit* null allele characterized by the insertion of a bacterial lacZ gene in exon 1 of *Kit*, allowed us to specifically and reliably label melanoblasts during development. In fact, previous results have shown that the nuclear βGAL produced by *Kit*^tm1Alf^ is not affected by *Mitf* mutations, at least not in melanoblasts (Hou *et al.* 2000). It needs to be kept in mind, however, that *Kit*^tm1Alf^/*Kit*^+^ mice have white feet, tail tips and belly spots as only two fully functional *Kit* alleles allow for completely normal melanoblast development. Hence, the use of *Kit*^tm1Alf^ gave us the added opportunity to compare the phenotypic effects of the different targeted *Mitf* alleles in conjunction with a separate mutation affecting melanogenesis. Intercrosses showed, however, that homozygosity for *Mitf*^mi-S73A^ and *Mitf*^mi-S-S73A^ did not grossly change the *Kit*^tm1Alf^/*Kit*^+^ phenotype except that on average, the belly spots seemed slightly larger with both *Mitf* alleles. We then harvested corresponding E12.5 and E15.5 embryos as well as P1 skin and subjected the specimens to Xgal labeling (Fig. 5). At E12.5, in a representative area around the developing eye, *Kit*^tm1Alf^/*Kit*^+^;*Mitf*^mi-S-S73A^/*Mitf*^mi-S-S73A^ embryos showed similar numbers of Xgal-labeled cells as *Kit*^tm1Alf^/*Kit*^+^;*Mitf*^mi-S73A^/*Mitf*^mi-S73A^ embryos. At E15.5 and P1, however, representative areas showed slightly, but significantly higher numbers of labeled cells in *Kit*^tm1Alf^/*Kit*^+^;*Mitf*^mi-S-S73A^/*Mitf*^mi-S-S73A^ compared to *Kit*^tm1Alf^/*Kit*^+^;*Mitf*^mi-S73A^/*Mitf*^mi-S73A^ mice. This was also reflected in the number of labeled cells in pigmented hair follicles in a representative dorsal area between the forelimbs. The results suggest that the absence of the entire exon 2B, and the selective absence of a phosphorylatable

17

residue at position 73, affect the accumulation of melanoblasts and melanocytes differentially. The findings are consistent with the facts that the presence of the S-S73A allele in some allelic combinations leads to decreased sizes of white spots (or increased numbers of pigmented spots) compared to mice carrying the S73A allele (see Fig. 4A,B; F,G; Suppl. Fig 2B).

Because *Mitf*^mi-S73A^ is a complex allele, giving rise to both exon 2B- as well as exon 2B+ protein (see Fig. 3G), we finally assessed what the separate effects of each of these two isoforms might be in cells in culture. For this, we used ARPE19 cells, which are spontaneously immortalized human retinal pigment epithelial cells that are low in endogenous MITF and yet are derived from a pigmented cell type, and infected them with retroviral vectors expressing either (wild-type) MITF 2B+ (as derived from the *Mitf*^mi-S-S73S^ allele), MITF^S73A^ or MITF^Δ2B^ proteins, each fused with the estrogen-responsive portion of the estrogen receptor (ER) (termed ER WT, ER S73A and ER 2B- in Fig. 6). In such cells, MITF proteins normally are found in the cytoplasm at relatively low levels but accumulate at high levels in nuclei after tamoxifen induction. In fact, western blots revealed the expected MITF bands and electrophoretic mobilities after tamoxifen induction (Fig. 6A). The cells were then subjected to flow cytometry, using two-color fluorescence labeling for MITF protein expression and total DNA content (DAPI) for cell cycle analysis. As shown in Fig. 6B, 48 hours of tamoxifen induction increased the percentage of gated cells showing above-threshold levels of MITF protein. Intriguingly, wild-type MITF-expressing cells showed distinct MITF^low^ and Mitf^high^ populations, whereas MITF^S73A^ and MITF^Δ2B^ expressing cells had a distinctly lower MITF^low^ population. This suggested that the MITF^low^ population was generated by a net reduction of MITF by degradation of the S73-phosphorylated form of MITF. As shown in Fig. 6C, tamoxifen induction of the different MITF isoforms had differential effects on DNA content of cells. While there was little change when the tag alone and no ectopic MITF

18

was present, wild-type MITF^{high} cells showed a decrease in the percentage of cells in S phase and an increase in the percentage of cells in G0/G1 48 hours after tamoxifen induction. In contrast, the percentage of MITF[S73Ahigh] and MITF[Δ2B-high] cells in S-phase was increased, rather than decreased, after tamoxifen induction, though less prominently with MITF[Δ2B] compared to MITF[S73A]. This in vitro analysis with heterologous cells and overexpressed, cDNA-derived inducible proteins suggested that wild-type MITF has antiproliferative activities but that the lack of exon 2B, or the absence of phosphorylation at residue 73, have no such antiproliferative activity. The results confirm earlier findings with an S73A mutated protein analyzed in different cells (BISMUTH *et al.* 2005) and are consistent with the in vivo genetic observations that the relative increased accumulation of non-phosphorylatable MITF protein leads to increased melanoblast/melanocyte numbers, increases in the size and extent of pigmentation in certain heteroallelic combinations, and increased ability to compensate a strong dominant-negative allele, *Mitf[Mi-wh]*.

Discussion

Numerous in vitro assays have shown that MITF is regulated by post-translational modifications, which in turn depend on the presence of the exons carrying the modifiable residues. Nevertheless, among the many spontaneous and induced *Mitf* mutations from zebrafish to man, few have been found so far to affect splicing or a specific post-translationally modifiable residue. This is not surprising given the fact that, for instance, targeted mutations in the serine-73 phosphoacceptor site as described here, along with those used in BAC transgenic rescue strategies (BAUER *et al.* 2009), produce little if any phenotypes on their own. It is only in conjunction with additional perturbations, such as the reduction in overall *Mitf* RNA levels or the combination with other *Mitf* alleles, that we

start to see the effects of mutations in serine-73, or, in addition, the subtle differences between a serine-73 mutation and the lack of the entire exon carrying serine-73.

Our analysis of the phenotypes produced by the targeted alleles benefited from the wide dynamic range of pigmentation and from the fact that the targeted mutations were produced in the endogenous gene rather than in BACs. Targeting the endogenous gene allows for a direct comparison between the different lines as their transcript levels are all similar to wild-type. In contrast, *Mitf* BAC transgenic lines show variable RNA expression levels (BAUER *et al.* 2009) likely due to the fact that the available BACs do not contain the entire 214 kb *Mitf* gene and so may lack the boundary elements necessary for sufficient insulation from neighboring sequences encountered at random transgene insertion sites. Comparable RNA expression levels were all the more important because the task was to evaluate the effects of mutations that may affect the stability of the mutated proteins. It has been shown in vitro that serine-73 mutated MITF has a similar activity on a test target gene promoter as non-phosphorylated wild-type MITF, but a lower activity when compared to phosphorylated wild-type MITF (HEMESATH *et al.* 1998). In subsequent in vitro experiments, it was reported that S73A singly mutated MITF or S73A/S409 doubly mutated MITF have an increased stability. Hence, it became important to determine whether there might be similar increases in the stability of mutated MITF protein in vivo, and whether a possible reduction in transcriptional activity was compensated for by increased protein stability.

The simplest explanation for all genetic results presented in this paper is indeed an increased stability of the mutated proteins. First, we find that both in an unrelated tissue, the heart, and in melanocytes, S73A mutated MITF accumulates to higher levels than corresponding wild-type MITF. Interestingly, in heart, S73D mutated MITF accumulates to levels intermediate between those in S73A and S73S mutated MITF, reflecting the intermediate phenotype that the *Mitf^{mi-S-S73D}* allele produces in some allelic

20

combinations. This suggests that a permanent negative charge at residue-73 neither reflects fully the properties of serine-73 phosphorylated MITF nor those of residue-73 non-phosphoryated MITF. Second, homozygotes for the mutations with wild-type transcript levels are all fully pigmented. Third, the two mutations resulting in MITF that cannot be phosphorylated at residue 73 ($Mitf^{mi-S-S73A\Delta Neo}$ and $Mitf^{mi-S73A\Delta Neo}$) are capable of partially compensating the effects of the strongly dominant-negative $Mitf^{Mi-wh}$ allele. Fourth, when the Mitf RNA expression levels of the neo-cassette-containing alleles were further reduced in compound heterozygotes with the null mutant $Mitf^{mi-vga-9}$, MITF^{S73A}-expressing mice, with the lowest RNA levels, produced the most extensive pigmentation, and MITF^{S73S}-expressing mice, with higher RNA levels, the least amount of pigmentation. Fifth, in vitro, both MITF^{S73A} and MITF$^{\Delta 2B}$ have milder anti-proliferative effects than corresponding wild-type MITF, or they may even stimulate cell proliferation given the non-limiting amounts of growth factors to which cultured cells are normally exposed. Nevertheless, despite this in vitro finding, the number of melanocytes found postnatally in vivo is not substantially different in mutants compared to wild type. This is likely due to the fact that only excess amounts of growth factors such as KIT ligand or endothelin-3 would allow for prolonged survival of supernumerary melanocytes in vivo.

The above observations imply that increased accumulation of the mutated MITF proteins may not only compensate for the reduction of their activities observed in vitro, but may even over-compensate such activity reductions. This underscores the in vivo importance of post-translational modifications that would seem to allow for precise regulation of the activities of MITF. The results presented in this paper also imply that MITF^{S73A} and MITF$^{\Delta 2B}$ have slightly different effects in vivo. Although $Mitf^{mi-S73A}$ can produce both full-length and exon 2B-deleted MITF, and although the full-length MITF^{S73A} protein may be relatively more stable than the internally truncated one, $Mitf^{mi-S73A}$ and $Mitf^{mi-S-S73A}$ mice still differ slightly in melanoblast/melanocyte numbers when

they are counted during development and postnatally, or in extent of pigmentation in the adult if RNA levels are reduced below a threshold amount by presence of a neo cassette in combination with the *Mitf* null allele *Mitf^{mi-vga9}*. Although subtle differences in the total levels of MITF may explain these variations, it is equally plausible that exon 2B has additional functions besides simply providing the substrate for serine-73 phosphorylation. In fact, it is conceivable that wild type MITF, MITF^{S73A} and MITF^{Δ2B} differentially stimulate their target genes. This may be important when considering allele-specific genetic interactions of *Mitf^{mi-bws}*, an *Mitf* allele with an exon 2B splice bias but low RNA levels and a wild type serine-73 (WEN *et al.* 2010). It may also be important to explain the recent finding that human MITF^{Δ2B}, when used to rescue pigmentation in zebrafish with a temperature-sensitive mutation in *mitfa*, leads to increased divisions of differentiated, pigmented cells (TAYLOR *et al.* 2011). Moreover, it may become important to explain the recent finding that a melanoma metastasis carries a somatic mutation at the downstream exon 2B splice junction that leads to elimination of exon 2B (CRONIN *et al.* 2009). Although alterations in *MITF* may be only one among many pathways whose changes allow for differentiated cells or melanoma cells to escape normal control of cell proliferation, it may well be that MITF splice alterations, genomically fixed or dynamically regulated, provide for both efficient and precise modulation of melanocyte or melanoma physiology.

Acknowledgments

Literature Cited

ARNHEITER, H., 2010 The discovery of the microphthalmia locus and its gene, Mitf. Pigment Cell Melanoma Res **23:** 729-735.

ARNHEITER, H., L. HOU, M. T. T. NGUYEN, K. BISMUTH, T. CSERMELY *et al.*, 2006 Mitf—A matter of life and death for the developing melanocyte in *From Melanocytes to Melanoma: The progression to malignancy*, edited by V. HEARING and S. P. L. LEONG. Humana Press, Totowa, NJ.

BAUER, G. L., C. PRAETORIUS, K. BERGSTEINSDOTTIR, J. H. HALLSSON, B. K. GISLADOTTIR *et al.*, 2009 The role of MITF phosphorylation sites during coat color and eye development in mice analyzed by bacterial artificial chromosome transgene rescue. Genetics **183:** 581-594.

BERNEX, F., P. DE SEPULVEDA, C. KRESS, C. ELBAZ, C. DELOUIS *et al.*, 1996 Spatial and temporal patterns of c-kit-expressing cells in WlacZ/+ and WlacZ/WlacZ mouse embryos. Development **122:** 3023-3033.

BHARTI, K., J. DEBBACHE, X. WANG and H. ARNHEITER, 2010 The basic-helix-loop-helix-leucine zipper gene Mitf: analysis of alternative promoter choice and splicing. Methods Mol Biol **647:** 237-250.

BHARTI, K., W. LIU, T. CSERMELY, S. BERTUZZI and H. ARNHEITER, 2008 Alternative promoter use in eye development: the complex role and regulation of the transcription factor MITF. Development **135:** 1169-1178.

BISMUTH, K., D. MARIC and H. ARNHEITER, 2005 MITF and cell proliferation: the role of alternative splice forms. Pigment Cell Res **18:** 349-359.

BISMUTH, K., S. SKUNTZ, J. H. HALLSSON, E. PAK, A. S. DUTRA *et al.*, 2008 An unstable targeted allele of the mouse Mitf gene with a high somatic and germline reversion rate. Genetics **178:** 259-272.

CARREIRA, S., J. GOODALL, I. AKSAN, S. A. LA ROCCA, M. D. GALIBERT *et al.*, 2005 Mitf
cooperates with Rb1 and activates p21Cip1 expression to regulate cell cycle
progression. Nature **433:** 764-769.

CRONIN, J. C., J. WUNDERLICH, S. K. LOFTUS, T. D. PRICKETT, X. WEI *et al.*, 2009
Frequent mutations in the MITF pathway in melanoma. Pigment Cell Melanoma
Res **22:** 435-444.

HALLSSON, J. H., J. FAVOR, C. HODGKINSON, T. GLASER, M. L. LAMOREUX *et al.*, 2000
Genomic, transcriptional and mutational analysis of the mouse microphthalmia
locus. Genetics **155:** 291-300.

HEMESATH, T. J., E. R. PRICE, C. TAKEMOTO, T. BADALIAN and D. E. FISHER, 1998 MAP
kinase links the transcription factor Microphthalmia to c-Kit signalling in
melanocytes. Nature **391:** 298-301.

HODGKINSON, C. A., K. J. MOORE, A. NAKAYAMA, E. STEINGRÍMSSON, N. G. COPELAND *et
al.*, 1993 Mutations at the mouse microphthalmia locus are associated with
defects in a gene encoding a novel basic-helix-loop-helix-zipper protein. Cell **74:**
395-404.

HOEK, K. S., and C. R. GODING, 2010 Cancer stem cells versus phenotype-switching in
melanoma. Pigment Cell Melanoma Res **23:** 746-759.

HOU, L., J. J. PANTHIER and H. ARNHEITER, 2000 Signaling and transcriptional regulation
in the neural crest-derived melanocyte lineage: interactions between KIT and
MITF. Development **127:** 5379-5389.

MANN, M., and O. N. JENSEN, 2003 Proteomic analysis of post-translational
modifications. Nat Biotechnol **21:** 255-261.

NILSEN, T. W., and B. R. GRAVELEY, 2010 Expansion of the eukaryotic proteome by
alternative splicing. Nature **463:** 457-463.

STEINGRÍMSSON, E., K. J. MOORE, M. L. LAMOREUX, A. R. FERRE-D'AMARE, S. K. BURLEY *et al.*, 1994 Molecular basis of mouse microphthalmia (mi) mutations helps explain their developmental and phenotypic consequences [see comments]. Nat Genet **8:** 256-263.

STRUB, T., S. GIULIANO, T. YE, C. BONET, C. KEIME *et al.*, 2011 Essential role of microphthalmia transcription factor for DNA replication, mitosis and genomic stability in melanoma. Oncogene **30:** 2319-2332.

SVIDERSKAYA, E. V., S. P. HILL, T. J. EVANS-WHIPP, L. CHIN, S. J. ORLOW *et al.*, 2002 p16(Ink4a) in melanocyte senescence and differentiation. J Natl Cancer Inst **94:** 446-454.

TAYLOR, K. L., J. A. LISTER, Z. ZENG, H. ISHIZAKI, C. ANDERSON *et al.*, 2011 Differentiated melanocyte cell division occurs in vivo and is promoted by mutations in Mitf. Development **138:** 3579-3589.

WANG, X., J. DEBBACHE and H. ARNHEITER, 2009 Alternative splicing and cell cycle regulation in vertebrate pigment cells. Developmental Biol **331:** 468-468.

WEN, B., Y. CHEN, H. LI, J. WANG, J. SHEN *et al.*, 2010 Allele-specific genetic interactions between Mitf and Kit affect melanocyte development. Pigment Cell Melanoma Res **23:** 441-447.

WU, M., T. J. HEMESATH, C. M. TAKEMOTO, M. A. HORSTMANN, A. G. WELLS *et al.*, 2000 c-Kit triggers dual phosphorylations, which couple activation and degradation of the essential melanocyte factor Mi. Genes Dev **14:** 301-312.

WU, T. D., and S. NACU, 2010 Fast and SNP-tolerant detection of complex variants and splicing in short reads. Bioinformatics **26:** 873-881.

XU, W., L. GONG, M. M. HADDAD, O. BISCHOF, J. CAMPISI *et al.*, 2000 Regulation of microphthalmia-associated transcription factor MITF protein levels by association with the ubiquitin-conjugating enzyme hUBC9. Exp Cell Res **255:** 135-143.

Zaidi, M. R., S. Davis, F. P. Noonan, C. Graff-Cherry, T. S. Hawley *et al.*, 2011a Interferon-gamma links ultraviolet radiation to melanomagenesis in mice. Nature **469:** 548-553.

Zaidi, M. R., C. P. Day and G. Merlino, 2011b Fluorescent protein-assisted purification for gene expression profiling. Methods Mol Biol **699:** 393-405.

Zaidi, M. R., T. J. Hornyak and G. Merlino, 2011c A genetically engineered mouse model with inducible GFP expression in melanocytes. Pigment Cell Melanoma Res **24:** 393-394.

Figure Legends

Figure 1. Detection of *Mitf* isoforms in melanocytes in vivo. (A) GFP positive melanoblasts from bi-transgenic (iDct-GFP) embryos and postnatal pups of the indicated ages were isolated and subjected to sorting by FACS. Corresponding RNA-seq data were analyzed as described in Materials and Methods. The ratios of the reads across exon 2A/exon 3 and exon 2B/exon 3 [2B$^-$/(2B$^-$ + 2B$^+$)] as well as the total number of reads analyzed are shown. (B) The relative abundance of Mitf 2B+ and Mitf 2B- RNA prepared from in vivo isolated P1 and P3 melanocytes, expressing GFP and FACS-sorted as for (A), was determined by qRT-PCR using the appropriate primer pairs (Suppl. Table 1). In addition, RNA from melanocyte cell lines derived from either B6•*Cdkn2a$^{-/-}$;Mitf$^+$/Mitf$^+$* and B6•*Cdkn2a$^{-/-}$;Mitf$^{mi-S73A}$/Mitf$^{mi-S73A}$* P1 dorsal skins and cultured for 10 passages served as controls. The calculated percentages correspond to the ratio of 2B$^-$/(2B$^-$ + 2B$^+$).

Figure 2. Generation of four knock-in *Mitf* alleles. (A) Schematic representation of the *Mitf* genomic structure and the mutations generated in *Mitf$^{mi-S73Aneo}$* [previously described (BISMUTH *et al.* 2008) and re-targeted for the purpose of this study] and in the three novel splice alleles. Sequence modifications at the exon 2A-2B junction as well as at the S73 codon are highlighted in red, and the position of the neomycin resistance cassette in intron 2 is shown. (B,C) Differential restriction profile of the *Mitf* locus before and after targeting and Southern blot analysis of wild-type and one line each of homozygous targeted mice. DNA was digested as indicated and probed with the respective 5' and 3' probes shown in (B).

Figure 3. Mitf exon 2B alternative splicing profile at the RNA and protein level in melanocyte lines. (A) RNA extracts were prepared from passage 10 *Cdkn2a$^{-/-}$*

melanocyte lines from wild-type B6, *Mitf*$^{mi-S73A\triangle Neo}$ (S73A) and *Mitf*$^{mi-S-S73A\triangle Neo}$ (S-S73A) mice and subjected to RT-PCR. (B) Schematic diagram of select prost-translational modifications of MITF seen in melanocytes and other cell types. Indicated are phsophorylation, sumoylation and caspase cleavage sites, while sites for acetylation, ubiquitination and other modificatiions are not shown. (C) Western blots of protein extract of the cell lines used in (A), probed with 6A5 anti-MITF antibodies. The double band seen in the wild-type sample corresponds to phosphorylated and non-phosphorylated exon 2B+ MITF. *Mitf*$^{mi-S73A}$ cells show both a minor band corresponding to 2B- MITF and a major band corresponding to 2B+ MITF, in addition to a band of higher molecular weight and one of lower molecular weight (arrows). *Mitf*$^{mi-S-S73A}$ cells show a predominant 2B+ MITF band and no 2B- MITF band. Also, there is a band of higher molecular weight and one of lower molecular weight (arrows). MITF quantification relative to the endogenous β-Tubulin is indicated below the gel.

Figure 4. Phenotypes associated with the four knock-in alleles alone and in combination with extant *Mitf* alleles. (A-J) Controls and neo-cassette-containing lines. (A-D) White belly spots found in homozygotes of the indicated genotypes. Note that *Mitf*$^{mi-S-S73A}$ homozygotes show no belly spot, in contrast to the other lines. (E) *Mitf*$^{mi-vga9}$ heterozygotes show no pigmentary phenotype while (H) *Mitf*$^{mi-vga9}$ homozygotes are completely white and microphthalmic. (F,G,I,J) Heteroallelic combinations with *Mitf*$^{mi-vga9.}$. Note different degrees of white spotting with the different targeted alleles. (K-R) Lines lacking the neo cassette (△Neo). (K-N) Regardless of the genotype, all homozygotes are normally pigmented and indistinguishable by visual inspection from wild-type B6 mice, except that *Mitf*$^{mi-S73A\triangle Neo}$/*Mitf*$^{mi-S73A\triangle Neo}$ mice have a tail with generally lighter pigmentation compared to the other genotypes. (O-R) Heteroallelic combinations with *Mitf*$^{Mi-wh}$. Note the darker pigmentation seen in combinations with either *Mitf*$^{mi-S73A\triangle Neo}$ or

Mitf^mi-S-S73AΔNeo^ compared to combinations with *Mitf*^mi-S-S73DΔNeo^, which yield mice with a coat that was only slightly darker, and combinations with *Mitf*^mi-S-S73SΔNeo^, which yield mice that are indistinguishable from *Mitf*^Mi-wh^/*Mitf*^+^ heterozygotes. Each photograph in O-R represents littermates.

Figure 5. Melanocyte numbers in developing embryos. Embryos homozygous for either *Mitf*^mi-S73AΔNeo^ or *Mitf*^mi-S-S73AΔNeo^ and heterozygous for *Kit*^tm1Alf^ were Xgal-labeled and blue cells counted in selected regions at E12.5, E15.5 and in P1 skin and P1 pigmented hair follicles. Numbers from 7-10 fields from at least three embryos are shown relative to those observed in *Kit*^tm1Alf^/*Kit*^+^ control samples. Statistical significance (2 tailed unpaired t-test) is indicated (* $p<0.1$; ** $p<0.01$; *** $p<0.001$).

Figure 6. Effects of the S73A mutation and exon 2B deletion on protein levels and DNA content in stable cell lines inducibly expressing MITF. ARPE-19 cells expressing either pBABE-ER (ER- Ø), MITF wild-type S73 (ER-WT), MITF S73A (ER-S73A), or MITF 2B-(ER-2B-) proteins were treated with 4-OH-tamoxifen (Tm) for 48h before collection, and total extracts were probed with 6A5 anti-MITF antibodies. Wild-type MITF expressing cells show the characteristic double band of S73-phosphorylated and non-phosphorylated MITF protein, S73A-MITF expressing cells only one band corresponding to non-phosphorylated MITF, and 2B- MITF-expressing cells a single band corresponding to the 2B- isoform. (B,C) ER-MITF and ER-only (ER- Ø) expressing ARPE-19 cell lines were incubated with or without 4-OH-tamoxifen, harvested after 48 hours, and labeled for MITF and DNA content, using DAPI. (B) Flow cytometric analysis displays the percentage of cells expressing relatively low (L) or high (H) MITF intensity and (C) their relative cell cycle stages based on DNA content. Gating was determined empirically and applied equally for all samples.

Supplemental Figure 1. Sequence changes at the 5' alternative splice site and codon-73. The exon 2A-2B junction closely matches the exon-intron consensus motif required for recognition by the spliceosome. Multiple nucleotide changes were made in order to alter this conserved motif while keeping the encoded protein sequence unchanged. In parallel, codon-73 was changed as indicated and the *Apa*L1 site present in *Mitf*$^{mi-S73A}$ was reverted to the wild-type sequence in the novel splice-mutant alleles.

Supplemental Figure 2. (A) cDNA generated from hearts of wild-type and homozygous knock-in mice were amplified using a primer pair across exons 2A and 3. Wild-type B6 cDNA (first lane) shows predominantly the 2B+ isoform while *Mitf*$^{mi-S73A}$ cDNA (second lane) shows predominantly the 2B- isoform and cDNAs of each of the splice mutant lines only the 2B+ isoform. Quantification by qRT-PCR, using appropriate mutant-specific primer pairs (see Supplemental Table 1) is shown in (B). (C) qRT-PCR of heart Mitf RNA from homozygotes carrying the indicated alleles after removal of the neo cassette. The results averaged from using primers spanning exon 6B-7 and 7-8 junctions are given and compared to those obtained from wild-type B6 and *Mitf*$^{mi-S73AΔneo}$/*Mitf*$^{mi-vga9}$ mice, the latter known to express no Mitf RNA from the *Mitf*$^{mi-vga9}$ null allele. The measurements showed no statistically significant changes in *Mitf* expression levels in the knock-in mice compared to wild type. (D) Effect of the neo cassette on *Mitf* expression in heart. The expression levels of Mitf 2B- in *Mitf*$^{mi-S73ANeo}$ mice and Mitf 2B+ in *Mitf*$^{mi-S-S73ANeo}$, *Mitf*$^{mi-S-S73DNeo}$ and *Mitf*$^{mi-S-S73SNeo}$ mice (Neo) was compared to those of the corresponding mice lacking the neo cassette (ΔNeo). The results show a reduction of 50% to 75% of Mitf expression in Neo-containing alleles. (E) MITF protein expression in heart tissue. Whole protein extracts were immunoprecipitated with a rabbit-anit-MITF serum from wild-type, *Mitf*$^{mi-vga9}$/*Mitf*$^{mi-vga9}$ and ΔNeo knock-in mice, subjected to SDS-polyacrylamide gel electrophoresis, and probed with 6A5 antibodies, which recognize the C-terminal part of

MITF protein. *Mitf*^{mi-S73A} hearts show a band corresponding to exon 2B- MITF in addition to possible degradation products and a background band representing IgG (arrows). Heart extracts from mice homozygous for the 3' splice mutation each show a major band corresponding to exon 2B+ MITF. Their expression levels relative to the internal β-Tubulin control and S-S73S as reference are shown below the gel. The S73A sample was not quantified because of the overlap of some MITF isoforms with the background IgG band. (F) Western blots of heart extracts of various mutants and their combinations. Protein extracts were prepared an d processed as for (E). Alleles and allelic combinations are as indicated. Note MITF 2B+ phospho and non-phospho form in wild type (lane 1), absence of MITF in *Mitf*^{mi-vga-9} homozygotes (lane 2), and absence of MITF 2B+ phospho form in Mitf^{mi-S73AΔneo} homozygotes. Arrows indicate a band corresponding to IgG heavy chain.

Supplemental Figure 3. Additional phenotypes associated with heteroallelic combinations between the targeted and extant *Mitf* alleles. The genotypes of the depicted mice are indicated. Note that in combinations with *Mitf*^{Mi-wh}, all four targeted alleles containing the Neo cassette produce a similar lightly tanned coat and variably sized white belly spots (A). In combination with *Mitf*^{mi}, the mice become largely white with small black spots that are most frequent with *Mitf*^{mi-S-S73Aneo} and totally absent in *Mitf*^{mi-S-S73Sneo} (B). (C,D) No phenotypic distinctions are seen in heteroallelic combinations with *Mitf*^{mi} or *Mitf*^{mi-vga9} once the neo cassette has been removed, except for *Mitf*^{mi-S73AΔNeo}/*Mitf*^{mi}, *Mitf*^{mi-S-S73SΔNeo}/*Mitf*^{mi}, and *Mitf*^{mi-S-S73SΔNeo}/*Mitf*^{mi-vga9} mice, which displayed variable, though more extensive depigmentation of the tail tip compared to normal C57BL/6 mice.

A   RNA-seq analysis of Mitf exon 2B alternative splicing profile
on GFP-positive sorted melanoblasts and melanocytes

Embryo stage	Ratio $\frac{2B-}{(2B- \mathbf{+} 2B+)}$	Total Mitf Reads Containing Exon 3 junctions
E15.5	2.7%	37
E17.5	0.7%	277
Post natal 1 Day	2.2%	557
Post natal 7 Days	1.9%	206
Total averaged	1.8%	1077

B   RT-PCR analysis of Mitf exon 2B alternative splicing profile
on both GFP-sorted and purified cultured melanocytes
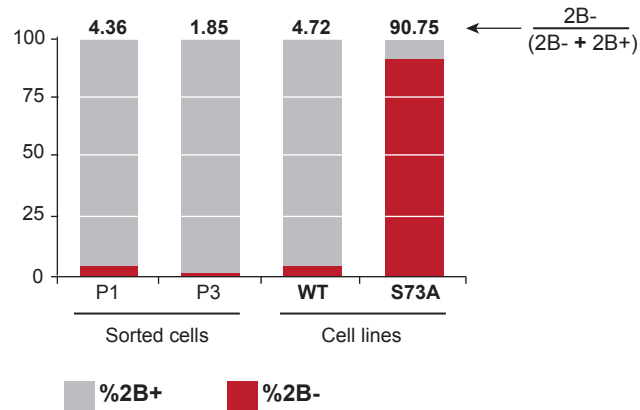
A Genomic modifications of 4 *Mitf* knock-in alleles
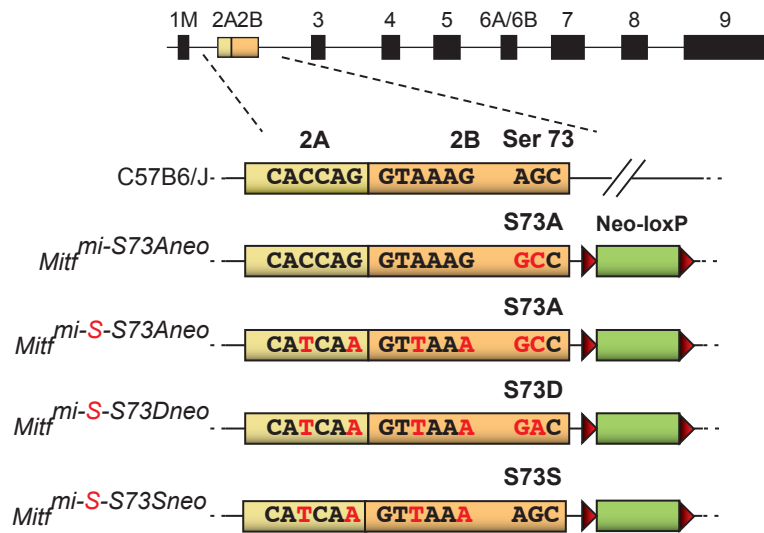
B Schematic diagram of *Mitf* before and after targeting
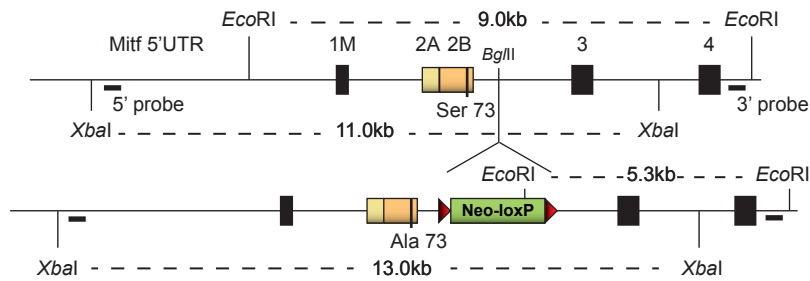
C Southern analysis of homozygous *Mitf* knock-in mice

Debbache et al., Figure 2
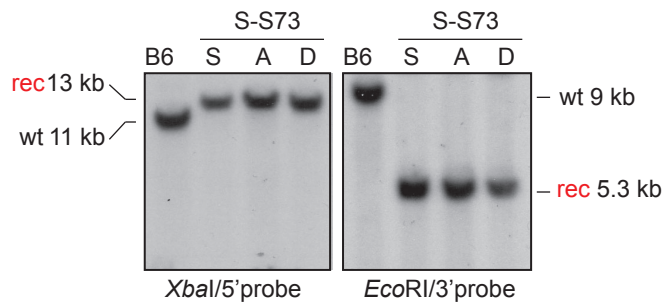
A Mitf transcript expression in melanocyte lines
derived from wild-type and mutant mice

— Mitf 2B+
— Mitf 2B-
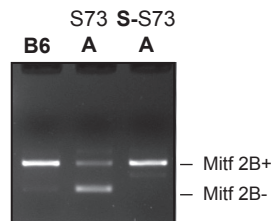
B Positions of select post-translational modifications
sites in MITF

1M   2A/B   3   4   5   6A/B   7   8   9

2A   2B

b-H   H-LZ

Loop

S73   S173 K182   S298 K316 D345   S409
S307

■ Phosphorylation   ● SUMOylation   ■ Caspase cleavage

C MITF protein expression in melanocyte lines
derived from wild-type and mutant mice

89 kD —
MITF S73-P —
MITF S73

— MITF 2B+
— MITF 2B-

β-Tubulin

$Mitf^{mi-S73Aneo}/Mitf^{mi-S73Aneo}$

$Mitf^{mi-S-S73Aneo}/Mitf^{mi-S-S73Aneo}$

$Mitf^{mi-vga9}/Mitf^{+}$

$Mitf^{mi-S73Aneo}/Mitf^{mi-vga9}$

$Mitf^{mi-S-S73Aneo}/Mitf^{mi-vga9}$

$Mitf^{mi-S-S73Dneo}/Mitf^{mi-S-S73Dneo}$

$Mitf^{mi-S-S73Sneo}/Mitf^{mi-S-S73Sneo}$

$Mitf^{mi-vga9}/Mitf^{mi-vga9}$

$Mitf^{mi-S-S73Dneo}/Mitf^{mi-vga9}$

$Mitf^{mi-S-S73Sneo}/Mitf^{mi-vga9}$

$Mitf^{mi-S73A\Delta neo}/Mitf^{mi-S73A\Delta neo}$

$Mitf^{mi-S-S73A\Delta neo}/Mitf^{mi-S-S73A\Delta neo}$

$Mitf^{Mi-wh}/Mitf^{+}$ $Mitf^{mi-S73A\Delta neo}/Mitf^{Mi-wh}$ $Mitf^{Mi-wh}/Mitf^{+}$ $Mitf^{mi-S-S73A\Delta neo}/Mitf^{Mi-wh}$

$Mitf^{mi-S-S73D\Delta neo}/Mitf^{mi-S-S73\Delta Dneo}$

$Mitf^{mi-S-S73S\Delta neo}/Mitf^{mi-S-S73S\Delta neo}$

$Mitf^{Mi-wh}/Mitf^{+}$ $Mitf^{mi-S-S73D\Delta neo}/Mitf^{Mi-wh}$ $Mitf^{Mi-wh}/Mitf^{+}$ $Mitf^{mi-S-S73S\Delta neo}/Mitf^{Mi-wh}$

Debbache et al., Figure 4

Relative number of LacZ positive cells compared to Mitf wild-type embryos

E12.5

E15.5

P1

P1 hair follicles

Debbache et al., Figure 5

A MITF expression in stably transfected
ARPE-19 cell lines
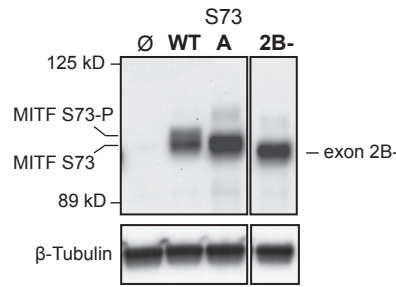
B FACS Analysis of MITF versus DAPI labelling of stably transfected ARPE-19 cell lines
with an inducible ER-MITF vector with or without Tamoxfien.

Tm -

Region	% Gated	Y Mean
MITF (-)	99.96	2.51
MITF (L)	0.03	20.95
MITF (H)	0.01	153.71

Region	% Gated	Y Mean
MITF (-)	59.39	3.40
MITF (L)	22.52	28.40
MITF (H)	18.29	213.25

Region	% Gated	Y Mean
MITF (-)	55.00	3.27
MITF (L)	19.22	27.72
MITF (H)	25.99	240.85

Region	% Gated	Y Mean
MITF (-)	39.56	3.47
MITF (L)	19.05	29.76
MITF (H)	41.56	241.66

Tm +

Region	% Gated	Y Mean
MITF (-)	99.98	2.37
MITF (L)	0.02	15.64
MITF (H)	0.00	***

Region	% Gated	Y Mean
MITF (-)	47.00	3.68
MITF (L)	27.46	28.23
MITF (H)	25.75	195.56

Region	% Gated	Y Mean
MITF (-)	39.48	3.76
MITF (L)	31.00	30.60
MITF (H)	29.84	140.77

Region	% Gated	Y Mean
MITF (-)	30.13	3.71
MITF (L)	31.28	35.12
MITF (H)	38.97	126.30

C DAPI-based cell cycle distribution of MITF-gated ARPE-19 cell lines with or
without Tamoxifen

Tm -

Cell cycle position	ER Ø	ER WT		ER S73A		ER 2B-	
	Mitf Negative	Mitf Low	Mitf High	Mitf Low	Mitf High	Mitf Low	Mitf High
% G0/G1	69.35	68.15	67.82	63.4	63.48	63.73	63.62
% S	18.21	18.62	17.95	18.5	18.82	17.74	18.68
% G2/M	12.67	13.41	14.42	18.24	17.99	18.78	17.98

Tm +

Cell cycle position	ER Ø	ER WT		ER S73A		ER 2B-	
	Mitf Negative	Mitf Low	Mitf High	Mitf Low	Mitf High	Mitf Low	Mitf High
% G0/G1	71.39	70.98	77.44	62.69	61.28	70.33	66.06
% S	19.17	19.98	14.64	21.6	27.62	19.85	23.49
% G2/M	9.55	9.19	8.06	16.01	11.53	10.12	10.86

Debbache et al., Figure 6

	Exon	Intron
Consensus :	A/CAG	GURAGU

	Ex2A	Ex2B
Wild Type Sequence:	CACCAG	GUAAAG
	***	****
	H Q	V K

Mutated Sequence:	CAUCAA	GUUAAA
	**	** *
	H Q	V K

	Ex2A	Ex2B		ApaLI	S73
Wild Type :	CACCAG	GTAAAG-----AGCGCACCCAAC**AGC**CCT
S73A :	CACCAG	GTAAAG-----A<u>GTGCAC</u>CCAAC**GCC**CCT
S-S73A:	CA**T**CA**A**	GT**T**AA**A**-----AGCGCACCCAAC**GCC**CCT
S-S73D:	CA**T**CA**A**	GT**T**AA**A**-----AGCGCACCCAAC**GAC**CCT
S-S73S:	CA**T**CA**A**	GT**T**AA**A**-----AG**C**GCACCCAAC**AGC**CCT

Debbache et al., Suppl. Fig.1

A PCR of heart cDNA
(Mitf exon 2A to exon 3)

ΔNeo

B6 S73 **S**-S73 **S**-S73 **S**-S73
     A   A   D   S

2B+
2B-
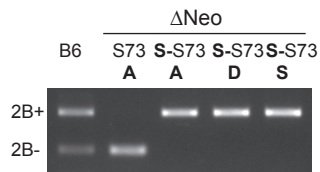
B qRT-PCR of Mitf 2B+ and Mitf 2B- cDNA from
mutant mouse heart

87.71 1.64 99.81 100 100

ΔNeo
■ % 2B+
■ % 2B-

B6 S73 **S**-S73 **S**-S73 **S**-S73
     A   A   D   S
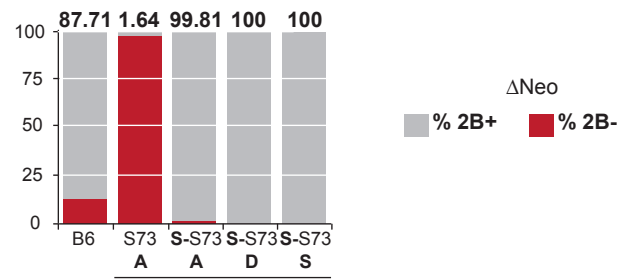
C Relative Mitf expression
in heart tissue of the different
mutants

***

B6 S73**A**/ S73 **S**-S73 **S**-S73 **S**-S73
    vga9   A   A   D   S

ΔNeo
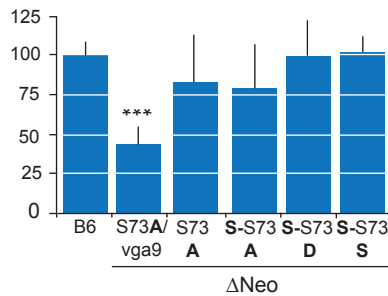
D Relative Mitf expression in hearts of lines
with or without the neo-cassette

S73**A**   **S**-S73**A**   **S**-S73**D**   **S**-S73**S**

ΔNeo Neo ΔNeo/   ΔNeo Neo   ΔNeo Neo   ΔNeo Neo
           vga9
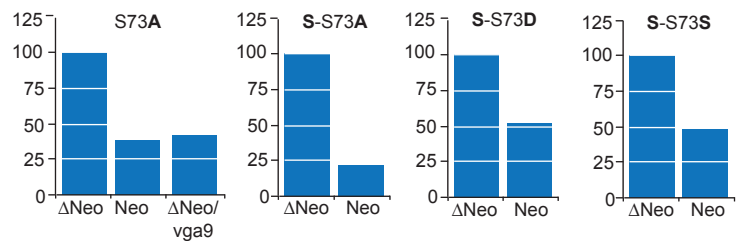
E MITF expression in heart tissue of wild-type
C57BL/6 and homozygous mutant mice

ΔNeo

S73   **S**-S73
A   A   D   S

89 kD —

MITF 2B- —   — MITF 2B+

β-Tubulin

ND 165.0 129.8 100.0   MITF relative
                          expression
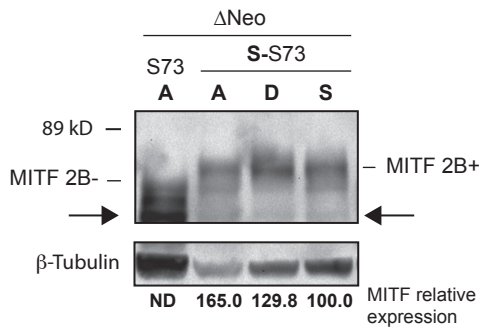
F MITF expression in heart tissue of different
mutant combinations

1 2 3 4 5 6 7 8

MITF 2B+ P —
MITF 2B+ —
MITF 2B- —

1: $Mitf^{+}/Mitf^{+}$

2: $Mitf^{mi-vga9}/Mitf^{mi-vga9}$

3: $Mitf^{mi-S73AΔneo}/Mitf^{mi-S73AΔneo}$

4: $Mitf^{mi-S73AΔneo}/Mitf^{mi-vga9}$

5: $Mitf^{mi-S73AΔneo}/Mitf^{Mi-wh}$

6: $Mitf^{Mi-wh}/Mitf^{mi-vga9}$

7: $Mitf^{Mi-wh}/Mitf^{+}$

8: $Mitf^{Mi-wh}/Mitf^{Mi-wh}$

Debbache et al., Suppl. Fig. 2
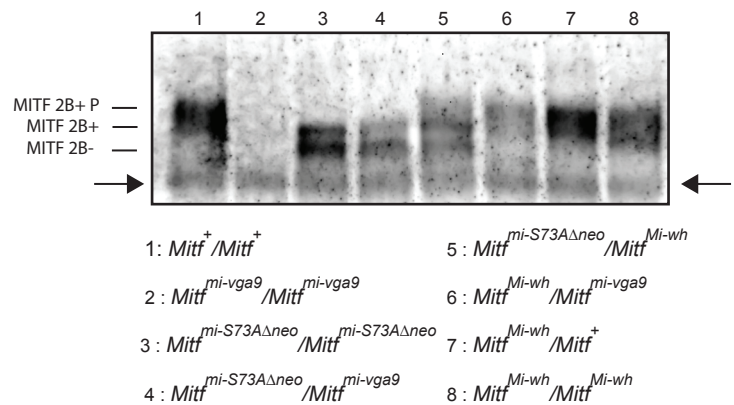
A

$Mitf^{mi-S73Aneo}/Mitf^{Mi-wh}$ | $Mitf^{mi-S-S73Aneo}/Mitf^{Mi-wh}$
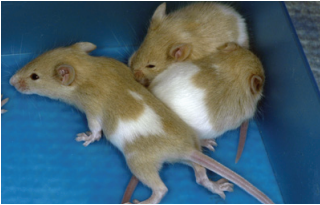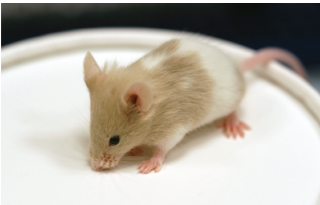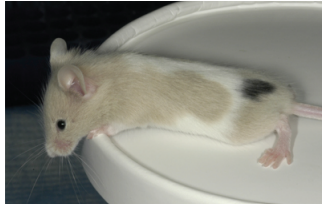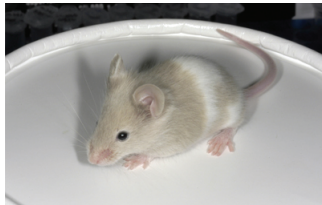
$Mitf^{mi-S-S73Dneo}/Mitf^{Mi-wh}$ | $Mitf^{mi-S-S73Sneo}/Mitf^{Mi-wh}$
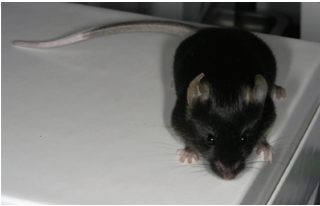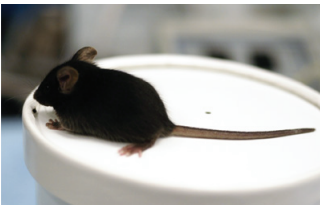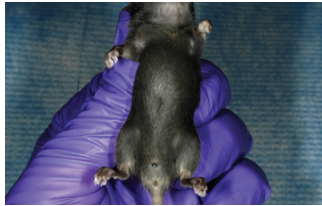
B

$Mitf^{mi-S73Aneo}/Mitf^{mi}$ | $Mitf^{mi-S-S73Aneo}/Mitf^{mi}$

$Mitf^{mi-S-S73Dneo}/Mitf^{mi}$ | $Mitf^{mi-S-S73Sneo}/Mitf^{mi}$

C
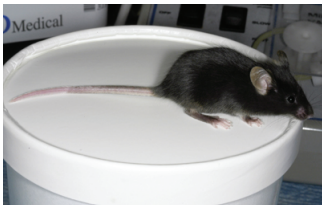
$Mitf^{mi-S73A\Delta neo}/Mitf^{mi}$ | $Mitf^{mi-S-S73A\Delta neo}/Mitf^{mi}$
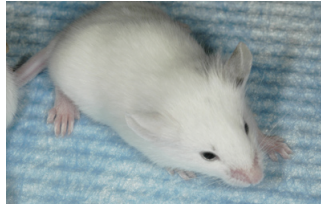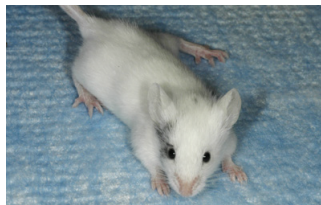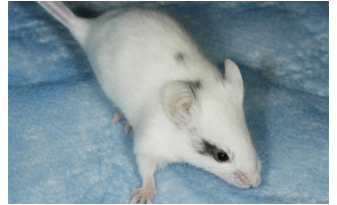
$Mitf^{mi-S-S73D\Delta neo}/Mitf^{mi}$ | $Mitf^{mi-S-S73S\Delta neo}/Mitf^{mi}$

D

$Mitf^{mi-S73A\Delta neo}/Mitf^{mi-vga9}$ | $Mitf^{mi-S-S73A\Delta neo}/Mitf^{mi-vga9}$
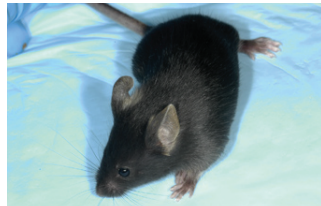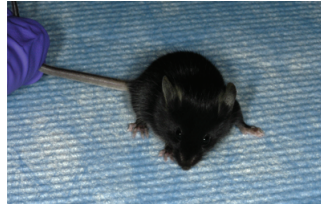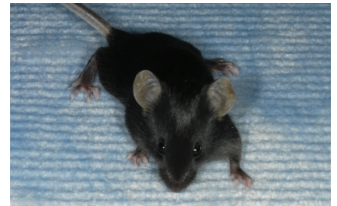
$Mitf^{mi-S-S73D\Delta neo}/Mitf^{mi-vga9}$ | $Mitf^{mi-S-S73S\Delta neo}/Mitf^{mi-vga9}$

Debbache et al., Suppl. Fig. 3
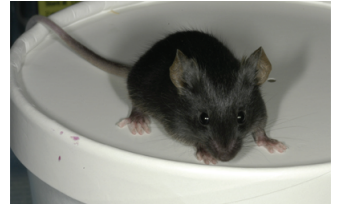
Supplemental Table 1: List of primers used

Primers for mutagenesis of *Mitf*^mi-S-S73^ alleles and pBABE constructs	Specific purpose
5'–CAGCAAGCTCAGAGGCATCAAGTTAAACAGTACCTTTCTACC–3' F 5'–GGTAGAAAGGTACTGTTTAACTTGATGCCTCTGAGCTTGCTG–3' R	Exon 2A-2B junction mutation
5'–CCAGTGCCGGGGAGCAGCGCACCCAACAGCCCTATGGCTATGC–3' F 5'–GCATAGCCATAGGGCTGTTGGGTGCGCTGCTCCCCGGCACTGG–3' R	S73S codon mutation
5'–CCAGTGCCGGGGAGCAGCGCACCCAACGCCCCTATGGCTATGC–3' F 5'–GCATAGCCATAGGGGCGTTGGGTGCGCTGCTCCCCGGCACTGG–3' R	S73A codon mutation
5'–CCAGTGCCGGGGAGCAGCGCACCCAACGACCCTATGGCTATGC–3' F 5'–GCATAGCCATAGGGTCGTTGGGTGCGCTGCTCCCCGGCACTGG–3' R	S73D codon mutation
5'–CAGCAAGCTCAGAGGCACCAGGCATTTTATAAGTTTGAG–3' F 5'–CTCAAACTTATAAAATGCCTGGTGCCTCTGAGCTTGCTG–3' R	Δ2B mutation
Primers for Mitf sequence verification and cloning	
5'–AGCACAATGGCCAGTACCTT–3' F 5'–TTGGTGACAATGACCAGGTG–3' R	Genomic sequencing from M-Mitf Intron 1 to Intron 2
5'–TGCTGGAAATGCTAGAATACAGTC–3' F 5'–TAGCTCCTTAATGCGGTCGT–3' R	cDNA sequencing from M-Mitf exons 1M to 7
5'–CATTGGCTAAAGAGAGGCAGA–3' F 5'–CTAGCCTGCATCTCCAGCTC–3' R	cDNA sequencing from M-Mitf exons 6B to 9
5'–GGGCGGCAAATTGTTTTATAAAGC–3' F 5'–GAAGTCAGCAAATGGTGGTGG–3' R	5' *Bam*HI fragment
5'–TGCTTTAGGTAAGAAAGGACCAAG–3' F 5'–CGGCTCGTATGTTGTGTGGAA–3' R	3' *Bam*HI fragment
5'–ACGTGAATTCTGATTTAAACATGGCAATATTTCTG–3' F 5'–ACGTAAGCTTGGGGGAACTTCCTGACTAGG–3' R	EcoRI-HindIII Mitf PCR cloning
Primers for qRT-PCR	
5'–AAGCTCAGAGGCACCAGGTAAAG–3' F 5'–ATGGTGAGCTCAGGACTTGG–3' R	qPCR Mitf 2B+
5'–GCTCAGAGGCACCAGGCATTTT–3' F 5'–GACGCTCGAGAGTGCGTGTT–3' R	qPCR Mitf 2B-
5'–GCAAGCTCAGAGGCATCAAGTTAAA–3' F 5'–ATGGTGAGCTCAGGACTTGG–3' R	qPCR Mitf 2B+ on mutated Exon2A-2B junction
5'–CAAGCTCAGAGGCATCAAGCATTTT–3' F 5'–GACGCTCGAGAGTGCGTGTT–3' R	qPCR Mitf 2B- on mutated Exon2A-2B junction
5'–CATTGGCTAAAGAGAGGCAGA–3' F 5'–TAGCTCCTTAATGCGGTCGT–3' R	qPCR Mitf 6B - 7
5'–CCCCAAGTCAAATGATCCAG–3' F 5'–GCAACTTCCGGATGTAGTCC–3' R	qPCR Mitf 7 - 8
5'–GGACCTTGAAAACCGACAGAAG–3' F 5'–CTAGCCTGCATCTCCAGCTC–3' R	qPCR Mitf 8 - 9
5'–CAGGGCTCAGAGGCACTACT–3' F 5'–GCTCCCTCCCTGCAATACTT–3' R	qPCR USF1

Debbache et al.

Supplemental Table 1: List of primers used (ct)

Primers for genotyping and Southern probes	Specific purpose
5'–CACCATGATATTCGGCAAGCAGGC–3' F 5'–TGACTGGGCACAACAGACAATCGG–3' R	Presence of Neo cassette
5'–GTGCAGACCCACCTGGAAAAC–3' F 5'–ACTCATCTAAGGACGGTGAT–3' R	Presence of LoxP site Removal of Neo cassette
5'–ATGACAGGCCCTTTCTAGT–3' F 5'–ACATGCAGTTCATGTGAG–3' R	5' probe generation
5'–GTAAGCGCAGCCTGCTCAG–3' F 5'–TCTTGACCTGAAATCGCAGC–3' R	3' probe generation

Debbache et al.

6 – La caractérisation d'un nouvel allèle du gène *Mitf* associé à un gain de d'activité.

Bien que les cribles de mutants suppresseurs aient souvent produit des données intéressantes dans la compréhension de la fonction de certains gènes chez plusieurs organismes, leur utilisation chez la souris reste restreinte. Dans cette étude nous décrivons l'isolation d'une mutation intra-génique de l'allèle « *spotted* » *Mitf*$^{mi-sp}$ du facteur de transcription murin Mitf. Ce nouvel allèle corrige largement les phénotypes pigmentaires associés à la présence combinée de l'allèle *Mitf*$^{mi-sp}$ et d'autres allèles de Mitf. La mutation localisée dans l'allèle *Mitf*$^{mi-sp}$ entraine l'absence de l'exon alternatif 6A qui code pour 6 acides aminés proche du domaine basique de fixation a l'ADN. Le nouvel allèle nommé « *spotless* » ou *Mitf*$^{mi-sl}$ conserve le défaut d'épissage alternatif de l'exon 6A mais dispose d'un site de terminaison de la traduction prématuré à l'acide amine 316. Ce codon STOP entraine une perte de 104 acide aminés de la partie Carboxy-terminale de MITF qui contient plusieurs sites de régulation post-traductionnelle de la protéine dont la K316 et S409. Même si nous ne trouvons pas de différences concernant la stabilité de la protéine ou l'affinité de fixation à l'ADN entre les protéines correspondantes, des expériences de gène rapporteur montrent une augmentation de l'activité transcriptionnelle de la protéine MITF^{mi-sl} ainsi qu'une augmentation de la stabilité leurs homodimers. Cependant, aucune différence n'a été observée en ce qui concerne le développement des mélanocytes entre les souris *Mitf*$^{mi-sp}$ et *Mitf*$^{mi-sl}$ homozygotes, que ce soit en terme de prolifération cellulaire ou du nombre total de mélanocytes, bien que la pigmentation postnatale de ces derniers soit différée dans les

souris *Mitf^{mi-sl}*. Ces résultats indiquent que la partie carboxy-terminale de MITF n'est pas essentielle à sa fonctionnalité, et qu'au contraire elle pourrait avoir un rôle négatif dans la régulation de son activité.

Les résultats expérimentaux liés à cette étude sont présentés dans l'**Article 6**.

The following expriments describe the characterization of a new allele identified in a N-ethyl-N-nitrosurea (ENU) mutagenesis screen on a *Mitf^{mi-sp}*/*Mitf^{mi-sp}* sensitized background. The aim of the screen was to discover new pigmentation gene modifiers that would either enhance or rescue the phenotype observed in *Mitf^{mi-sp}*/ *Mitf^{mi-ew}* mice.

In this study, we describe the molecular analysis of one particular mutant allele, which results in the correction of the pigmentation defect of *Mitf^{mi-sp}* when crossed with null or dominant-negative *Mitf* mutants. Intriguingly, this new modifier allele was found to be genetically linked to the *Mitf* locus, and by further sequencing, it happened to be a additional modification on the mutant *Mitf^{mi-sp}* allele. The new allele, named *Mitf^{mi-sl}* (spotless), results in the truncation of MITF protein due to the appearance of an early stop codon at the position 316.

While the *Mitf^{mi-sl}* allele displays a gain-of-function when crossed with other Mitf mutants compared to *Mitf^{mi-sp}*, *Mitf^{mi-sl}*/*Mitf^{mi-sl}* homozygotes display a coat color dilution, turning them from black to brownish. In this study, we present the analysis of this complex and unique *Mitf* allele and we attempt to explain both molecularly and developmentally the rescue of the pigmentation phenotype observed when crossed with other mutant Mitf alleles.

The details of this research study are described in the following **Article 6**.

Article 6

An induced suppressor mutation at the microphthalmia locus in the mouse reveals novel insights into bHLH-LZ transcription factor function

En préparation pour PNAS

An induced suppressor mutation at the *microphthalmia* locus in the mouse reveals novel insights into bHLHZip transcription factor function.

(DRAFT)

Eiríkur Steingrímsson[a,1], Heinz Arnheiter[b], Kristín Bergsteinsdóttir[a], Julien Debbache[b], Christian Praetorius[a], Keren Bismuth[b], Bryndís K. Gísladóttir[a], Adalheidur G. Hansdottir[a], Latasha Crawford[b], Melanie Gasper[b], Anjali Parekh[b], Susan Skuntz[b], Michael C. Dean[c], Deborah A. Swing[d], Jón H. Hallsson[a], David E. Fisher[e], Neal G. Copeland[d, f] and Nancy A. Jenkins[d, f]

[a]Department of Biochemistry and Molecular Biology, Faculty of Medicine, University of Iceland, Vatnsmýrarvegur 16, 101 Reykjavik, Iceland.
[b]Mammalian Development Section, NINDS, NIH, Bethesda, MD 20892-3706.
[c]Laboratory of Experimental Immunology, NCI, Frederick, MD 21702-1201.
[d]Mouse Cancer Genetics Program, NCI, Frederick, MD 21702-1201.
[e]Massachusetts General Hospital, Harvard Medical School, Boston, MA 02115.
[f]Current address: The Methodist Hospital Research Institute, Houston, Texas.

[1]Corresponding author: Phone: +354-525-4270
                                 FAX: +354-525-4886
                                 E-mail: eirikurs@hi.is

Running Head: *Mitf* suppressor mutation

Key words: *Mitf*, transcription factor, mutagenesis, suppressor

The analysis of mutations which suppress or compensate the effects of other mutations has revealed important insights into gene function in many organisms. Here we report the isolation of an intragenic mutation in the *Mitf^mi-spotted* (*Mitf^mi-sp*) allele of the mouse bHLHZip transcription factor gene *Mitf*, which largely corrects the phenotypic enhancement observed when this allele is combined with other *Mitf* mutations. The *Mitf^mi-sp* mutation leads to the absence of the alternatively spliced exon 6A, which encodes 6 residues close to the DNA-binding basic domain of MITF. The novel suppressor mutation, termed *spotless* or *Mitf^mi-sl*, retains this splice alteration but introduces a stop codon at amino acid 316, leading to the loss of 104 residues at the carboxyl terminus of MITF. Although we find no differences in protein stability or DNA binding between the corresponding proteins, reporter assays show increased transcription activation potential of the MITF^mi-sl protein, and the stability of MITF^mi-sl homodimers seems to be increased. Nevertheless, developmental studies show no differences between *Mitf^mi-sp* and *Mitf^mi-sl* homozygotes in cell proliferation or melanocyte numbers although the postnatal onset of pigmentation is delayed in *Mitf^mi-sl* homozygotes. Our data indicate that the carboxyl-end of MITF is not essential for the function of *Mitf* in melanocytes and may rather play a negative role. We conclude that searching for suppressor mutations in the mouse is feasible and provides a powerful tool for generating unexpected insights into gene function.

The analysis of suppressor mutations, many of them identified by suppressor screens, has provided many insights into gene function, gene interactions and genetic pathways in organisms ranging from bacteria to Drosophila. In mice, however, few suppressor screens have been performed, but the analysis of spontaneous suppressor mutations such as the *dilute-suppressor* suggest that such mutations may lead to important mechanistic insights also in this species. The *dilute-suppressor* is an allele of the gene *Mreg* (*Mreg^dsu*) that acts on *Myo5a*, whose mutations affect coat pigmentation (1). In fact, alterations in coat pigmentation provide for an ideal phenotype when screening for suppressors because more than 150 genes affecting pigmentation have been cloned already, coat pigmentation allows for a readily visible and highly sensitive read-out of gene function, and alterations

in pigmentation are usually compatible with normal life and breeding. Here, we describe experiments in which we screened for suppression of a mutation in the pigment gene *Mitf.*

Mutations at the mouse *microphthalmia* locus (*Mitf*) affect the development of several different cell types including neural crest-derived melanocytes, pigmented epithelial cells of the eye, mast cells, and osteoclasts. The many mutations found at the locus over the last 60 years have different phenotypic effects and can be arranged in an allelic series. The original and most severe allele, $Mitf^{mi}$, affects all of the above cell types and results in death at 3-4 weeks of age while the mildest allele, $Mitf^{mi\text{-}spotted}$ ($Mitf^{mi\text{-}sp}$), creates no visible phenotype even when homozygous. Nevertheless, this latter allele is named "*mi-spotted*" because it induces or enhances a white spotting phenotype when combined with other mutations at the locus (reviewed by (2, 3). Some of these other *Mitf* alleles are inherited semidominantly and show white spotting on their own when heterozygous with wild type, but their white spotting is enhanced in compound heterozygotes with $Mitf^{mi\text{-}sp}$. Most *Mitf* alleles, however, are recessive and do not exhibit white spotting when heterozygous, and yet when combined with $Mitf^{mi\text{-}sp}$, white spotting becomes visible and can indeed be quite extensive (reviewed in (3).

The MITF protein is a member of the MYC family of basic-Helix-Loop-Helix-leucine zipper (bHLH-Zip) transcription factors and is closely related to the TCFE3, TCFEB and TCFEC proteins (formerly known as TFE3, TFEB and TFEC proteins) (4, 5). The basic domain is the DNA binding domain of the protein while the HLH and Zip domains are responsible for dimerization. Other domains in the MITF protein include distinct activation domains, several conserved domains of unknown function and many sites for posttranslational modifications including phosphorylation, sumoylation, and caspase cleavage (6-13). The MITF protein can bind DNA as homodimers or heterodimers with other TFE family members [Hemesath, 1994]. It is a nuclear protein (14) which regulates the expression of genes involved in cell specification, differentiation and function, cell survival, and cell cycle regulation (15-17). In melanoma cells, MITF plays a critical role as a lineage-survival oncogene (18) and may act as a molecular switch that determines whether cells proliferate or become quiescent, thus allowing migration and formation of metastasis (19). Genome-wide analysis suggests that MITF is

indeed involved in DNA replication and genome stability in melanoma cells, and ChIP-sequencing studies show that MITF binds predominantly to two related E-box sequences, CACGTG and CATGTG (20). Given its multiple roles, MITF can be considered a master regulator of both normal melanin-bearing pigment cells as well as their malignant derivatives.

The molecular defects associated with most of the *Mitf*-alleles in mice and other vertebrates have been determined and their biochemical properties analyzed (21). The *Mitf^{mi-sp}* mutation is characterized by an extra cytosine in the alternatively spliced 18 bp exon 6A that encodes 6 amino acids just upstream of the basic domain. The extra base may affect the splicing reaction directly, leading to a decrease in mRNAs containing the 6A exon. It may also subject RNAs still containing exon 6A to non-sense-mediated decay, as the mutation leads to a premature stop codon in the adjacent exon 6B. In contrast to wild-type mice where the 6A+ and the 6A- RNAs are made in approximately equal proportion in most cell types, the 6A+ version is missing in *Mitf^{mi-sp}* homozygotes and, as we show here, the overall *Mitf* mRNA levels are reduced. The corresponding MITF+ and MITF- (MITF^{mi-sp}) proteins have similar DNA binding properties, but the DNA binding stability of the latter protein is slightly reduced (22). The combination of reduced mRNA levels and reduced DNA binding may explain why the pigment enzyme encoded by the *Mitf* target gene *Tyrosinase* and the survival of melanocytes are somewhat impaired in *Mitf^{mi-sp}* homozygotes (23, 24). These negative effects may be counteracted in part by the fact that, based on ectopic expression in heterologous cells in vitro, the MITF+ protein inhibits DNA synthesis whereas the MITF- protein has only mild if any effects (25). Interestingly, in melanoma cells, the 6A+/6A- ratio is regulated by the MAP kinase pathway, and a subset of melanoma samples shows a decreased ratio of 6A+/6A- RNAs (26).

Besides *Mitf^{mi-sp}*, there is a second allele, *Mitf^{Mi-White}* (*Mitf^{Mi-Wh}*), that underscores the importance of exon 6A. This allele is inherited semidominantly and results in coat color dilution and a belly spot in heterozygotes (2, 3, 27). It is characterized by a point mutation changing residue 212 from isoleucine to asparagine (21). This position lies in the middle of the DNA-binding basic region of the protein and is conserved in the three TCFE (formerly known as TFE) family members. Biochemical analysis using proteins

truncated at both the amino- and carboxyl termini showed that neither version of the MITF^{Mi-Wh} protein, containing or lacking the 6 residues, bind DNA as homodimers, suggesting that the *Mitf*$^{Mi-wh}$ mutation has dramatic effects on DNA binding. However, as dimers with wild-type MITF or the wild-type TCFE3, the MITF^{Mi-Wh}+ protein was shown to bind DNA at normal levels (22). Based on these studies, DNA binding of the MITF^{Mi-Wh} protein depends on the presence of both the alternative 6 residues and a wild-type dimerization partner. Nevertheless, an explanation for why the 6 residues are important in this context may require detailed structural analyses. Interestingly, the combination of *Mitf*$^{Mi-wh}$ with *Mitf*$^{mi-sp}$ results in mice that do not only show an enhanced white spotting compared to *Mitf*$^{Mi-wh}$/*Mitf*$^{+}$ heterozygotes but also a pale tan color as opposed to the mild dilution seen with *Mitf*$^{Mi-wh}$/*Mitf*$^{+}$ heterozygotes. This suggests that these alleles engage in complex interactions that affect melanocyte development as well as differentiation.

The variety of coat pigmentation alterations obtained with *Mitf*$^{mi-sp}$ made this allele ideal for an N-ethyl-N-nitrosurea (ENU) mutagenesis screen. Such a screen would not only allow identification of mutations that enhance the phenotype of compound heterozygotes but also of mutations that alleviate it. Using this approach we expected to find mutations in novel genes participating in the molecular pathways through which *Mitf* regulates pigment cell development and melanogenesis. In fact, we were able to isolate a suppressor mutation, but intriguingly, it does not represent an allele of a different gene but is a derivative of the *Mitf*$^{mi-sp}$ allele itself, perhaps further highlighting the central role that *Mitf* plays in melanocyte biology.

Results and Discussion

Generation and analysis of an *Mitf* suppressor mutation. We designed a simple F$_1$ mutagenesis screen for dominant coat color changes of the mouse *Mitf* mutation After testing for tolerance to the mutagen and for male and female fertility, the *Mitf*$^{mi-sp}$ and *Mitf*$^{mi-eyeless white}$ (*Mitf*$^{mi-ew}$) mutations were chosen for the mutagenesis experiment. While *Mitf*$^{mi-sp}$ homozygotes have no visible coat color phenotype, animals homozygous for the *Mitf*$^{mi-ew}$ mutation are white, severely microphthalmic and exhibit mild hyperosteosis (28) (Supplementary Table 1). Compound heterozygotes for these two mutations have a "salt-and-pepper" body color with white head, belly and feet (Fig. 1A). For the experiment,

homozygous C57BL/6 (B6)-*Mitf*$^{mi\text{-}sp}$ males were treated four times at one week intervals with 100 mg/kg ENU. After a 6-8 week recovery time, the males were mated to NAW-*Mitf*$^{mi\text{-}ew}$/*Mitf*$^{mi\text{-}ew}$ females and the resulting F1s, which all should show the identical "salt-and-pepper" body color with white head, belly and feet, were screened for coat pigmentation changes. Numerous B6-*Mitf*$^{mi\text{-}sp}$/*Mitf*$^{mi\text{-}sp}$ males were treated with ENU and mated to 63 NAW-*Mitf*$^{mi\text{-}ew}$/*Mitf*$^{mi\text{-}ew}$ females of which only 44% bred, resulting in the generation of a total of 470 offspring. In one of the matings, a deviant female, marked by a * to indicate the presence of a mutagenized chromosome, showed a considerably darker coat (near-black coat with pale ears, tails and toes) compared to littermates (Fig. 1A).

When this female with the genotype *Mitf*$^{mi\text{-}ew}$/*Mitf*$^{mi\text{-}sp}$ * was bred to a B6-*Mitf*$^{mi\text{-}ew}$/*Mitf*$^{mi\text{-}ew}$ male, two classes of offspring resulted: white microphthalmic mice of the genotype *Mitf*$^{mi\text{-}ew}$/*Mitf*$^{mi\text{-}ew}$ and mice with the same phenotype as the mother: near-black coat with pale ears, tails and toes and the genotype *Mitf*$^{mi\text{-}ew}$/*Mitf*$^{mi\text{-}sp}$ * (Supplemental Fig. 1A). Again, these animals were considerably more pigmented than the corresponding B6-*Mitf*$^{mi\text{-}sp}$/*Mitf*$^{mi\text{-}ew}$ mice. This suggested that the mutation altering the *Mitf* phenotype is dominant, at least with respect to the combination of these two alleles. Also, because the above crosses did not yield mice with the phenotype expected for *Mitf*$^{mi\text{-}ew}$/*Mitf*$^{mi\text{-}sp}$ mice, the novel suppressor mutation is likely closely linked with *Mitf*$^{mi\text{-}sp}$, or lies within the gene itself, rather than on a different chromosome. Furthermore, crossing the near-black mice to C57BL/6J or B6-*Mitf*$^{mi\text{-}sp}$ animals only resulted in black offspring showing that the new suppressor does not alter the heterozygous phenotypes of these alleles.

When the near-black *Mitf*$^{mi\text{-}ew}$/*Mitf*$^{mi\text{-}sp}$ * mice were mated to *Mitf*$^{Mi\text{-}wh}$/*Mitf*$^{Mi\text{-}wh}$ homozygotes, there were again two classes of offspring: white mice with normal eye size (*Mitf*$^{mi\text{-}ew}$/*Mitf*$^{Mi\text{-}wh}$ heterozygotes) and "steel"-colored mice with pale ears, tail, toes and a belly spot (*Mitf*$^{Mi\text{-}wh}$/*Mitf*$^{mi\text{-}sp}$ * animals, Fig. 1B). The coat color of the latter animals is much darker than that of the corresponding *Mitf*$^{Mi\text{-}wh}$/*Mitf*$^{mi\text{-}sp}$ animals which are light tan with white spots (24) (Fig. 1B). In fact, the color is even darker when compared to *Mitf*$^{Mi\text{-}wh}$/*Mitf*$^{+}$ mice, suggesting that the new mutant represents a gain-of-function compared to wild type. Similar effects were also seen when animals carrying the new *Mitf*$^{mi\text{-}sp}$ * mutation were crossed to the dominant-negative *Mitf*^{mi} (Fig 1C), *Mitf*$^{Mi\text{-}or}$ and *Mitf*$^{Mi\text{-}b}$ mutations (Supplemental Fig. 1B-D). In all these cases, the coat was more pigmented

than when the respective mutations were crossed to the original $Mitf^{mi-sp}$ mutation. The effect was most dramatic when comparing the $Mitf^{mi}/Mitf^{mi-sp}$ * and $Mitf^{mi}/Mitf^{mi-sp}$ compound heterozygotes (Fig. 1C). These observations showed that the suppressing effects of the new mutation were not restricted to the $Mitf^{mi-ew}$ allele and were seen regardless of genetic background (compare Fig. 1A to Supplemental Fig. 1A and Supplemental Figs. 1B to 1C).

Interestingly, the new mutation also improves the phenotype of a loss-of-function mutation in *Mitf*. The $Mitf^{mi-vga9}$ mutation is caused by a transgene insertion into the *Mitf* regulatory region which eliminates expression of the *Mitf* gene and results in a severe eye and coat color phenotype (4, 29). When animals homozygous for the new suppressor mutation were crossed to B6-$Mitf^{mi-vga9}/Mitf^{mi-vga9}$ animals, the resulting progeny were black with a small belly spot, in contrast to B6-$Mitf^{mi-vga9}/Mitf^{mi-sp}$ mice which show extensive white spotting (Fig. 1E, F). The fact that the $Mitf^{mi-vga9}/Mitf^{mi-sp}$ * animals exhibit near-normal pigmentation suggests that the $Mitf^{mi-sp}$ * mutation can restore pigmentation to areas which otherwise would be unpigmented, suggesting that the mutation restores the effects of *Mitf* during melanocyte development. The new mutation does not affect the coat color of the recessive $Mitf^{mi-rw}$ allele as compared to $Mitf^{mi-rw}/Mitf^{mi-sp}$ animals (Fig. 1H), reflecting the fact that the latter animals are already black and no further improvement in coat color is possible. Similarly, no effects were observed on eye size or bone development in any of the combinations since both phenotypes are normal in $Mitf^{mi-sp}$ homozygotes or their compound heterozygotes.

Intercrosses of B6-$Mitf^{+}/Mitf^{mi-sp}$ * heterozygotes produced two classes of offspring: normal non-agouti (black) mice and mice with a diluted "brownish" coat color, in a 3 to 1 ratio. Genotyping showed that the "brownish" animals were homozygous for the $Mitf^{mi-sp}$ mutation (compare Figs. 1G to 1H). Thus, intriguingly, the new mutation suppresses the spotting phenotype of most combinations of *Mitf* alleles but causes the $Mitf^{mi-sp}$ mutation to express a neomorphic function.

Molecular analysis of the new mutation. From the various crosses described above it was clear that the new mutation is either tightly linked to *Mitf* on chromosome 6, or is an intragenic mutation. We therefore performed RT-PCR and sequencing studies of the *Mitf*

gene in total RNA isolated from homozygous *Mitf*^mi-sp^ * heart and kidney. Consistent with the induced origin of the mutation, sequencing of the cDNA revealed the previously characterized *Mitf*^mi-sp^ mutation, namely the lack of the 18 bp alternative exon (21). In addition, an A to T transversion was detected at nucleotide 1075 of the cDNA (4) resulting in a Lys316Stop mutation and a predicted premature truncation of the protein (Fig. 2A). The presence of the Stop codon was confirmed by genomic sequencing of the last *Mitf* exon, exon 9, which encodes Lys316. Thus, the new mutation is an intragenic re-mutation at the *Mitf*^mi-sp^ allele. We have termed the new mutation *Mitf*^mi-spotless^ (*Mitf*^mi-sl^) in order to distinguish it from the *Mitf*^mi-sp^ mutation on which it arose. Accordingly, the mutant MITF^mi-sl^ protein contains the bHLHZip domain, the amino-terminal activation domain and the Ser73 phosphorylation site but is missing 104 residues of the carboxyl end, including a SUMOylation site (Lys 316) (11), a caspase cleavage site (Asp 345) (8), a phosphorylation site implicated in the MAP kinase signal transduction pathway (Ser 409) (13)), and a putative transcription activation domain (12). To confirm that the carboxyl-end of MITF indeed is missing from the *Mitf*^mi-sl^ mutant, we labeled melanocyte cultures and eye sections from *Mitf*^mi-sl^ and *Mitf*^mi-sp^ mutants with the monoclonal antibody 6A5, which reacts with the carboxyl terminus of MITF (30). As shown in Fig. 2B, the antibody did not give a signal in *Mitf*^mi-sl^ cells or eye sections whereas *Mitf*^mi-sp^ cells and sections exhibited clear nuclear staining; eye sections from both genotypes were stained with a polyclonal rabbit anti-MITF antibody. The results indicated that the MITF protein is present in *Mitf*^mi-sl^ mutants but lacks the carboxyl-end. Further proof that MITF^mi-sp^ and MITF^mi-sl^ proteins accumulate in the nuclei of cells came from experiments in which we transfected cells with corresponding GFP fusion constructs or labeled the expressed proteins directly with the C5 anti-MITF antibody (Suppl. Fig. 2). Nevertheless, as these assays would not be able to detect minor differences in the efficiencies of nuclear translocation, potential differences in nuclear accumulation cannot be entirely excluded to explain the mutant phenotype.

Mitf^mi-sl^/_Mitf_^mi-sl^ homozygotes show normal melanoblast development but delayed onset of pigmentation. Conceivably, the above suppressor phenotype might be explained by increased proliferation of melanoblasts or melanocytes induced by the MITF^mi-sl^

protein. To investigate this possibility, we first tested BrdU incorporation in HEK293 cells expressing MITF[mi-sp] or MITF[mi-sl] proteins from corresponding expression vectors. However, these assays revealed no significant difference in BrdU incorporation between the two different mutations ($69 \pm 2\%$ BrdU positivity in MITF[mi-sp] -expressing cells versus $71 \pm 2\%$ BrdU positivity in MITF[mi-sl] -expressing cells). To count melanoblast numbers during development in vivo, we generated *Mitf*[mi-sp] and *Mitf*[mi-sl] homozygous embryos carrying a melanoblast marker transgene, Dct-LacZ (31). In wild type C57BL/6 embryos, the Dct-LacZ marker (as determined by blue cells after Xgal staining) showed, as expected, an increase of labeled cells with developmental time. Similar increases were seen in *Mitf*[mi-sp] and *Mitf*[mi-sl] homozygotes, although the total number of labeled cells seemed on average reduced compared to wild type. Possibly because of varying degrees of transgene silencing, however, there was a great variability in staining from embryo to embryo. Therefore, we switched to a different marker, Kit-LacZ, in which we expected less variability because the LacZ gene was inserted by targeted mutagenesis into the endogenous *Kit* gene (32). As *Kit* was rendered non-functional by targeting and *Kit* is involved in the regulation of melanocyte development, *Kit-LacZ* heterozygotes have a reduced number of melanocytes, phenotypically manifested as white feet and tail tips, and, in our colony, a white belly spot. Hence, by introducing *Kit-LacZ* into *Mitf*[mi-sp] and *Mitf*[mi-sl] mice, we also could evaluate whether the suppressor mutant was able to suppress white spotting created by the *Kit* mutation. In fact, the white spotting associated with *Kit-LacZ* heterozygosity was not influenced by the presence of either *Mitf* allele, suggesting that the suppressor mutation acts only on *Mitf* itself (data not shown). The analysis of X-gal staining in the respective embryos is shown in Fig. 3A,B. At 12.5 days, the mutant embryos have fewer melanocytes than wild type. However, no differences were observed between *Mitf*[mi-sp] and *Mitf*[mi-sl]. At 15.5 days, no difference was seen when the cells were counted in the hind-limb region whereas a region around the ear showed that *Mitf*[mi-sp] and *Mitf*[mi-sl] had more melanocytes than wild type and *Mitf*[mi-sl] had the highest levels. This suggests that generally, the numbers of melanocytes are the same in the two mutations although there may be region-specific differences.

In order to determine if the phenotypic suppression of *Mitf*[mi-sl] is due to effects on developmental timing, the appearance of pigmentation was traced both in neural crest

cultures established at E9.5 and in newborn *Mitf*^mi-sp and *Mitf*^mi-sl mice. In *Mitf*^mi-sp cultures, the first pigmented melanocytes appear at day 10 of culture (N=38) and their number increases steadily through day 17 (N=372) (Supplemental Fig. 3A). In *Mitf*^mi-sl cultures, the first pigmented melanocytes appear at day 14, i.e. 3 days later than in *Mitf*^mi-sp cultures, and their average number is lower (N=95) (Supplemental Fig. 3A). Nevertheless, in both *Mitf*^mi-sp and *Mitf*^mi-sl cultures, melanoblasts can be detected by expression of the MITF protein as early as day 1 of culture (Supplemental Fig. 3, inset, for day 3 of culture), suggesting that the delay in pigmentation is not due to a delay in melanoblast appearance. Comparing pups of the two genotypes shows that pigmentation appears later in *Mitf*^mi-sl mice than in *Mitf*^mi-sp animals, particularly striking at postnatal day 2 and 3 (Supplemental Fig. 3B). However, this difference is only seen when the mice are homozygous for these alleles and not when they are combined, for instance, with *Mitf*^mi-vga9 (Supplemental Fig. 3C, comapre mice labeled #1 and #3). Hence, it is conceivable that delayed onset of pigmentation reflects the appearance of the "brownish" color which also requires homozygosity for *Mitf*^mi-sl. In any event, the above results suggest that the delayed onset of pigmentation in *Mitf*^mi-sl cultures and pups is not due to an extended period of cell proliferation that would delay the beginning of differentiation.

RNA expression and protein stability. In order to determine expression levels of the *Mitf* gene in the mutants, we first quantitated *Mitf* RNA expression in the heart, an organ that is not overtly affected in any of the extant *Mitf* mutants. Quantitative RT-PCR (33) showed that expression of *Mitf* RNA is reduced to 65.7% in *Mitf*^mi-sp hearts compared to wild-type controls but remains at wild-type levels (115.8%) in *Mitf*^mi-sl hearts. Similar observations were made when RNA obtained from skin was quantitated (Fig. 4A). Indeed, increased *Mitf* RNA expression or stability would explain the phenotypic suppression observed with the *Mitf*^mi-sl mutation. The results may indicate either that MITF regulates its own expression, with MITF^mi-sl protein being a more potent activator than MITF^mi-sp, or that MITF^mi-sl may bias the exon 6A splice reaction such that less of the *Mitf* RNA is removed by non-sense mediated degradation.

The MAPK signalling pathway has been shown to lead to phosphorylation of Ser73 and Ser409 of MITF, resulting in increased transcription activation potential and reduced

protein stability (13).   The MITF[mi-sl] mutant protein is missing the Ser409 phosphorylation site and might therefore be more stable, thus explaining the more normal phenotype observed in compound heterozygotes. Protein kinetic studies were therefore performed in transfected Cos cells to test if the *Mitf*[mi-sl] mutation differentially affects the stability of the corresponding proteins.   The results show that whereas there is less MITF[mi-sl] protein expressed in the cells to begin with, its stability is not affected by the deletion mutation or by the absence of the 6 amino acid insert sequence (Fig. 4B). This is consistent with the above observation that reduced MAPK activity as seen in *Kit-LacZ/Kit*[+] mice does not alter the *Mitf*[mi-sl] phenotype and with previous results that showed that transgenic Mitf BACs with a Ser409Ala mutation can fully rescue the phenotype of *Mitf*[mi-vga9]/*Mitf*[mi-vga9] mice (34).

DNA binding and transcription activation. The DNA binding abilities of the MITF[mi-sl], MITF[mi-sp] and MITF[+] proteins were determined using electrophoretic mobility shift assays (EMSA).   Previous DNA binding studies have shown that the MITF[mi-sp] and MITF[+] proteins bind DNA with similar steady state affinities (22).   Our EMSA results are in agreement with this (Fig. 4C, lane 2, 6). Consistent with its smaller size the MITF[mi-sl] protein results in a band that moves faster in the gel than the wild-type and MITF[mi-sp] proteins; this band is also more diffuse (Figure 4C, compare lanes 2, 6 and 10). In order to determine if dimerization ability was affected, the three proteins were co-translated with the dominant negative MITF[mi] protein before performing the EMSA. This mutant protein carries a deletion of one of three arginines in the DNA binding domain (21), is unable to bind DNA but can still dimerize with its partners and thus interfere with their DNA-binding (22). Co-translating this protein with the wild type, MITF[mi-sp] and MITF[mi-sl] proteins and then performing gel shift experiments shows that increasing amounts of the MITF[mi] protein interfere with the DNA binding of all three proteins.   However, quantitation of the bands revealed that MITF[mi] is twice as effective at interfering with the wild type protein (MITF+) than with either of the mutant proteins, suggesting that the lack of exon 6A confers reduced dimerization abilities (Fig. 4C).   Nevertheless, according to this analysis, the C-terminal truncation has no additional effects. A slightly different picture emerges when the proteins were translated separately and mixed before

the EMSA. Again, the MITF^{mi} protein is more effective at interfering with binding of the wild type protein than with the MITF^{mi-sp} and MITF^{mi-sl} proteins. In this case, however, it is even less effective at interfering with the MITF^{mi-sl} protein (Fig. 4D) than with MITF^{mi-sp}. This suggests that, once formed, the MITF^{mi-sl} dimers are more stable than either the wild type or MITF^{mi-sp} dimers and thus less prone to interference by the MITF^{mi} protein. More stable MITF^{mi-sl} dimers might explain the suppressor phenotype.

In order to test the transcription activation potential of the MITF^{mi-sl} mutant protein, co-transfection assays were performed. When transfected into 293T cells, the Mitf^{mi-sp} protein is a less potent transcription activator than MITF+ on all promoters tested. However, the MITF^{mi-sl} protein was a more potent transactivator than the MITF^{mi-sp} protein on the *tyrosinase* promoter as well as on all other promoters tested and was in all cases similar to the wild type protein (Fig. 5).   Similar results were obtained in 501mel melanoma cells. This is consistent with the suppressor phenotype as increased activity of the MITF^{mi-sl} protein might improve the phenotype in compound heterozygotes. This is also consistent with the increased expression of the *Mitf* gene in heart of *Mitf^{mi-sl}* mutant animals, again suggesting that MITF regulates its own expression. It has also been shown that the carboxyl end of MITF is important for maintaining transcription activation of the tyrosinase promoter (12).   These results suggested the presence of an important transcription activation domain between amino acids 293 and 324. As the MITF^{mi-sl} protein is truncated at residue 316, yet maintains transcription activation ability, the domain important for transcription activation must lie between residues 293 and 316. Alternatively, the 6 amino acids lacking in the MITF^{mi-sp} and MITF^{mi-sl} proteins may contain an activation domain that depends on the carboxyl-end of MITF such that in the absence of both, other activation domains dominate, leading to increased activation. Nevertheless, it needs to be kept in mind that all experiments of Takeda et al. (2000) were performed using MITF which contains the 6 amino acids and a reporter containing a larger segment of the tyrosinase promoter than was used here.

Conclusions. We have generated a novel intragenic suppressor mutation at the *Mitf* locus in the mouse, characterized the molecular lesion involved and the biochemical effects *in vitro*. The mutation is a re-mutation at the *Mitf* locus which results in a truncation of the

already mutated *Mitf^{mi-sp}* protein. In the homozygous condition, the *Mitf^{mi-sl}* mutation results in a brownish coat color, suggesting a neomorphic action as compared to the *Mitf^{mi-sp}* mutation on which it arose which leads to a normal black coat. However, in compound heterozygous conditions with other *Mitf* mutations, including severe mutations at the locus such as *Mitf^{mi}*, *Mitf^{Mi-or}*, *Mitf^{Mi-wh}*, *Mitf^{mi-ew}* and the loss-of-function mutation *Mitf^{mi-vga9}*, the *Mitf^{mi-sl}* mutation improves the phenotype as compared to the same alleles combined with the original *Mitf^{mi-sp}* mutation. A molecular explanation of this mutation needs to consider its contradictory genetic behaviour. Some of our data is consistent with the altered pigmentation observed in homozygotes. For example, developmental analysis shows a delay in pigmentation. However, other data is consistent with the suppressor phenotype, including the increased expression of the *Mitf* gene in *Mitf^{mi-sl}* hearts, the increased ability of MITF^{mi-sl} to activate expression and the increased stability of dimers formed by the MITF^{mi-sl} protein. Recently, two independent reports showed association of mutations in the human MITF gene with melanoma [Bertolotto, 2011; Brown, 2011]. The mutation involved is an E318K mutation that affects sumoylation of the protein and leads to increased transcription activation potential, thus leading to oncogenic ability. This is consistent with the results observed with the MITF^{mi-sl} protein which lacks the sumoylation site and has increased transcription activation ability. This mouse may therefore be useful as a model for MITF-mediated melanoma.

Our analysis suggests that the *Mitf^{mi-sl}* mutation may affect several different aspects of MITF function. The effects of the *Mitf^{mi-sl}* mutation, although clearly visible in the mouse, would not have been predicted a priori based on DNA or protein sequence. We therefore conclude that generating suppressor mutations in the mouse is an interesting and feasible option for studying gene function and may reveal unexpected aspects of protein function or regulation, leading to novel insights into protein activity in the living organism.

Methods

Mouse strains used, mutagenesis and genotyping. The following *Mitf* mutants were used in this study: C57BL/6J-*Mitf^{mi-sp}*, C57BL/6J-*Mitf^{mi-eyeless white}* (*Mitf^{mi-ew}*), NAW-*Mitf^{mi-eyeless white}* (*Mitf^{mi-ew}*), C57BL/6J-*Mitf^{Mi-Wh}*, C57BL/6J-*Mitf^{mi-red-eyed white}* (*Mitf^{mi-rw}*), C57BL/6J-

Mitf^{*microphthalmia*}, 82UT-*Mitf*^{*mi-Oak ridge*} (*Mitf*^{*Mi-Or*}), C57BL/6J-*Mitf*^{*mi-oak ridge*} (*Mitf*^{*Mi-or*}), 82UT-*Mitf*^{*mi-brownish*} (*Mitf*^{*mi-b*}) and a [C3H/C57BL/6J]-*Mitf*^{*mi-vga-9*} strain (Table 1). These strains are maintained at the NCI in Frederick, MD and at the NINDS, NIH in Bethesda, MD. The mice were mated systematically in order to generate the different allelic combinations. In order to screen for Mitf suppressor mutations, homozygous B6-*Mitf*^{*mi-sp*} males were treated four times at one week intervals with 100 mg/kg ethylnitrosourea (ENU). After a 6-8 week recovery period, the males were mated to NAW-*Mitf*^{*mi-ew*}/*Mitf*^{*mi-ew*} females and the resulting offspring, which all should show an identical phenotype, screened for more normally pigmented deviates. DNA-HPLC was used to confirm the presence of the *Mitf*^{*mi-sp*} mutation. The Kit-LacZ mice, involving C57BL/6J, C3H/HeJ and 129/Sv, were originally obtained from Jean-Jacques Panthier.

RT-PCR and sequencing. Total RNA was isolated from hearts of wild type and mutant mice using the RNAwiz kit from Ambion. The RNA was reverse transcribed by SuperScript reverse transcriptase (Invitrogen) and the resulting cDNA phenol/chloroform extracted. Alternatively, RNA was isolated using the Macherey Nagel RNAII kit. The entire *Mitf* cDNA was amplified by PCR using overlapping primers and the resulting PCR products sequenced directly using Big Dye Terminator Cycle Sequencing kit (ABI) and the ABI 377 sequencer. The results were confirmed by sequencing additional animals as well as several controls animals, on which the mutation was induced, in order to confirm the alterations.

Generation of plasmid constructs. The wild type and mutant expression clones were all generated in pcDNA3, by subcloning and/or in vitro mutagenesis. In order to determine nuclear localization experiments, fusion proteins were generated where wild type and mutant versions of the *Mitf* gene were fused to Green Fluorescent Protein (GFP). All the constructs were sequence verified.

Co-transfection experiments

Co-transfection experiments were performed in 293T cells maintained in Dulbecco´s modified Eagle medium (DMEM) supplemented with 10% Fetal Bovine Serum (FBS), 2

mM L-glutamine and penicillin/streptomycin (50 U/mL). Cells were grown at 37°C in a humidified atmosphere of 5% CO_2. Cells were split on Nunc 12-well plates 24 hours prior to transfection such that cells were ~50-60% confluent at the time of DNA addition. At harvest, the cells were washed with ice cold PBS and lysed with passive lysis buffer (PLB) from the Dual Luciferase assay Kit (Promega). Then a part of the cell lysaste was used to evaluate luciferase activity; all reactions were preformed according to manufacturer's suggestions.

DNA binding studies. Electrophoretic Mobility Shift Assays were performed using proteins expressed in the TNT T7 Coupled Reticulocyte Lysate System (Promega, WI), according to the manufacturer´s recommendation. DNA binding reactions were performed in 10 mM Hepes (pH 7.9), 50 mM NaCl, 5 mM $MgCl_2$, 0.1 mM EDTA, 2 mM dithiothreitol (DTT), 5% ethylene glycol and 5% glycerol. The buffer was mixed in 2X concentration and was diluted to 1X concentration in the binding reaction which was composed of 10 µL of 2X binding buffer, 2.5 µL of TNT translated Mitf protein, 1.4 ng of labeled probe, 4 µg of bovine serum albumin (BSA) (35) and water adjusting the reaction volume to 20 µL. For supershifts, 0.5 µL of C5-Mitf antibody was added to the reaction. The samples were incubated on ice for 30 minutes to allow binding to proceed. The resulting DNA-protein complexes were resolved on 6% non-denaturing polyacrylamide gels, placed on a storage phosphor screen and then scanned on a Typhoon Phosphor Imager 8610 (Molecular Dynamics) for analysis.

Protein kinetic studies. COS cells were transfected with constructs expressing the *Mitf$^+$*, *Mift^{mi-sp}*, and *Mitf^{mi-sl}* proteins (in pCDNA3) and grown in DMEM plus 10% fetal bovine serum. The cells were then treated with 100 nM TPA (Sigma) and 15µg/ml cyclohexamide (Sigma) and incubated for 0, 1, 2 and 3 hrs before harvesting. The cells were then lysed in SDS buffer and the expression of the Mitf proteins determined by Western-blotting using the C5 monoclonal Mitf antibody (36).

Neural crest cells cultures and staining. Neural crest cells were prepared from *Mitf^{mi-sp}*/ *Mitf^{mi-sp}* and *Mitf^{mi-sl}*/ *Mitf^{mi-sl}* embryos following the protocol previously described (37).

The cultures were observed daily for the appearance of pigmented melanocytes. The number of pigmented melanocytes was counted for each mutant in 4 independent cultures. The presence of MITF positive cells was detected by immunofluorescence using anti-microphthalmia C5 antibody (Neomarkers) and anti-mouse-FITC secondary antibody (Sigma).

Proliferation assay. HEK 293 cells were transfected with Mitf^{mi-sp} or Mitf^{mi-sl} cDNA and 18 hours after transfection, the cells were incubated in 10 μM BrdU (Sigma) for 30 min at 37 °C. The cells were then fixed in 4% paraformaldehyde and processed for MITF staining using anti-microphthalmia C5 antibody (Neomarkers) and rat-absorbed anti-mouse-FITC antibody (Southern Biotech) after post-fixation in 4% paraformaldehyde. BrdU labeling was performed using rat anti-BrdU (Accurate Chemical) and mouse absorbed anti-rat TRITC (Southern Biotech). One hundred cells were counted per transfection, whereby each transfection was done in triplicate, in 3 independent experiments.

1. O'Sullivan TN, *et al*. (2004) dsu functions in a MYO5A-independent pathway to suppress the coat color of dilute mice. *Proc Natl Acad Sci U S A* 101: 16831-16836.
2. Arnheiter H (2010) The discovery of the microphthalmia locus and its gene, Mitf. *Pigment Cell Melanoma Res* 23: 729-735.
3. Steingrimsson E, Copeland NGJenkins NA (2004) Melanocytes and the microphthalmia transcription factor network. *Annu Rev Genet* 38: 365-411.

4. Hodgkinson CA, *et al*. (1993) Mutations at the mouse microphthalmia locus are associated with defects in a gene encoding a novel basic-helix-loop-helix-zipper protein. *Cell* 74: 395-404.

5. Hughes MJ, Lingrel JB, Krakowsky JMAnderson KP (1993) A helix-loop-helix transcription factor-like gene is located at the mi locus. *J Biol Chem* 268: 20687-20690.

6. Hallsson JH, *et al*. (2007) Evolutionary sequence comparison of the Mitf gene reveals novel conserved domains. *Pigment Cell Res* 20: 185-200.

7. Hemesath TJ, *et al*. (1998) MAP kinase links the transcription factor Microphthalmia to c-Kit signalling in melanocytes. *Nature* 391: 298-301.

8. Larribere L, *et al*. (2005) The cleavage of microphthalmia-associated transcription factor, MITF, by caspases plays an essential role in melanocyte and melanoma cell apoptosis. *Genes Dev* 19: 1980-1985.

9. Mansky KC, Sankar U, Han JOstrowski MC (2002) Microphthalmia transcription factor is a target of the p38 MAPK pathway in response to receptor activator of NF-kappa B ligand signaling. *J Biol Chem* 277: 11077-11083.

10. Miller AJ, *et al*. (2005) Sumoylation of MITF and its related family members TFE3 and TFEB. *J Biol Chem* 280: 146-155.

11. Murakami HArnheiter H (2005) Sumoylation modulates transcriptional activity of MITF in a promoter-specific manner. *Pigment Cell Res* 18: 265-277.

12. Takeda K, *et al*. (2000) Ser298 of MITF, a mutation site in Waardenburg syndrome type 2, is a phosphorylation site with functional significance. *Hum Mol Genet* 9: 125-132.

13. Wu M, *et al*. (2000) c-Kit triggers dual phosphorylations, which couple activation and degradation of the essential melanocyte factor Mi. *Genes Dev* 14: 301-312.

14. Takebayashi K, *et al*. (1996) The recessive phenotype displayed by a dominant negative microphthalmia-associated transcription factor mutant is a result of impaired nucleation potential. *Mol Cell Biol* 16: 1203-1211.

15. Du J, *et al*. (2004) Critical role of CDK2 for melanoma growth linked to its melanocyte-specific transcriptional regulation by MITF. *Cancer Cell* 6: 565-576.

16. Loercher AE, Tank EM, Delston RBHarbour JW (2005) MITF links differentiation with cell cycle arrest in melanocytes by transcriptional activation of INK4A. *J Cell Biol* 168: 35-40.

17. McGill GG, *et al*. (2002) Bcl2 regulation by the melanocyte master regulator Mitf modulates lineage survival and melanoma cell viability. *Cell* 109: 707-718.

18. Garraway LA, *et al*. (2005) "Lineage addiction" in human cancer: lessons from integrated genomics. *Cold Spring Harb Symp Quant Biol* 70: 25-34.

19. Hoek KSGoding CR (2010) Cancer stem cells versus phenotype-switching in melanoma. *Pigment Cell Melanoma Res* 23: 746-759.

20. Strub T, *et al*. (2011) Essential role of microphthalmia transcription factor for DNA replication, mitosis and genomic stability in melanoma. *Oncogene* 30: 2319-2332.

21. Steingrimsson E, *et al*. (1994) Molecular basis of mouse microphthalmia (mi) mutations helps explain their developmental and phenotypic consequences. *Nat Genet* 8: 256-263.

22. Hemesath TJ, *et al*. (1994) microphthalmia, a critical factor in melanocyte development, defines a discrete transcription factor family. *Genes Dev* 8: 2770-2780.

23. Boissy RELamoreux ML (1995) In vivo and in vitro morphological analysis of melanocytes homozygous for the misp allele at the murine microphthalmia locus. *Pigment Cell Res* 8: 294-301.

24. Wolfe HGColeman DL (1964) Mi-spotted:a mutation in the mouse. *Genet Res Camb* 5: 432-440.

25. Bismuth K, Maric DArnheiter H (2005) MITF and cell proliferation: the role of alternative splice forms. *Pigment Cell Res* 18: 349-359.

26. Primot A, *et al*. (2010) ERK-regulated differential expression of the Mitf 6a/b splicing isoforms in melanoma. *Pigment Cell Melanoma Res* 23: 93-102.

27. Steingrimsson E (2010) Interpretation of complex phenotypes: lessons from the Mitf gene. *Pigment Cell Melanoma Res* 23: 736-740.

28. Steingrimsson E, *et al*. (2002) Mitf and Tfe3, two members of the Mitf-Tfe family of bHLH-Zip transcription factors, have important but functionally redundant roles in osteoclast development. *Proc Natl Acad Sci U S A* 99: 4477-4482.

29. Tachibana M, *et al*. (1992) Cochlear Disorder associated with melanocyte anomaly in mice with a transgenic insertional mutation. *Mol Cell Neurosci* 3: 433-445.

30. Bharti K, *et al*. (2008) Alternative promoter use in eye development: the complex role and regulation of the transcription factor MITF. *Development* 135: 1169-1178.

31. Silver DL, *et al*. (2008) The secreted metalloprotease ADAMTS20 is required for melanoblast survival. *PLoS Genet* 4: e1000003.

32. Bernex F, *et al*. (1996) Spatial and temporal patterns of c-kit-expressing cells in WlacZ/+ and WlacZ/WlacZ mouse embryos. *Development* 122: 3023-3033.

33. Bharti K, Debbache J, Wang XArnheiter H (2010) The basic-helix-loop-helix-leucine zipper gene Mitf: analysis of alternative promoter choice and splicing. *Methods Mol Biol* 647: 237-250.

34. Bauer GL, *et al*. (2009) The role of MITF phosphorylation sites during coat color and eye development in mice analyzed by bacterial artificial chromosome transgene rescue. *Genetics* 183: 581-594.

35. Lee M, *et al*. (2000) Direct regulation of the Microphthalmia promoter by Sox10 links Waardenburg-Shah syndrome (WS4)-associated hypopigmentation and deafness to WS2. *J Biol Chem* 275: 37978-37983.

36. Weilbaecher KN, *et al*. (1998) Age-resolving osteopetrosis: a rat model implicating microphthalmia and the related transcription factor TFE3. *J Exp Med* 187: 775-785.

37. Opdecamp K, *et al*. (1997) Melanocyte development in vivo and in neural crest cell cultures: crucial dependence on the Mitf basic-helix-loop-helix-zipper transcription factor. *Development* 124: 2377-2386.

Figure legends

Figure 1.   Phenotypic behavior of the induced $Mitf^{mi-sp}*$ suppressor mutation. *(A)* NAW-$Mitf^{mi-ew}$/B6-$Mitf^{mi-sp}$ and NAW-$Mitf^{mi-ew}$/B6-$Mitf^{mi-sp}*$ compound heterozygotes. *(B)* B6-$Mitf^{Mi-Wh}$/B6-$Mitf^{mi-sp}*$ and B6-$Mitf^{Mi-Wh}$/B6-$Mitf^{mi-sp}$ compound heterozygotes. *(C)* B6-$Mitf^{mi-sp}$/B6-$Mitf^{mi}$ *and B6-*$Mitf^{mi-sp}*$/B6-$Mitf^{mi}$ compound heterozygotes. Notice the dramatic suppression of the phenotype from near-white to black coat color. *(D)* B6-$Mitf^{mi-sp}$/B6-$Mitf^{mi-rw}$ and B6-$Mitf^{mi-sp}*$/B6-$Mitf^{mi-rw}$ animals. *(E) B6-*$Mitf^{mi-sp}*$/B6-$Mitf^{mi-vga9}$. *(F) B6-*$Mitf^{mi-sp}$/B6-$Mitf^{mi-vga9}$. *(G) B6-*$Mitf^{mi-sp}$/$Mitf^{mi-sp}$. *(H)* B6-$Mitf^{mi-sp}*$/$Mitf^{mi-sp}*$.

Figure 2.   The molecular alteration associated with the $Mitf^{mi-sl}$ suppressor mutation. *(A)* The $Mitf^{mi-sl}$ mutation is a A to T transversion at nucleotide 1075, replacing Lys316 with a stop codon, resulting in the absence of a large portion of the carboxyl end of the protein. Like the $Mitf^{mi-sp}$ mutation, the $Mitf^{mi-sl}$ RNA is also missing the alternative 18 bp exon encoding a 6 amino acid alternatively spliced insert sequence. *(B)* The 6A5 monoclonal antibody, which recognizes the C-end of MITF, shows that $Mitf^{mi-sl}$ tissues and cells express a truncated form of MITF. The polyclonal rabbit anti-MITF antibody recognizes the MITF protein in both $Mitf^{mi-sp}$ and $Mitf^{mi-sl}$ tissues.

Figure 3.   Melanocyte numbers in developing embryos. The Kit-LacZ transgene was crossed into $Mitf^{mi-sl}$ and $Mitf^{mi-sp}$ mice and the number of melanocytes, as determined by the presence of blue cells, determined in selected regions in 12.5 and 15.5 day old embryos (indicated by red boxes). Statistically significant differences (Student's t-test) are indicated by **.

Figure 4.   RNA expression levels and MITF protein stability and DNA binding ability. (*A*) Relative RNA expression levels in wild type, $Mitf^{mi-sp}$ and $Mitf^{mi-sl}$ heart and skin, as detrmined by qRT-PCR. (*B*) Stability of the MITF, MITF^{mi-sp} or MITF^{mi-sl} proteins. In order to determine effects on stability, Cos cells were transfected with expression constructs containing wild type MITF, MITF^{mi-sp} and MITF^{mi-sl} proteins. The cells were then stimulated with TPA in the presence of cyclohexamide and the amount of

MITF protein after 0, 1, 2 and 3 hrs compared by Western blotting using the monoclonal C5 anti-MITF antibody.   Anti-tubulin antibodies were used as a control. (*C,D*) Electrophoretic mobility shift assays were performed using the M-box sequence as a probe. *(C)* Wild-type, MITF^{mi-sp} and MITF^{mi-sl} proteins were expressed using the TNT system alone (lanes 1, 2, 6, 10 and 11) or co-expressed with the dominant negative MITF^{mi} protein (lanes 3-5, 7-9 and 12-14) and then incubated with the labelled probe. The binding is specific since the presence of the C5 monoclonal MITF antibody results in a supershift (Ab). *(D)* The same experiment as in (*C*), except the proteins were translated separately and then incubated for half an hour in presence of DNA to allow heterodimerization before performing the mobility shift experiment.

Figure 5.   Promoter-specific   differences   in   transcription   activation   ability. Cotransfection studies comparing the transcription activation potential of the wild-type MITF, MITF^{mi-sp}, MITF^{mi-sl} and MITF^{mi-ew} proteins from two different promoters. *(A)*The MITF^{mi-sp} and MITF^{mi-sl} proteins are both less effective at activating transcription from the *tyrosinase* promoter than the wild type MITF protein. The MITF^{mi-sl} protein is less active from this promoter than the MITF^{mi-sp} protein. The MITF^{mi-ew} protein is lacking the basic domain and therefore cannot bind DNA or activate gene expression. *(B)* The MITF^{mi-sl} protein is a better transactivator than the MITF^{mi-sp} protein from the synthetic 4x M-box promoter. In fact, it is as effective as the wild type MITF protein in activating this promoter.

Supplementary Figures

Supplementary Figure 1. Phenotypic behavior of the induced $Mitf^{mi\text{-}sp*}$ suppressor mutation. *(A)* B6-$Mitf^{mi\text{-}ew}$/B6-$Mitf^{mi\text{-}sp}$ and B6-$Mitf^{mi\text{-}ew}$/B6-$Mitf^{mi\text{-}sp*}$ compound heterozygotes. *(B)* 82UT-$Mitf^{Mi\text{-}Or}$/B6-$Mitf^{mi\text{-}sp*}$ and 82UT-$Mitf^{Mi\text{-}Or}$/B6-$Mitf^{mi\text{-}sp}$ compound heterozygotes. *(C)* B6-$Mitf^{mi\text{-}sp*}$/B6-$Mitf^{Mi\text{-}Or}$ *and* B6-$Mitf^{mi\text{-}sp}$/B6-$Mitf^{Mi\text{-}Or}$ compound heterozygotes. *(D)* B6-$Mitf^{mi\text{-}sp*}$/B6-$Mitf^{Mi\text{-}b}$ and B6-$Mitf^{mi\text{-}sp}$/B6-$Mitf^{Mi\text{-}b}$ animals.
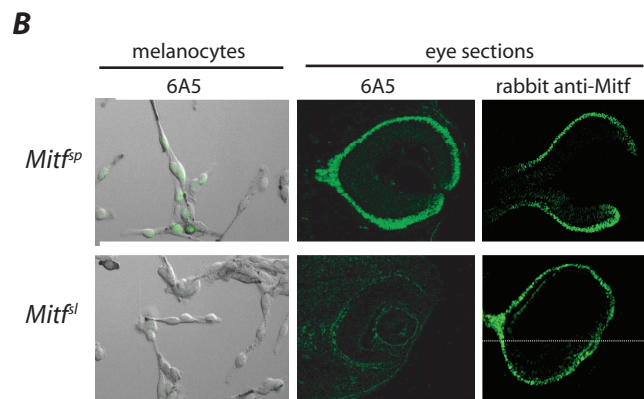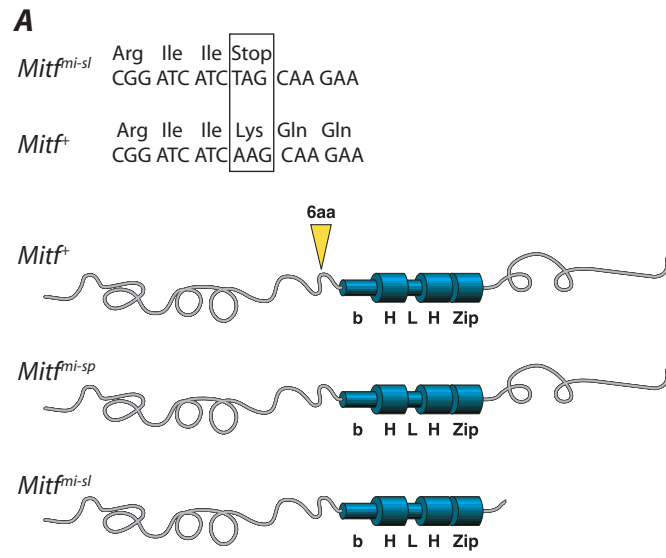
Supplementary Figure 2. The mutations do not affect nuclear localization of MITF. The nuclear localization of the MITF, MITF$^{mi\text{-}sp}$, MITF$^{mi\text{-}sl}$ and MITF$^{mi\text{-}ew}$ proteins were determined using two different methods. First, by fusing the respective MITF proteins to GFP, transforming the constructs into 293T cells and then tracing the location of the GFP protein (top panel), the protein was exclusively seen in the nucleus (counterstaining by TOPRO). Second, constructs expressing the different versions of MITF (not as GFP fusions) were transformed into 293T cells and the cells stained with the C5 antibody to detect the presence of MITF. The nuclear localization of the MITF$^{mi\text{-}ew}$ proteins contradicts the results of (14) who showed this protein to be both cytoplasmic and nuclear. This difference may be due to the fact that the protein is overexpressed in our system.

Supplementary Figure 3. The $Mitf^{mi\text{-}sl}$ mutation results in delayed pigmentation. *(A)* Melanocytes differentiating from neural crest cultures from $Mitf^{mi\text{-}sl}$ and $Mitf^{mi\text{-}sp}$ animals show that pigmentation is severely delayed in $Mitf^{mi\text{-}sl}$ homozygotes as compared to $Mitf^{mi\text{-}sp}$ homozygotes. Nevertheless, melanoblasts are present as evidenced by anti-MITF antibody staining (inset). *(B)* Homozygous $Mitf^{mi\text{-}sl}$ newborns show delayed onset of pigmentation as compared to $Mitf^{mi\text{-}sp}$ homozygotes, particularly clearly visible at postnatal day 2 and 3. (*C*) No difference in onset of pigmentation in compound heterozygous condition with $Mitf^{mi\text{-}vga9}$. Compare mice labeled #1 ($Mitf^{mi\text{-}sp}$/$Mitf^{mi\text{-}vga9}$) with mcie labeled #3 ($Mitf^{mi\text{-}sl}$/$Mitf^{mi\text{-}vga9}$).

$Mitf^{mi-sp}/Mitf^{mi-ew}$ $Mitf^{mi-sp*}/Mitf^{mi-ew}$ $Mitf^{mi-sp*}/Mitf^{Mi-Wh}$ $Mitf^{mi-sp}/Mitf^{Mi-Wh}$ $Mitf^{mi-sp}/Mitf^{mi}$ $Mitf^{mi-sp*}/Mitf^{mi}$ $Mitf^{mi-sp}/Mitf^{mi-rw}$ $Mitf^{mi-sp*}/Mitf^{mi-rw}$

$B6\text{-}Mitf^{mi-sp*}/B6\text{-}Mitf^{mi-vga9}$ $B6\text{-}Mitf^{mi-sp}/B6\text{-}Mitf^{mi-vga9}$ $B6\text{-}Mitf^{mi-sp}/B6\text{-}Mitf^{mi-sp}$ $B6\text{-}Mitf^{mi-sp*}/B6\text{-}Mitf^{mi-sp*}$

Steingrimsson et al., Figure 1

A

Mitf^mi-sl

Arg Ile Ile Stop
CGG ATC ATC TAG CAA GAA

Mitf^+

Arg Ile Ile Lys Gln Gln
CGG ATC ATC AAG CAA GAA

Mitf^+

6aa

b H L H Zip

Mitf^mi-sp

b H L H Zip

Mitf^mi-sl

b H L H Zip

B

	melanocytes	eye sections	
	6A5	6A5	rabbit anti-Mitf

Mitf^sp

Mitf^sl

Steingrimsson et al., Figure 2

A

| 12.5 day, eye-region | 15.5 day, ear-region | 15.5 day, hind-region |

B

Steingrimsson et al, Fig. 3

A

Heart

Skin

B

Mitf+   Mitf^mi-sp   Mitf^mi-sp*

Mitf
Mitf

Tubulin

0 1 2 3   0 1 2 3   0 1 2 3   TPA + CHX

C

Mitf^mi   Mitf^mi   Mitf^mi

Ab   Mitf +   Mitf^mi-sp   Mitf^mi-sl

1 2 3 4 5   6 7 8 9   10 11 12 13 14

6.61   3.77   3.79

D

Mitf^mi   Mitf^mi   Mitf^mi

Mitf +   Mitf^mi-sp   Mitf^mi-sl

1 2 3 4   5 6 7 8   9   10 11 12 13

3.87   2.60   1.98

Steingrimsson et al, Fig. 4

Steingrimsson et al., Fig. 5

$Mitf^{mi-sp}/B6-Mitf^{mi-ew}$ $Mitf^{mi-sp*}/B6-Mitf^{mi-ew}$ $Mitf^{mi-sp*}/82UT-Mitf^{Mi-Or}$ $Mitf^{mi-sp}/82UT-Mitf^{Mi-Or}$

$Mitf^{mi-sp*}/B6-Mitf^{Mi-Or}$ $Mitf^{mi-sp}/B6-Mitf^{Mi-Or}$ $Mitf^{mi-sp*}/Mitf^{Mi-b}$ $Mitf^{mi-sp}/Mitf^{Mi-b}$

Steingrimsson et al., Supplementary Figure 1

EGFP vector　　EGFP-Mitf+　　EGFP-Mitf^{mi-sp}　　EGFP-Mitf^{mi-sl}　　EGFP-Mitf^{mi-ew}

Mitf+　　Mitf^{mi-sp}　　Mitf^{mi-sl}　　Mitf^{mi-ew}

Steingrimsson et al., Supplementary Figure 2

A

day 12   day 14

$Mitf^{mi-sp}/Mitf^{mi-sp}$

$Mitf^{mi-sl}/Mitf^{mi-sl}$

Appearance of melanocytes

d   10   11   12   13   14   15   16   17

300
200
100

number of pigmented cells per culture

50

number of pigmented cells per culture

B

1 d   2 d   3 d   4 d   5 d   6 d   7 d

$Mitf^{mi-sp}/Mitf^{mi-sp}$

$Mitf^{mi-sl}/Mitf^{mi-sl}$

C

1 d   2 d   3 d   4 d   5 d   6 d   7 d   14d

1   $Mitf^{mi-sp}/Mitf^{mi-vga9}$

2   $Mitf^{mi-sp}/Mitf^{+}$

3   $Mitf^{mi-sl}/Mitf^{mi-vga9}$

4   $Mitf^{mi-sl}/Mitf^{+}$

one agouti pup separated out and grouped with a second one

Steingrimsson et al., Supplemental Figure 3

Table 1. The *Mitf* mutants used in this study

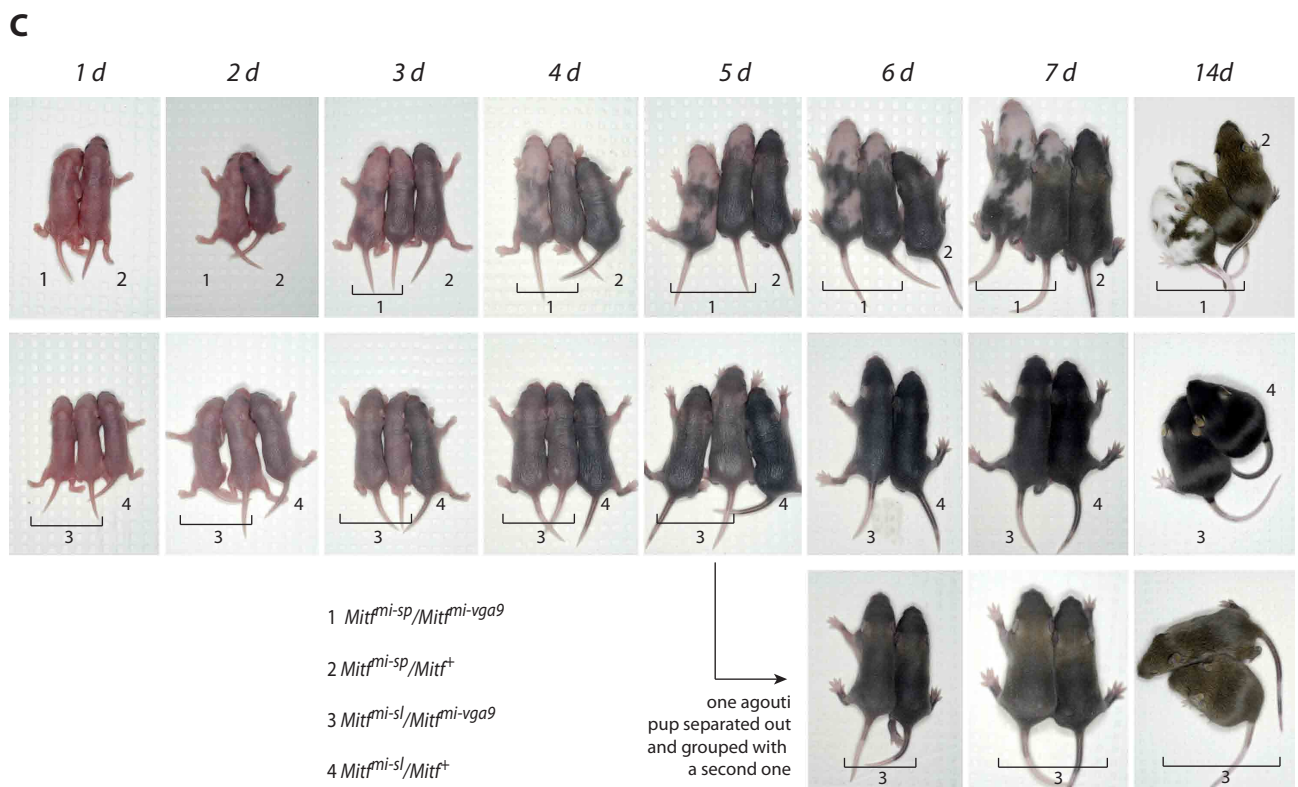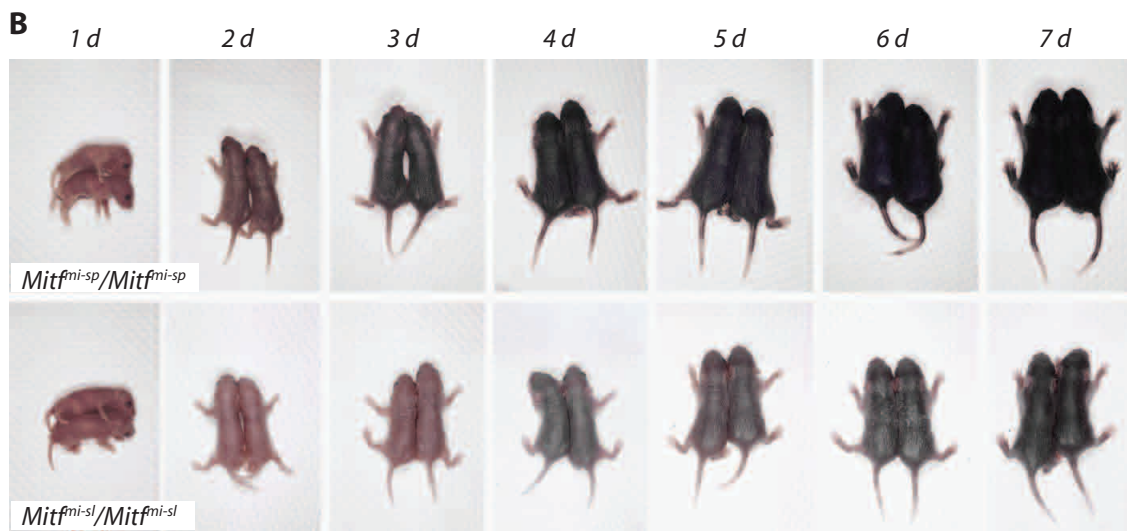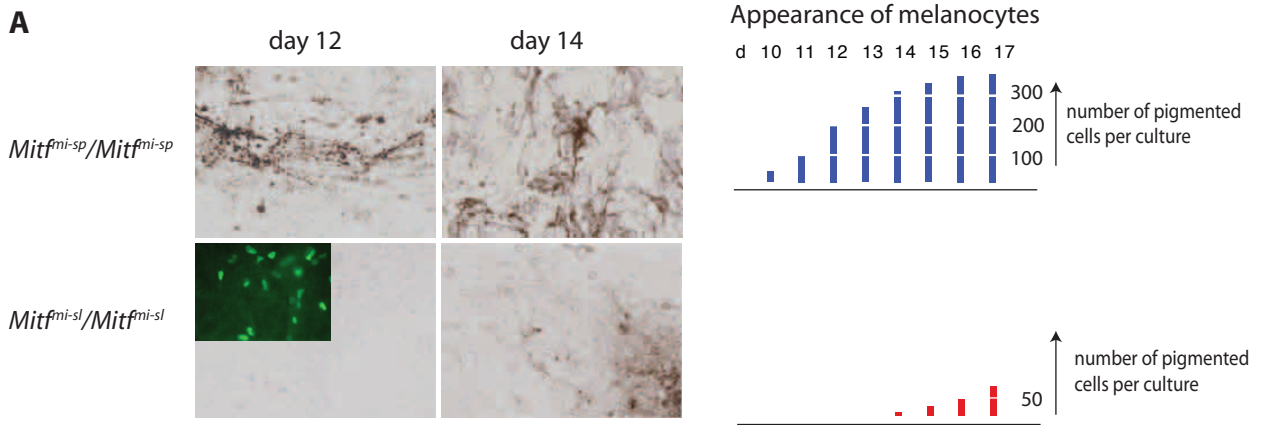| Allele	Symbol	Mode of induction	Phenotype* Heterozygote	Homozygote	Lesion
micropthalmia	*Mitf*mi	X-irradiation	Iris pigment less than in wild type; occasional spots on belly, head or tail	White coat, eyes small and red; deficiency of mast cells, incisors fail to erupt, osteopetrosis; inner ear defects	3 bp deletion in basic domain
oak ridge	*Mitf*mi-or	gamma-irradiation	Pale ears and tail; belly streak or head spot	White coat, eyes small and red; incisors fail to erupt, osteopetrosis	R216K
white	*Mitf*Mi-Wh	spontaneous or X-irradiation	Coat color lighter than dilute (*d/d*); eyes dark ruby; spots on feet, tail and belly	White coat; eyes small and slightly pigmented; inner ear defects	I212N
brownish	*Mitf*Mi-b	spontaneous	Fur diluted brownish with pale ears and tail	White coat, reduced eye pigment, eyes of normal size	G244E
eyeless-white	*Mitf*mi-ew	spontaneous	Normal	White coat, eyes almost absent, eyelids never open	25 amino acid deletion (splicing)
VGA-9	*Mitf*mi-vga9	transgene insertion	Normal	White coat, eyes red and small; inner ear defects	transgene insertion and 882 bp deletion
red-eyed white	*Mitf*mi-rw	spontaneous	Normal	White with pigmented spot on head and rump; eyes small and red	Upstream genomic deletion
spotted	*Mitf*mi-sp	spontaneous	Normal (reduced tyrosinase activity in skin)	Normal (reduced tyrosinase activity in skin). *Mitf*Mi-Wh/*Mitf*mi-sp animals are light yellow with white spots on coat; eyes are pigmented	Additional cytosine in polypyrimidine tract; 18 bp exon missing
Spotless	*Mitf*mi-sl	ENU	Normal	"Brownish" coat color. Compound heterozygotes with other Mitf mutations show a more normal coat color than is seen with *Mitf*mi-sp mice.	Additional cytosine in polypyrimidine tract; 18 bp exon missing. In addition, Lys316STOP

* The phenotypes of the mutant alleles have been described by different researchers and to different extents. Features described for all the mutants are coat and eye color, eye size and tooth and bone defects.

Discussion

Discussion

The *Mitf* transcription factor gene is a highly, if not the most important gene for the pigment cell lineage. It controls biological features as diverse as proliferation, differentiation, migration, and survival and so has been called the master regulator of melanocyte biology. Alterations of MITF activities are very often associated with abnormalities of development and maintenance of this cell type, as well as of melanocytic cancers. Therefore, tight regulations of Mitf levels, target gene activation and target gene specificity are crucial factors in the maintenance of melanocyte homeostasis in the skin. The net activity of MITF is the result of the integration of transcription activation of Mitf isoform specific promoters, alternative splicing, Mitf mRNA stability, translation initiation, post-translational modification, MITF protein degradation, and MITF DNA binding activation. For this reason, we developed several methods to quantify distribution of Mitf isoforms both *in vivo* and *in vitro*.

The MAPK signaling pathway is vital to melanocytes and its constitutive activation in one of the essential steps towards melanoma genesis. Intriguingly, it is also known to be associated with most of the regulatory processes of MITF activity, such as M-Mitf transcriptional activation, Mitf exon 6A alternative splicing, and the regulation of MITF stability. By using several genetic approaches, we show that the role of MITF phosphorylation at the Ser73 position is a critical modulator MITF activity. *In vitro*, MITF S73 phosphorylation was found to lead to a gain of transcriptional activity as well

as to a reduction of MITF stability in conjunction with MITF S409 phosphorylation, (Hemesath et al., 1998; Wu et al., 2000). Furthermore, the absence of phosphorylation at both S73 and S409 sites resulted in a protein that was transcriptionally inactive. While the phenotype of the *Mitf*[mi-S73A] knock-in mice clearly indicated that MITF S73 phosphorylation is not required for the normal development of melanocytes (Bismuth et al., 2008), the molecular analysis of this mutant mouse revealed that the absence of a overt phenotype might be the consequence of the absence of exon 2B rather than the prevention of S73 phosphorylation. The phenotypes resulting from mouse lines expressing mutant *Mitf* BAC transgenes confirmed, first, that exon 2B is not required for the normal development of melanocytes and, second, that the alteration of the Ser73 codon was leading to increased exclusion of exon 2B from Mitf messages (Bauer et al., 2009). Furthermore, this transgenic study showed that the mutation of both S73 and S409 into alanines was still able to rescue the *Mitf*[mi-vga9] phenotype. However, in that particular case, it is difficult to assess whether the rescue can be attributed to MITF S73/409A protein or whether the exclusion of exon 2B may help in the rescue effect by increasing the amount of MITF 2B- S409A protein. In addition, the inherent variabilities of Mitf levels between different lines are of concern and may not allow a full assessment of the role of phosphorylation in MITF activity regulation. This led us to use a different mutagenesis strategy, allowing us to dissociate the Ser73 mutation from exon 2B alternative splicing. Hence, we generated three *Mitf* knock-in alleles, *Mitf*[mi-S-S73A], *Mitf*[mi-S-S73D] and *Mitf*[mi-S-S73S] by targeting both the 5' alternative splice site and the codon for residue-73. The phenotypic analysis of these Mitf S73 mutants in combination with additional Mitf mutant alleles demonstrated a gain-of-function of the non-

phosphorylatable MITF 2B+ isoform. We attribute this gain of function to a significant increase in protein stability. The specific activity of the protein was, however, not determined and would require additional micro array experiments with respect to *in vivo* expression profiling and chromatin binding.

In a study not directly related to the question of exon 2B splicing and phosphorylation, we also presented the molecular and phenotypic characterizations of a gain of function modifier allele obtained by ENU mutagenesis on a *Mitf* pre-sensitized background. This new mutant allele happened to be an additional alteration of the *Mitf* mutant allele *Mitf^{mi-sp}*. The resulting MITF protein truncation leads to a rescue of the spotted phenotype that is produced when *Mitf^{mi-sp}* mice are crossed with mice carrying other *Mitf* mutations. This suppressor phenotype is linked to an apparent upregulation of transcriptional activity of MITF^{sl}.

The integration of the results obtained in the above-described studies rises 3 main discussion topics:

1) The physiological consequences of the lack of Mitf exon 2B

2) The discrepancies between *in vitro* and *in vivo* experiments

3) Mitf gain-of-function and melanoma

1) The physiological consequences of the lack of Mitf exon 2B

As described earlier, Mitf is subject to alternative splicing at exon 2B that gives rise to 2 isoforms, MITF 2B+ and MITF 2B(-). MITF 2B- lacks 56 amino acids. This serine/proline-rich sequence is thought to play a role in the CBP/P300 interaction but no

co-immunoprecipitation assay has been demonstrated to indicate that MITF 2B- protein is, indeed, unable to bind CBP/P300. Within this sequence also lies the critical S73 phosphorylation site that we have been studying here. Hence MITF 2B- lacks this critical regulation site and can therefore not be phosphorylated at this position. By modulating the level of exon 2B incorporation in Mitf transcripts, cells can therefore regulate the amount of phosphorylatable MITF. The importance of exon 2B and/or S73 phosphorylation has been further supported by several studies, indicating that MITF 2B- plays a fundamentally different role with respect to proliferation in melanocytes (Cronin et al., 2009; Taylor et al., 2011). In a melanoma sample screen looking for tumor-specific genomic alterations, Y. Samuels' group identified several somatic mutations in *MITF* that affected the coding sequence. While no mutation was found to affect S73 phosphorylation itself, one of them, called MITF4TΔ2B, leads to the exclusion of exon 2B in a melanoma metastasis sample. Reporter assays were performed to assess the activity of this mutant MITF protein among the others and led the authors to conclude that MITF 2B- was more active on certain target genes. Although the expression of MITF 2B- leads to an increase in luciferase induction, based on the western blot results, the amount of MITF 2B- protein reported relative to the loading control was much higher compared to wild-type MITF (Cronin et al., 2009). This would still support an increased transcription activation linked to the expression of MITF 2B(-), but not through an increase of the specific activity of MITF. The interesting differential activation of genes controlling differentiation processes compared to cell proliferation subsequently caught the interest of Patton's group. This MITF4TΔ2B mutant was used in rescue experiments on Mitf null zebrafish in order to determine its *in vivo* implication for development. The

results show that MITF 2B- protein is able to rescue pigmented cells more efficiently than wild-type MITF. In addition, MITF 2B- expressing pigmented melanocytes are still able to perform several division cycles while the wild-type MITF expressing cells stop dividing when they become pigmented (Taylor et al., 2011). Similar results have been observed *in vitro* where MITF 2B- transfected cells incorporate more BrdU than MITF 2B+ transfected cells. A higher proliferation rate was also observed in NCC derived from *Mitf*$^{mi-S73A}$ mutant mice compared to wild-type explants (Bismuth, PhD Thesis). While more cell divisions are observed in seemingly differentiated melanocytes, it is interesting that no increased pigmentation due to the presence of comparatively higher numbers of melanocytes, was observed in zebrafish or mouse. This suggests that independently of their differential growth rate, MITF 2B- expressing pigmented cells do not overcome the dependence on extracellular growth factors. It is important to note that in the zebrafish developmental study, dividing pigmented cells were considered as differentiated melanocytes (Taylor et al., 2011). While it is true that pigmentation is the primary goal of a differentiating melanoblasts, pigmentation is not the only parameter of differentiation. For instance, Tyrosinase negative melanocytes are unable to produce melanin but, apart from the lack of pigment, are otherwise most similar to wild type melanocytes. Hence, additional morphological and molecular markers should be taken into consideration to state that these proliferating cells were indeed differentiated and were not just early pigmented precursor cells.

With regards to our mouse models, the initial *Mitf*$^{mi-S73A}$ knock-in mutant turned out to be a rather complicated genetic entity. We demonstrated that the mutation of the S73 codon reduces the binding affinity for SRp40, which subsequently leads to the exclusion of exon

2B in the majority of Mitf mRNA. It is, however, important to note that despite this Mitf alternative splicing defect, resulting in 95% Mitf 2B- and only 5% Mitf 2B+ at the mRNA level, the respective protein isoform do not seem to faithfully reflect the ratios of the mRNA. Endogenous MITF expression from heart tissue as well as primary melanocyte cultures from *Mitf^{mi-S73A}* mutant mice show that MITF 2B+ represent between 30 to 50% of total MITF protein. The discrepancies between RNA and protein ratios is conceivably due to the fact that MITF 2B+ and MITF 2B- have different stabilities. In this genetic context, both MITF 2B+ S73A and MITF 2B- proteins cannot be phosphorylated. The significant amount of MITF 2B+ S73A protein seen in *Mitf^{mi-S73A}* mice could be an explanation for the phenotypic similarities observed between mice carrying the S73A and S-S73A alleles. The additional amount of full-length protein found in *Mitf^{mi-S-S73A}* mice, which cannot include exon 2B, might then be a plausible explanation for the slight gain in pigmentation observed by comparing *Mitf^{mi-S73A}* and *Mitf^{mi-S-S73A}* mice mice. In order to identify specific target genes subject to regulation by MITF 2B+ and MITF 2B(-), microarray gene expression analysis could be performed from either skin-derived sorted melanocytes or transgenic mouse-derived melanocyte cell lines cultured *in vitro*. While the first approach seems to be the most accurate with respect to expression profiling of melanocytes in their native environment, it also has several technical disadvantages. First of all, iDct-GFP bi-transgenic mice would need to be intercrossed with the *Mitf* mutant mice (Zaidi et al., 2011). Secondly, the GFP-sorted cell population obtained from these animals is heterogeneous as it consists of three subpopulations, undifferentiated melanocyte stem cells, differentiating melanoblasts and fully differentiated melanocytes. All of these three subpopulations might display

differential expression profiles and in this case would be pooled together. Another subject of concern is that the induction of the GFP system is under the control of the Dct promoter, which itself is controlled by Mitf activity. Cell sorting based on an MITF target driven reporter on a Mitf mutant genetic background might skew the threshold of detection and therefore bias the population sampling between mutants.

The *in vitro* alternative does not come without a cost either, as it has the major disadvantage that the *in vitro* culture conditions only partially reflect the *in vivo* situation. As I explain in more detail in the second part of the discussion, in specific cases, culture conditions might strongly influence the expression profile of the cell population. In addition, when placed in culture, the vast majority of the cells do not survive. Only the cells that are in the appropriate proliferation state or able to adapt will be able to survive in culture, thereby potentially introducing a cell population-specific selection. *In vitro* modeling implies that the cells are able to divide indefinitely, or at least for several passages. In a non-inducible system of differentiation versus proliferation, the cell population that is in the process of differentiation might be lost after only a few passages. Nevertheless, using melanocyte cell lines we performed preliminary experiments in order to decipher Mitf exon 2B regulations. In unpublished results, Wang *et al.* demonstrate that exon 2B incorporation in Mitf mRNA is regulated through the cell cycle with a preferential exclusion of exon 2B during S phase. While the level of significance of this fluctuation with respect to the pool of MITF protein has not yet been tested, the temporal synchronization between the decrease of a S-phase inhibiting isoform and the S-phase is indeed intriguing.

2) The discrepancies between *in vitro* and *in vivo* experiments

One of the most important points of this thesis centers on the demonstration that *in vitro* and *in vivo* results can lead to different conclusions. The original experiments testing the role of MITF S73 phosphorylation suggested that phosphorylation leads to an increase of MITF transcriptional activity and a reduction of its stability, and that the S73A mutation prevents these changes. The *in vivo* results show, however, that the prevention of S73 phosphorylation by the introduction of an alanine at this position produces a net gain-of-function, perhaps because an increased stability of the MITF protein might compensate its possible reduction in activity. In this context, then, we demonstrate that under normal circumstances, S73 phosphorylation-mediated transcriptional activation does not play any significant role in the development of melanocytes. Nevertheless, once Mitf levels are reduced in a sensitized background, S73 phosphorylation becomes important as it increases white spotting.

The *Mitf^{mi-S73A}* mouse model is a perfect example supporting these discrepancies between *in vivo* and *in vitro* results. In the NCC experiment performed *in vitro* from *in vivo* tissue, cells clearly show an increased proliferative rate, while in the animal, absolutely no difference in cell numbers can be observed. A likely hypothesis to explain this difference is based on the consideration that *in vitro* and *in vivo* conditions are vastly different with respect to availability of growth factors. It is known that in order to maintain *in vitro* melanocyte cultures, one has to add excess amounts of growth factors to compensate for the lack of cellular matrix provided by the *in vivo* environment. Unlike normal melanocytes *in vivo*, *in vitro* cultures of pigmented cells are perpetually in a growth state,

perhaps similar to what is observed in the cancers. In order to sustain this level of growth, it is very likely that the dose of growth factors or their response to them, would be above the *in vivo* threshold of signaling activity.

How is this related to the MITF phosphorylation and activity topic? As I mentioned earlier, one of the major factors involved in melanocyte proliferation is KIT Ligand, which activates the MAPK pathway. The same signaling pathway is involved in MITF phosphorylation. Hemesath *et al.* show that they can induce complete phosphorylation of MITF within 8 minutes of incubation with MAPK activators *in vitro*. Wu *et al.* show that MITF expression disappears within 4 hours of MAPK activation due to ubiquitin-mediated degradation. It is therefore puzzling to link the disappearance of MITF expression within 4h and the upregulation of target genes 8h after induction, especially when no MITF protein levels were shown in the luciferase activation test (Hemesath et al., 1998; Wu et al., 2000). Without MAPK induction, the 50% of phosphorylated MITF protein do not show a higher activation of the reporter gene. An upregulation of MITF activity is therefore only observed subsequently to the replenishment of newly synthesized MITF protein after ubiquitination-mediated depletion of the MITF protein pool. Hence, the upregulation of Mitf target gene activation can be seen as a compensatory mechanism following prior depletion of MITF as newly synthesized protein might be transcriptionally more active than older protein. Considering the *in vivo* situation, it is conceivable, therefore, that this extent of MITF phosphorylation *in vitro* would not reflect the state of phosphorylation *in vivo*.

With respect to proliferation, the same remarks regarding the association of an over activation of the MAPK and MITF are valid. The differential effects on proliferation

between MITF 2B+ and MITF 2B- are only seen *in vitro*, where the MAPK activation threshold is likely higher than *in vivo*. We know from several publications that constitutive activation of the MAPK pathway in melanocytes leads to senenscence-mediated cell cycle arrest. Intriguingly, similar phenomenons happen in melanoma.

3) Mitf gain-of-function and melanoma.

In early stages of melanoma, constitutively active BRAF or NRAS lead to senescence. The association of the MITF 2B- isoform in this context would then correlate with the *in vitro* NCC experiments, because MITF 2B- expressing cells would continue to proliferate despite MAPK-signaling. This could be tested by introducing an MITF S73A mutant, for instance, on a melanocyte-specific BRAF V600E background and by studying tumor formation in such mice.

In contrast, *in vivo* reductions of endogenous Kit signaling leads to a slightly more severe pigmentation defect in absence of a phosphorylatable serine. This might demonstrate the role of MITF phosphorylation in the survival/proliferation balance. Mitf phosphorylation would promote cell differentiation and survival and inhibit cell proliferation, whereas Mitf 2B- and Mitf 2B+ S73A might promote differentiation and proliferation.

The large majority of previously identified Mitf mutant alleles are loss-of-function mutations, ultimately resulting in a loss, or reduced number, of the neural crest-derived pigment cells. Here, we presented new Mitf alleles that show apparent gain-of-

function compared to wild type. As described earlier, melanoma is often associated with an increased copy number of the *Mitf* gene, and a likely associated gain of activity. While none of our *Mitf* alleles in mice displayed spontaneous formations of melanoma tumors on their own, it may be interesting to investigate their potential interaction with other known tumor promoting factors besides constitutively active MAPK, such as PTEN knock-outs. The alleles described here are very particular because, unlike wild-type, they lead to MITF proteins that lose critical regulation sites that may be important for cancer progression. The study of the specific interaction of these MITF regulation mutants with oncogenic pathways may reveal potential therapeutic targets or at least help understand how MITF activity is involved in the tumor formation process.

In conclusion, we have identified several key mechanisms of Mitf post-transcriptional and post-translational regulations, which seem to play major roles with respect to net MITF activity. Although we identified several alleles with hypermorphic functions, they did not produce striking phenotypes by themselves *in vivo*. These results combined with recent findings from other groups, however, prompt a series of new questions that would be interesting to answer:

♦ Exon 2B alternative splicing: Is exon 2B alternative splicing linked to the MAPK signaling pathway as it is for exon 6A alternative splicing? And is exon 2B splicing or MITF phosphorylation regulated during the cell cycle?

♦ <u>Protein interaction:</u> What are the factors binding specifically to MITF S73-P, potentially explaining the difference in cell proliferation inhibition?

♦ <u>Transcriptional activation:</u> Are the expression profiles of these mice similar or do they present major differences that could explain their distinct phenotypes?

♦ <u>Melanoma:</u> Would Mitf gain of function alleles result in a higher melanoma progression on a mouse cancer model, or would it prevent cell proliferation?

Synthèse

Synthèse du travail de thèse

L'épissage alternatif et les modifications post-traductionnelles font partie des mécanismes biologiques grâce auxquels un seul et unique gène peut générer plusieurs protéines de fonction diverse. Grâce à l'analyse de résultats issus de techniques récentes telles que le séquençage de nouvelle génération aussi appelé « RNA-seq » et la protéomique, on a pu mettre en évidence que la grande majorité des ARN pré-messagers comportant plusieurs exons sont sujets à des modifications post-trancriptionnelles d'épissage alternatif, et que de telles modifications post-traductionnelles modulent l'activité de bon nombre de protéines de cellules eucaryotes. Dans ce travail de thèse, nous nous sommes intéressés à un modèle génétique murin grâce auquel nous avons pu tester *in vivo* l'effet de mutations ponctuelles de sites de phosphorylation connus pour affecter la fonction d'un facteur de transcription crucial pour la lignée mélanocytaire : MITF.

La lignée mélanocytaire et son utilisation dans l'étude d'interactions génétiques et de modulations de l'activité de ces constituants, présente plusieurs avantages. Premièrement, la fonctionnalité de ce type cellulaire n'est pas requise pour la survie de l'animal, deuxièmement, les phénotypes de pigmentation sont aisément identifiables et quantifiables sans intervention nécessaire sur l'animal et enfin le processus de pigmentation de la peau met en jeu la majorité des processus de régulation cellulaires tels que la prolifération, la différentiation, la maintenance de l'état différencié et la survie cellulaire. Jusqu'à maintenant, 179 gènes ont été identifiés comme ayant un impact sur la

biologie des mélanocytes et la pigmentation. Au centre de cette vaste liste se trouve le facteur de transcription Microphthalmia, qui est le régulateur principal de ce type cellulaire. Il régule à la fois la prolifération, la différentiation et la survie des mélanocytes. Ainsi l'étude des processus de régulation de l'activité de ce facteur de transcription permet de comprendre comment des fonctions si diverses et parfois opposées comme l'activation de la prolifération et de la différentiation peuvent être régulées par un seul gène.

Chez la souris, l'importance du gène *Mitf* est d'autant plus soulignée par une pléthore de plus de 30 allèles différents, qui ont été identifiés depuis son clonage (Hodgkinson et al., 1993). Le domaine basique de MITF permet la fixation à l'ADN tandis que les domaines HLH et LZ jouent un rôle important dans l'homo et l'hétérodimérisation avec ses partenaires. La grande majorité des allèles identifiés de *Mitf* par le passé, tels que *Mitf*^{mi}, *Mitf*$^{mi\text{-}wh}$, *Mitf*$^{mi\text{-}ce}$, *Mitf*$^{mi\text{-}ew}$, *Mitf*$^{mi\text{-}or}$, *Mitf*$^{mi\text{-}vit}$, sont des mutations qui altèrent l'un ou l'autre de ces deux domaines, ce qui provoque une perte partielle ou totale de l'activité de la protéine.

Chez l'homme les mutations du gène *MITF* provoquent des défauts de pigmentation de la peau et du développement de l'œil ainsi que, dans certains cas, une surdité congénitale. L'ensemble des symptômes présentés par ces sujets est généralement regroupé sous un sous type du syndrome de Waardenburg, lequel rassemble des mutations d'autres gènes tels que *SOX10* ou *PAX3*, tous deux situés dans la voie d'activation de la transcription de *MITF* dans les mélanocytes.

Le gène Mitf appartient à la superfamille de facteurs de transcription de type bHLH-LZ (basic Helix-Loop-Helix Leucine-Zipper), tels que Myc, Mad ou Max, et a une structure génétique relativement complexe, constituée de 9 promoteurs alternatifs. L'activation transcriptionnelle de certaines isoformes est hautement spécifique du type cellulaire. Les isoformes A-Mitf ou H-Mitf sont exprimées de façon ubiquitaire contrairement à l'isoforme M-Mitf qui est spécifique aux Melanocytes. Outre la régulation du niveau d'expression, chacun de ces transcrits est régulé par des mécanismes d'épissage alternatif sur deux sous-exons : 6A et 2B. Le rôle du premier a été associé à une augmentation de la stabilité de fixation à l'ADN lorsqu'il est présent dans la protéine et également à l'inhibition de la prolifération médiée par Mitf. L'exon 2B, quant à lui, contient un site de phosphorylation lié à la voie des MAPK, la Serine 73, qui a été associé *in vitro* comme jouant un rôle important dans la régulation de l'activité de MITF ainsi que sa stabilité (Bismuth et al., 2005; Hemesath et al., 1998; Wu et al., 2000). Au total, Mitf peut donc donner naissance à 36 transcrits différents.

Du fait de cette complexité moléculaire, un premier travail de recherche a été dédié à l'élaboration de méthodes quantitative et qualitatives par RT-PCR afin d'identifier et de mesurer l'expression de ces isoformes multiples dans divers tissus. Nous avons ainsi présenté une méthode simple de quantification de transcrits complexes, applicable à d'autres gènes sujets aux mêmes types de régulations transcriptionnelles et d'épissages alternatifs.

Intrigué par la dualité fonctionnelle apparente du rôle de la phosphorylation de la Serine 73 *in vitro*, notre groupe de recherche avait préalablement tenté de déterminer le rôle de celle-ci *in vivo* en mutant S73 en une alanine non phosphorylable, de façon endogène. Bien que cette mutation ait été effective sur le plan génomique par une substitution du codon S73 en codon A73, elle a également provoque un effet inattendu sur la régulation de l'épissage de l'exon 2B sur lequel se situe le site de phosphorylation. L'altération du codon S73 entraine une forte augmentation de l'exclusion de l'exon 2B quelque soit le contexte génétique. Une seconde tentative par insertion de transgènes codant pour MITF S73A a eu le même effet sur le profile d'épissage de l'exon 2B. Cette étude réalisée par le laboratoire du Dr Steingrimsson a cependant apporté des éléments nouveaux concernant le rôle de la phosphorylation de la S409 ainsi que l'absence totale de l'exon 2B. Ce travail a démontré que ni la phosphorylation de la serine S73 ni la présence de l'exon 2B ni la phosphorylation de la S409 ne sont requises pour conserver l'activité transcriptionnelle de MITF *in vivo*.

Parallèlement, dans le but de comprendre les raisons de l'association entre la mutation du codon de la S73 et de l'exclusion préférentielle de l'exon 2B des transcrits Mitf, notre laboratoire a donc étudié de façon approfondie les mécanismes moléculaires impliqués dans cette observation. Nous avons ainsi identifié que le codon de la S73 fait partie d'un site de fixation d'un facteur de régulation de l'épissage de la famille des « Serine/Arginine rich proteins » SRp40. La mutation du codon S73 entraine une diminution de la fixation de ce facteur et favorise ainsi le choix de la jonction exon2A-2B comme site d'épissage préférentiel. De ce fait, l'inclusion de l'exon 2B est

intrinsèquement liée au statut du codon S73. Afin d'étudier le rôle de la phosphorylation de cette serine indépendamment de l'exclusion de l'exon 2B qui la comporte, nous avons entrepris de re-cibler le gène Mitf endogène en apportant des altérations de séquences supplémentaires qui permettent l'inclusion de l'exon 2B dans 100% des transcrits quelque soit la séquence du codon 73. La jonction entre l'exon 2A et 2B correspond à la séquence consensus qui définit la limite entre l'extrémité 3' d'un exon et le début d'un intron. Ainsi, notre stratégie a été de modifier cette séquence afin qu'elle ne soit plus reconnue par le complexe d'épissage, en conjonction avec l'altération du codon S73.

Les résultats décrits dans ce travail démontrent que l'absence de phosphorylation de MITF sur la Serine 73 non seulement n'est pas indispensable à l'activité transcriptionelle, mais provoque aussi un gain de stabilité suffisant de la protéine qui a pour conséquence un gain de fonction au niveau phénotypique. Nous avons également pu lier l'absence de phosphorylation à la perte totale ou partielle d'inhibition de la progression dans le cycle cellulaire.

Du fait de son rôle central sur la survie, la différentiation et la prolifération des melanocytes, il n'est pas surprenant de retrouver Mitf associé au mélanome. Le dérèglement pathologique de ce type cellulaire est dans la très forte majorité associé à une activation constitutive de la voix des MAPK et à un gain de l'activité de MITF. Nous suggérons donc que la perte de phosphorylabilité de MITF par une augmentation de l'exclusion de l'exon 2B (déjà rapportée dans des métastases de mélanome (Cronin et al., 2009)) ou par l'altération de la réaction de phosphorylation (augmentation de l'activité des phosphatases ou mutation du site de phosphorylation) peuvent être des éléments déterminant dans le développement du processus tumoral du mélanome.

En outre, en collaboration avec le laboratoire du Dr Steingrimsson, nous avons participé à la caractérisation d'un nouvel allèle du gène *Mitf* de type suppresseur. Au cours de ce travail basé sur un crible de mutations aléatoires sur un fond génétique sensibilisé de souris homozygotes pour l'allèle *Mitf*$^{mi-sp}$, nous avons identifié une mutation intragénique de *Mitf*$^{mi-sp}$ produisant un nouvel allèle nommé *Mitf*$^{mi-sl}$. *Mitf*$^{mi-sl}$ possède, en plus de la mutation *Mitf*$^{mi-sp}$, qui provoque la dégradation par « Non-sense mediated decay » des transcrits MITF 6A+, un codon stop prématuré qui tronque la protéine à l'acide amine 315. MITF perd ainsi plusieurs sites de modifications post traductionnelles, tels que la Lysine 316 impliquée dans la réduction de l'activité de MITF par SUMOylation. Cette modification post-traductionnelle a d'ailleurs été récemment liée à un risque accru de contracter un mélanome lorsqu'elle est perdue ou altérée (Bertolotto et al., 2011). Ainsi nous avons démontré que ce nouvel allèle possédait un gain d'activité transcriptionnelle *in vitro* ainsi qu'un gain phénotypique associé à une augmentation du niveau d'expression transcriptionnelle de Mitf *in vivo*.

En conclusion, nous avons identifié certains mécanismes de régulations post transcriptionnelles et post traductionnelles jouant des rôles importants dans le contrôle de la biologie des mélanocytes par MITF. Bien que les nouveaux allèles de Mitf, décrits dans cette thèse, présentent des gains de fonction sans qu'aucun mélanome spontané ne soit apparu, certaines des données obtenues in vitro suggèrent qu'il est probable que ces allèles puissent avoir un potentiel oncogénique supérieur à l'allèle témoin en présence de mutations de type BRAF V600E ou PTEN-/-.

Bibliographie

Bibliographie

Aksan, I., and Goding, C.R. (1998). Targeting the microphthalmia basic helix-loop-helix-leucine zipper transcription factor to a subset of E-box elements in vitro and in vivo. Mol Cell Biol 18, 6930-6938.

Amae, S., Fuse, N., Yasumoto, K., Sato, S., Yajima, I., Yamamoto, H., Udono, T., Durlu, Y.K., Tamai, M., Takahashi, K., et al. (1998). Identification of a novel isoform of microphthalmia-associated transcription factor that is enriched in retinal pigment epithelium. Biochem Biophys Res Commun 247, 710-715.

Bauer, G.L., Praetorius, C., Bergsteinsdottir, K., Hallsson, J.H., Gisladottir, B.K., Schepsky, A., Swing, D.A., O'Sullivan, T.N., Arnheiter, H., Bismuth, K., et al. (2009). The role of MITF phosphorylation sites during coat color and eye development in mice analyzed by bacterial artificial chromosome transgene rescue. Genetics 183, 581-594.

Bennett, D.C. (2008). How to make a melanoma: what do we know of the primary clonal events? Pigment Cell Melanoma Res 21, 27-38.

Bertolotto, C., Abbe, P., Hemesath, T.J., Bille, K., Fisher, D.E., Ortonne, J.P., and Ballotti, R. (1998). Microphthalmia gene product as a signal transducer in cAMP-induced differentiation of melanocytes. J Cell Biol 142, 827-835.

Bertolotto, C., Lesueur, F., Giuliano, S., Strub, T., de Lichy, M., Bille, K., Dessen, P., d'Hayer, B., Mohamdi, H., Remenieras, A., et al. (2011a). A SUMOylation-defective MITF germline mutation predisposes to melanoma and renal carcinoma. Nature 480, 94-98.

Bertolotto, C., Lesueur, F., Giuliano, S., Strub, T., de Lichy, M., Bille, K., Dessen, P., d'Hayer, B., Mohamdi, H., Remenieras, A., et al. (2011b). A SUMOylation-defective MITF germline mutation predisposes to melanoma and renal carcinoma. Nature.

Bharti, K., Liu, W., Csermely, T., Bertuzzi, S., and Arnheiter, H. (2008). Alternative promoter use in eye development: the complex role and regulation of the transcription factor MITF. Development 135, 1169-1178.

Bharti, K., Nguyen, M.T., Skuntz, S., Bertuzzi, S., and Arnheiter, H. (2006). The other pigment cell: specification and development of the pigmented epithelium of the vertebrate eye. Pigment Cell Res 19, 380-394.

Bismuth, K., Maric, D., and Arnheiter, H. (2005). MITF and cell proliferation: the role of alternative splice forms. Pigment Cell Res 18, 349-359.

Bismuth, K., Skuntz, S., Hallsson, J.H., Pak, E., Dutra, A.S., Steingrimsson, E., and Arnheiter, H. (2008). An unstable targeted allele of the mouse Mitf gene with a high somatic and germline reversion rate. Genetics 178, 259-272.

Boissy, R.E., and Lamoreux, M.L. (1995). In vivo and in vitro morphological analysis of melanocytes homozygous for the misp allele at the murine microphthalmia locus. Pigment Cell Res 8, 294-301.

Calloni, G.W., Le Douarin, N.M., and Dupin, E. (2009). High frequency of cephalic neural crest cells shows coexistence of neurogenic, melanogenic, and osteogenic differentiation capacities. Proc Natl Acad Sci U S A 106, 8947-8952.

Carreira, S., Goodall, J., Denat, L., Rodriguez, M., Nuciforo, P., Hoek, K.S., Testori, A., Larue, L., and Goding, C.R. (2006). Mitf regulation of Dia1 controls melanoma proliferation and invasiveness. Genes Dev 20, 3426-3439.

Cronin, J.C., Wunderlich, J., Loftus, S.K., Prickett, T.D., Wei, X., Ridd, K., Vemula, S., Burrell, A.S., Agrawal, N.S., Lin, J.C., et al. (2009). Frequent mutations in the MITF pathway in melanoma. Pigment Cell Melanoma Res 22, 435-444.

Dahl, C., and Guldberg, P. (2007). The genome and epigenome of malignant melanoma. APMIS 115, 1161-1176.

de Snoo, F.A., and Hayward, N.K. (2005). Cutaneous melanoma susceptibility and progression genes. Cancer Lett 230, 153-186.

Dhomen, N., Reis-Filho, J.S., da Rocha Dias, S., Hayward, R., Savage, K., Delmas, V., Larue, L., Pritchard, C., and Marais, R. (2009). Oncogenic Braf induces melanocyte senescence and melanoma in mice. Cancer Cell 15, 294-303.

Dorsky, R.I., Moon, R.T., and Raible, D.W. (1998). Control of neural crest cell fate by the Wnt signalling pathway. Nature 396, 370-373.

Dunn, K.J., Brady, M., Ochsenbauer-Jambor, C., Snyder, S., Incao, A., and Pavan, W.J. (2005). WNT1 and WNT3a promote expansion of melanocytes through distinct modes of action. Pigment Cell Res 18, 167-180.

Dunn, K.J., Williams, B.O., Li, Y., and Pavan, W.J. (2000). Neural crest-directed gene transfer demonstrates Wnt1 role in melanocyte expansion and differentiation during mouse development. Proc Natl Acad Sci U S A 97, 10050-10055.

Dupin, E., Real, C., Glavieux-Pardanaud, C., Vaigot, P., and Le Douarin, N.M. (2003). Reversal of developmental restrictions in neural crest lineages: transition from Schwann cells to glial-melanocytic precursors in vitro. Proc Natl Acad Sci U S A 100, 5229-5233.

Fuse, N., Yasumoto, K., Takeda, K., Amae, S., Yoshizawa, M., Udono, T., Takahashi, K., Tamai, M., Tomita, Y., Tachibana, M., et al. (1999). Molecular cloning of cDNA encoding a novel microphthalmia-associated transcription factor isoform with a distinct amino-terminus. J Biochem 126, 1043-1051.

Galibert, M.D., Yavuzer, U., Dexter, T.J., and Goding, C.R. (1999). Pax3 and regulation of the melanocyte-specific tyrosinase-related protein-1 promoter. J Biol Chem 274, 26894-26900.

Garraway, L.A., Widlund, H.R., Rubin, M.A., Getz, G., Berger, A.J., Ramaswamy, S., Beroukhim, R., Milner, D.A., Granter, S.R., Du, J., et al. (2005). Integrative genomic analyses identify MITF as a lineage survival oncogene amplified in malignant melanoma. Nature 436, 117-122.

Gast, A., Scherer, D., Chen, B., Bloethner, S., Melchert, S., Sucker, A., Hemminki, K., Schadendorf, D., and Kumar, R. (2010). Somatic alterations in the melanoma genome: a high-resolution array-based comparative genomic hybridization study. Genes Chromosomes Cancer 49, 733-745.

Giblin, A.V., and Thomas, J.M. (2007). Incidence, mortality and survival in cutaneous melanoma. J Plast Reconstr Aesthet Surg 60, 32-40.

Haflidadottir, B.S., Bergsteinsdottir, K., Praetorius, C., and Steingrimsson, E. (2010). miR-148 regulates Mitf in melanoma cells. PLoS One 5, e11574.

Hallsson, J.H., Favor, J., Hodgkinson, C., Glaser, T., Lamoreux, M.L., Magnusdottir, R., Gunnarsson, G.J., Sweet, H.O., Copeland, N.G., Jenkins, N.A., et al. (2000). Genomic, transcriptional and mutational analysis of the mouse microphthalmia locus. Genetics 155, 291-300.

Hallsson, J.H., Haflidadottir, B.S., Schepsky, A., Arnheiter, H., and Steingrimsson, E. (2007). Evolutionary sequence comparison of the Mitf gene reveals novel conserved domains. Pigment Cell Res 20, 185-200.

Hari, L., Brault, V., Kleber, M., Lee, H.Y., Ille, F., Leimeroth, R., Paratore, C., Suter, U., Kemler, R., and Sommer, L. (2002). Lineage-specific requirements of beta-catenin in neural crest development. J Cell Biol 159, 867-880.

Hart, M.J., de los Santos, R., Albert, I.N., Rubinfeld, B., and Polakis, P. (1998). Downregulation of beta-catenin by human Axin and its association with the APC tumor suppressor, beta-catenin and GSK3 beta. Curr Biol 8, 573-581.

Hemesath, T.J., Price, E.R., Takemoto, C., Badalian, T., and Fisher, D.E. (1998). MAP kinase links the transcription factor Microphthalmia to c-Kit signalling in melanocytes. Nature 391, 298-301.

Hemesath, T.J., Steingrimsson, E., McGill, G., Hansen, M.J., Vaught, J., Hodgkinson, C.A., Arnheiter, H., Copeland, N.G., Jenkins, N.A., and Fisher, D.E. (1994). microphthalmia, a critical factor in melanocyte development, defines a discrete transcription factor family. Genes Dev 8, 2770-2780.

Hershey, C.L., and Fisher, D.E. (2004). Mitf and Tfe3: members of a b-HLH-ZIP transcription factor family essential for osteoclast development and function. Bone 34, 689-696.

Hertwig, P. (1942). Neue Mutationen und Kopplungsgruppen bei der Hausmaus. Z Indukt Abstammungs- u Vererbungsl 80, 220-246.

Hodgkinson, C.A., Moore, K.J., Nakayama, A., Steingrimsson, E., Copeland, N.G., Jenkins, N.A., and Arnheiter, H. (1993). Mutations at the mouse microphthalmia locus are associated with defects in a gene encoding a novel basic-helix-loop-helix-zipper protein. Cell 74, 395-404.

Hodgkinson, C.A., Nakayama, A., Li, H., Swenson, L.B., Opdecamp, K., Asher, J.H., Jr., Arnheiter, H., and Glaser, T. (1998). Mutation at the anophthalmic white locus in Syrian hamsters: haploinsufficiency in the Mitf gene mimics human Waardenburg syndrome type 2. Hum Mol Genet 7, 703-708.

Hoek, K.S., and Goding, C.R. (2010). Cancer stem cells versus phenotype-switching in melanoma. Pigment Cell Melanoma Res 23, 746-759.

Hou, L., Panthier, J.J., and Arnheiter, H. (2000). Signaling and transcriptional regulation in the neural crest-derived melanocyte lineage: interactions between KIT and MITF. Development 127, 5379-5389.

Huber, W.E., Price, E.R., Widlund, H.R., Du, J., Davis, I.J., Wegner, M., and Fisher, D.E. (2003). A tissue-restricted cAMP transcriptional response: SOX10 modulates alpha-melanocyte-stimulating hormone-triggered expression of microphthalmia-associated transcription factor in melanocytes. J Biol Chem 278, 45224-45230.

Izumi, K., Kohta, T., Kimura, Y., Ishida, S., Takahashi, T., Ishiko, A., and Kosaki, K. (2008). Tietz syndrome: unique phenotype specific to mutations of MITF nuclear localization signal. Clin Genet 74, 93-95.

Jonsson, G., Dahl, C., Staaf, J., Sandberg, T., Bendahl, P.O., Ringner, M., Guldberg, P., and Borg, A. (2007). Genomic profiling of malignant melanoma using tiling-resolution arrayCGH. Oncogene 26, 4738-4748.

Kuhlbrodt, K., Herbarth, B., Sock, E., Hermans-Borgmeyer, I., and Wegner, M. (1998). Sox10, a novel transcriptional modulator in glial cells. J Neurosci 18, 237-250.

Le Douarin, N.M., Calloni, G.W., and Dupin, E. (2008). The stem cells of the neural crest. Cell Cycle 7, 1013-1019.

Lee, M., Goodall, J., Verastegui, C., Ballotti, R., and Goding, C.R. (2000). Direct regulation of the Microphthalmia promoter by Sox10 links Waardenburg-Shah syndrome (WS4)-associated hypopigmentation and deafness to WS2. J Biol Chem 275, 37978-37983.

Levy, C., Khaled, M., and Fisher, D.E. (2006a). MITF: master regulator of melanocyte development and melanoma oncogene. Trends Mol Med 12, 406-414.

Levy, C., Khaled, M., Robinson, K.C., Veguilla, R.A., Chen, P.H., Yokoyama, S., Makino, E., Lu, J., Larue, L., Beermann, F., et al. (2010). Lineage-specific transcriptional regulation of DICER by MITF in melanocytes. Cell 141, 994-1005.

Levy, C., Lee, Y.N., Nechushtan, H., Schueler-Furman, O., Sonnenblick, A., Hacohen, S., and Razin, E. (2006b). Identifying a common molecular mechanism for inhibition of MITF and STAT3 by PIAS3. Blood 107, 2839-2845.

McGill, G.G., Horstmann, M., Widlund, H.R., Du, J., Motyckova, G., Nishimura, E.K., Lin, Y.L., Ramaswamy, S., Avery, W., Ding, H.F., et al. (2002). Bcl2 regulation by the melanocyte master regulator Mitf modulates lineage survival and melanoma cell viability. Cell 109, 707-718.

Meyle, K.D., and Guldberg, P. (2009). Genetic risk factors for melanoma. Hum Genet 126, 499-510.

Miller, A.J., Levy, C., Davis, I.J., Razin, E., and Fisher, D.E. (2005). Sumoylation of MITF and its related family members TFE3 and TFEB. J Biol Chem 280, 146-155.

Mollaaghababa, R., and Pavan, W.J. (2003). The importance of having your SOX on: role of SOX10 in the development of neural crest-derived melanocytes and glia. Oncogene 22, 3024-3034.

Murakami, H., and Arnheiter, H. (2005). Sumoylation modulates transcriptional activity of MITF in a promoter-specific manner. Pigment Cell Res 18, 265-277.

Murakami, M., Iwata, Y., and Funaba, M. (2007). Expression and transcriptional activity of alternative splice variants of Mitf exon 6. Mol Cell Biochem 303, 251-257.

Nakayama, A., Nguyen, M.T., Chen, C.C., Opdecamp, K., Hodgkinson, C.A., and Arnheiter, H. (1998). Mutations in microphthalmia, the mouse homolog of the human deafness gene MITF, affect neuroepithelial and neural crest-derived melanocytes differently. Mech Dev 70, 155-166.

Nishimura, E.K. (2011). Melanocyte stem cells: a melanocyte reservoir in hair follicles for hair and skin pigmentation. Pigment Cell Melanoma Res 24, 401-410.

Nishimura, E.K., Jordan, S.A., Oshima, H., Yoshida, H., Osawa, M., Moriyama, M., Jackson, I.J., Barrandon, Y., Miyachi, Y., and Nishikawa, S. (2002). Dominant role of the niche in melanocyte stem-cell fate determination. Nature 416, 854-860.

Nobukuni, Y., Watanabe, A., Takeda, K., Skarka, H., and Tachibana, M. (1996). Analyses of loss-of-function mutations of the MITF gene suggest that haploinsufficiency is a cause of Waardenburg syndrome type 2A. Am J Hum Genet 59, 76-83.

Opdecamp, K., Vanvooren, P., Riviere, M., Arnheiter, H., Motta, R., Szpirer, J., and Szpirer, C. (1998). The rat microphthalmia-associated transcription factor gene (Mitf) maps at 4q34-q41 and is mutated in the mib rats. Mamm Genome 9, 617-621.

Phung, B., Sun, J., Schepsky, A., Steingrimsson, E., and Ronnstrand, L. (2011). C-KIT signaling depends on microphthalmia-associated transcription factor for effects on cell proliferation. PLoS One 6, e24064.

Pingault, V., Bondurand, N., Kuhlbrodt, K., Goerich, D.E., Prehu, M.O., Puliti, A., Herbarth, B., Hermans-Borgmeyer, I., Legius, E., Matthijs, G., et al. (1998). SOX10 mutations in patients with Waardenburg-Hirschsprung disease. Nat Genet 18, 171-173.

Pingault, V., Ente, D., Dastot-Le Moal, F., Goossens, M., Marlin, S., and Bondurand, N. (2010). Review and update of mutations causing Waardenburg syndrome. Hum Mutat 31, 391-406.

Price, E.R., Horstmann, M.A., Wells, A.G., Weilbaecher, K.N., Takemoto, C.M., Landis, M.W., and Fisher, D.E. (1998). alpha-Melanocyte-stimulating hormone signaling regulates expression of microphthalmia, a gene deficient in Waardenburg syndrome. J Biol Chem 273, 33042-33047.

Primot, A., Mogha, A., Corre, S., Roberts, K., Debbache, J., Adamski, H., Dreno, B., Khammari, A., Lesimple, T., Mereau, A., et al. (2010). ERK-regulated differential expression of the Mitf 6a/b splicing isoforms in melanoma. Pigment Cell Melanoma Res 23, 93-102.

Rowan, S., Chen, C.M., Young, T.L., Fisher, D.E., and Cepko, C.L. (2004). Transdifferentiation of the retina into pigmented cells in ocular retardation mice defines a new function of the homeodomain gene Chx10. Development 131, 5139-5152.

Saito, H., Yasumoto, K., Takeda, K., Takahashi, K., Yamamoto, H., and Shibahara, S. (2003). Microphthalmia-associated transcription factor in the Wnt signaling pathway. Pigment Cell Res 16, 261-265.

Seldin, M.F., Martinez, L., Howard, T.A., Naylor, S.L., and Sakaguchi, A.Y. (1990). Localization of mouse melanoma growth stimulatory activity gene (Mgsa) between Afp and Gus on chromosome 5 using interspecific backcross mice. Cytogenet Cell Genet 54, 68-70.

Shiohara, M., Shigemura, T., Suzuki, T., Tanaka, M., Morii, E., Ohtsu, H., Shibahara, S., and Koike, K. (2009). MITF-CM, a newly identified isoform of microphthalmia-associated transcription factor, is expressed in cultured mast cells. Int J Lab Hematol 31, 215-226.

Sommer, L. (2011). Generation of melanocytes from neural crest cells. Pigment Cell Melanoma Res 24, 411-421.

Steingrimsson, E., Moore, K.J., Lamoreux, M.L., Ferre-D'Amare, A.R., Burley, S.K., Zimring, D.C., Skow, L.C., Hodgkinson, C.A., Arnheiter, H., Copeland, N.G., et al. (1994). Molecular basis of mouse microphthalmia (mi) mutations helps explain their developmental and phenotypic consequences. Nat Genet 8, 256-263.

Steingrimsson, E., Tessarollo, L., Pathak, B., Hou, L., Arnheiter, H., Copeland, N.G., and Jenkins, N.A. (2002). Mitf and Tfe3, two members of the Mitf-Tfe family of bHLH-Zip transcription factors, have important but functionally redundant roles in osteoclast development. Proc Natl Acad Sci U S A 99, 4477-4482.

Strub, T., Giuliano, S., Ye, T., Bonet, C., Keime, C., Kobi, D., Le Gras, S., Cormont, M., Ballotti, R., Bertolotto, C., et al. (2011). Essential role of microphthalmia transcription factor for DNA replication, mitosis and genomic stability in melanoma. Oncogene 30, 2319-2332.

Tachibana, M. (1999). Sound needs sound melanocytes to be heard. Pigment Cell Res 12, 344-354.

Tachibana, M. (2000). MITF: a stream flowing for pigment cells. Pigment Cell Res 13, 230-240.

Takebayashi, K., Chida, K., Tsukamoto, I., Morii, E., Munakata, H., Arnheiter, H., Kuroki, T., Kitamura, Y., and Nomura, S. (1996). The recessive phenotype displayed by a dominant negative microphthalmia-associated transcription factor mutant is a result of impaired nucleation potential. Mol Cell Biol 16, 1203-1211.

Takeda, K., Takemoto, C., Kobayashi, I., Watanabe, A., Nobukuni, Y., Fisher, D.E., and Tachibana, M. (2000a). Ser298 of MITF, a mutation site in Waardenburg syndrome type 2, is a phosphorylation site with functional significance. Hum Mol Genet 9, 125-132.

Takeda, K., Yasumoto, K., Takada, R., Takada, S., Watanabe, K., Udono, T., Saito, H., Takahashi, K., and Shibahara, S. (2000b). Induction of melanocyte-specific microphthalmia-associated transcription factor by Wnt-3a. J Biol Chem 275, 14013-14016.

Tassabehji, M., Newton, V.E., and Read, A.P. (1994). Waardenburg syndrome type 2 caused by mutations in the human microphthalmia (MITF) gene. Nat Genet 8, 251-255.

Taylor, K.L., Lister, J.A., Zeng, Z., Ishizaki, H., Anderson, C., Kelsh, R.N., Jackson, I.J., and Patton, E.E. (2011). Differentiated melanocyte cell division occurs in vivo and is promoted by mutations in Mitf. Development 138, 3579-3589.

Vance, K.W., and Goding, C.R. (2004). The transcription network regulating melanocyte development and melanoma. Pigment Cell Res 17, 318-325.

Verastegui, C., Bille, K., Ortonne, J.P., and Ballotti, R. (2000). Regulation of the microphthalmia-associated transcription factor gene by the Waardenburg syndrome type 4 gene, SOX10. J Biol Chem 275, 30757-30760.

Watanabe, A., Takeda, K., Ploplis, B., and Tachibana, M. (1998). Epistatic relationship between Waardenburg syndrome genes MITF and PAX3. Nat Genet 18, 283-286.

Wen, B., Chen, Y., Li, H., Wang, J., Shen, J., Ma, A., Qu, J., Bismuth, K., Debbache, J., Arnheiter, H., et al. (2010). Allele-specific genetic interactions between Mitf and Kit affect melanocyte development. Pigment Cell Melanoma Res 23, 441-447.

Wu, M., Hemesath, T.J., Takemoto, C.M., Horstmann, M.A., Wells, A.G., Price, E.R., Fisher, D.Z., and Fisher, D.E. (2000). c-Kit triggers dual phosphorylations, which couple activation and degradation of the essential melanocyte factor Mi. Genes Dev 14, 301-312.

Yajima, I., Sato, S., Kimura, T., Yasumoto, K., Shibahara, S., Goding, C.R., and Yamamoto, H. (1999). An L1 element intronic insertion in the black-eyed white

(Mitf[mi-bw]) gene: the loss of a single Mitf isoform responsible for the pigmentary defect and inner ear deafness. Hum Mol Genet 8, 1431-1441.

Yasumoto, K., Amae, S., Udono, T., Fuse, N., Takeda, K., and Shibahara, S. (1998). A big gene linked to small eyes encodes multiple Mitf isoforms: many promoters make light work. Pigment Cell Res 11, 329-336.

Yokoyama, S., Woods, S.L., Boyle, G.M., Aoude, L.G., MacGregor, S., Zismann, V., Gartside, M., Cust, A.E., Haq, R., Harland, M., et al. (2011). A novel recurrent mutation in MITF predisposes to familial and sporadic melanoma. Nature 480, 99-103.

Zaidi, M.R., Hornyak, T.J., and Merlino, G. (2011). A genetically engineered mouse model with inducible GFP expression in melanocytes. Pigment Cell Melanoma Res 24, 393-394.

Zhao, X., Fiske, B., Kawakami, A., Li, J., and Fisher, D.E. (2011). Regulation of MITF stability by the USP13 deubiquitinase. Nat Commun 2, 414.

RESUME

Le facteur de transcription Microphthalmia (Mitf) et la voie de signalisation des « Mitotic Activated Protein Kinase » (MAPK) sont des éléments déterminants pour la différentiation, la prolifération et la survie des melanocytes. L'altération des fonctions de l'un ou l'autre se manifeste par une perte totale ou partielle de ce type cellulaire. A l'inverse, le mélanome est associé très majoritairement à une activation constitutive des MAPK, et parfois, à un gain d'activité de MITF. Afin d'étudier les interactions entre les MAPK et l'activité de MITF, nous nous sommes intéressés aux modifications post transcriptionnelles qui permettent la génération d'isoformes multiples dotées d'activité différentes. MITF contient un site de phosphorylation, la serine 73 (S73), qui a été démontré par le passé comme jouant un rôle à la fois dans l'augmentation de l'activité et dans la réduction de la stabilité de MITF in vitro. Pour comprendre le rôle de cette serine in vivo, une tentative de mutation S73A de *Mitf* a été réalisée. Ce codon fait parti d'un « Exon splicing Enhancer » et sa mutation réduit l'affinité de fixation de la protéine SRp40 et l'exclusion de l'exon 2B dans lequel est situé ce site de phosphorylation. Pour dissocier l'exclusion de l'exon 2B de sa phosphorylation, nous avons donc altéré la jonction de l'exon 2A-2B afin qu'elle ne soit plus reconnue par le spliceosome. En conséquence, l'exon 2B ne peut plus être exclu des transcrits Mitf quelque soit le statut du codon 73. La comparaison de 3 nouveaux allèles *Mitf* S-S73A S-S73D et S-S73S, où l'inclusion de l'exon 2B est forcée, nous a permis d'associer l'absence de phosphorylation à un gain d'activité de MITF.

Mots-clés : Microphthalmia (Mitf), facteur de transcription, phosphorylation, épissage alternatif, souris knock-in, mélanocyte

Laboratoire : Mammalian Development Section, National Institute of Neurological Disorders and Stroke, National Institutes of Health, Building 35 Room 2A/102, 35 Convent Drive, Bethesda, MD USA

Affiliation : Régulation Transcriptionnelle et Oncogenèse, Institut de Génétique et Développement de Rennes, UMR CNRS 6061, 2 avenue du Professeur Léon Bernard, CS 34317, 35043 Rennes CEDEX